ANALYSIS OF PREDICTION ERRORS IN PARTIAL LEAST SQUARES CALIBRATION MODELS USING NEAR INFRARED SPECTROSCOPY BY THREE EXPERIMENTAL SYSTEMS

By

Carlos Alberto Ortega Zúñiga

A dissertation submitted in partial fulfillment of the requirements for the degree of

DOCTOR OF PHILOSOPHY
In
Applied Chemistry

UNIVERSITY OF PUERTO RICO
MAYAGUEZ CAMPUS
2019

Approved by:

_____	_____
Rodolfo J. Romañach, PhD. President, Graduate Committee	Date
_____	_____
Nairmen Mina Camilde, PhD. Member, Graduate Committee	Date
_____	_____
Alberto Santana, PhD. Member, Graduate Committee	Date
_____	_____
Rafael Mendez Román, PhD. Member, Graduate Committee	Date
_____	_____
Oscar Juan Perales Perez, PhD. Representative of Graduate Studies	Date
_____	_____
Enrique Melendez, PhD. Chairperson of the Department	Date

ABSTRACT

This dissertation is focused on understanding the absorption and scattering effects of solid materials in the near infrared (NIR) spectral region and their impact on the prediction errors observed in NIR calibration models developed using partial least squares (PLS) regressions. Four different studies were performed using three experimental settings with four levels of heterogeneity of the materials.

The first study consisted in the use of polypropylene films varying the number of layers stacked together which provided a system with reduced heterogeneity. NIR spectra were acquired using two experimental setups with the integrating sphere module of a Fourier transform NIR (FT-NIR) spectrometer. The depth of penetration of the radiation into the polymer layers was estimated using the O-H stretching mode related to first and second overtones of talc, which ranged from 2.95 to 3.12 mm. PLS models were developed using 30 film layers and bias values were not significantly different from zero at the 95% confidence level. Seven spectral regions were evaluated using different spectral preprocessing, the results showed that optical sampling is unbiased and there is an absence of systematic error by the NIR method. A calibration model using 50 film layers was also evaluated and it presented high statistical errors and bias due the depth of penetration of NIR radiation (optical sampling). This study highlights the lack of systematic error in the NIR method as long as the calibration is representative of the variation to be modelled by PLS regression.

A second study was performed using two polymer films (polypropylene and polyethylene) with similar thickness to vary the heterogeneity of the samples and to evaluate the prediction errors observed in PLS models due to light scattering. Two FT-NIR were used to acquire the spectra of the samples. The spectra from the first instrument was used to

develop the calibration models. NIR spectra from both instruments obtained on three days chosen at random order were used as prediction set to evaluate the linearity and reproducibility of the calibration model. Calibration models were developed based on polyethylene percent content varying the placement and composition below the infinite depth of the radiation. The results based on ANOVA of the predictions shown that PLS models using second derivative as preprocessing in the spectral region of 6500 – 5000 cm^{-1} provided low residual values with no statistical differences on both instruments. This study provides a straightforward and economic analytical method to test the linearity and reproducibility of two FT-NIR instruments using low heterogeneous polymer films.

The third study was developed for real time determination of drug concentration, powder density, and porosity of powder blends at low active pharmaceutical ingredient (API) concentration (3.00 %w/w) within a feed frame. The feed frame provides the most representative stage for measurement of API before the final process. However, changes in the materials' physical properties (e.g. powder density, particle size, flowability, and cohesivity) have a significant effect on NIR spectra. Therefore, this represents a challenge in the development of the calibration model. NIR calibration models using second derivative as spectral preprocessing explained the changes in API concentration, bulk density, and porosity of the powder blends with low error and bias values.

The fourth study shows an applied case in a commercial manufacturing plant in Puerto Rico. Tablets with a combination medicine with two APIs at low concentration were analyzed by PLS regression models for real time release testing (RTRt) in a continuous manufacturing (CM) process. This study provides a better understanding of changes in the manufacturing process and their impact in the predictions of NIR calibration, furthermore,

the evaluation serves for the improvement of control strategies in the manufacturing of a drug product.

RESUMEN

Esta disertación está enfocada en la comprensión de los efectos de absorción y dispersión de materiales sólidos en la región espectral de infrarrojo cercano y su impacto en los errores de predicción observados en modelos de calibración de infrarrojo cercano desarrollados usando regresión de mínimos cuadrados parciales. Cuatro estudios diferentes fueron realizados usando tres montajes experimentales con cuatro niveles de heterogeneidad de los materiales.

El primer estudio consistió en el uso de películas de polipropileno variando el número de capas apiladas juntas lo cual proporcionó un sistema con heterogeneidad reducida. Los espectros de infrarrojo cercano fueron adquiridos usando dos montajes experimentales con el módulo de esfera integradora de un espectrómetro de infrarrojo cercano con transformada de Fourier. La profundidad de penetración de la radiación dentro de las capas de polímeros fue estimada usando el modo de estiramiento O-H relacionado al primer y segundo sobretono de talco, la cual varió en un rango de 2.95 a 3.12 mm. Modelos de mínimos cuadrados parciales fueron desarrollados usando 30 capas de películas y los valores de sesgo no fueron significativamente diferentes de cero al 95% de nivel de confianza. Siete regiones espectrales fueron evaluadas usando diferentes preprocesamientos espectrales, los resultados mostraron que el muestreo óptico es sin sesgo y hay una ausencia de error sistemático por el método de infrarrojo cercano. Un modelo de calibración utilizando 50 capas de películas fue también evaluado y presentó altos errores estadísticos y sesgo debido a la penetración de la radiación de infrarrojo cercano (muestreo óptico). Este estudio destaca la falta de error sistemático en el método de infrarrojo cercano siempre y cuando la calibración es representativa de la variación que va a ser modelada por la regresión de mínimos cuadrados parciales.

Un segundo estudio fue realizado usando dos filmes poliméricos (polipropileno y polietileno) con espesor similar para variar la heterogeneidad de las muestras y evaluar los errores de predicción observados en regresión de mínimos cuadrados parciales debido a la dispersión de la luz. Dos espectrómetros de infrarrojo cercano con transformada de Fourier fueron usados para adquirir los espectros de las muestras. Los espectros del primer instrumento fueron usados para desarrollar los modelos de calibración. Espectros de infrarrojo cercano de ambos instrumentos obtenidos en tres días escogidos en orden aleatorio fueron usados como set de predicción para evaluar la linealidad y reproducibilidad del modelo de calibración. Los modelos de calibración fueron desarrollados basados en el contenido porcentual de polietileno variando la posición y composición por debajo de la penetración infinita de la radiación. Los resultados basados en ANOVA de las predicciones muestran que los modelos de regresión de mínimos cuadrados parciales usando segunda derivada como pretratamiento en la región espectral de 6500 – 5000 cm^{-1} proveyó bajos valores de residuales sin diferencia estadística en ambos instrumentos. Este estudio provee un método analítico económico y sencillo para probar la linealidad y reproducibilidad de dos espectrómetros de infrarrojo cercano con transformada de Fourier usando filmes poliméricos con baja heterogeneidad.

El tercer estudio fue desarrollado para la determinación de concentración de droga en tiempo real, densidad de polvo y la porosidad de mezclas en polvo a baja concentración del ingrediente activo farmacéutico (3.00 %w/w) dentro de un marco de alimentación. El marco de alimentación proporciona la etapa más representativa para la medición de ingrediente activo farmacéutico antes del proceso final. Sin embargo, cambios en propiedades físicas de los materiales debido al proceso (densidad de polvo, tamaño de partícula, fluidez, y

cohesividad) tienen un efecto significativo en los espectros de infrarrojo cercano. Por lo tanto, esto representa un reto en el desarrollo del modelo de calibración. Modelos de calibración de infrarrojo cercano usando segunda derivada como preprocesamiento espectral explicaron cambios en ingrediente activo farmacéutico, densidad aparente y porosidad de las mezclas en polvo con bajos valores de error y sesgo.

El cuarto estudio muestra un caso aplicado en una planta de manufactura comercial en Puerto Rico. Tabletas con una combinación de medicinas de dos ingredientes activos farmacéuticos a baja concentración fueron analizados por modelos de regresión de mínimos cuadrados parciales para las pruebas de liberación en tiempo real in un proceso de manufactura continua. Este estudio proporciona un mejor entendimiento de los cambios en los procesos de manufactura y su impacto en las predicciones de calibraciones de infrarrojo cercano, y la evaluación sirve para el mejoramiento de estrategias de control en la manufactura de un producto de droga.

ACKNOWLEDGEMENTS

During the development of my PhD studies in the University of Puerto Rico at Mayaguez I want to thank several persons:

First thanks to God for the opportunity to contribute for science. I have the belief that the rules of the nature and life were created by a supreme being, and we are part of this work.

My family for their trust in me.

Professor Rodolfo Romañach for accept me in their group lab and his guidance in several areas of the PhD and life.

Graduate committee for his time to review and evaluate this dissertation.

Professor Kim H. Esbensen for helpful discussions on chemometric analysis and the theory of sampling, Professor Don Dahm for discussions on the physics of diffuse reflection, and my friend Andres Roman for his help and advice.

All my friends who help me in the moment that I needed.

This work was funded by the National Science Foundation Engineering Research Center on Structured Organic Particulate Systems, through Grant NSF-ECC 0540855. The funding of the Puerto Rico Science Technology Research Trust, I-Corps 1659082 and SBIR 1621688 grants is gratefully acknowledged.

Graduate Research and Innovation Center (GRIC) and the Graduate Writing Facilitators that help me in the drafting of this dissertation.

Table of Contents

List of Figures

List of Tables

List of Abbreviations and Symbols

APAP	Acetyl-para-aminophenol (acetaminophen)
API	Active pharmaceutical ingredient
CM	Continuous manufacturing
DoE	Design of experiment
FT-NIR	Fourier transform near infrared
GMP	Good manufacturing practice
ICH	International Conference on Harmonisation
LC	Label claim
MCC	Microcrystalline cellulose
MgSt	Magnesium stearate
MIR	Mid infrared
MLR	Multiple linear regression
MPA	Multi-purpose analyzer
NIR	Near infrared
PAT	Process analytical technology
PC	Principal components
PCA	Principal component analysis
PCR	Principal components regression
PLS	Partial least squares
PSD	Particle size distribution
QbD	Quality by design
RMSEC	Root mean square error of calibration
RMSECV	Root mean square error of cross-validation
RMSEP	Root mean square error of prediction
RPM	Revolutions per minute
RSD	Relative standard deviation
RSEP	Relative standard error of prediction
RSVV	Relative specific void volume

RTRt	Real time release testing
SiO_2	Colloidal silicon dioxide
SNV	Standard normal variate
TOS	Theory of sampling
US-FDA	United States Food and Drug Administration

CHAPTER 1: INTRODUCTION

1.1. MOTIVATION AND JUSTIFICATION

Near infrared (NIR) spectroscopy is considered one of the most suitable and fast method for sensing of organic materials in areas such as pharmaceutical manufacturing, agricultural science, medical diagnostics, material science, astronomical spectroscopy, among others, because it is a non-destructive technique. In NIR spectroscopy most of the absorption phenomenon involves vibrations from the stretching and bending of hydrogen atoms associated with carbon, nitrogen, and oxygen atoms. The progress in NIR spectroscopy is due to the fast evolution of instrumentation for diffuse reflectance and its combination with chemometric methods. However, there are factors that have an impact in NIR calibrations as sources of error and need to be minimized by the experimental method. The knowledge of the sources of error in a NIR calibration and how they can be controlled (or minimized) is important to facilitate the evaluation of the materials' properties, processing, or analytical method without undesired disturbances that affect the analysis.

The purpose of this research is the evaluation of prediction errors in near infrared (NIR) calibration models by performing three studies using solid materials with different heterogeneity. CHAPTER 1 presents a brief introduction of NIR spectroscopy and the chemometric methods used in this dissertation. For a detailed explanation of the terms, the reader is cited to the specific references.

Chapter 2 shows the first study which consisted in the use of a low heterogeneous material. A polymer film provided a system with reduced heterogeneity to evaluate the impact on prediction errors in partial least squares (PLS) models due to absorption and

scattering effects, spectral preprocessing, and number of calibration and validation samples. This evaluation serves to understand NIR calibration models without errors due to heterogeneity of the sample and to estimate the minimal error of the NIR method.

Chapter 3 shows a variation of the first chapter using two different polymer materials (polypropylene and polyethylene) with similar thickness to evaluate the prediction errors due to light scattering into the samples. Two FT-NIR instruments were used to acquire the spectra using mix of polymer films below the infinite depth to avoid sampling errors due the depth of penetration of the NIR radiation. Linearity and reproducibility on both FT-NIR instruments were tested by analyzing the PLS predictions of samples acquired at three random days. This study provides a straightforward and economic analytical method to test the linearity and reproducibility of two FT-NIR instruments using low heterogeneous polymer films.

Chapter 4 describes a NIR method for real time prediction of powder blends at low concentration of active pharmaceutical ingredient (API) 3.00% w/w, within a feed frame which it is the most representative stage for measurement of API before the final process. This concentration level is challenging for the NIR method; however, is not impossible as long as the heterogeneity of the materials, and the manufacturing process does not present the major source of prediction errors. This study provides a method for evaluation of critical properties within the feed frame such as tablet mass, hardness and dissolution in batch and continuous manufacturing processes.

Chapter 5 shows an applied case for tablets with a combination medicine of two APIs at low concentration within a commercial manufacturing plant in Puerto Rico for real time release testing (RTRt) in a continuous manufacturing (CM) process where the heterogeneity

is critical for sensing of the materials. The development of the method follows the technical requirements of United States Food and Drug Administration (US-FDA), the guidelines of the International Conference on Harmonisation (ICH). This study provides a better understanding of changes in manufacturing process and the impact in the predictions of the NIR calibration. Also, this evaluation serves for the improvement of control strategies in the manufacturing of a drug product.

1.2. **FUNDAMENTAL BACKGROUND**

2.3.1. Near infrared spectroscopy

This dissertation presents several applications of near infrared (NIR) spectroscopy to understand the interaction of the radiation with heterogeneous materials and their effects in the errors observed in chemometrics models. NIR spectroscopy methods have gained the interest of many areas for real time analysis of materials. Research in areas such as chemical composition and production of foods and fibers in agriculture (Batten, 1998), quality control for cosmetic preparations (Blanco, Alcalá, Planells, & Mulero, 2007), non-invasive medical devices for research and clinical studies of biological tissue (Torricelli et al., 2014), pharmaceutical industry for manufacturing of drug products (Vargas et al., 2018), prediction of polymer composition (Furukawa, Watari, Siesler, & Ozaki, 2003; Rohe, Becker, Kölle, Eisenreich, & Eyerer, 1999; Sulub & DeRudder, 2013), among others have done a gradual substitution of conservative analytical techniques such as Gas Chromatography (GC), High Performance Liquid Chromatography (HPLC), Mass Spectrometry (MS), Nuclear magnetic resonance (NMR), and Ultraviolet and visible (UV-Vis) absorption spectroscopy. An

increasing demand of NIR spectroscopy methods has been seen because this is a non-destructive technique, it is also environmentally compatible because it does not generate waste, and with respect to conservative techniques it is a non-time-consuming method, in other words, a real-time in situ technique (Siesler, 2007).

Despite the potential of NIR spectroscopy, there are some chief disadvantages that make the technique complex. The disadvantages are instrumentation response, dependence of the calibration method, NIR spectral data preprocessing, sampling procedures, high sensitivity to environmental conditions and low sensitivity to minor constituents, and the physics of diffuse reflectance (Norris, 1989). However, the development of the NIR instrumentation and the combination with chemometrics make possible the use of NIR spectroscopy methodologies for fast analysis of materials.

This chapter will briefly review basic concepts of Near Infrared Spectroscopy and chemometrics. However, the references to scientific articles and books related to the topics will be addressed for a deep understanding.

1.2.2. Basic principles of molecular vibrations

The near infrared (NIR) region is complementary to the fundamental vibrations observed in Mid infrared (MIR) and Raman. **Table 1** shows a short comparative summary between NIR, MIR, and Raman. For more detailed information the reader is referred to the following literature (D. J. Dahm & Dahm, 2001; Miller, 2001; Norris, 1989; Siesler, 2007; Workman & Weyer, 2012). The three techniques are different in several aspects; however,

their basic principle is the same: the signals observed in Raman, MIR, and NIR are a result of the molecular vibrations due to the interaction of radiation with the molecules.

Table 1. Principles of Raman, MIR, and NIR spectroscopy. From (Siesler, 2007).

Raman	**Mid infrared**	**Near infrared**
Fundamental vibrations	Fundamental vibrations	Overtones and combinations
4000 – 50 cm^{-1}	4000 – 200 cm^{-1}	14000 – 4000 cm^{-1}
Scattering technique	Absorption techniques	
Source: Monochromatic radiation Laser VIS-NIR	Sources: (Dispersed) Polychromatic radiation Globar tungsten	
Polarizability	Dipole moment	Anharmonicity
Homonuclear e.g., C=C	Polar e.g., C=O	Polar, $m_2 \ll m_1$ C-H/O-H/N-H m_2: H; m_1: C, O, N.

The vibrational energy is calculated using the harmonic oscillator model by the view of oscillation of atoms in a molecule attached by a bond like a spring following the equation (1-1):

$$E = \frac{h}{2\pi}\sqrt{\frac{k}{\mu}} \tag{1-1}$$

Where E: is the energy of the molecular vibration, h: is Planck's constant, and μ is the reduced mass given by the equation (1-2):

$$\mu = \frac{m_1 m_2}{m_1 + m_2} \tag{1-2}$$

m_1: the mass of atom 1, and m_2: the mass of the atom 2.

Equations 1 and 2 shows that energy of molecular vibrations is very sensitive to the structure, and this is the wide application of MIR in structure elucidation.

The potential energy of the vibrating system (V) at any given time is a quadratic function of the displacement of the atoms involved in the vibration following Hooke's law, which is shown in **Figure 1** and given by the equation (1-3):

$$V = \frac{1}{2}kx^2 = \frac{1}{2}k(r - r_e)^2 \quad (1\text{-}3)$$

Where V: is the potential energy of the vibrating system, k: is the force constant of the bond (also named restoring force), x: represents the displacement of the atoms from the equilibrium position (displacement coordinate), r: is the internuclear distance during the vibration, and r_e: is the equilibrium internuclear distance.

From equation 1 and 3, the vibrational frequency of the system (ν_0) is given by the equation (1-4):

$$\nu_0 = \frac{1}{2\pi}\sqrt{\frac{k}{\mu}} \quad (1\text{-}4)$$

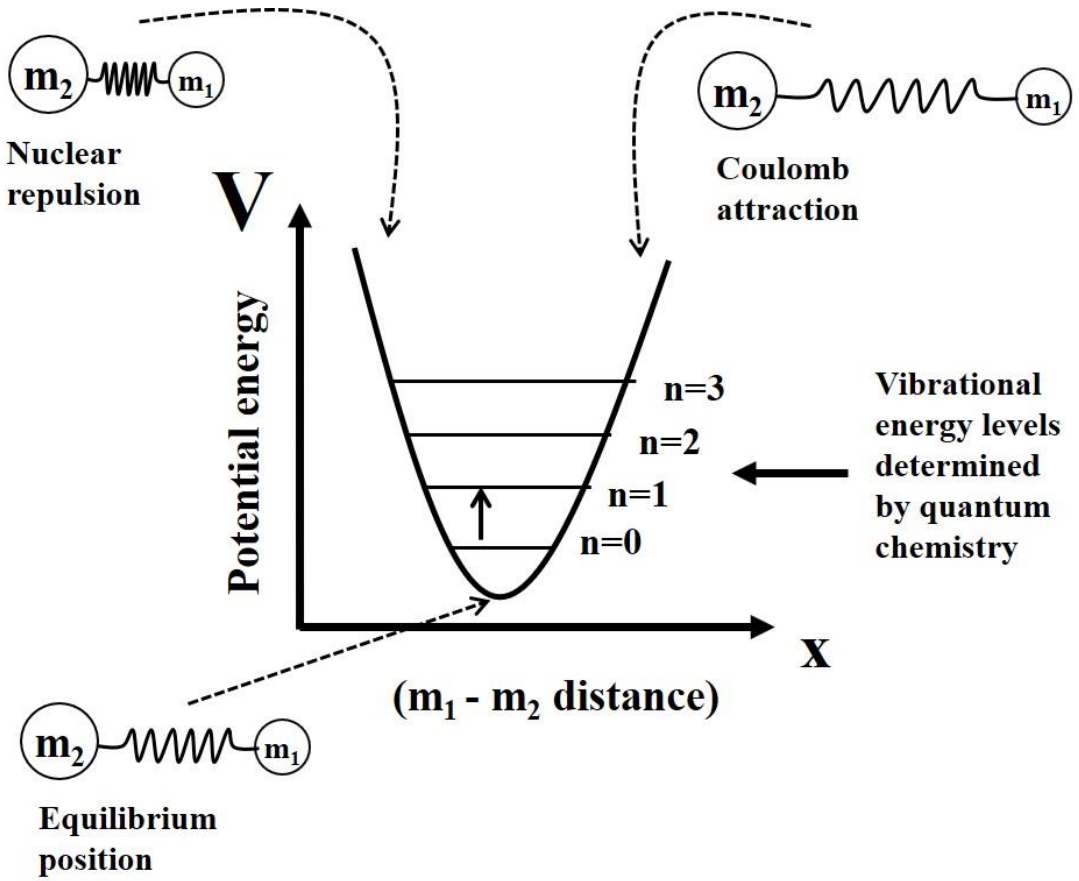

Figure 1. Representation of the harmonic oscillator model. Potential energy (V) vs internuclear distance during the vibration. From (Miller, 2001).

The vibrational energy has discrete values that are calculated by a quantum mechanical treatment by the Schrodinger equation, and these values are given by the equation (1-5):

$$E = h\nu_0\left(n + \frac{1}{2}\right) \qquad (1\text{-}5)$$

Where h is Planck's constant, ν_0 is the vibrational frequency defined in equation 4, and n is the vibrational quantum number that can only have integer values (0, 1, 2, 3, …).

Diatomic molecules are useful to demonstrate and explain the concept of vibrational energy; however, real molecules have more than two atoms and their vibrations are more

complex. Furthermore, NIR vibrational spectroscopy relies on nonidealities of the harmonic oscillator (Miller, 2001). The potential energy curve for NIR vibrations follow an asymmetric Morse function represented in **Figure 2**.

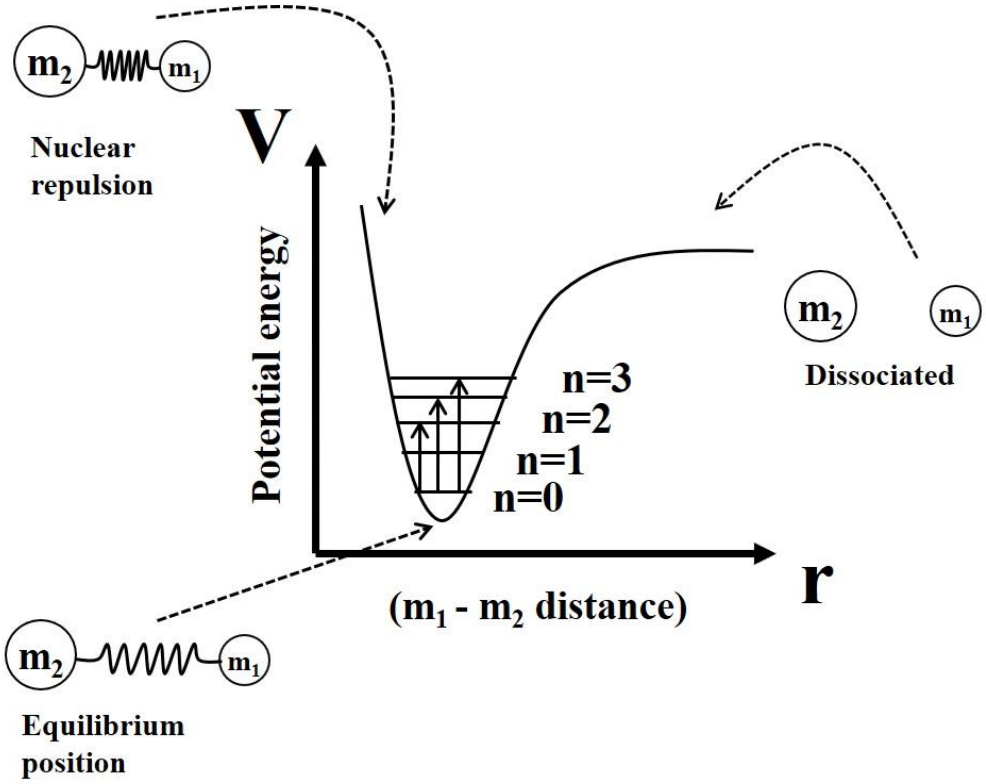

Figure 2. Representation of the anharmonic oscillator model. Potential energy (V) vs internuclear distance during vibration. From (Miller, 2001).

The existence of NIR vibrational spectroscopy relies on two main deviations of the harmonic oscillator model:

1. Mechanical anharmonicity: most of the real molecules present anharmonic vibrations rather than harmonic.

2. Electrical anharmonicity: the dipole moment for a couple of atoms in a molecule, is not exactly a function of interatomic distance.

For in depth reading of this subject these authors have extensive review: (D. J. Dahm & Dahm, 2001; Norris, 1989; Siesler, 2007). From **Figure 2**, there are three important points to mention that are consequence of anharmonicity and make NIR spectroscopy possible:

1. Overtones: these molecular vibrations are a result of the transition from a vibration number higher than one, for example n=0 to n=2, 3, …, and so on.
2. Combinations: this mode of vibration involves two or more different vibrations from absorption of a single photon; they must have the same symmetry and must involve the same functional group.
3. The separation levels of the transitions are not equally separate, as the harmonic oscillator.

The frequency of the overtone vibrations is approximately equal to integer numbers of the fundamental vibrations. The combination bands are approximately the sum of frequencies that makes the combination. **Figure 3** shows an example of two fundamental vibrations for a methylene (-CH_2-) group, their overtone frequencies, and the combination band. As show in figure 3, the frequency of the overtones are integer values of the fundamental vibrations. However, the frequency value is smaller because the anharmonicity and the point three (3) mentioned before.

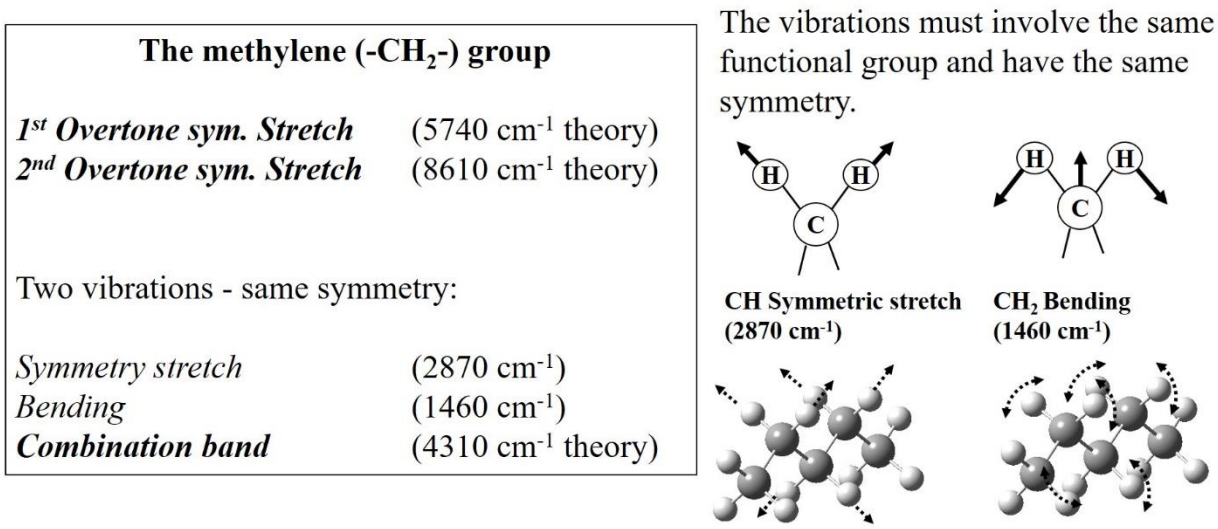

Figure 3. Representation of two fundamental vibrations of methylene group. Geometry representation, frequency, overtones, and combination bands. From (Miller, 2001).

1.2.3. NIR spectral acquisition

Near infrared spectroscopy is a technique with a wide usage in several analytical areas because it is a non-destructive, fast and it is sensitive to chemical and physical variation in the sample. However, due to sensitivity to physical changes it is necessary to use a correct sensor that can detect the desired variation to analyze without loss of information or undesired disturbances. **Figure 4** shows four of the most used setups for sample measurement in NIR spectroscopy. The first setup (**Figure 4a**) is for measurement in liquid samples in transmission mode; in this mode is used approximately 1 – 2 mL of the sample in a cell. The second setup (**Figure 4b**) is the mode of diffuse reflectance using the solid probe for solids. The third setup (**Figure 4c**) is the mode of diffuse reflectance using the integrating sphere module for solids. The fourth setup (**Figure 4c**) is the transmission mode for solids such as tablets.

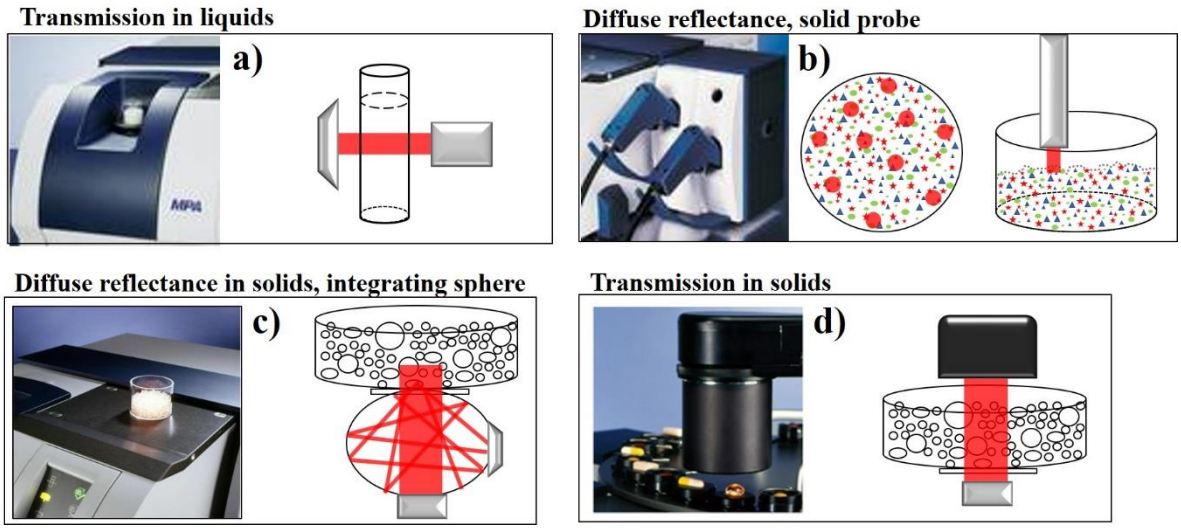

Figure 4. Representation of four used sample measurements in NIR spectroscopy. a) Transmission in liquids. b) Diffuse reflectance using a NIR probe. c) Diffuse reflectance using a integrating sphere module. d) Transmission in solids. Instrument images from Bruker optics.

1.2.4. Multivariate data analysis

Multivariate data analysis was used in all studies described in this dissertation. In this section the basic concepts of multivariate data analysis in the chemometrics field with NIR spectroscopy are addressed. For a comprehensive explanation of the topics, the reader is cited to the following references: (Beebe, Pell, & Seasholtz, 1998; Kim H Esbensen, Guyot, Westad, & Houmoller, 2002; Mark & Workman Jr, 2010; Næs, Isaksson, Fearn, & Davies, 2002).

Most of the data from science is multivariate and depends on several variables. Calibration is a mathematical model to relate an instrument response as output from a property of a sample (Beebe et al., 1998), If the instrument response used for construction of the calibration is only one per each property of the sample, the calibration is univariate. However, there are many cases where the combination of multiple instrument responses with

the property of the sample provide better results; this is a multivariate calibration (Næs et al., 2002).

The use of multivariate analysis with statistical and mathematical procedures to extract information of chemical (or physical) data to solve problems that are not easily resolved with univariate analysis, lead to the creation of Chemometrics (Kim H Esbensen et al., 2002; Næs et al., 2002). Some of the most used methods of multivariate calibration are Principal Component Analysis (PCA) and Partial Least Squares (PLS). However, multivariate data can be complex; this is because the response of the instrument depends not only in the property of the sample to be modelled but also the noise part that is "everything else" (contributions from other components, instrumental noise, analytical errors (Kim H Esbensen et al., 2002). There are a diverse number of factors that can produce an unknown source of variation, **Figure 5** shows some of the most common variations in NIR spectral data. There are additive effects that cause a baseline variation in the spectra; multiplicative effects that cause variations in the intensity of the spectral bands; and combinations of additive and multiplicative effects is the most common variation observed because they are presented randomly in the data (Kohler, Zimonja, Segtnan, & Martens, 2009). The instrument variation in spectral acquisition is another source of variation that affects the data. Sideways shifts affect the peak position of the instrument response of the sample. Random noise heteroscedasticity, i.e. high instrument response (e.g. high absorbance) tend to have high uncertainty that small instrument response. Response curvature depends on the concentration of the sample, if the concentration is high, the detector will be saturated and it will not be possible to observe a correct band intensity (Kohler et al., 2009).

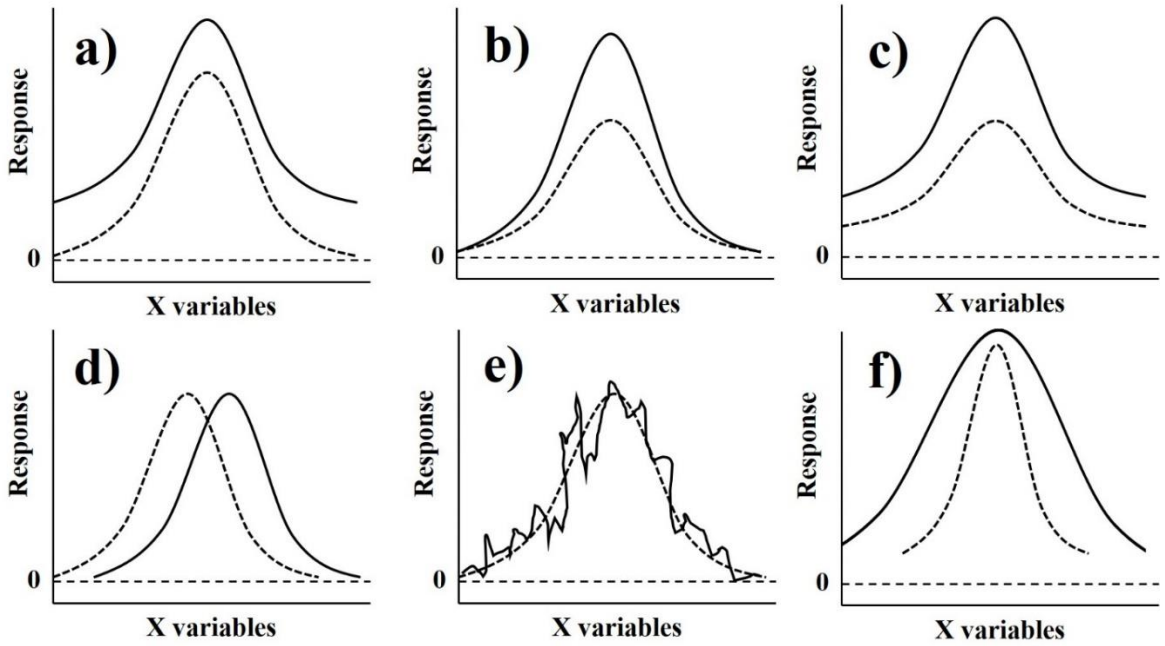

Figure 5. Representation of the most common variations in NIR spectra. a) Additive effects, b) multiplicative effects, c) combination of additive and multiplicative effects, d) sideways shift, e) random noise, and f) response curvature. From (Kohler et al., 2009).

NIR spectra provides information on the chemical composition of the samples and physical properties; however, there are diverse sources of irrelevant information of the spectra that affect the data analysis (Norris, 1989). Prior to data analysis it is necessary to remove or reduce irrelevant source of information, this is the data preprocessing step. This need has been called one of the six habits of the chemometrician (Beebe et al., 1998). Some of the basic data preprocessing methods are smoothing, Standard Normal Variate (SNV), derivatives, and a combination of these methods.

1.2.4.1. Savitzky-Golay smoothing

Savitzky-Golay smoothing method was used in this research to reduce noise by applying a moving polynomial function to the data. This function is created using a specific

number of points (this number of points must be odd and ≥5) and creating a sub-model that smoothes the original data. This preprocessing does not remove baseline or spectral slope in the spectra (Savitzky & Golay, 1964).

1.2.4.2. Standard normal variate

The preprocessing standard normal variate (SNV) was applied to raw spectra acquired in the studies of this dissertation to normalize the set of spectra. This preprocessing is used to reduce multiplicative, baseline, and wavelength shifts (Cao, 2013). SNV performs a normalization of the spectra reducing scattering effects due to packing heterogeneity or path-length variations. Also, it improves instrument transferability (Cao, 2013). SNV preprocessing applies a subtraction of the mean and divide with the standard deviation (Barnes, Dhanoa, & Lister, 1989). Equation (1-6) shows the SNV preprocessing given by:

$$SNV = \frac{(x - \bar{x})}{\sqrt{\frac{(x - \bar{x})^2}{n-1}}} \tag{1-6}$$

where x represents the absorbance of the sample at the specific wavenumber, and $\bar{x}$ represents the average of all absorbances of the sample.

Figure 6 shows an example of how it works the SNV pretreatment on the spectra with a real case using a commercial refined sugar (sucrose) obtained from supermarkets. The granules of sugar were grinded manually in a mortar to obtain fine particles of this material. NIR spectra of powder samples based on grinded granules (grinded sugar) and powder samples from raw material (refined sugar) were acquired using the solid probe of the FT-NIR

instrument. The difference of these materials is the particle size; grinded sugar had lower particle size than refined sugar due the result of grinding the raw granules in a mortar. The NIR spectra of grinded sugar had a lower baseline than the spectra of refined sugar because more radiation reach the detector due that there is more reflected radiation by the particles (**Figure 6a**). After SNV pretreatment (**Figure 6b**) the spectra of grinded sugar and refined sugar presented a similar baseline with changes in some parts due to the absorption of the material and the wavenumber of the radiation. However, this pretreatment reduces the difference due to the baseline and it allows to evaluate the difference in absorbance of the materials.

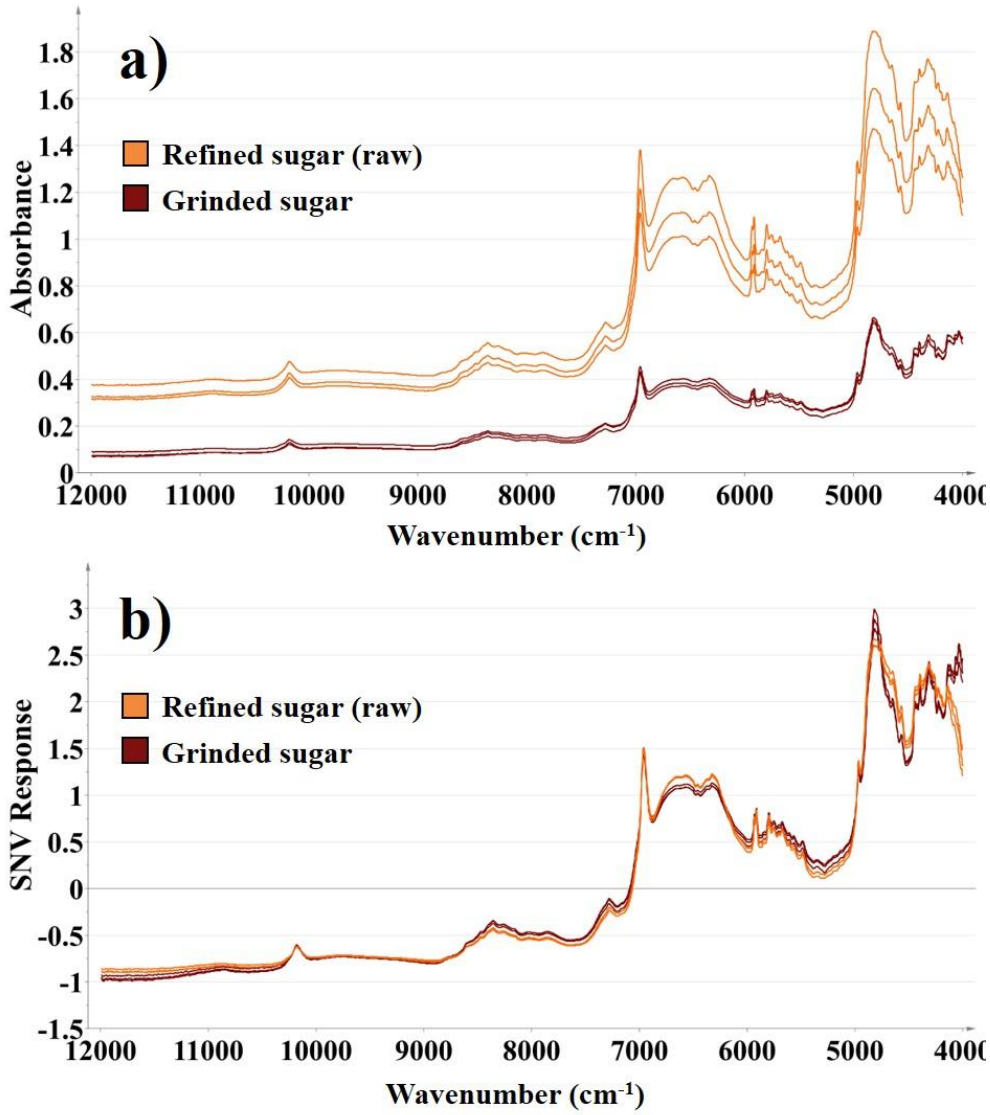

Figure 6. Representation of the SNV pretreatment with NIR spectra of sugar fine and ground sugar. a) NIR spectra without pretreatment, b) SVN spectra.

1.2.4.3. Derivatives Savitzky-Golay

The derivatives (first and second derivative) were the most used preprocessing methods in this dissertation to evaluate the spectra and to perform NIR calibrations. Derivatives are functions utilized to reduce scatter effects of continuous spectra using the polynomial Savitzky-Golay smooth (Savitzky & Golay, 1964). The first derivative preprocessing is usually used to reduce additive baseline ("offset"), where the second derivative preprocessing

also involves removal of linear baseline. Similar to how the Savitzky-Golay smoothing works, the derivatives generate a new function that depends on the number of points used (Næs et al., 2002).

Figure 7 shows an example of how it works the first derivative pretreatment for a set of NIR spectra using the solid probe of the FT-NIR instrument of powder blends with three components at different concentration levels. **Figure 7a** shows the NIR spectra of particulate materials such as powder blends which presented differences in spectral baseline due to the complex interaction of particles with different size and composition. Additionally, the NIR spectra of each powder blend presented differences in the absorption bands due to concentration of the materials; for this case is acetaminophen (APAP), lactose (lac), and microcrystalline cellulose (MCC). After first derivative pretreatment (**Figure 7b**) the differences in spectral baseline were minimized and it is possible to observe their differences in absorption bands due to concentration of the components.

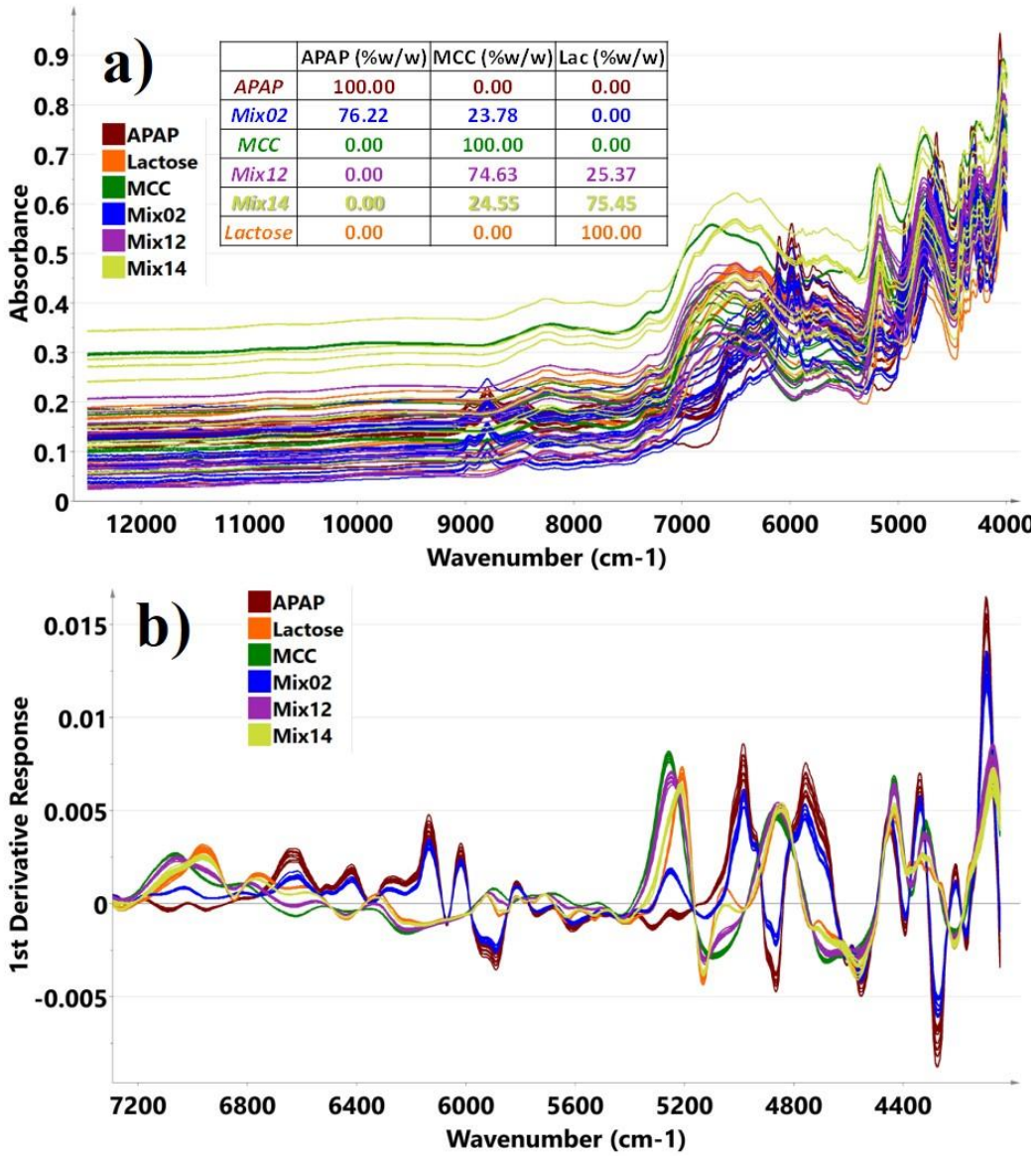

	APAP (%w/w)	MCC (%w/w)	Lac (%w/w)
APAP	100.00	0.00	0.00
Mix02	76.22	23.78	0.00
MCC	0.00	100.00	0.00
Mix12	0.00	74.63	25.37
Mix14	0.00	24.55	75.45
Lactose	0.00	0.00	100.00

Figure 7. Representation of the first derivative pretreatment with NIR spectra of powder blends at several levels of acetaminophen (APAP), lactose (Lac), and microcrystalline cellulose (MCC) concentration. a) NIR spectra without pretreatment, b) first derivative spectra.

Combination of preprocessing techniques such as SNV + first or second derivatives, are used as methods for scatter correction to reduce the physical variability such as particle size between samples and adjustment for baseline shift over the long period of data collection (Cao, 2013).

The most common methods of multivariate calibration are Principal Components Analysis (PCA), Principal Components Regression (PCR), and Partial Least Squares (PLS). A brief description of these methods are presented; however, it is recommended to read these references: (Beebe et al., 1998; Kim H Esbensen et al., 2002; Næs et al., 2002).

1.2.4.4. Principal Components Analysis

Principal Component Analysis (PCA) was utilized in this dissertation as projection method which provided an interpretable overview of the main multidimensional data matrix. PCA takes information carried by the original variables and projects them onto a smaller number of latent variables called Principal Components (PC). Each PC explains a certain amount of the total information contained in the original data and the first PC contains the greatest source of information in the data set. Each subsequent PC contains, in order, less information than the previous one. By plotting PCs, important sample and variable interrelationships can be revealed, leading to the interpretation of certain sample groupings, similarities or differences (Beebe et al., 1998; Kim H Esbensen et al., 2002; Næs et al., 2002). **Figure 8** shows a graphical description of a PCA., and corresponding scores plots in two and three dimensions. Each NIR spectra contains the absorption at each wavenumber (variable), making it a vector for each sample. After performing the PCA, the number of variables is reduced to a small number (called the PC). The scores (dots in the new space) represent the projection of the original variables into the new space. In this case the first source of variation is the concentration level starting at 70% LC and finalizing at 130% LC.

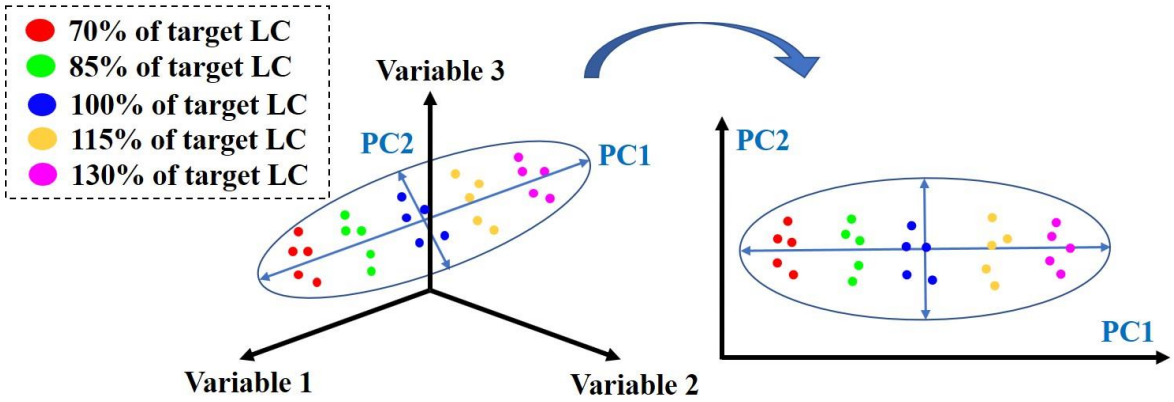

Figure 8. Graphical description of a PCA, and corresponding scores plots. Left: variable 1, variable 2, and variable 3 (**X**-variables). Right: (PC1 and PC2).

PCA can be used to reveal the hidden structure within large data sets. It provides a visual representation of the relationships between the samples and variables, and it provides insights into how measured variables cause some samples to be similar, or how they differ between them. **Figure 9** shows an example of the use of a PCA with the compressibility profile of two lactose powders with different particle size within a FT4 powder rheometer. Lactose 70 (blue triangles) presents higher particle size than lactose 140 (orange boxes). As exploratory data analysis, using all the NIR spectra shows two cluster groups related to the particle size of the two powders (**Figure 9a**). After divide the datasets by particle size and process, the PCA shows the variation based on the compressibility of the powders within the FT4 (**Figure 9b**).

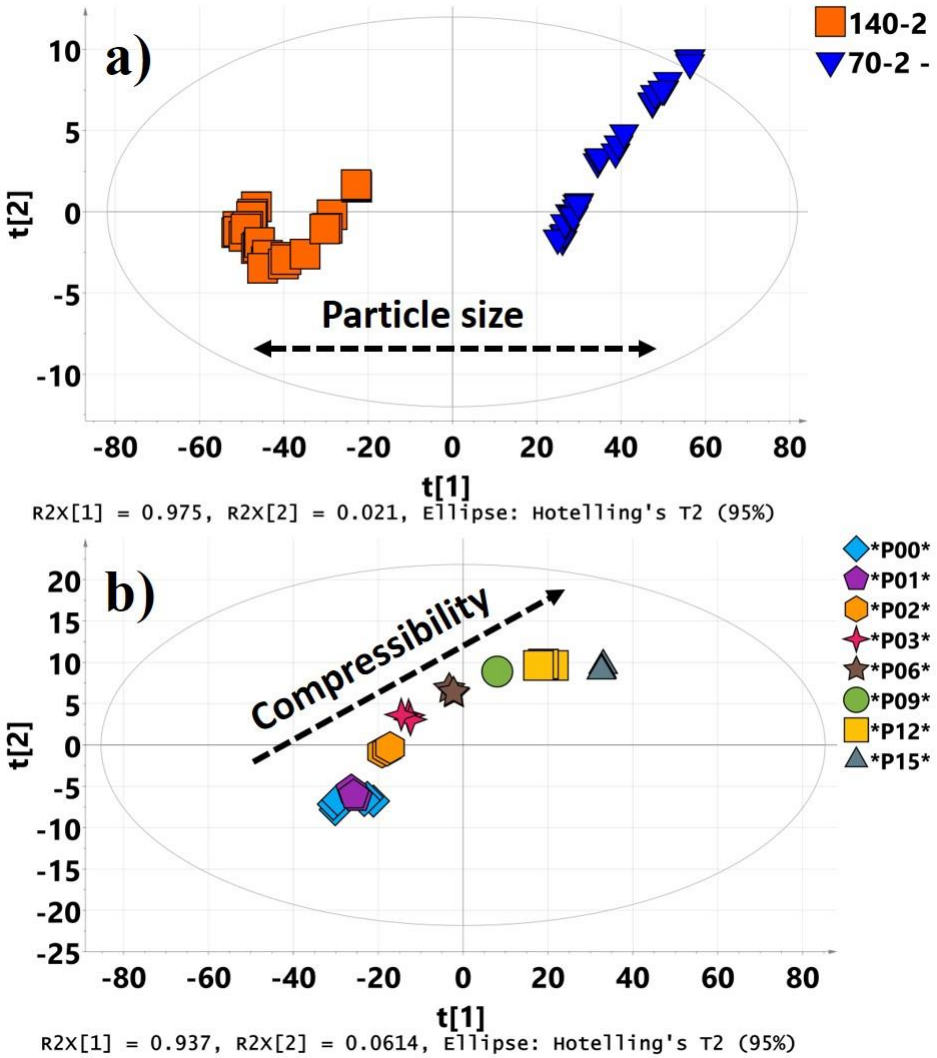

Figure 9. PCA of two datasets for two powder blends of lactose with two particle size within a compressibility profile in a FT4 powder rheometer. a) Lactose 70 (blue triangles) presents higher particle size than lactose 140 (orange boxes). b) Compressibility profile at 0, 1, 2, 3, 6, 9, 12, and 15 kilo Pascal.

1.2.4.5. Multiple Linear Regression

Multiple linear regression (MLR), is a classical regression method that combines a set of several predictor or **X**-variables in linear combinations, which correlate as closely as possible to a corresponding single response or **Y**-vector (Beebe et al., 1998; Kim H Esbensen et al., 2002; Næs et al., 2002).

MLR has the following properties and behavior:

- The number of **X**-variables must be smaller than the number of samples;
- In case of collinearity among **X**-variables, the b-coefficients are not reliable, and the model may be unstable;
- MLR tends to overfit when noisy data is used.

1.2.4.6. Principal Component Regression

Principal Component Regression (PCR), is a method for relating the variance in a response variable (**Y**-variable) to the variance of several predictors (**X**-variables), with explanatory or predictive purposes. It is a two-step procedure which first decomposes an **X**-matrix by PCA, then fits an MLR model, using the PC scores instead of the original **X**-variables as predictors (Beebe et al., 1998; Kim H Esbensen et al., 2002; Næs et al., 2002).

This method performs particularly well when the various **X**-variables express common information, i.e. when there is a large amount of correlation, or even collinearity. Since the scores are orthogonal, the MLR solution is stable and therefore the PCR model does not suffer from collinearity effects. It is the belief of some data analysis scientists that PCR is superior to PLS since it forces analysts to better understand their data and its preprocessing (transformations) before the application of a regression procedure (Beebe et al., 1998; Kim H Esbensen et al., 2002; Næs et al., 2002).

1.2.4.7. Partial Least Squares

Partial Least Squares (PLS) Regression, also sometimes referred to as Projection to Latent Structures or just PLS was the method for multivariate calibration used in the studies described in this dissertation to obtain a relationship of the spectra (**X**-variables) and the properties (**Y**-variables) to model. PLS models both the **X**- and **Y**-matrices simultaneously to find the latent (or hidden) variables in X that will best predict the latent variables in **Y**. These PLS components are similar to principal components but will be referred to as factors (Beebe et al., 1998; Kim H Esbensen et al., 2002; Næs et al., 2002).

PLS maximizes the covariance between **X** and **Y** data. In this case, convergence of the system to a minimum residual error is often achieved in fewer factors than using PCR. This contrasts with PCR, which first performs PCA on **X** and then regresses the scores (**T**) vs. the **Y** data (Beebe et al., 1998; Kim H Esbensen et al., 2002; Næs et al., 2002).

1.2.4.8. Statistical Evaluation of the results and validation

The performance of the multivariate calibration method used was evaluated in terms of the following statistical parameters: bias, standard deviation, Root Mean Square Error of Prediction (RMSEP), and Relative Standard Error of Prediction, RSEP (%) (Beebe et al., 1998; Kim H Esbensen et al., 2002; Næs et al., 2002).

The bias is the average difference between the predicted and measured values for the validation set, is a measure of the accuracy, expressed by equation (1-7):

$$bias = \frac{\sum_{i=1}^{n}(\hat{y}_i - y_i)}{n} \quad (1\text{-}7)$$

Where $\hat{y}_i$ and y_i are, respectively, the predicted and measured values of sample i of the n samples in the validation set. A model that is not representative of the validation set will lead to significant bias.

The RMSEP is the average prediction error calculated by equation (1-8):

$$RMSEP = \sqrt{\frac{\sum_{i=1}^{n}(\hat{y}_i - y_i)^2}{n}} \quad (1\text{-}8)$$

If both calibration and validation sets are representative of future prediction errors, the RMSEP should be a good estimation for future predictions. High RMSEP values could be an indication of a lack of accuracy and/or precision. However, a high RMSEP does not necessarily mean a poor method; if the samples are highly heterogeneous, the accuracy and precision will be affected.

The Relative Standard Error of Prediction, RSEP (%), is a measure of the error in comparison with the measured values in the validation set, and is calculated by equation (1-9):

$$RSEP(\%) = 100 \times \sqrt{\frac{\sum_{i=1}^{n}(\hat{y}_i - y_i)^2}{\sum_{i=1}^{n}(y_i)^2}} \quad (1\text{-}9)$$

CHAPTER 2: STUDY OF NIR CHEMOMETRIC MODELS WITH LOW HETEROGENEITY FILMS. THE ROLE OF SAMPLING AND SPECTRAL PREPROCESSING ON PLS ERRORS

Based on the Work Published in: *Journal of Near Infrared Spectroscopy* 25(2), 2017, 103–115.

Carlos Ortega-Zuñiga, Kerimar Reyes-Maldonado, Rafael Méndez and Rodolfo J Romañach.

This chapter is not an exact copy of the published paper. It contains original information.

2.1. INTRODUCTION

This work was performed to investigate the effect of depth of penetration, scattering and absorption of NIR radiation on the errors observed in reflectance measurements with PLS calibration models. The understanding of systematic and random errors is extremely important in NIR spectroscopy, and in all the analytical methods available to chemists who provide valuable information to society. However, NIR spectroscopy is subject to a number of errors associated with the fact that the samples analyzed are usually solids, with significant scattering. The sources of error are different than in an HPLC method where samples are dissolved, filtered, and centrifuged. Thus, the importance of investigating the effect of depth of penetration and scattering on quantitative PLS measurements.

Sampling errors also affect the quality of data reported by analytical chemists. According to the Theory of Sampling (TOS), the combined sampling errors are one or two orders of magnitude higher than analytical errors, therefore, the quality of the data is almost entirely dependent upon proper sampling practices.(Kim H. Esbensen & Geladi, 2010; Kim H. Esbensen & Paasch-Mortensen, 2010; Petersen, Minkkinen, & Esbensen, 2005) TOS also

indicates that heterogeneity is the source of all sampling errors. NIR spectroscopy is often performed with samples that are mixtures and where heterogeneity leads to sampling errors.(Kim H. Esbensen & Paasch-Mortensen, 2010; K. H. Esbensen, Roman-Ospino, Sanchez, & Romanach, 2016; Petersen et al., 2005) However, the errors in NIR spectroscopy are also related to the complex interaction between light and particles (scattering), and the optical set up used.

The interaction of the radiation with solids is complex and does not follow Beer's law (D. Dahm & Dahm, 2014). **Figure 10** shows an idealized case of layer of particles and the interaction with NIR radiation. **Figure 10** shows that particles such as pharmaceutical powders are not organized in that way, because particles have physical properties as segregation, consolidation, cohesion, among other that makes the bulk material to be heterogeneous. The interaction of NIR radiation is in a random way as particles in solids have a random distribution. This complex interaction makes NIR spectra difficult to evaluate for newcomers in this area. Nevertheless, NIR spectroscopy is considered one of the most suitable and fast non-destructive methods for analysis of materials. NIR scattering is affected by physical differences of the materials, such as particle size,(D. Dahm, 2005; Frake et al., 1998; Himmelsbach, Barton, & Akin, 1986; Sarraguca, Cruz, Amaral, Costa, & Lopes, 2011) density,(D. R. Ely, Thommes, & Carvajal, 2008; Gupta, Peck, Miller, & Morris, 2005; Román-Ospino et al., 2016) and thickness,(Heymann, Mirschel, & Scherzer, 2010; Heymann, Mirschel, Scherzer, & Buchmeiser, 2009; Römer, Heinämäki, Strachan, Sandler, & Yliruusi, 2008) This scattered radiation was studied using different numbers of layers of similar polymer sheets to describe the representative layer theory (D. J. Dahm & Dahm,

2001) and to find the absorption and remission fractions for layers which best fit the observed log(1/R) values.(D. Dahm, Dahm, & Norris, 2000),(D. Dahm, Dahm, & Norris, 2002) The mathematics described by the equations of Benford used in the study are in agreement with the behavior of the absorption/remission of samples with plane parallel layers. A substantial error was found to fit perfectly the experimental data as result of incomplete detection of the remitted radiation by differences in sample roughness. In spite of the complexity of the interaction between radiation and particles, NIR spectroscopy is applied in many industries.

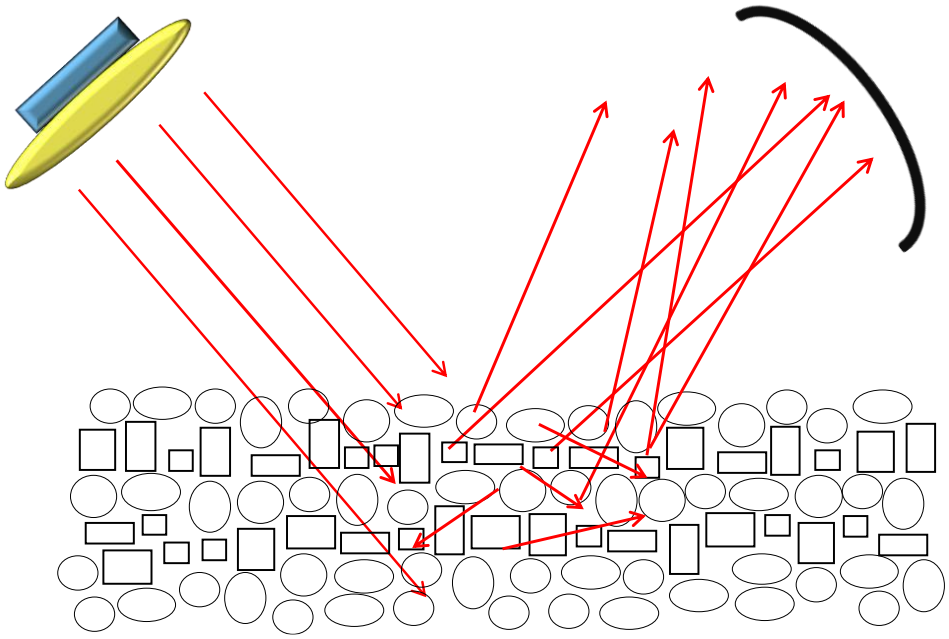

Figure 10. Idealized case of organized particle layers; in reality pharmaceutical powders do not have organized particle layers.

Table 2 provides a summary of applications using NIR spectroscopy and chemometrics for quantification purposes in different industries. The summary in **Table 2** was difficult to create because of differences in the way that NIR results are reported in publications and

different industries and is not considered a complete description of the errors observed in NIR spectroscopy. **Table 2** indicates that liquid samples present the lowest errors with RSEP(%) less than 2%. Polymer blends and pellets present RSEP(%) lower than 6%. Pharmaceutical powder blends and granulates present RSEP of 7.5% and lower, and pharmaceutical tablets have been determined with RSEP (%) of 0.9–7.5%.

Table 2. Summary of studies using NIR spectroscopy and chemometrics for quantification purposes. T: transmission, R: diffuse reflection, and TF: transflection. * RSEP values presented in percent (%).

Reference	Error value*	Method	Samples
Tankeu et al(Tankeu, Vermaak, Kamatou, & Viljoen, 2014)	< 2	T	lavender oils
Alves and Poppi(Alves & Poppi, 2013)	< 2	TF	ternary fuel blends
Rohe et al(Rohe et al., 1999)	< 2	T	polymer blends
Heymann et al(Heymann et al., 2010)	< 2	TF	polymer film coatings
Sulub and Derudder(Sulub & DeRudder, 2013)	< 3	R	polymer blends
Rosas et al(Rosas, Blanco, Santamaría, & Alcalà, 2013)	6.2	R	ternary mixture pellets
Colón et al(Colón, Florian, Acevedo, Méndez, & Romañach, 2014)	2.5	R	pharm. powder blends
Vanarase et al(Vanarase, Alcalà, Jerez Rozo, Muzzio, & Romañach, 2010)	7.5	R	pharm. powder blends
Dou et al(Dou, Sun, Ren, Ju, & Ren, 2005)	1.07	R	pharm. powder blends
Cárdenas et al(Càrdenas, Blanco, & Alcalà, 2014)	1.90	R	lab. powder blends and ind. gran.
Blanco et al(Blanco, Bautista, & Alcalá, 2008)	3.9 and 1.6	R	pharm. powder blends (granules)
Cárdenas et al(Cárdenas, Cordobés, Blanco, & Alcalà, 2015)	0.81 – 2.68	R	pharm. powder blends and tablets
Sánchez-Paternina et al(Adriluz Sánchez-Paternina et al., 2016)	< 5	T	pharm. powder blends
Blanco et al(Blanco, Coello, Iturriaga, Maspoch, & Pou, 2001)	< 1.6	R	powder blends (milled tablets)
Dou et al(Dou et al., 2005)	1.2	R	two components tablets
Blanco and Alcalá(Blanco & Alcalá, 2006)	0.9 – 6.8	R	pharm. Tablets
Abrahamsson et al(Abrahamsson, Johansson, Andersson-Engels, Svanberg, & Folestad, 2005)	2.5	T	intact pharm. Tablets

Polymer films that are much less heterogeneous than powder samples, such as pharmaceutical materials, were selected in this application to reduce sampling errors. The polymer films were used to minimize sampling errors but maintain scattering to study its effect on the errors in PLS calibration models. The reduction of sampling errors facilitates the study of the effect of: 1. Scattering and depth of penetration, 2. the selection of spectral regions and 3. the effect of preprocessing on the errors observed in PLS calibration models.

2.1.1. Scientific literature and contribution

This dissertation is based on the experimental setup of the representative layer theory (RLT) for diffuse reflectance (D. Dahm et al., 2000). In the theory, the theoretical description of the spectroscopic absorption, remission, and transmission fractions of the samples with different thickness using plane parallel mathematics are examined and tested. The RLT assumes that samples are composed of plane parallel layers, each individual layer is representative of the entire sample. The application of discontinuous mathematics (D. Dahm et al., 2000) was used to determine the absorption and remission coefficients of the samples. The authors tested the theory using two polymer films composed of polyethylene (plastic sheets) with uniform thickness and different surface roughness. The authors described efficiently the absorption and remission behavior of the samples by the mathematics of plane parallel layers. They found a substantial experimental error attributed to the remitted radiation primarily surface reflection that did not reach the detector. This left an open door to investigate the impact of the error due to light scattering in NIR diffuse reflection models.

Representative layer theory has been studied using polymer films with uniform thickness and also have been applied to real systems such as powdered samples (Cairós, Coello, & Maspoch, 2008), milk (D. J. Dahm, 2013), and it has been used in combination with linear polarization spectroscopy to powder and milk samples (Gobrecht, Bendoula, Roger, & Bellon-Maurel, 2015). However, the experimental setup mentioned in the test of the RLT does not consider the optical sampling of the NIR radiation and its effect on the errors in the model. Therefore, this chapter was undertaken to determine the impact of depth of penetration into low heterogeneous materials such a polymer films with uniform thickness on the statistical errors observed in NIR calibration models. The scientific contribution of this work is to develop an experiment that can be helpful to understand the complex of absorption and scattering of NIR radiation into solids materials using low heterogeneous polymers. This is the first study reported to estimate by multivariate data analysis the maximum depth of penetration of NIR radiation into polymer film materials and to calculate the minimum statistical error in the NIR calibration method avoiding the undesired effect of the heterogeneity of particulate systems. This work presents an extension of a previous article to train students in NIR spectroscopy, which has been used in a number of trainings of new students and industrial scientists (Romañach, Hernández-Torres, Roman-Ospino, Pastrana-Otero, & Semidei-Ortiz, 2014) based on the study of Dahm et al (D. Dahm et al., 2000).

2.2. **MATERIALS AND METHODS**

2.2.1. Polypropylene polymers

Samsill® No. S43496 non-glare sheet protectors composed of heavy weight polypropylene top load were used in this study (**Figure 11**). Films of 21 cm length and 7 cm width were cut

from these sheet protectors into smaller pieces sufficiently large to cover the integrating sphere window of the NIR system.

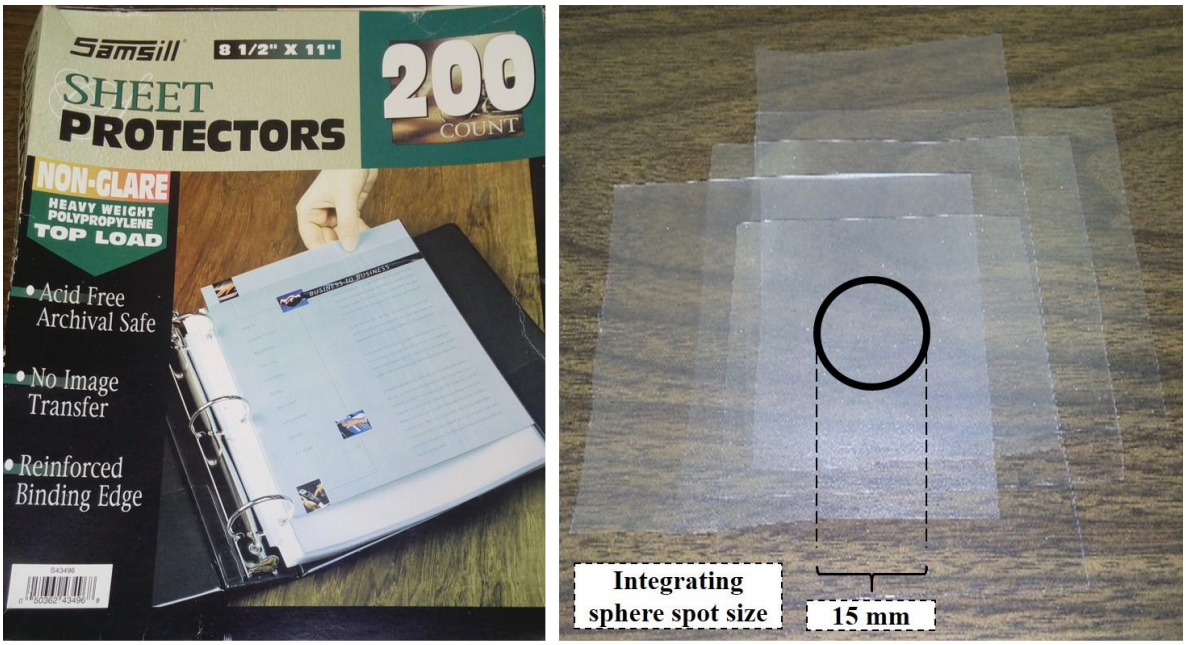

Figure 11. Samsill® No. S43496 non-glare sheet protectors composed of heavy weight polypropylene top load were used in this study.

2.2.2. Layer thickness measurements of individual films

Fifty polypropylene films were numbered on the bottom corner and the thickness of the polymer films was measured using a digital micrometer (Marathon, 0-25mm, resolution: 0.001mm, accuracy: 0.002 mm). The left, center, and right sides of the films were measured with the digital micrometer as shown in **Figure 12** to determine whether significant variations existed from film to film. The thickness of each individual film used in this study was obtained, and the thickness values of different combinations of film layers was determined. The thickness of the polymer films stacked together was also determined taking into consideration the variation of combination with different film layers. The purpose of this

combination of film layer is to obtain the variation of different layers, because in practice is not possible to use exactly the same film layers and the same position of the film polymer.

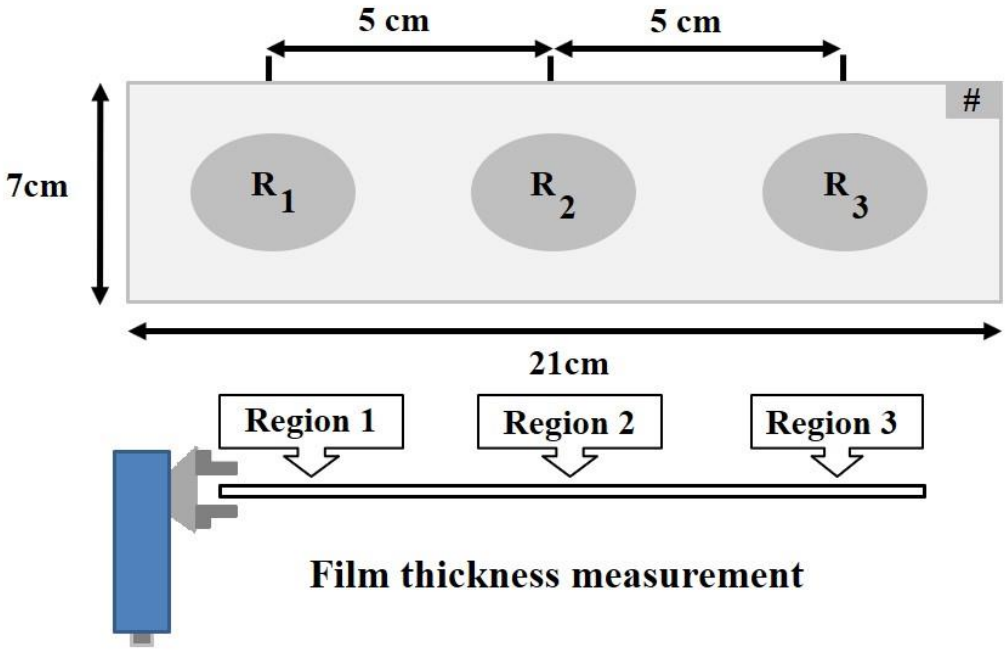

Figure 12. Thickness measurements in three different regions of the layer.

2.2.3. Acquisition of NIR spectra

NIR spectra were acquired using the integrating sphere module in a Bruker MPA (Multi-Purpose) FT-NIR Analyzer (Massachusetts, USA) equipped with a semiconductor room temperature sulphide lead (RT-PbS) external detector that works from 12800 to 3600 cm^{-1} (780 to 2780 nm). The integrating sphere is fixed within the spectrometer; unlike the fiber optic probe which can be moved. Single and stacked polymer films were placed over the integrating sphere of the MPA. The macrosample set up was used providing a NIR beam diameter of 15 mm. All NIR spectra were acquired over 12500 to 3500 cm^{-1} (800 to 2857 nm) spectral range at a resolution of 8 cm^{-1}, with 64 scans for background and 64 scans for the sample.

The remitted radiation was acquired in reflection mode in the first experimental setup (**Figure 13a**). The term remitted radiation refers to light that has been absorbed and then sends back by the summation of external reflection (specular and diffuse), internal reflection, and backward scattering (radiation that leaves the sample in opposite direction as the incident beam) (D. Dahm et al., 2000; D. J. Dahm, 2013). The second experimental setup (**Figure 13b**) was used to collect spectra in transflection mode. This second setup included a metallic plate on top of the film layers. The plate provides a reflective surface to force the radiation back through the films. The transflection spectra were the result of the radiation passing at least twice through the films.(D. Dahm & Dahm, 2014),(D. Dahm et al., 2000) The metallic plate and a metallic cylinder were also helpful in pressing the polymer film layers to minimize the effect of trapped air between the layers.

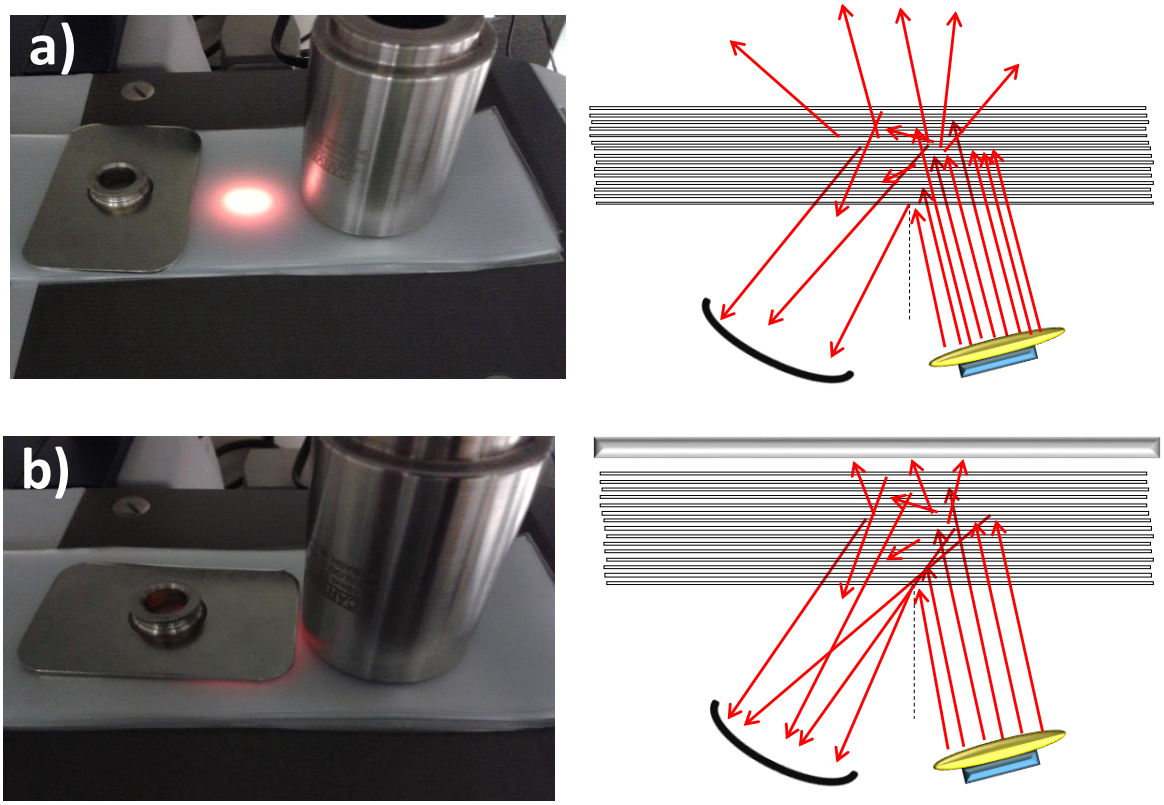

Figure 13. Experimental setup for the acquisition of films spectra. a) NIR acquisition film spectra using the integrating sphere macrosample setup. b) NIR acquisition film spectra using the integrating sphere macrosample setup with the metallic plate on top of the films working as a reflective surface. In the instrumental setup the metallic plate and the metallic cylinder were used to minimize the air between the films.

2.2.4. NIR sampling depth into polymer layers

Powder talc obtained by commercial talc product was used to estimate the optical sampling depth of the NIR radiation into the polymers. The effective sampling depth into polymer film layers was estimated by placing powder talc (hydrated magnesium silicate, $Mg_3Si_4O_{10}(OH)_2$) (Ferrage et al., 2003) on top of films. The amount of powder talc was enough to cover the emerging light of the integrating sphere module. NIR spectra were then obtained with the integrating sphere as described above.

2.2.5. Development of Multivariate Calibration Models

Principal component analysis (PCA) and partial least squares (PLS) regression calibration models were obtained using the SIMCA software, version 14 (MKS Umetrics AB, Umeå, Sweden).

The quality of the models was determined in terms of the bias, equation (2-1), the standard deviation, the root mean square error of prediction (RMSEP), equation (2-2), and the relative standard errors of prediction RSEP (%), equation (2-3), defined as:

$$Bias = \sum_{i=1}^{n} \frac{\left(Y_i^{pred} - Y_i^{ref}\right)}{n} \quad (2\text{-}1)$$

$$RMSEP = \sqrt{\frac{\sum_{i=1}^{n} (Y_i^{pred} - Y_i^{ref})^2}{n}} \quad (2\text{-}2)$$

$$RSEP\ (\%) = 100 \times \sqrt{\frac{\sum_{i=1}^{n} (Y_i^{pred} - Y_i^{ref})^2}{\sum_{i=1}^{n} (Y_i^{ref})^2}} \quad (2\text{-}3)$$

where n is the number of samples used in the test set, Y^{pred} and Y^{ref} the predicted and measured reference values. The number of PLS factors was chosen by the minimum error (RMSEP or RSEP (%)) and bias calculated.

2.3. **RESULTS AND DISCUSSION**

2.3.1. NIR spectra of film layers with and without metal plate

Figure 14 shows the NIR spectra of the films in the first experimental setup. The boxed area shows the vibrational combination bands of the stretching and deformation modes of methyl and methylene groups of polypropylene in the 7350-7070 cm^{-1} spectral region and the second overtones of the asymmetric stretching mode of methyl and methylene groups in the 8400-8200cm^{-1} region (Furukawa et al., 2003; Watari & Ozaki, 2004; Workman Jr., 2001). In **Figure 14**, the spectrum of one film shows a high baseline and weak absorption bands. This high baseline is observed because most of the radiation is transmitted through the film away from the detector. Only a minor portion of the radiation is remitted (back-scattered to the detector). As the number of films increases, the baseline decreases, and the intensity values of absorption bands increase. Despite these spectral differences due the number of films, the chemical heterogeneity remains equivalent from film layer to film layer. The correlation coefficient of the NIR spectra of the film layers has values that range from 0.954 to 0.999, that all films are very similar. This experiment was first performed in the description of the representative layer theory (D. Dahm et al., 2000),(D. Dahm et al., 2002). The present work presents an extension of a previous article to train students in NIR spectroscopy (Romañach et al., 2014) based on the study of Dahm et al (D. Dahm et al., 2000). The baseline changes and depth of penetration observed in NIR spectra which are extremely important to understand NIR applications (Berntsson et al., 1999; Berntsson, Danielsson, & Folestad, 1998; Clarke, Hammond, Jee, & Moffat, 2002; Iyer, Morris, & Drennen III, 2002; Johansson, Sparén, Svensson, Folestad, & Claybourn, 2007; Mauritz, Morrisby, Hutton, Legge, & Kaminski, 2010; Oelkrug, Brun, Rebner, Boldrini, & Kessler, 2012; Romañach et al., 2014;

A Sánchez-Paternina et al., 2015; Shi & Anderson, 2010). The experiment is now used to study the effect of scattering on the errors observed in PLS regression predictions.

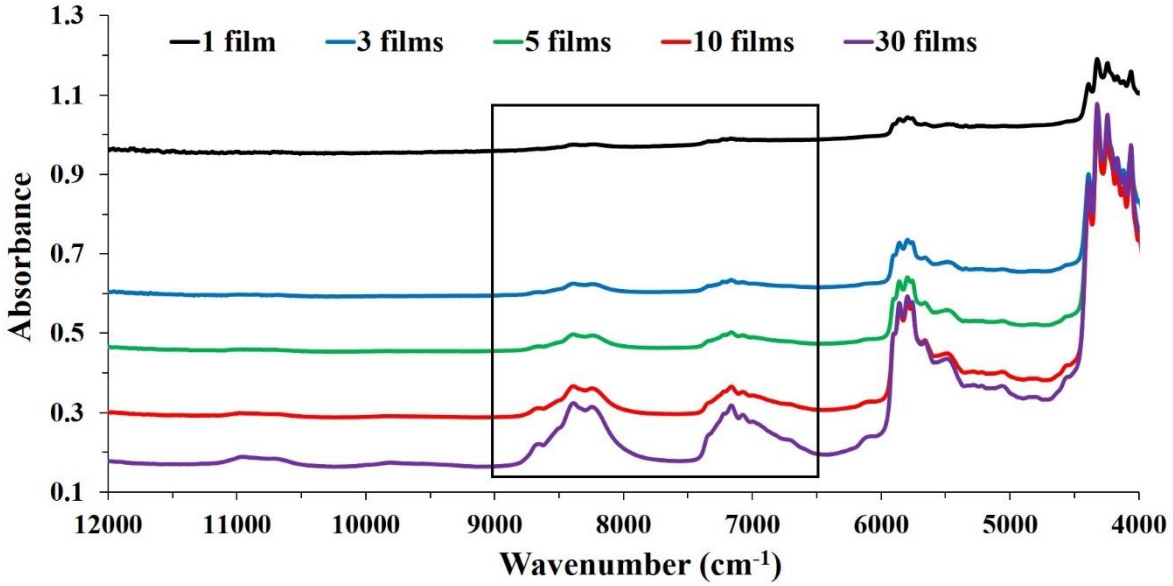

Figure 14. Spectral region for acquisition without metal plate and spectral region used in chemometric models.

Figure 15 shows the spectra of the films for the second experimental setup (transflection mode). In this case, the metallic plate was placed at the top of the film layers. The baseline is lower than in the previous spectra because the metallic plate reflects the radiation through the polymer films. The radiation passed at least twice through the films, and there are three important properties of the interaction of light with the films: the absorption of the molecular vibration modes of the molecules, the transmission through the thickness of the film layers, and the remission or radiation that reached the detector. In this experimental setup the radiation passed at least twice through the films, increasing the pathlength and therefore

transmission and absorption by the material. The metallic plate worked as a reflective surface that increased the remission of the radiation.(Koçak, Lucania, & Berets, 2009)

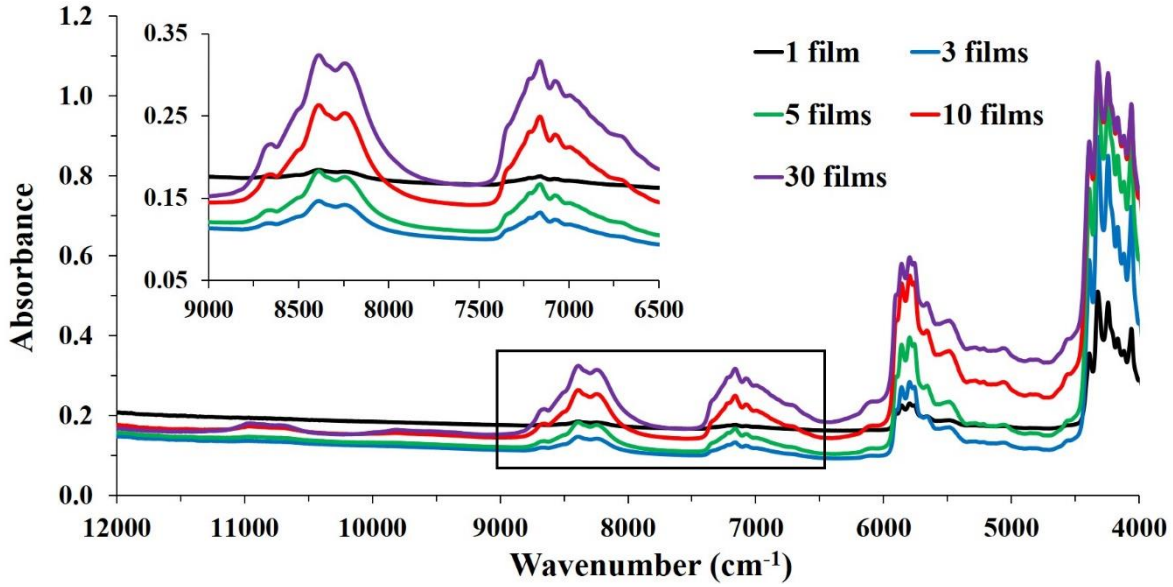

Figure 15. Spectral region for acquisition with metal plate and spectral region used in chemometrics models.

2.3.2. NIR spectra of individual film with metal plate and PCA evaluation

Figure 16 (up) shows the NIR spectra of 30 individual films with the metallic plate. As shown the figure, the spectra have minor differences of baseline, and this is due to physical effects when the polymer film is placed over the window of the integrating sphere in the FT-MPA. As shown by **Figure 16** (bottom), a spectral pretreatment such as standard normal variate (SNV), reduces the differences in baseline in the spectra. As shown by **Figure 16** (up), a PCA evaluation of the NIR spectra without spectral pretreatment does not have a distribution of the scores (**Figure 17**, up), but the PCA of the SNV spectra (**Figure 17**, bottom) shows a distribution around the center of the PC1 and PC2. This indicates that SNV

spectra have similar pattern that makes the scores to be equivalent. Equation (2-4) shows the SNV preprocessing given by:

$$SNV = \frac{(x - \bar{x})}{\sqrt{\frac{(x - \bar{x})^2}{n-1}}} \tag{2-4}$$

where x represents the absorbance of the sample at the specific wavenumber, and $\bar{x}$ represents the average of all absorbances of the sample.

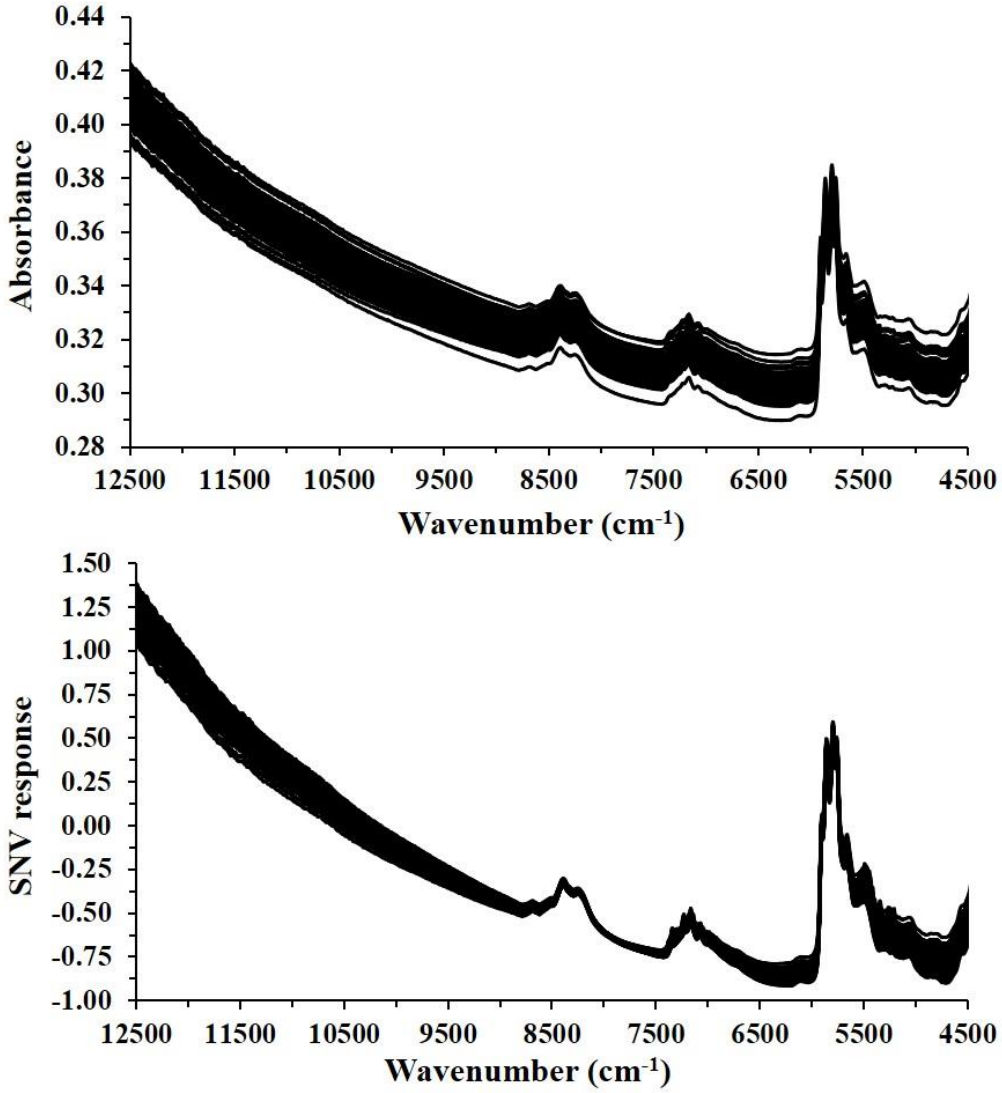

Figure 16. NIR spectra of individual polypropylene films (up). Normalized spectra (SNV) of individual films (bottom).

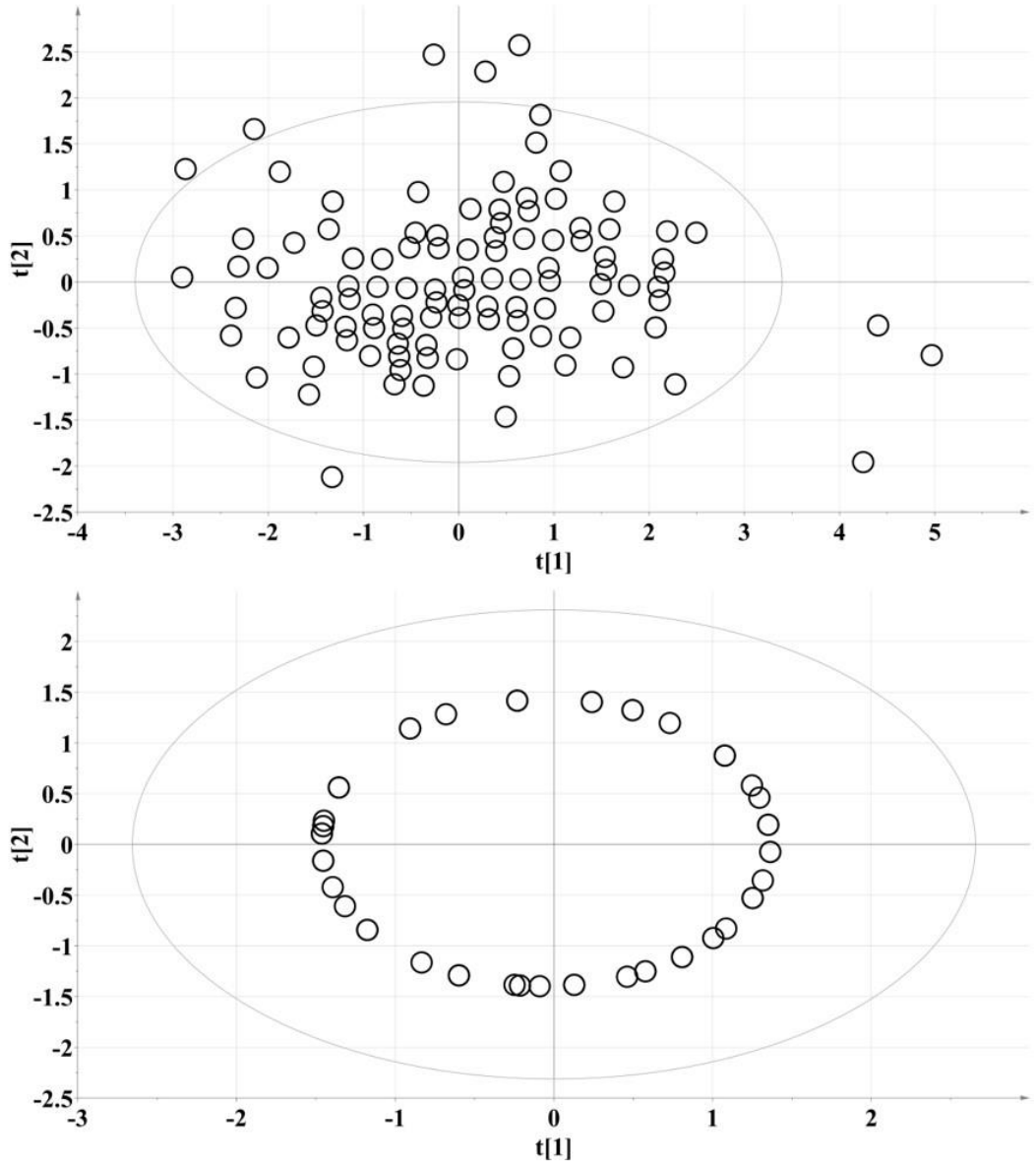

Figure 17. Top – PCA scores plot obtained with NIR spectra of individual polypropylene films (). Bottom-PCA scores plot after normalized spectra (SNV) of individual films (bottom).

2.3.3. Thickness of polypropylene film layers

The thickness of the polymer films was measured in the left, center, and right sides of the individual films to evaluate if there was heterogeneity in film thickness which could affect the results. **Table 3** shows that film thickness was very uniform from side to side, and from film to film. This low heterogeneity is an advantage for this study, since heterogeneity is

recognized as the major source of sampling errors (Kim H. Esbensen & Geladi, 2010; Kim H. Esbensen & Paasch-Mortensen, 2010; Petersen et al., 2005).

Table 3. Average and standard deviation for the thickness measurements on the different of fifty films. Values are in mm.

n = 50	**Region 1**	**Region 2**	**Region 3**	**Average 3 Regions**
Average (mm)	0.08563	0.08558	0.08563	0.08561
Std dev (mm)	0.00220	0.00198	0.00167	0.00196

The thickness from one to thirty stacked polymer films in three different combinations of layers was measured. These measurements were performed to evaluate whether air trapped between the layers were affecting the measured film thickness. The average thickness of one film was 0.086 mm and the average for thirty films was 2.520 mm. A linear regression between the number of film layers and the thickness shows that R^2 is 0.9998 the slope is 0.084 and the intercept is -0.002 (**Figure 18**). The average film thickness (0.086 mm), this value is similar to the slope (0.084) obtained in the measurement from one to thirty film layers. These results show that the differences in film thickness between individual and stacked films are very low, and the possible effect of air trapped between the layers has been minimized.

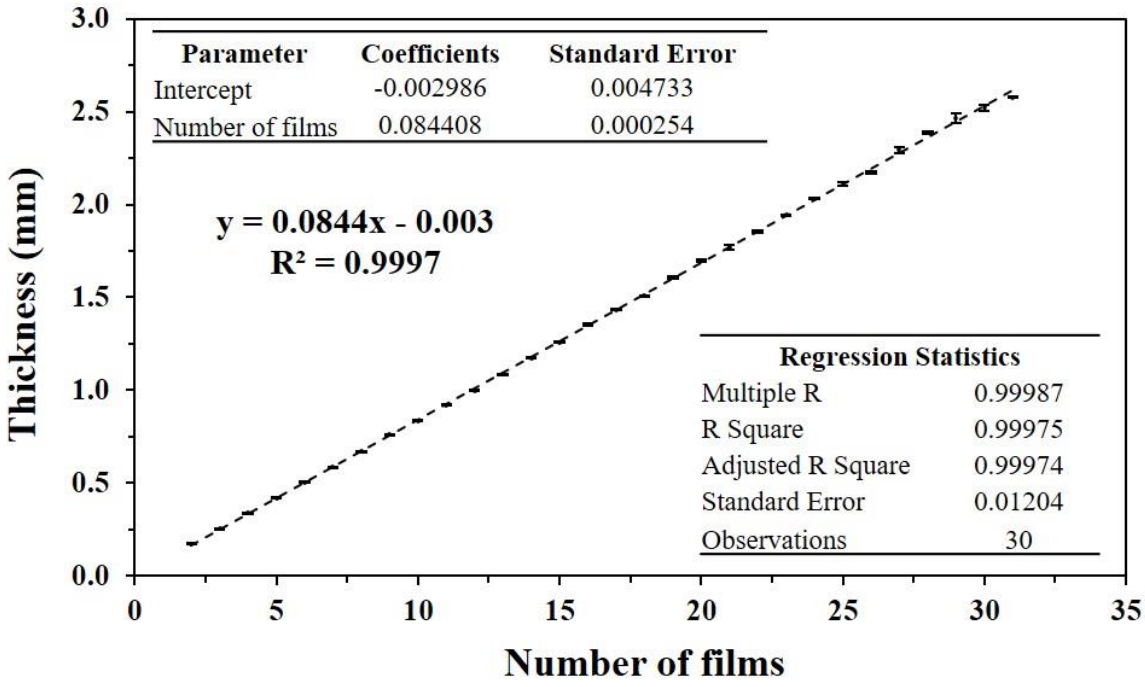

Figure 18. Thickness measurement vs number of films.

2.3.4. Depth of penetration of NIR radiation into polymer layers

The depth of penetration of NIR radiation in polymer film layers was determined first to learn how it affects PLS regression models. The effective sampling depth of penetration was estimated by placing talc (hydrated magnesium silicate, $Mg_3Si_4O_{10}(OH)_2$) on top of the films. The amount of powder talc was enough to cover the emerging light of the integrating sphere module. The film layers were increased up to 50 films with a thickness of 4.25 mm. **Figure 19a** shows that the second overtone of O-H stretching of talc is observed at 10534 cm^{-1}, while **Figure 19b** shows the first overtone overtones at 7186 and 7154 cm^{-1}.(Zhang et al., 2006) When more than thirty-six film layers were used (3.04 mm), the absorption band of the second overtones of O-H stretching in talc (hydrated magnesium silicate, $Mg_3Si_4O_{10}(OH)_2$) were not observed and the spectra did not vary significantly. Thus, the depth of penetration

of NIR radiation was estimated as 3.04 mm (thickness of 36 film layers) through visual inspection of the spectra.

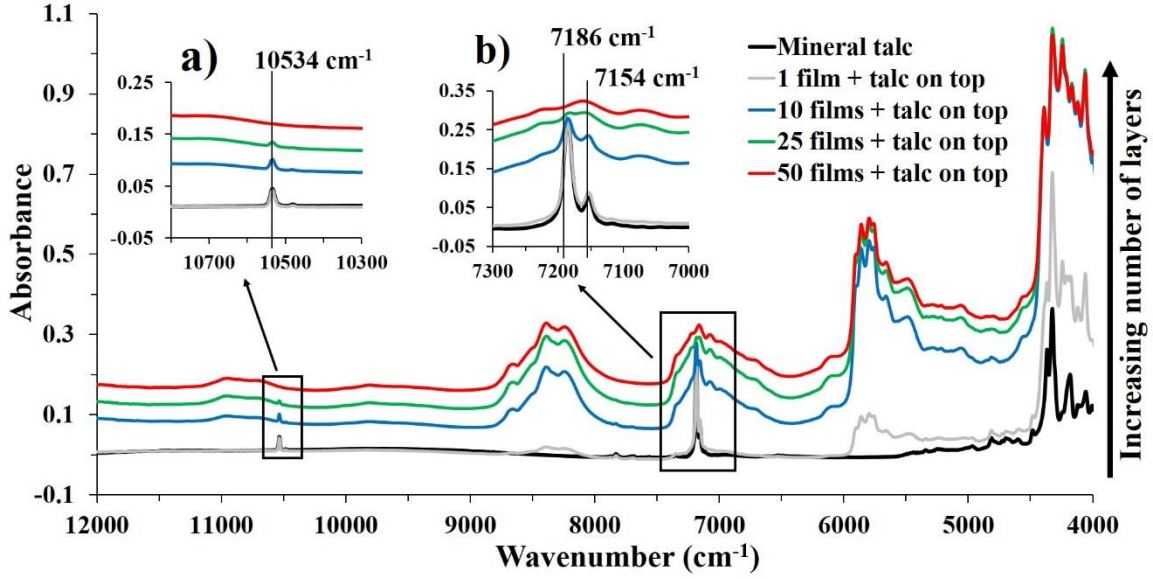

Figure 19. Film spectra with talc powder on top side. a) Second overtone of O-H stretching of talc (hydrated magnesium silicate, $Mg_3Si_4O_{10}(OH)_2$), and b) first overtones of OH stretching of talc.

A second assessment of the depth of penetration of the NIR radiation was performed in the second overtone region (10560 – 10510 cm^{-1}) using SNV spectral preprocessing and PCA in this region. **Figure 20** shows the NIR spectra of the second overtone region of O-H stretching band of talc on top of 28 to 50 layers (2.36 to 4.22 mm), and **Figure 20** shows an expanded view. **Figure 21** and **Figure 22** shows the PCA on the second overtone region of O-H stretching of talc using SNV as spectral preprocessing in the region of 10560 – 10510 cm^{-1}. **Figure 21** shows the PCA score plot for spectra of one to 36 film layers (0.08 to 3.04 mm). The score plot is enlarged in **Figure 22** shows the distribution from twenty-four to thirty-six film layers (2.02 to 3.04 mm). In **Figure 22**, the scores vary linearly along the first principal

component from 24 to 35 films. When more than thirty-five film layers (2.95 mm) are used, this linear trend is no longer observed as shown in **Figure 22**. In summary, the depth of penetration of NIR radiation in the second overtone region of talc (10534 cm^{-1}) was estimated through PCA as 2.95 mm into polymer film layers which is similar to the result by visual inspection (3.04 mm) described in the previous paragraph.

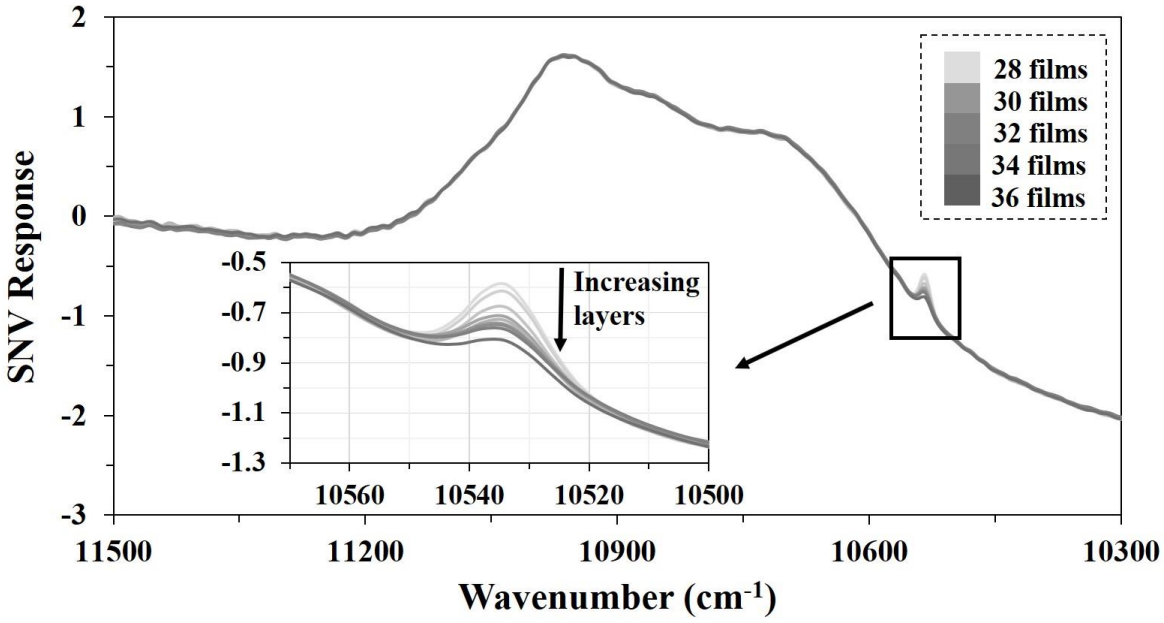

Figure 20. Evaluation of the depth of penetration of radiation based on the intensity of the second overtone of O-H stretching of talc (hydrated magnesium silicate, $Mg_3Si_4O_{10}(OH)_2$). Film spectra with talc powder on the top side on the spectral region of 11500 – 10300 cm^{-1}. Box zone is the zoom in the second overtone of O-H stretching of talc.

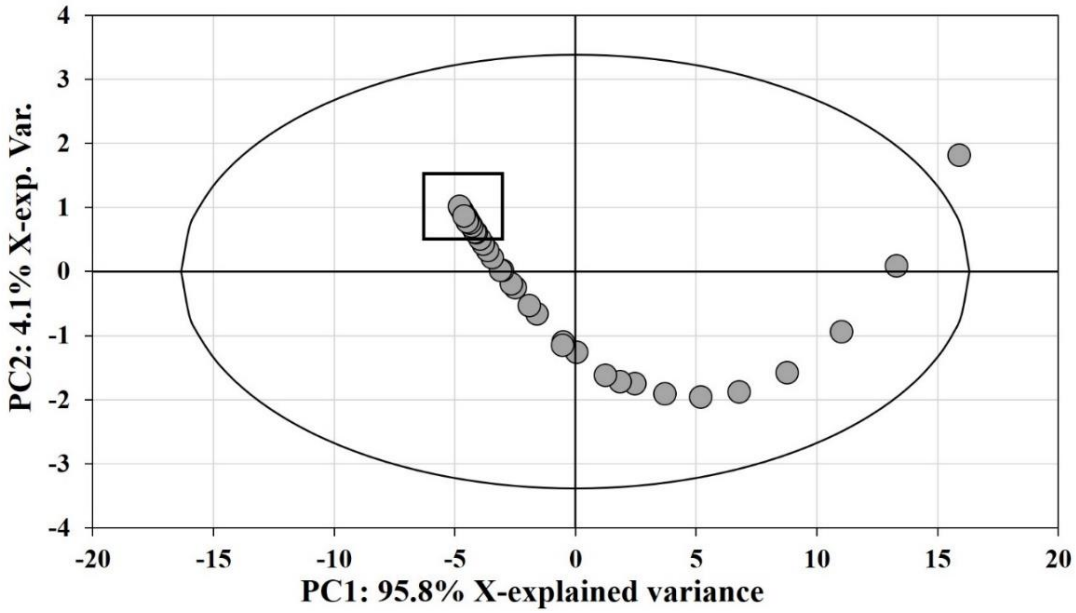

Figure 21. PCA performed using SNV on the spectral region 10560-10510 cm-1. Box zone is the zoom of PCA from twenty-four to fifty film layers.

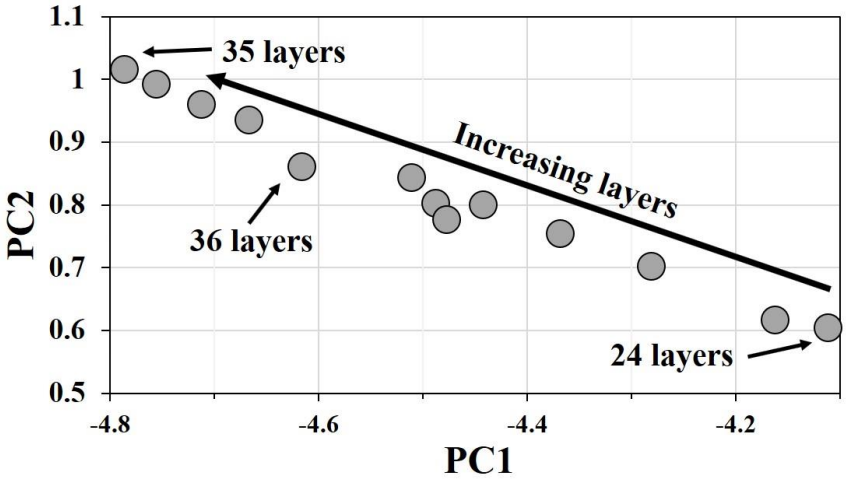

Figure 22. Zoom of the PCA from twenty-four to fifty film layers performed using SNV on the spectral region 10560-10510 cm^{-1}.

The first overtones of O-H stretching of talc (hydrated magnesium silicate, $Mg_3Si_4O_{10}(OH)_2$) are shown in **Figure 19b** at 7186 and 7154 cm^{-1}.(S. Petit, Decarreau, Martin, & Buchet, 2004; Sabine Petit, Martin, Wiewiora, De Parseval, & Decarreau, 2004; Zhang et al., 2006) This

region contains bands with moderate intensity (significantly stronger than bands located in the second overtone region), which facilitated this study in a spectral region widely used in NIR calibration models.(Norris, 1989) PCA was performed to estimate the depth of penetration of NIR radiation in the polypropylene films in this region. **Figure 23** shows the NIR spectra of talc placed on top of 16 to 50 film layers (1.35 to 4.22 mm) in the region of 9000 to 6500 cm^{-1} using SNV as preprocessing. **Figure 24** shows the first overtone of the O-H stretching bands of talc from 7270 to 7110 cm^{-1}. **Figure 25** and **Figure 26** show the evaluation of the PCA on the first overtone region of O-H stretching of talc using SNV as spectral preprocessing on the region of 7270 to 7100 cm^{-1}. **Figure 25** shows the distribution of the score plots from one to thirty-seven film layers (0.085 to 3.12 mm). The box contains the score plot distribution from twenty-five to thirty-seven film layers (2.11 to 3.12 mm) at **Figure 26**. In summary, the depth of penetration of NIR radiation in the first overtones region of talc (7186 and 7154 cm^{-1}) was estimated as 3.12 mm into polymer film layers.

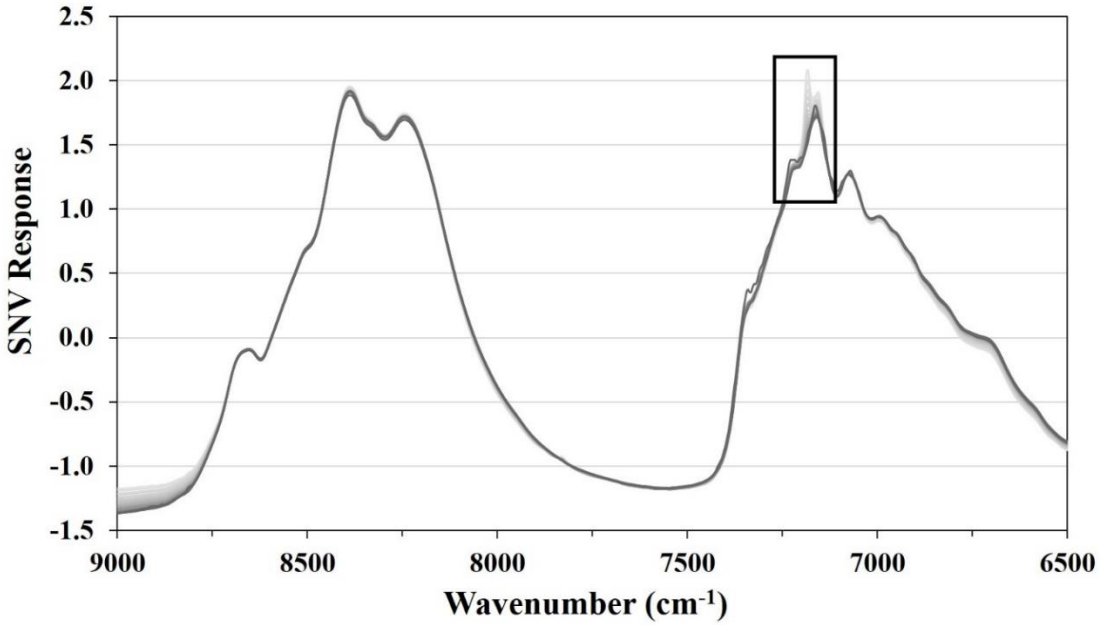

Figure 23. Evaluation of the depth of penetration of radiation on the first overtone of O-H stretching of talc (hydrated magnesium silicate, $Mg_3Si_4O_{10}(OH)_2$). Film spectra with talc powder on the top side on the spectral region 9000 – 6500 cm^{-1}. Zoom in the first overtones of O-H stretching of talc powder.

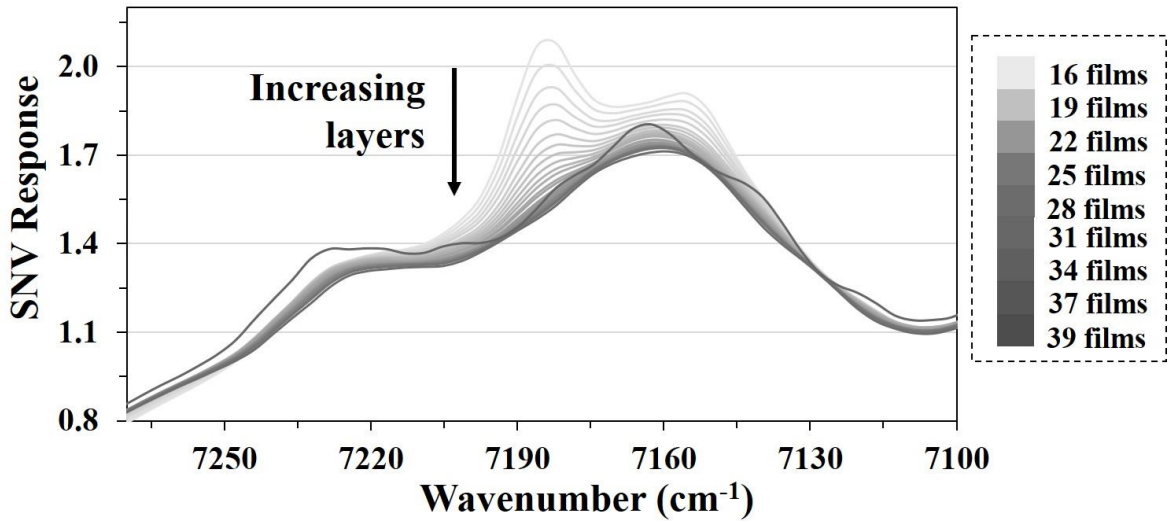

Figure 24. Evaluation of the depth of penetration of radiation on the first overtones of O-H stretching of talc (hydrated magnesium silicate, $Mg_3Si_4O_{10}(OH)_2$). Zoom in the first overtone of O-H stretching of talc.

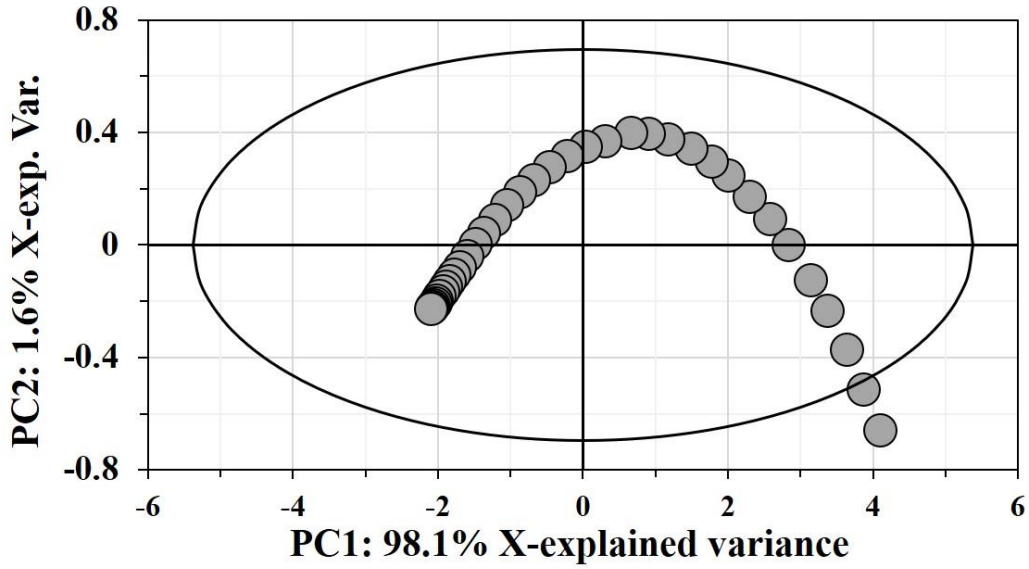

Figure 25. PCA performed using SNV on the spectral region 7270 – 7100 cm^{-1}.

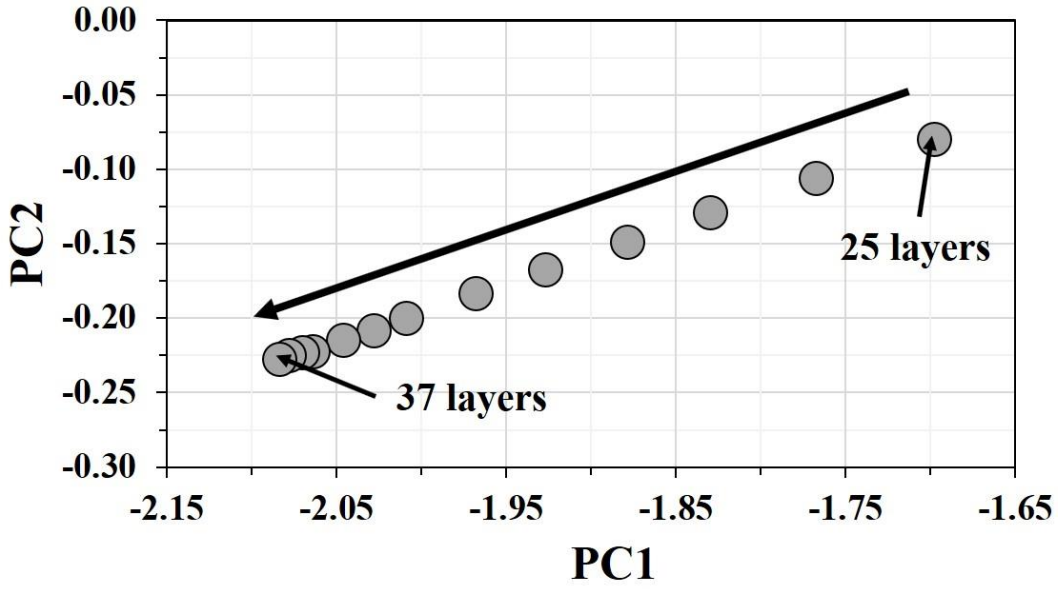

Figure 26. Zoom of the PCA from twenty-four to fifty film layers on the spectral region 7270 – 7100 cm^{-1}.

The analysis performed shows an estimate of sampling depth of 2.95 mm for polypropylene films near 10534 cm^{-1}, and 3.12 mm around 7186 and 7154 cm^{-1}. This result is in agreement with previous studies that show a depth of penetration from 1.9 and 2.7 mm at 1210 nm (8264 cm^{-1}) and 1186 nm (8432 cm^{-1}) respectively in diffuse reflectance measurements of tablets.(Iyer et al., 2002) In transmission measurements the depth of penetration reported is from 3.4 to 4.9 mm at 1210 nm (8264 cm^{-1}) and 1186 nm (8432 cm^{-1}) respectively.(Iyer et al., 2002) In pharmaceutical powders samples the depth of penetration of NIR radiation at 1123 nm (8907 cm^{-1}) is 2.4 mm in samples with 10% of active pharmaceutical ingredient in diffuse reflection mode.(Bellamy, Nordon, & Littlejohn, 2008)

2.3.5. Prediction of number of films

The development of the NIR calibration model for the prediction of number of film layers was based on the results of the penetration of radiation in the polymer films. **Figure 27** shows the calibration design (C.D.) used in this study. The first set of PLS models were based on the sampling depth of penetration below the infinite depth. Thirty film layers were used to develop these models, with the exclusion of every fifth film as shown in **Figure 27a**. In this case the radiation does not reach infinite depth, and this guarantees that all the samples are analysed by NIR radiation. Even though there are 30 films (below infinite depth) – this represents a case with multiple pathlengths.(Oelkrug et al., 2012) Some of the radiation is being scattered through 15 films, other by 22 films, etc. A second calibration model was developed with 50 film layers as shown in **Figure 27b**. **Table 4** shows the results of PLS models with and without the metallic plate in the 9000 – 6500 cm^{-1} region. The results show the lowest error values using first derivative with 25 points as spectral preprocessing. The bias for all calibration models is low,(Bondi, Igne, Drennen, & Anderson, 2012) and the confidence intervals of the bias includes zero in all the calibration models developed regardless of the spectral preprocessing used. This result highlights that sampling is unbiased,(Kim H. Esbensen, Paoletti, & Minkkinen, 2012) and there is an absence of systematic error by the NIR method. Thus, the RMSEP and RSEP (%) summarize the random error in the measurements, and values are low after all spectral preprocessing, even though SNV models have higher error values. In this experiment, the first derivative calibration model shows lower RMSEP and RSEP (%) values. The accuracy of the results is somewhat lower using the metallic plate than models without the metallic plate, however, all calibration

models developed with the metallic plate include zero within the 95% confidence interval of the bias. These results are obtained in two optical designs both with multiple pathlengths.

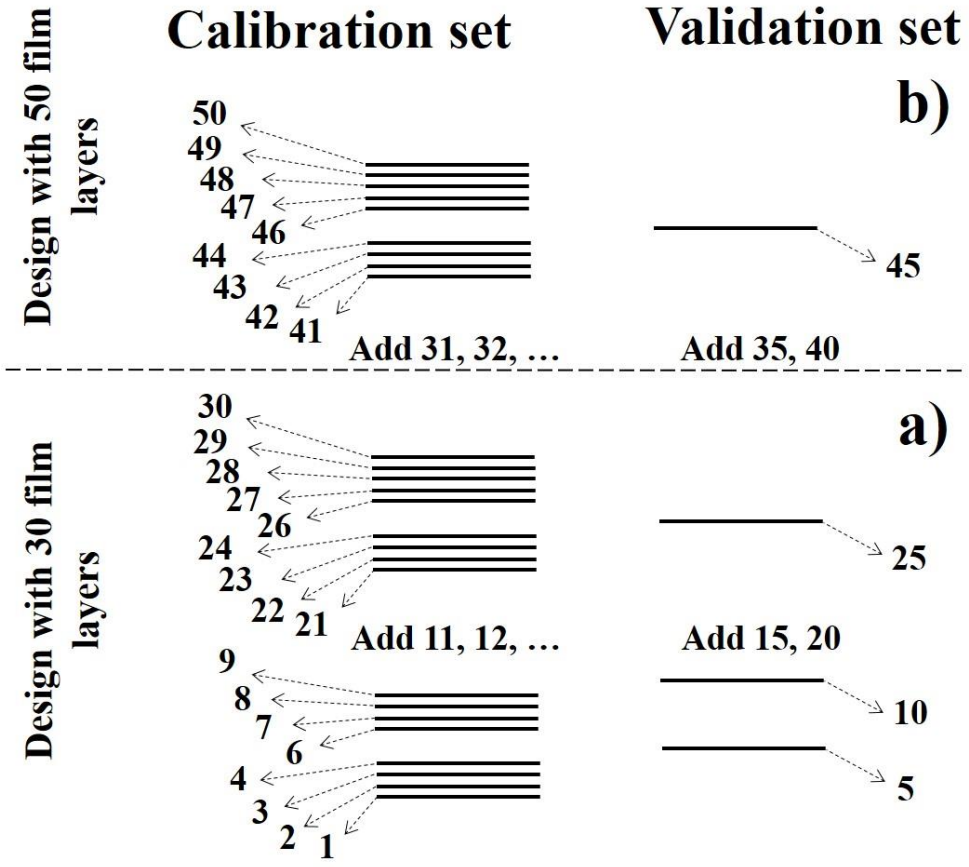

Figure 27. Calibration designs used in the study. a) Design using a total number of thirty film layers, excluding each fifth layers up until twenty-five film layers, and b) design using a total number of fifty film layers, excluding each fifth layers up until forty-five film layers. Number of films used for calibration set (left) and validation set (right).

Table 4. RMSEP, RSEP (%), bias for the PLS models performed with and without metallic plate on top for models using thirty film layers on the spectral region 9000 – 6500 cm^{-1}. * units: number of films layers.

SPECTRAL PREPROCESSING	POINTS	WITHOUT METAL PLATE (n=30)			WITH METAL PLATE (n=30)		
		RMSEP*	RSEP (%)	Bias	RMSEP*	RSEP (%)	Bias
No pretreatment	-	0.40	2.42	-0.03	1.00	6.01	0.37
SNV	-	1.02	6.15	-0.05	0.68	4.11	0.14
Savitzky-Golay	9	0.40	2.42	-0.03	0.99	5.99	0.37
Savitzky-Golay	15	0.40	2.41	-0.03	1.00	6.00	0.37
1st Derivative	15	0.30	1.79	0.04	0.27	1.60	0.11
1st Derivative	**25**	**0.29**	**1.77**	**0.03**	**0.27**	**1.65**	**0.10**
Savitzky-Golay + SNV + 1st Derivative	15	0.91	5.51	-0.03	0.44	2.64	0.14
SNV + 1st Derivative	15	0.93	3.49	-0.01	0.61	3.70	0.15
2nd Derivative	15	0.58	3.49	0.00	0.39	2.35	0.17
2nd Derivative	25	0.37	2.21	-0.01	0.32	1.90	0.14
SNV + 2nd Derivative	15	1.69	10.19	0.24	1.10	6.61	0.17
Row Center	-	0.32	1.92	0.00	0.55	3.34	0.07
MSC	-	0.55	3.30	-0.03	0.70	4.21	0.11
Row Center + 1st Derivative	15	0.30	1.79	0.04	0.27	1.60	0.11
MSC + 1st Derivative	15	1.08	6.54	0.14	1.08	6.52	0.38

Table 5 shows the predictions obtained in PLS models using 50 films in the spectral region of 9000 - 6500 cm^{-1} without the metallic plate removing every fifth film layer (as shown in Figure 13b). **Table 5** shows that the best prediction result was for the model without spectral preprocessing, RSEP (%) = 5.38 and bias = 0.21. This low result was surprising because most NIR calibration models include spectral preprocessing. In this experiment the changes observed in the baseline of the spectra are related to the number of films, thus making the prediction possible without preprocessing. The calibration models are being developed according to physical changes (varying the number of polymer film layers) and an increasing pathlength for the radiation in the layers. The results show that spectral preprocessing should

be performed based on an understanding of the physics and chemistry of the material.(Beebe et al., 1998; Pell, Seasholtz, Beebe, & Koch, 2014)

The right side of **Table 5** shows the results of models performed from one to thirty film layers as calibration set and with a prediction set that varied from thirty-one to fifty film layers. The authors recognize that the larger number of films in the validation set should increase the error. However, this is a simulation of a situation that frequently occurs in NIR spectroscopic calibration models due to sample heterogeneity. Calibration models are built obtaining spectra of the sample that is illuminated by the NIR radiation. However, a larger sample size could be analyzed with a reference method (e.g. HPLC) and the material outside of the area interrogated by the NIR radiation could be different. In this case the RMSEP and RSEP (%) values are higher and the bias has a confidence interval that does not include zero, indicating a systematic error that is also a sampling error. These comparison models show the importance of the depth of penetration of near infrared radiation. If the sample has a high heterogeneity, sampling errors will occur.(Kim H. Esbensen & Geladi, 2010; Kim H. Esbensen & Paasch-Mortensen, 2010; K. H. Esbensen et al., 2016; Petersen et al., 2005)

Table 5. RMSEP, RSEP (%), and bias for the PLS models performed without metallic plate for models using fifty film layers on the spectral region 9000 – 6500 cm^{-1}. * units: number of films layers.

SPECTRAL PREPROCESSING	POINTS	VALIDATION SET (5, 10, 15, …, 45 FILMS)			VALIDATION SET (31 – 50 FILMS)		
		RMSEP*	RSEP (%)	Bias*	RMSEP*	RSEP (%)	Bias*
No preprocessing	-	1.51	5.38	0.21	7.24	17.70	-6.21
SNV	-	3.03	10.77	0.15	9.09	22.21	-8.17
1st Derivative	15	2.27	8.07	0.43	8.66	21.17	-7.54
1st Derivative	25	2.18	7.73	0.10	8.52	20.82	-7.40
SNV + 1st Derivative	15	3.92	13.94	0.43	10.54	25.77	-9.59
2nd Derivative	15	2.42	8.59	0.13	8.97	21.94	-7.84
2nd Derivative	25	2.41	8.57	0.63	8.92	21.80	-7.77
SNV + 2nd Derivative	15	4.20	14.93	0.33	11.10	27.12	-10.10

The effect of selection of spectral region was also studied (**Table 6**). This evaluation was performed because the depth of penetration of NIR radiation depends on the wavelength of radiation and the heterogeneity of the material, therefore the statistical errors in NIR calibration models will also depend on depth of penetration.(Berntsson et al., 1998) **Table 6** shows the RSEP (%) values of PLS models performed in seven spectral regions with different spectral preprocessing without metallic plate using thirty film layers. The first region (9000-6500 cm^{-1}) comprises the combination bands and second overtones of the asymmetric stretching modes of methyl and methylene groups of polypropylene, where the spectral bands have moderate intensity. The second region (9000-4500 cm^{-1}) includes the first overtones of methyl and methylene groups of polypropylene, which have high absorbance. The third region (11500-4500 cm^{-1}) comprises almost the entire spectrum except for the strongest bands observed below 4500 cm^{-1} related to C-H combination bands, and above 11500 cm^{-1}. The fourth region (6500-4500 cm^{-1}) comprises the first overtones of the asymmetric and symmetric stretching modes of methyl and methylene groups of polypropylene. The fifth region (11500-6500 cm^{-1}) comprises the second overtones and combination bands, and it

includes the third overtone which has low intensity values. The sixth region (11500-10300 cm^{-1}) comprises the third overtone region, and the seventh region (12500-3500 cm^{-1}) comprises the entire spectral region acquired by the NIR method. The PLS models in the spectral regions evaluated in this study show that first derivative has the lower error values (in terms of RSEP (%)). The lower errors were observed in models that includes the first, second and combination bands of methyl and methylene groups of polypropylene and excludes the limits of the detector with high spectral noise (S.R.1: 9000-6500 cm^{-1}, S.R.2: 9000-4500 cm^{-1}, S.R.3: 11500-4500 cm^{-1}).

Table 6. RSEP(%)/bias values for the PLS models performed without metallic plate using thirty film layers on the spectral region (S.R.): S.R.1: 9000-6500 cm^{-1}, S.R.2: 9000-4500 cm^{-1}, S.R.3: 11500-4500 cm^{-1}, S.R.4: 6500-4500 cm^{-1}, S.R.5: 11500-6500 cm^{-1}, S.R.6: 11500-10300 cm^{-1}, and S.R.7: 12500-3600 cm^{-1}. NP: no spectral preprocessing, SNV: Standard Normal Variate, 1^{st}: first derivative (25 points), SNV-1^{st}: SNV + first derivative (25 points), 2^{nd}: second derivative (25 points), and SNV-2^{nd}: SNV + second derivative (25 points).

SPEC. PREP.	**S.R.1**	**S.R.2**	**S.R.3**	**S.R.4**	**S.R.5**	**S.R.6**	**S.R.7**
NP	2.42/-0.03	4.14/0.04	4.16/0.03	4.88/0.09	2.38/-0.02	2.82/0.00	5.79/0.18
SNV	6.15/-0.05	3.76/-0.08	5.42/0.04	3.23/0.08	10.73/0.20	4.67/0.12	4.10/0.01
1^{st}	**1.77/0.03**	**1.94/-0.07**	**2.01/-0.05**	2.20/-0.08	2.52/0.02	3.24/0.12	4.68/0.08
SNV-1^{st}	2.21/-0.01	2.49/-0.04	2.73/0.02	2.87/-0.03	3.17/0.01	5.27/0.17	5.86/0.17
2^{nd}	3.49/-0.01	3.61/-0.11	4.66/-0.06	3.83/-0.04	7.57/0.00	6.83/0.00	6.34/0.03
SNV-2^{nd}	10.19/0.24	4.92/-0.05	7.69/0.04	4.92/-0.07	9.72/-0.10	9.22/0.49	9.01/0.10

The lowest error value obtained in this study is for the model using first derivative with 25 points on the 9000 – 6500 cm^{-1} spectral region. **Figure 28** shows the loading line plot (up) and the spectra using first derivative (bottom). The model using the metallic plate has similar error values than model without the metallic plate, but bias is somewhat higher. An evaluation of loading weights in the model without the metallic plate shows the first loading w*c with R^2X=0.996 and a correlation with the first derivative spectra of 0.9993.

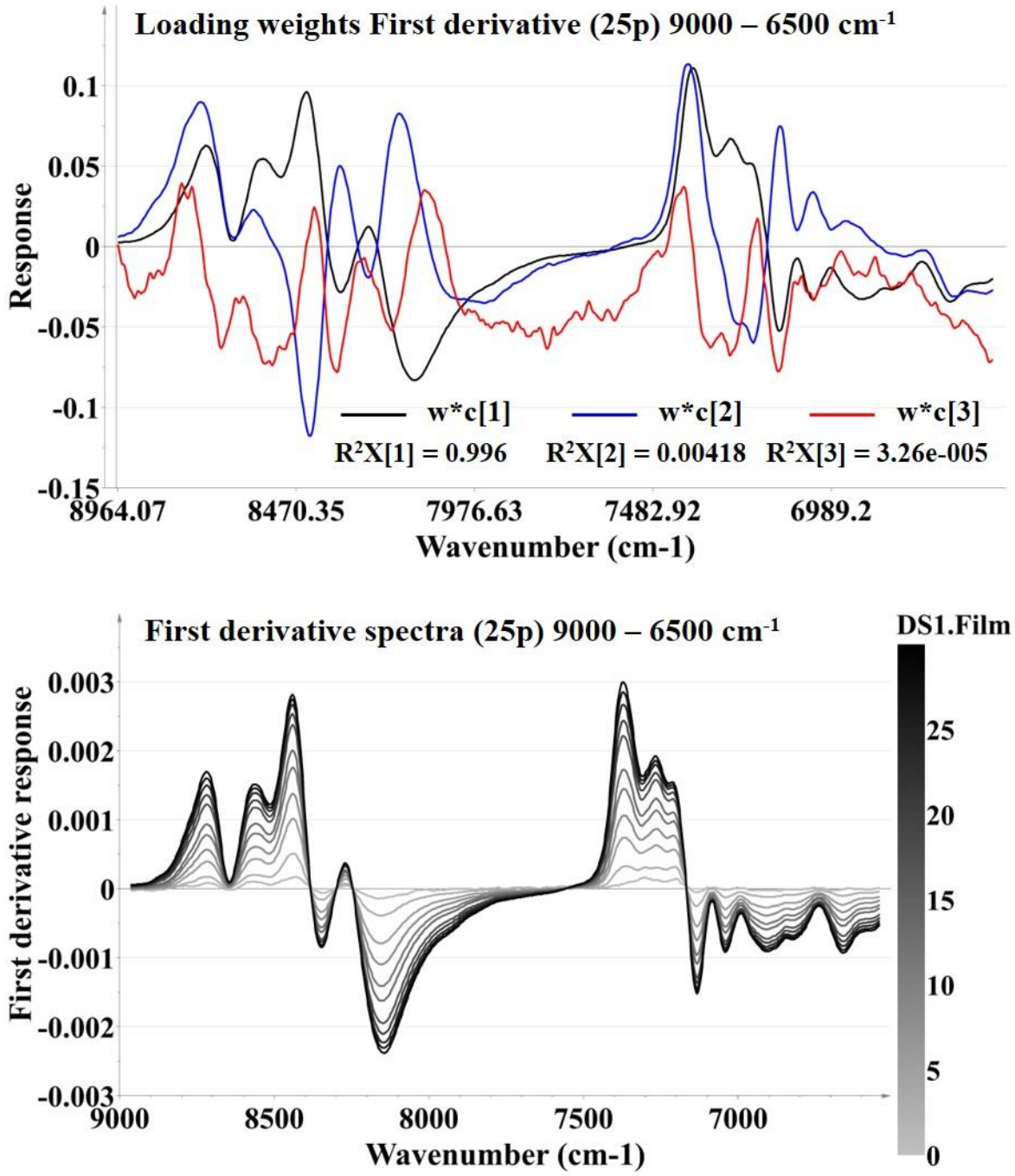

Figure 28. Loading weight lines and first derivative spectra. up) Loading line plot w*c performed on the spectral region 9000-6500 cm^{-1} using 1st derivative (25 points) as preprocessing, and bottom) film spectra on the spectral region 9000 - 6500 cm^{-1} using 1st derivative (25 points) as preprocessing.

2.3.6. Evaluation of models varying the number of samples in C.S.

Eight different calibration sets were evaluated varying the number of polymer film layers in the calibration and validation sets as shown in **Table 7**. The top part of **Table 7** provides a summary of the calibration models developed and the bottom part the details of the spectra used in the calibration model and the validation set. The first calibration set includes 26 calibration spectra and predicts every 6^{th} film layer (n =4) as outlined in Table 6. The second calibration set includes 25 calibration spectra and leaves out every fifth film for a total of 5 validation samples. The impact of a lower number of samples in the calibration set was evaluated in models that contains the samples separated each three (No. 6), four (No. 7), and five film layers (No. 8).

Table 7 (up) shows the results of the PLS models obtained by the different calibration sets with the 9000 – 6500 cm^{-1} using different spectral preprocessing. The table shows that the lower RSEP(%) values are obtained using first derivative with 25 points (preprocessing number 3) in all the calibration sets. The calibration performed using every fifth film layers as validation set (C.S. No. 2) presents the lowest RSEP(%) values. In almost all the models the bias is negligible, and the confidence interval of the bias includes zero, except in calibration set 6, 7 and 8, and which contain the lowest number of samples in the calibration set. The bias is significant when the number of calibration samples is less than elven. This result highlights the lack of systematic error by the NIR method, as long as the number of samples in the calibration set is representative of all the variation to be modelled by a PLS regression.

Table 7. RSEP(%) and bias values obtained by the different calibration set (C.S.) evaluated for the PLS models performed without metallic plate on top for models using a total of thirty film layers in the spectral region of 9000 – 6500 cm^{-1}. 1: no spectral preprocessing, 2: SNV, 3: first derivative (25 points), 4: SNV + first derivative (25 points), 5: second derivative (25 points), and 6: SNV + second derivative (25 points). n_{Cal}: number of samples for calibration set, n_{Val}: number of samples for validation set. *: the confidence interval does not include zero.

SPEC. PREP.	n_{Cal}=26 n_{Val}=4		**n_{Cal}=25 n_{Val}=5**		n_{Cal}=23 n_{Val}=7		n_{Cal}=21 n_{Val}=9		n_{Cal}=16 n_{Val}=14		n_{Cal}=11 n_{Val}=19		n_{Cal}=9 n_{Val}=21		n_{Cal}=7 n_{Val}=23	
	RSEP (%)	**Bias**	**RSEP (%)**	**Bias**	**RSEP (%)**	**Bias**	**RSEP (%)**	**Bias**	**RSEP (%)**	**Bias**	**RSEP (%)**	**Bias** *	**RSEP (%)**	**Bias** *	**RSEP (%)**	**Bias** *
NP	3.31	0.02	2.42	-0.03	2.54	0.03	3.13	0.05	2.77	-0.02	2.86	0.13	3.20	0.15	3.38	0.24
SNV	4.90	0.25	6.15	-0.05	5.62	-0.08	5.31	0.07	5.69	0.14	6.63	0.28	9.01	0.56	9.62	0.72
1st	2.75	0.08	**1.77**	**0.03**	1.96	0.02	2.41	0.10	2.12	0.00	2.27	0.07	2.48	0.15	2.83	0.19
SNV-1st	3.44	-0.08	2.21	-0.01	2.65	0.00	4.24	0.11	2.92	-0.08	3.67	0.12	4.01	0.17	4.60	0.32
2nd	4.41	0.19	3.49	-0.01	5.27	-0.15	4.64	0.14	5.30	0.05	5.76	0.12	7.22	0.36	8.73	0.24
SNV-2nd	6.63	0.77	10.19	0.24	8.87	-0.07	9.38	0.18	9.12	0.31	11.11	0.19	13.13	0.34	13.20	0.20
	C.S. No. 1		**C.S. No. 2**		**C.S. No. 3**		**C.S. No. 4**		**C.S. No. 5**		**C.S. No. 6**		**C.S. No. 7**		**C.S. No. 8**	
Calibration Number of layers	1, 2, 3, 4, 5, 7, 8, 9, 10, 11, 13, 14, 15, 16, 17, 19, 20, 21, 22, 23, 25, 26, 27, 28, 29, 30		**1, 2, 3, 4, 6, 7, 8, 9, 11, 12, 13, 14, 16, 17, 18, 19, 21, 22, 23, 24, 26, 27, 28, 29, 30**		1, 2, 3, 5, 6, 7, 9, 10, 11, 13, 14, 15, 17, 18, 19, 21, 22, 23, 25, 26, 27, 29, 30		1, 2, 4, 5, 7, 8, 10, 11, 13, 14, 16, 17, 19, 20, 22, 23, 25, 26, 28, 29, 30		1, 3, 5, 7, 9, 11, 13, 15, 17, 19, 21, 23, 25, 27, 29, 30		1, 3, 6, 9, 12, 15, 18, 21, 24, 27, 30		1, 4, 8, 12, 16, 20, 24, 28, 30		1, 5, 10, 15, 20, 25, 30	
Validation Number of layers	6, 12, 18, 24		**5, 10, 15, 20, 25**		4, 8, 12, 16, 20, 24, 28		3, 6, 9, 12, 15, 18, 21, 24, 28		2, 4, 6, 8, 10, 12, 14, 16, 18, 20, 22, 24, 26, 28		2, 4, 5, 7, 8, 10, 11, 13, 14, 16, 17, 19, 20, 22, 23, 25, 26, 28, 29		2, 3, 5, 6, 7, 9, 10, 11, 13, 14, 15, 17, 18, 19, 21, 22, 23, 25, 26, 27, 29		2, 3, 4, 6, 7, 8, 9, 11, 12, 13, 14, 16, 17, 18, 19, 21, 22, 23, 24, 26, 27, 28, 29	

2.3.7. Evaluation of models at the three different regions of the films

PLS calibration models were performed for the left, middle, and center regions of the films and compared to evaluate whether a significant difference exists between the three regions of the film layers. **Table 8** presents the RMSEP values for the models performed with and without metallic plate, the results shows a similar pattern using three PLS factors, at different spectral pretreatments in the 9000-6500 cm^{-1} spectral region. A correlation between the different PLS results from one to five PLS factors, show values above the 0.991, which demonstrate that the results in the three regions are similarly equivalent. An ANOVA single factor of these data (from one to five PLS factors) shows that F= 0.1541 with F_{crit}= 2.2939 (p-value= 0.9784), indicating that the results of pretreatments on the three regions of the film layers are statistically equivalent.

This evaluation demonstrate an uncomplicated method to analyze the results and it is suitable for low-heterogeneous materials, where differences due to sampling process have a low impact on the results, as long as instrumental setup allows a correct sampling procedure. If the polymer films presented non-uniformities in all the regions of the material, the results of ANOVA were statistically inequivalent.

Table 8. RMSEP values for the PLS models performed with and without metallic plate on top for models using thirty film layers at three different regions of the film layers.

SPECTRAL PREPROCESSING	PLS FACTORS	RMSEP WITH METAL PLATE			RMSEP WITHOUT METAL PLATE		
		Region 1	Region 2	Region 3	Region 1	Region 2	Region 3
No Pretreatment	1	3.88	3.83	4.04	5.85	5.84	5.81
	2	3.77	3.80	3.92	1.79	1.74	1.89
	3	1.84	1.76	1.80	1.05	0.81	0.93
	4	1.12	1.03	1.10	0.70	0.54	0.71
	5	0.60	0.78	1.21	0.80	0.55	0.65
SNV	1	5.48	5.51	5.57	7.88	7.52	7.64
	2	3.15	3.15	3.25	2.91	2.96	2.78
	3	2.09	1.94	1.99	1.81	1.27	1.48
	4	0.77	1.16	1.26	1.17	0.98	1.17
	5	0.36	0.77	0.66	1.08	0.95	1.11
1st derivative	1	4.25	4.27	4.35	2.25	2.27	2.37
	2	1.93	1.83	1.90	1.34	1.22	1.23
	3	1.32	1.20	0.91	0.95	0.79	0.96
	4	0.49	0.48	0.76	0.59	0.57	0.63
	5	0.40	0.37	0.57	0.60	0.50	0.52
2nd derivative	1	3.66	3.67	3.71	2.38	2.36	2.39
	2	2.27	2.21	2.24	2.07	2.02	2.05
	3	1.79	1.74	1.82	1.07	0.87	1.06
	4	0.89	0.73	0.95	0.86	0.74	0.82
	5	0.81	0.64	0.98	0.75	0.68	0.67

2.3.8. Comparing the number of film and thickness values as Y value

To evaluate the effect of using a parameter such as number of films layers or a physical parameter such as thickness on the PLS calibration, two sets of models were performed. The first set was done using the previous data of number of films and the second set was using the thickness values obtained before. **Table 9** shows the results of the comparison for the results of PLS calibration using the number of films and the thickness measurements. As shows the results, the models are quite similar between number of film and thickness measurements. An ANOVA single factor of these data (from one to five PLS factors) shows that F=0.2889 with F_{crit}= 2.725 (p-value= 0.8333),

indicating that the results of pretreatments using the thickness as Y value, that is a physical parameter, or using the number of film layers are statistically equivalent. This similarity can be confirmed with the results obtained between the relationship with thickness measurement average and the number of films (Table 2).

Table 9. RSEP (%) values for the PLS models performed with and without metallic plate on top for models using thirty film layers at three different regions of the film layers using Y-value the thickness and the number of film layers.

DATA PRETREATMENT	PLS FACTORS	RSEP (%) METAL		RSEP (%) NO METAL	
		THICKNESS	NUMBER OF FILM	THICKNESS	NUMBER OF FILM
No Pretreatment	3	9.82	9.44	5.59	5.24
SNV	3	10.75	10.70	10.75	10.70
1st derivative	3	7.22	6.95	5.00	4.67
2nd derivative	3	8.46	9.09	5.43	5.15

2.3.9. Evaluation of models on two different seasons of the year

The PLS calibration models were used for prediction at two different seasons of the year. The acquisition of the NIR spectra for the first models was in April 2015, and the second set of spectra was acquired on October 2015. The main difference between these seasons was the humidity in the environment. For this reason, the impact of the humidity in the laboratory on the PLS calibration was evaluated in this special case, using materials with a low grade of heterogeneity, high stability and low degradation with respect to time.

Table 10 shows the summarized results for the first experiments performed on April 2015 and the second experiments performed on October 2015. The PLS models of the first experiments have lower RMSEP values than the values of the second experiment. So, what can be the source of error that leads to this difference? There are two principal sources of error that answer this question. The

first one is the lamp source of NIR radiation. The effect of lamp aging is a subject of study in NIR calibration models. The second one is the humidity in the laboratory. This is another subject of study with a strong interest in the pharmaceutical industry and academic laboratories because the humidity affects the stability of the materials and causes degradation with time. To evaluate these two sources of error, the background single channel spectra of different sets of NIR data was analyzed. If intensity of lamp is decreased for aging the maximum value of the single channel will be decreased, and if the humidity affects the NIR spectra, the background single channel will present information of OH regions in the spectra.

Table 10. RMSEP values at two different seasons of the year using the metallic plate.

DATA PRETREATMENT	PLS FACTORS	FIRST EXPERIMENT	SECOND EXPERIMENT
No Pretreatment	3	1.00	1.39
SNV	3	0.68	1.77
1st derivative	3	0.26	1.33
2nd derivative	3	0.39	1.50

Figure 29 shows the evaluation of the background single channel of the first experiment acquired on April 2015 and the second experiment acquired on October 2015. The red single channel spectra correspond to the background acquired on April, and the blue single channel spectra corresponds to the background acquired on October. In both cases, due to the methodology used by comparing three different regions, a high amount of NIR spectral data was necessary. This caused that were used at least two days with two different background single channel to complete the set of data in each evaluation. For this reason, two background single channels for each set of data in the seasons were analyzed. The issue in this point is that the difference in background from the month of April is lower compared to the difference in background from the month of October. Taking in consideration that the absorbance is a logarithmic function, these difference in background single

channels in the same month cause bigger differences in the NIR spectra of the film polymers acquired on different days.

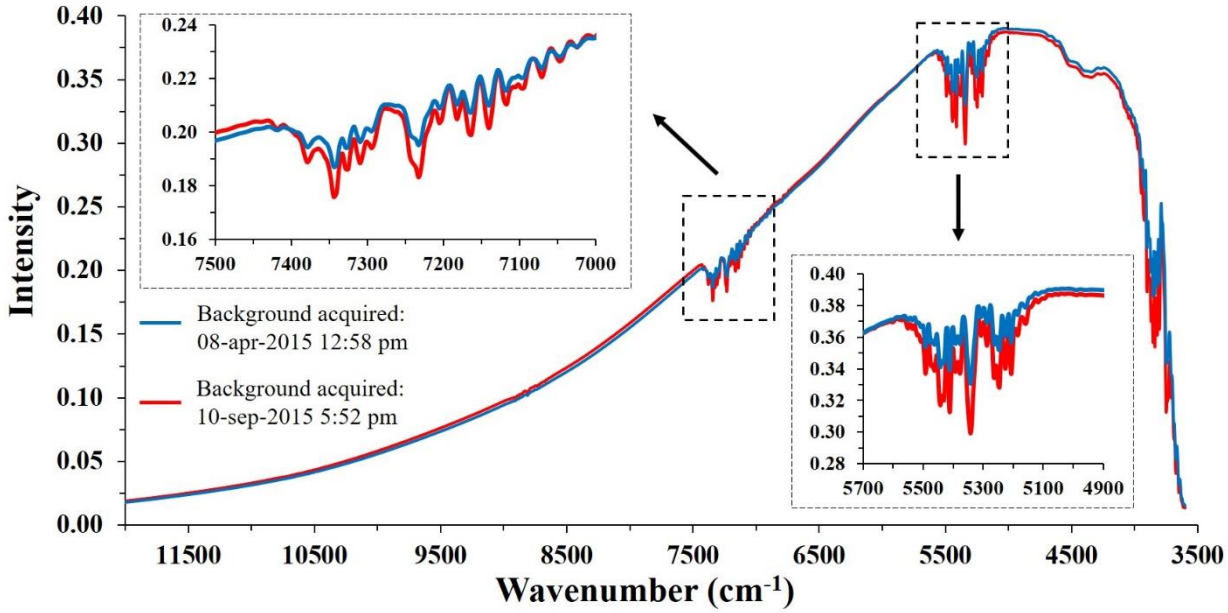

Figure 29. Single channel spectra of the background acquired at two different seasons of the year.

2.4. **CONCLUSIONS OF CHAPTER 2**

This study provides an uncomplicated method based on the test of representative layer theory to have a better understanding of absorption and scattering effects of NIR radiation into solid materials using low heterogeneous polypropylene non-glare films. The optical sampling of the NIR radiation into the polymer films was determined and it was estimated the maximum sampling depth that can penetrates the samples without a loss of information.

PLS calibration models were developed based on the results of the depth of penetration of NIR radiation into the samples and it was evaluated the effect of use more samples that beyond the

optical sampling. The results shown that NIR method is unbiased as long as the number of samples are within the depth of penetration of the NIR radiation.

This study also provides an economic and efficient method to test the reliability of the NIR instrument through the lifecycle of the lamp source and instrument parts. It is suggested to use polymer film standards to follow the quality guidance of the industry laboratories.

PLS models predicted the number of polypropylene films with high accuracy for calibration models built with up to 30 films. The PLS calibration models were developed with a system of low heterogeneity but with significant light scattering. Even though there are 30 films (below infinite depth) – this represents a case with multiple pathlengths. The radiation could be remitted to the detector after passing through only film, through 15, or through the 30 films. The radiation travels multiple pathlengths through the films, and the path travelled by the radiation is not known. In spite of these uncertainties, a systematic error is not observed with the calibration models developed with 30 films, and the six different preprocessing methods.

As long as the number of samples in the calibration set is representative of the variation to be modelled by a PLS regression, the sampling by the NIR method was unbiased. Sampling errors were obtained when the number of films used was greater than the depth of penetration of the NIR radiation. The results show the NIR spectroscopy is able to provide results with high accuracy as long as the sampling error is reduced. The sampling error was reduced by using a system with low heterogeneity in this study since as TOS indicates, heterogeneity is the major source of all sampling errors.

CHAPTER 3: STUDY OF NIR CHEMOMETRIC MODELS WITH LOW HETEROGENEITY FILMS PART II HETEROGENEITY. THE ROLE OF SAMPLING AND SPECTRAL PREPROCESSING ON PLS ERRORS

To be submitted to: *Journal of Near Infrared Spectroscopy*

Carlos Ortega-Zuñiga, Ricardo Navarro-Dent, and Rodolfo J. Romañach

This chapter is not an exact copy of the paper to be submitted. It contains original information.

3.1. **INTRODUCTION**

Near infrared (NIR) spectroscopy is widely used for non-destructive analysis in the agricultural, food, petrochemical and pharmaceutical industry and in process analytical technology (PAT) (Roggo et al., 2007; US-FDA, 2004). The understanding of NIR spectroscopy has grown as a result of thousands of studies, publications, and multiple books (D. Dahm & Dahm, 2014; D. Dahm et al., 2000, 2002; D. J. Dahm & Dahm, 2001; Norris, 1989; Romañach, Román-Ospino, & Alcalà, 2016; Williams & Norris, 1987; Workman & Weyer, 2012). One recent publication presented a procedure for the development and validation of NIR methods for pharmaceutical materials (Romañach et al., 2016). In spite of the progress made, there is still a need to understand the errors observed in NIR methods that can arise due to a number of sources. Partial least squares (PLS) regression methods require spectral variation that need to be enough representative of the property to model, and the presence of interferences with strong overlapping or spectral noise may result in biased predictions (Gowen, Downey, Esquerre, & O'Donnell, 2011; Kalivas & Palmer, 2014).

There are errors related to the NIR optical sampling of the materials (Ortega-Zuñiga, Reyes-Maldonado, Méndez, & Romañach, 2017). The NIR radiation that reaches the detector in diffuse

reflectance measurements is remitted from the top of 1-2 mm of the powder surface (K. H. Esbensen et al., 2016). A “mismatch error” may occur when the NIR measurement is on the top 1-2 mm of the surface, but the reference method is analyzing a 20 mm thick sample with a different composition (Romañach, 2017). This systematic sampling error is likely one of the most significant sources of error in NIR spectroscopy (Mark, 1991). There are also a number of other sampling errors that have been characterized within the field known as the Theory of Sampling (TOS) (K. Esbensen & Julius, 2009; Kim H. Esbensen & Paasch-Mortensen, 2010; Kim H. Esbensen et al., 2012; K. H. Esbensen et al., 2016; Kim H Esbensen & Wagner, 2014). TOS also explains that the material analysed by the NIR radiation, may not be representative of the full lot to be characterized. A sampling error, known as the fundamental sampling error, will occur due to the heterogeneity of the material analysed. This is an un-avoidable sampling error, but there are also a number of incorrect sampling errors which may occur. According to Theory of Sampling (TOS), sampling errors, which are caused by material heterogeneity and sampling process deficiencies are one or two orders of magnitude higher than analytical errors (Kim H. Esbensen & Paasch-Mortensen, 2010; Romañach, 2017). Therefore, data quality depends heavily on sampling methods (Kim H. Esbensen & Paasch-Mortensen, 2010; Roggo et al., 2007).

NIR radiation may interact with a particle one or more than times as shown in previous studies (Abrahamsson et al., 2005; Johansson et al., 2002). NIR radiation also penetrates more at high frequencies where less absorption occurs than at lower frequencies (Bellamy et al., 2008; Iyer et al., 2002; Ortega-Zuñiga et al., 2017). NIR spectroscopy could be visualized as occurring in a multiple path length cell since the depth of penetration varies according to the frequency of radiation and light scattering. Thus, NIR spectroscopy does not follow Beer’s law (D. Dahm & Dahm, 2014). The depth of penetration of NIR radiation can be estimated but the exact mass of

material that interacts with NIR radiation is not known (Colón et al., 2014; Adriluz Sánchez-Paternina et al., 2016). This complex interaction between light and particles (physics of diffuse reflectance) can also be considered a source of error in NIR spectroscopy.

A previous study evaluated the effect of light scattering on the determination of the number of polypropylene polymer films stacked together (Ortega-Zuñiga et al., 2017). The polymer films provided a system with a reduced heterogeneity to determine the error associated with light scattering. Experiments with similar polymer films were used to develop the Representative Layer Theory (RLT) (D. Dahm & Dahm, 2014; D. Dahm et al., 2000, 2002; D. J. Dahm & Dahm, 2001). Even though these films have very low heterogeneity in comparison to agricultural products and pharmaceutical powder mixtures, similar sampling errors are observed in these methods due to the physics of diffuse reflectance. Diffuse reflectance spectra of powder mixtures are based on the interaction of the radiation with the top 1 – 2 mm of the material (Colón et al., 2014; Adriluz Sánchez-Paternina et al., 2016), but the analysis of this top portion is frequently compared with that of a larger (thicker) sample. Thus, the experiment conducted with the film layers was considered a simulation of the analyses conducted with powder samples but with a reduction in sample heterogeneity.

In this study, NIR calibration models were developed using two polymers materials (polypropylene and polyethylene) with similar thickness (for the polyethylene film was 0.083 ± 0.002 mm, and the polypropylene film was 0.086 ± 0.002 mm) to understand the absorption and scattering effects on the errors observed by partial least squares when two materials are added to the sample. The polymers used in this experiment constitute a system with reduced heterogeneity, where the two films have similar thickness (polypropylene and polyethylene), and this represents a system with multiple pathlengths (Oelkrug et al., 2012). Calibration models were based on the

polyethylene percent content in the mix of films to evaluate the linearity of NIR predictions. All spectral measurements were performed with a number of films below the infinite depth of penetration to avoid this sampling error and guaranteeing that all the samples were analyzed by the NIR radiation (Ortega-Zuñiga et al., 2017). Additionally, calibration models were tested with the NIR spectra acquired in a second instrument to test the reproducibility of the models. This study therefore facilitated the study of more complex sample composition and the effects that: (1) materials with NIR spectra similarities for example excipients in pharmaceutical formulations, (2) evaluation of NIR calibration on a second instrument to test the reproducibility of the model, and (3) selection of spectral range and preprocessing to perform a NIR calibration model that works on two FT-NIR spectrometers in two different laboratories.

3.2. **MATERIAL AND METHODS**

3.2.1. Polymer films

Non-glare sheet protectors Samsill® (Lot. No. S43496; Samsill Corporation, 5740 Hartman Rd., Fort Worth, TX 76119) composed of heavy weight polypropylene top load were used in this study. Films were cut into rectangles sufficiently large to cover the integrating sphere window of the NIR system. Full Weight Plastic Sheet, 4X6-C Polyethylene Sheeting, 4-Mil, Clear, Poly-Cover® (Warp Bros manufacturer, 4647 W. Augusta Blvd. Chicago, IL 60651) were also cut into rectangles large enough to cover the integrating sphere window of the NIR system. The approximate thickness was measured by triplicate to determinate an average; for the polyethylene film was 0.083 ± 0.002 mm, and the polypropylene film was 0.086 ± 0.002 mm.

3.2.2. Layer thickness measurements

A digital micrometre (0-25mm, resolution: 0.001mm, and accuracy: 0.002 mm, manufactured by Marathon Management Company; Catalog No. S40502A; Fisher Scientific Company L.L.C.; 300 Industry Dr, Pittsburgh, PA 15275) was used to measure the thickness of the films. These were measured in triplicate (once on each side and once in the centre) to determine the average thickness of each sample and reduce variation.

3.2.3. Acquisition of NIR spectra

NIR spectra were obtained in the method development laboratory using the integrating sphere module in a Bruker MPA (Multi-Purpose Analyzer) FT-NIR (MA, USA) with a semiconductor room temperature lead sulphide (RT-PbS) external detector. A second Bruker MPA FT-NIR spectrometer from a different laboratory was used for the reproducibility study. The different arrangements of films were placed over the integrating sphere window of the FT-NIR spectrometer. The macro sample setup was used providing a NIR beam diameter of 15 mm. All NIR spectra were acquired over a 12000 – 4000 cm^{-1} (833.33 – 2500 nm) spectral range at a resolution of 16 cm^{-1}, with 32 scans for background and 32 scans for the sample. The remitted radiation was obtained in diffuse reflection mode. The films were pressed with a metallic plate and cylinder to minimize the effect of trapped air between the polymer films. This metal plate was removed from the top of the films before obtaining each spectrum.

The spectral bands related to NIR vibrations of the polyethylene and polypropylene were evaluated to find spectral regions where both components present differences that can be used to develop a NIR calibration model. Spectra of 10 polyethylene and 10 polypropylene films were

taken separately to evaluate the similarity of the NIR spectra of the materials. These were compared by determining their correlation coefficients using different spectral preprocessing with different spectral regions.

NIR infrared spectra were obtained for three layers of films as shown in **Figure 30**. The bottom set layer consisted of polypropylene films placed over the integrating sphere, the middle layer were polyethylene films and the top layer was polypropylene films. **Figure 30** shows the specific schemes for the arrangement of the three layers, the bottom and top layers were varied from one to six polypropylene films (maintaining a total sum of seven polypropylene films in each scheme) while the middle layer was varied from one to ten polyethylene films. The first spectrum for scheme 1 in **Figure 30** was obtained with one polypropylene film followed by one polyethylene film and six polypropylene films on top. This arrangement was maintained while the number of polyethylene films were increased up to ten films. This provided a total of ten sample arrangements for the first scheme. The scheme 2 in **Figure 30** included two polypropylene films on the bottom, while varying the polyethylene films from 1-10 in the middle and five polypropylene films on top. The scheme 6 in **Figure 30** consisted of six polypropylene films on the bottom as the number of polyethylene films in the middle was varied from 1 – 10 films and one polypropylene film was placed on top. These arrangements yielded a total of 60 different distributions of polyethylene and polypropylene films. NIR spectra were obtained in triplicate at each of these arrangements for a total of 180 spectra.

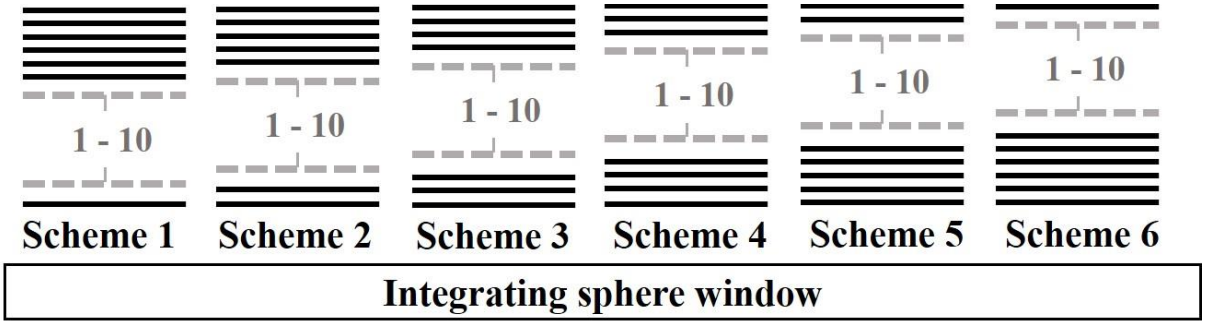

Figure 30. Sample arrangements. Polypropylene films in black line and polyethylene films in gray dashed line. The total number of spectra acquired were 180 (6 schemes, 10 sample arrangements, 3 spectra for each sample).

3.2.4. Development of Calibration Models

A total of 180 spectra were obtained for the calibration models using one FT-NIR spectrometer. Principal component analysis (PCA) and Partial Least Squares (PLS) regression were performed to develop the calibration models using the software SIMCA 15 (Sartorious Stedim Data Analytics Solutions, Umeå, Sweden). The calibration models were developed with: (1) No preprocessing (NP), (2) Standard Normal Variate (SNV), (3) first derivative (1^{st}der), (4) second derivative (2^{nd}der), (5) SNV+1^{st}der, and (6) SNV+2^{nd}der as spectral preprocessing.

The **Y**-variable evaluated was the percentage composition of polyethylene in total films of sample arrangement. This variable was chosen to obtain a parameter for the content of polyethylene based on the thickness of the whole sample using the equation (3-1). The average thickness of sample is a measurement of the total polymers (polyethylene and polypropylene films) stacked together, and the average thickness of polyethylene films is a measurement of the total number of polyethylene stacked together without the layers of polypropylene.

$$C_{Polyethylene}(\%) = 100 \times \left(\frac{Thickness\ of\ Polyethylene\ Films}{Thickness\ of\ sample}\right) \quad (3\text{-}1)$$

3.2.5. Validation of the Calibration Models

The calibration models were validated by repeating the spectral acquisition shown in **Figure 30** on three different days chosen randomly by two different analysts with a first FT-NIR spectrometer in the method development laboratory. A second FT-NIR spectrometer from a second laboratory was used to obtain the NIR spectra on three different days randomly to test the reproducibility of the method. The predictive capability of the models developed was assessed in terms of root mean squared error of prediction, RMSEP, equation (3-2); the relative root mean squared error of prediction, RSEP(%), equation (3-3); and bias, equation (3-4), defined as:

$$RMSEP = \sqrt{\frac{\sum_{i=1}^{n}\left(Y_i^{pred} - Y_i^{ref}\right)^2}{n}} \quad (3\text{-}2)$$

$$RSEP(\%) = \sqrt{\frac{\sum_{i=1}^{n}\left(Y_i^{pred} - Y_i^{ref}\right)^2}{\sum_{i=1}^{n}\left(Y_i^{ref}\right)^2}} \times 100 \quad (3\text{-}3)$$

$$Bias = \sum_{i=1}^{n} \frac{\left(Y_i^{pred} - Y_i^{ref}\right)}{n} \quad (3\text{-}4)$$

Where n is the number of samples used in the validation set, and Y_i^{pred} and Y_i^{ref} are the predicted and measured reference values based on the **Y**-variable used.

3.3. **RESULTS AND DISCUSSION**

3.3.1. NIR spectral evaluation

Figure 31 shows the NIR spectra of polyethylene and polypropylene corresponding to ten stacked films of each material separately. The two materials show significant spectral differences, with the polyethylene film showing narrower bands than the polypropylene film. For the polypropylene material the combination band of the first overtone and deformation mode of methyl and methylene groups are found in the 7350 – 7070 cm^{-1} spectral region; the second overtones of the asymmetric stretching mode of methyl ($-CH_3$) and methylene ($-CH_2-$) groups are found in the 8400 – 8200 cm^{-1} spectral region. **Table 11** and

Table 12 shows the assignment of the NIR bands of polypropylene and polyethylene materials based on previous studies. The intense band at 8227 cm^{-1} corresponds to the second overtone of the stretching mode of methylene in polyethylene, this band present a moderate intensity at 8242 cm^{-1} in polypropylene. The band at 8389 cm^{-1} corresponds to the second overtone vibrational mode of methyl group in polypropylene, while this is a weak band at 8420 cm^{-1} in polyethylene. These bands have been studied to monitor the density of polyethylene as quality control in a polymer production process by the ratio of the two absorption bands (Nagata, Ohshima, & Tanigaki, 2000). The density becomes lower as the number of polymer chain branches increases, and their backbone length kept constant. Methyl groups are located at the ends of branches as well as at the ends of the main chains. Therefore, the density and degree of branching was estimated by the ratio of the absorption bands of methyl and methylene groups (Nagata et al., 2000).

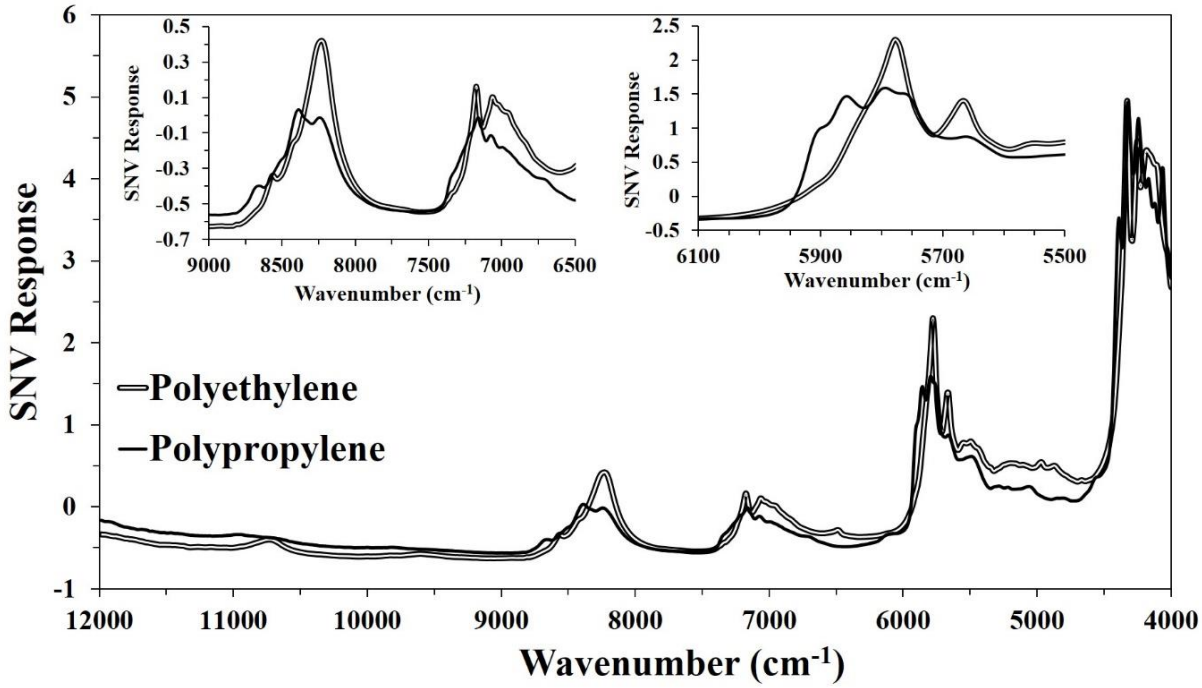

Figure 31. SNV spectra of polymer layers. Solid line for polypropylene and double line for polyethylene.

Table 11. Assignment of the NIR bands of polypropylene materials.

Polymer*	Assignation	nm (rep.)	cm^{-1} (rep.)	cm^{-1} (obs.)
Polypropylene	C-H str first overtone (CH_2)	1768 (Furukawa et al., 2003)	5656.11	5662
	C-H str first overtone (CH_2)	1730 (Furukawa et al., 2003)	5780.35	-
	C-H str first overtone (CH_3)	1726 (Workman & Weyer, 2012; Workman Jr., 2001)	5793.74	5797
	C-H str first overtone (CH_3)	1705.61	5863 (Watari & Ozaki, 2004)	5832
	C-H str first overtone (CH_3)	1700 (Furukawa et al., 2003; Workman & Weyer, 2012; Workman Jr., 2001)	5882.35	5893
	2x C-H str + C-H def (CH_2)	1413.83	7073 (Watari & Ozaki, 2004)	7077
	2x C-H str + C-H def (CH_2)	1424 (Furukawa et al., 2003)	7022.47	-
	2x C-H str + C-H def (CH_2)	1395.48	7166 (Watari & Ozaki, 2004)	7158
	C-H combination (CH_2 and CH_3)	1394 (Workman & Weyer, 2012; Workman Jr., 2001)	7173.60	-
	2x C-H str + C-H def (CH_2)	1390 (Furukawa et al., 2003)	7194.24	-
	2x C-H str + C-H def (CH_3)	1370 (Furukawa et al., 2003)	7299.27	-
	2x C-H str + C-H def (CH_3)	1382.74	7232 (Watari & Ozaki, 2004)	-
	C-H str second overtone (CH_3)	1220 (Workman & Weyer, 2012; Workman Jr., 2001)	8196.72	-
	C-H str second overtone (CH_2)	1216 (Furukawa et al., 2003)	8223.68	8242
	C-H str second overtone (CH_2)	1218.92	8204 (Watari & Ozaki, 2004)	-
	C-H str second overtone (CH_3)	1192 (Furukawa et al., 2003; Workman & Weyer, 2012; Workman Jr., 2001)	8389.26	8389
	C-H str second overtone (CH_3)	1193.18	8381 (Watari & Ozaki, 2004)	-
	C-H str second overtone (CH_3)	1151.81	8682 (Watari & Ozaki, 2004)	8655
	C-H str second overtone (CH_3)	1150 (Furukawa et al., 2003)	8695.65	-

Table 12. Assignment of the NIR bands of polyethylene materials.

Polymer*	Assignation	nm (rep.)	cm-1 (rep.)	cm-1 (obs.)
Polyethylene	C-H str first overtone (CH_2)	1764 (Shimoyama et al., 1998)	5668.93	5666
	C-H str first overtone (CH_2)	1728 (Shimoyama et al., 1998)	5787.04	5778
	2x C-H str + 1 C-H def (CH_2)	1438 (Workman & Weyer, 2012)	6954.10	6958
	2x C-H str + 1 C-H def (CH_2)	1416 (Shimoyama et al., 1998)	7062.15	7062
	2x C-H str + 1 C-H def (CH_2)	1410 (Workman & Weyer, 2012)	7092.20	-
	2x C-H str + 1 C-H def (CH_2)	1392 (Shimoyama et al., 1998)	7183.91	-
	2x C-H str + 1 C-H def (CH_2)	1394 (Workman & Weyer, 2012)	7173.60	7174
	2x C-H str + 1 C-H def (CH_3)	1374 (Shimoyama et al., 1998), (Workman & Weyer, 2012)	7278.02	-
	C-H str second overtone (CH_2)	1218 (Workman & Weyer, 2012)	8210.18	8227
	C-H str second overtone (CH_2)	1214 (Shimoyama et al., 1998)	8237.23	-
	C-H str second overtone (CH_2)	1190 (Workman & Weyer, 2012)	8403.36	-
	C-H str second overtone (CH_3)	1186 (Shimoyama et al., 1998)	8431.70	8420
	C-H str second overtone (CH_2)	1166 (Shimoyama et al., 1998)	8576.33	8562
	C-H str second overtone (CH_3)	1154 (Workman & Weyer, 2012)	8665.51	8655
	C-H str second overtone (CH_3)	1146 (Shimoyama et al., 1998)	8726.00	-
	C-H str second overtone (CH_3)	1130 (Workman & Weyer, 2012)	8849.56	-

Figure 32 shows the NIR spectra for schemes 1 and 6 as the number of polyethylene (PE) films was increased. The black color is used for the spectra of scheme 1 which has one polypropylene (PP) film at the bottom and six at the top, the gray color is for scheme 6 which has six films of polypropylene at the bottom and one at the top. **Figure 32** shows differences in spectral

baseline due to the portion of the radiation that was remitted (back-scattered to the detector). The spectral baseline is reduced as the number of PE films is increased. When the number of PE is the same for the schemes 1 and 6, their spectra present minor baseline differences and differences in the intensity of the bands. However, the spectra of the scheme 1 show the intense band of methylene (-CH_2-) in PE at 8227 cm^{-1}, and the NIR spectra of the scheme 6 shows diminished this band with an increment of the methyl (-CH_3) band in PP at 8389 cm^{-1}. These differences can be significant in the development of NIR calibration models, for example, API concentration in bilayer tablets or coating process, where the heterogeneity of the blend has a significant contribution in spectral features of the API (Andersson, Josefson, Langkilde, & Wahlund, 1999; Ito et al., 2010).

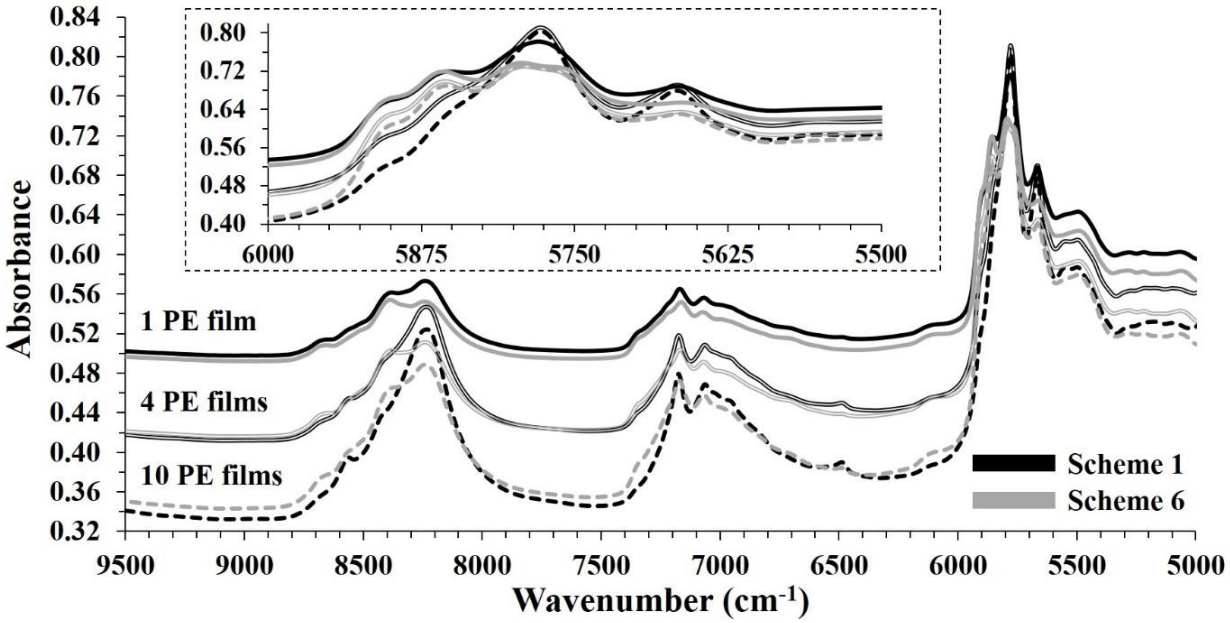

Figure 32. Polyethylene spectral changes as film number increases in the schemes 1 and 6. Black colour for scheme 1, gray colour for scheme 6, PE: polyethylene.

The correlation coefficient of the NIR spectra for polyethylene and polypropylene varied from 0.449 to 0.975 depending the spectral region and spectral preprocessing as described in **Table 13**. There are differences on the spectral range of 8800 – 8300 cm^{-1} due to molecular vibrations of the structures as discussed before. The use of NIR spectra with high similarity can be challenging, even, the use of SNV as spectral preprocessing presents a high correlation coefficient between the materials as shown in **Table 13**, which imply a challenge for model development. The correlation coefficient decreases significantly when derivatives are used as spectral preprocessing compared to raw spectra and SNV. The development of a calibration model using materials which present a high correlation coefficient in their NIR spectra, can be improved with the correct usage of the spectral region and preprocessing (Alcalà et al., 2013; Da-Col & Poppi, 2018). The correlation coefficient of PE and PP spectra throughout the 9500 – 6500 cm^{-1} and 6500 – 5000 cm^{-1} spectral regions between the materials become significantly lower when the first or second derivatives are used as spectral preprocessing as shown in **Table 13**.

Table 13. Correlation coefficient values for polyethylene and polypropylene in five spectral regions. NP: no spectral preprocessing; SNV: standard normal variate; 1^{st}: first derivative (25 points); SNV-1^{st}: SNV + first derivative (25 points); 2^{nd}: second derivative (25 points); SNV-2^{nd}: SNV + second derivative (25 points).

Preprocessing	**12000-4000 cm^{-1}**	**9500-6500 cm^{-1}**	**6500-5000 cm^{-1}**	**5000-4000 cm^{-1}**
NP	0.975	0.917	0.922	0.971
SNV	0.975	0.917	0.922	0.971
1^{st}	0.901	0.786	0.838	0.922
2^{nd}	0.560	0.474	0.449	0.616
SNV-1^{st}	0.901	0.786	0.838	0.922
SNV-2^{nd}	0.560	0.474	0.449	0.616

Table 14 shows the average percentage composition of polyethylene within each scheme arrangement on **Figure 30**. The arrangements of each scheme in **Figure 30** has a variation on the number of polyethylene films from one to ten, while the total number of polyethylene films

remains seven (7) in all the schemes. **Table 14** shows that the increments of thickness in the average sample and average polyethylene depends on the number of polyethylene films used in the arrangements, this increment is 0.083 mm. However, the average polyethylene percentage composition is a value that depends on the thickness of polyethylene films and the sample thickness, where the total number of polypropylene films is fixed to a total number of seven (**Equation 1**). **Table 14** shows the percentage composition of polyethylene (%PE) which does not present a constant variation, and the increment shows a rate of change that vary from 9.5% and 2.6%, as shown in **Figure 33**. **Table 14** shows the approximate change in the intensity of the absorbance band of methylene ($-CH_2-$) in PE at 8227 cm^{-1} in the scheme 1 and 6, after baseline correction. The approximate change in the scheme 1 is 0.009, while the approximate change in the scheme 6 is 0.013. A linear regression between the number of PE films and the approximate change in the intensity of methylene at 8227 cm^{-1} shows a R^2 of 0.9832 and 0.9573 for scheme 1 and 6, respectively. This is due to the NIR radiation that travels into the PE films in the scheme 6 pass firstly into a thicker layer of PP compared to the scheme 1. Therefore, the interaction of the NIR radiation with the PE films is lower. This approximate change in the intensity of the absorbance band of methylene can be a source of error in a NIR calibration model and the difference of the results of the different scheme need to be evaluated in deep.

Table 14. Description of polyethylene (PE) in each scheme. These variations were done for each of the six schemes. Seven polypropylene films were used in each scheme. Thickness for one polyethylene film: 0.083 ± 0.002 mm, thickness for one polypropylene film: 0.086 ± 0.002 mm.

PE Films	PP Films	Sample Thickness (±0.01 mm)	PE Thickness (±0.01 mm)	%PE Composition (±0.1 %)	Intensity* (CH_2) in PE 8227 cm^{-1} Scheme 1	Intensity* (CH_2) in PE 8227 cm^{-1} Scheme 6
1	7	0.69	0.08	12.1	0.075	0.059
2	7	0.77	0.17	21.6	0.097	0.071
3	7	0.85	0.25	29.3	0.116	0.085
4	7	0.93	0.33	35.5	0.135	0.094
5	7	1.02	0.42	40.8	0.149	0.103
6	7	1.10	0.50	45.3	0.156	0.115
7	7	1.18	0.58	49.1	0.171	0.127

8	7	1.27	0.66	52.4	0.182	0.129
9	7	1.35	0.75	55.4	0.186	0.136
10	7	1.43	0.83	58.0	0.191	0.144

* Band intensity after baseline correction of the NIR spectra.

Figure 33 shows the relationship between the percentage of polyethylene films vs the number of polyethylene films. The use of the number of films as **Y**-variable implies to consider a linear change based on the number of polyethylene films stacked together no matter the thickness of the materials. Therefore, the use percent of polyethylene in total films as **Y**-variable implies to consider the thickness of the polyethylene and polypropylene films stacked together as physical variable to represent the changes in content composition of the samples.

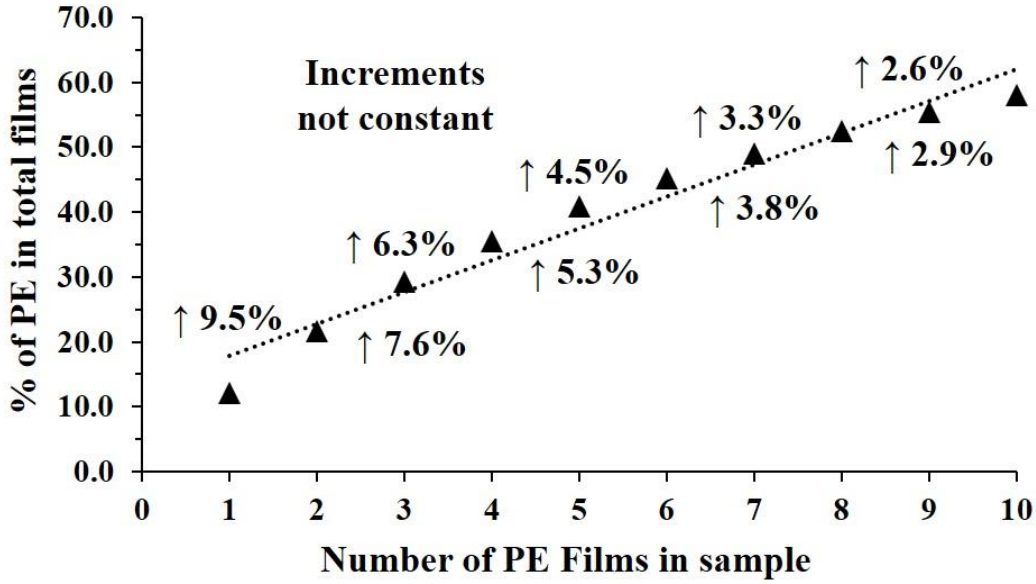

Figure 33. Percentage of polyethylene films vs number of polyethylene films.

3.3.2. PCA and spectral preprocessing evaluation

Figure 34 shows the PCA score plots of the NIR spectra in the spectral region of 9500 – 6500 cm^{-1} with the preprocessing: a) second derivative (25-point window) and b) SNV+1st

derivative (25-point window) of the calibration samples with the six schemes evaluated in this study. As shows the figure, for the second derivative preprocessing (**Figure 34a**), the first principal component represents the variation in the composition of polyethylene in the schemes with an explained variance of 92.2%. The second component has an explained variance of 7.6% and it depends of the schemes. For the scheme 1 the bottom layer has one film of polypropylene, and most of the radiation reaches the middle layer composed of the polyethylene films. The scheme 6 has six films of polypropylene in the bottom layer, and the radiation must travel into more PP films. Therefore, the spectra of the scheme 6 contain more information of the PP than the scheme 1, and the scores of this samples present a different pattern which can be explained with the first and second component of the PCA plot. The SNV+1st derivative (25-point window) preprocessing (**Figure 34b**) shows a pattern where the variation of polyethylene in the six schemes is similar with an explained variance in the first component of 96.7% and 3.1% in the second component.

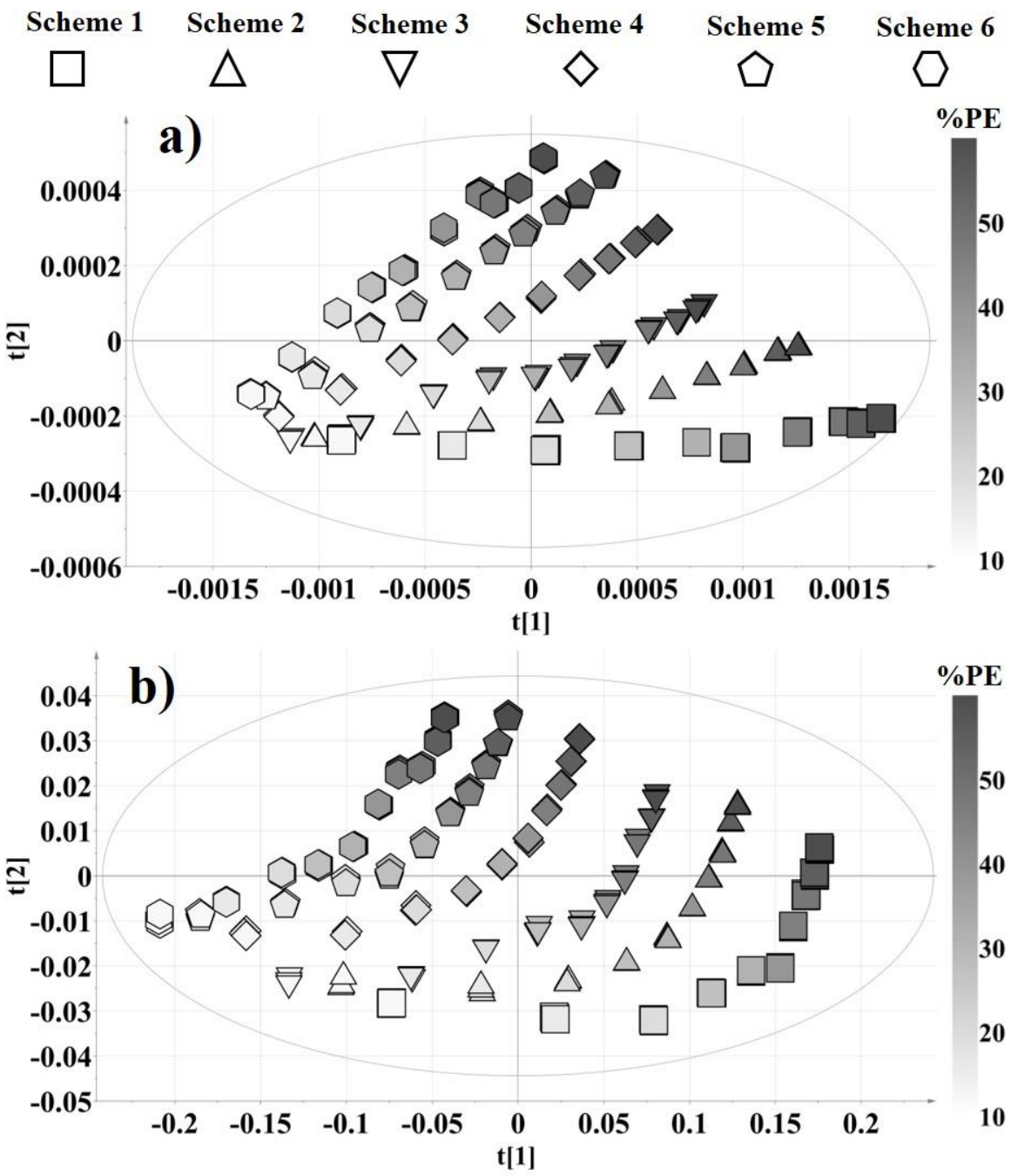

Figure 34. PCA scores plot of the NIR spectra for calibration samples (six schemes) acquired with the first instrument. Spectral region 9500 – 6500 cm^{-1} using the preprocessings: a) 2nd derivative (25-point window) and b) SNV+1st derivative (25-point window). Percentage of polyethylene increasing from white to black colour.

3.3.3. Evaluation of the validation sets over three replicates

The validation spectra were obtained by placing the films over the integrating sphere on three separate days in the same way as the calibration set. This procedure was performed using the first and second FT-NIR spectrometers. **Table 15** shows the global RMSEP, RSEP(%) and bias for each validation set in the spectral region of 9500 – 6500 cm^{-1} with first derivative (25-point window), and 2nd derivative (25-point window). These statistical results were calculated based on the predictions with one, two and three PLS factors for the six schemes in each validation set. The results in the first FT-NIR spectrometer shows that three PLS factors present the lower errors and bias. However, the use of this calibration model with three PLS factors in the second instrument result in higher errors and bias when SNV+1st derivative is used as spectral preprocessing. The calibration model using second derivative as preprocessing provides the lower errors and bias when used to predict spectra from the first and second FT-NIR spectrometers.

Table 15. Results of three validations acquired with the first and second instrument until three PLS factors using the spectral region 9500 – 6500 cm^{-1}. The RMSEP, RSEP(%), and bias values are calculated for the six schemes used in this study. The cells marked with '*' indicate that zero is included within the 95% confidence interval of the bias.

		Val 1 - NIR 1			**Val 2 - NIR 1**			**Val 3 - NIR 1**		
Preproc.	**PLS Factors**	**RMSEP**	**RSEP (%)**	**Bias**	**RMSEP**	**RSEP (%)**	**Bias**	**RMSEP**	**RSEP (%)**	**Bias**
2nder	1	8.10	19.08	0.40*	8.21	19.32	0.29*	8.43	19.86	0.20*
	2	2.55	6.01	1.33	1.76	4.15	1.01	1.50	3.52	0.01*
	3	2.52	5.93	1.39	1.66	3.92	1.12	1.32	3.10	-0.09*
SNV+1st der	1	11.14	26.24	0.07*	10.98	25.85	-0.18*	11.09	26.11	0.26*
	2	2.49	5.87	-0.85	2.66	6.25	-1.26	2.45	5.77	-1.09
	3	1.86	4.38	-0.78	1.96	4.62	-0.19*	2.04	4.80	-1.42
		Val 1 - NIR 2			**Val 2 - NIR 2**			**Val 3 - NIR 2**		
2nder	1	8.34	19.63	0.49*	8.53	20.08	0.72*	8.23	19.37	0.72*
	2	1.96	4.62	0.86	1.80	4.24	1.00	1.81	4.26	1.25
	3	1.87	4.41	0.96	1.68	3.95	1.03	1.64	3.86	1.28
SNV+1st der	1	10.86	25.57	0.00*	11.05	26.01	0.38*	11.12	26.19	0.38*
	2	8.73	20.56	-8.18	9.91	23.34	-9.49	9.61	22.62	-9.15
	3	10.66	25.10	-10.03	12.69	29.89	-12.17	12.33	29.03	-11.83

2nder: second derivative (25-point window); SNV+1stder: SNV + first derivative (25-point window).

Table **16** shows the statistical results by scheme averaging the three validations acquired with by the first and the second FT-NIR spectrometer; the results are presented using the second PLS factor as it was shown before that provides the lower errors and bias. The results using SNV+1st derivative provides lower errors and bias in the first FT-NIR spectrometer, however the calibration with this spectral preprocessing present a high error and bias when used to predict spectra acquired with the second instrument. The calibration model using second derivative provides the lower errors and bias in both instruments with RSEP(%) up to 5.27% and bias up to 1.67 percent of polyethylene. Previous results showed a RSEP(%) of 1.77 and 0.03 of bias. However, this result is based in one FT-NIR spectrometer and using one polymer (polypropylene) with variation of the number of film layers below the infinite depth of penetration of the NIR radiation into the material.(Ortega-Zuñiga et al., 2017) It should be noted that results using derivatives provide the lower error and bias when physical variation is present in the system to be modelled as previous studies show (Ortega-Zúñiga et al., 2019; Ortega-Zuñiga et al., 2017; Román-Ospino et al., 2016; Šašić, Blackwood, Liu, Ward, & Clarke, 2015).

Table 16. Statistical results by scheme of the three validations acquired with the first and second instrument using two PLS factors with the spectral region 9500 – 6500 cm^{-1}. The RMSEP, RSEP(%), and bias values were calculated for the six schemes used in this study.

NIR	***2nd derivative (25-point window)***						
	RMSEP/Bias	**Scheme 1**	**Scheme 2**	**Scheme 3**	**Scheme 4**	**Scheme 5**	**Scheme 6**
1	**Val 1**	2.40 / -2.04	2.44 / 1.95	3.50 / 3.35	2.02 / 1.81	1.59 / 0.38	2.91 / 2.54
	Val 2	1.50 / 0.52	2.11 / 1.85	1.49 / 0.65	1.95 / 1.55	1.56 / 1.07	1.87 / 0.43
	Val 3	1.35 / 1.20	1.55 / -0.70	1.48 / 1.03	1.36 / -0.52	1.23 / 0.5	1.92 / -1.43
	SNV +1st derivative (25-point window)						
	Val 1	2.83 / -1.67	1.6 / 0.13	1.61 / 0.88	1.05 / -0.24	3.84 / -2.88	2.88 / -1.32
	Val 2	3.39 / -2.56	1.55 / 0.33	2.19 / -0.46	1.73 / -0.15	2.59 / -1.38	3.73 / -3.35
	Val 3	1.51 / -0.44	2.66 / -1.47	1.39 / 0.24	2.1 / -0.96	1.72 / -0.27	4.16 / -3.66
2	***2nd derivative (25-point window)***						
	Val 1	1.90 / 1.31	3.02 / 2.74	1.37 / -0.34	2.06 / 1.53	1.31 / -0.45	1.61 / 0.36
	Val 2	2.66 / 2.45	1.72 / 1.24	1.47 / 0.84	1.63 / 1.02	1.35 / -0.43	1.67 / 0.86
	Val 3	1.55 / 0.97	1.34 / 0.75	1.90 / 1.51	1.96 / 1.54	2.20 / 1.62	1.78 / 1.13
	SNV +1st derivative (25-point window)						
	Val 1	10.35 / -9.72	7.89 / -7.2	8.27 / -7.69	6.73 / -6.27	9.28 / -9.07	9.39 / -9.13
	Val 2	8.94 / -8.33	9.37 / -8.85	9.09 / -8.70	9.32 / -9.02	11.32 / -11.09	11.16 / -10.97
	Val 3	10.38 / -9.67	9.47 / -8.92	8.48 / -7.99	8.96 / -8.69	8.72 / -8.44	11.32 / -11.18

A graphical evaluation of the calibration samples and the test sets of the first and second FT-NIR is presented in **Figure 35**. The figure shows the PLS score plots of the calibration and test sets of the first and second FT-NIR spectrometer using the second derivative (**Figure 35a**) and SNV+1st derivative (**Figure 35b**) as preprocessing in the spectral region of 9500 – 6500 cm^{-1}. As shown the figure, the score plot of the samples using the second derivative preprocessing presented a similar pattern and the plots are grouped by number of polyethylene films in each scheme. The samples are aligned by scheme allowing a separation and classification by number of polyethylene and by scheme in the experimental setup. In the case of the score plots using the SNV+1st derivative preprocessing the samples of the test set with the second FT-NIR presented a bias. However, these samples maintained the pattern of the score plots of the calibration set. A possible way to correct this bias is a method of slope/bias correction or mathematical treatment of the score plots of this test set; however, in this study was evaluated a second spectral region where the raw materials

presented differences. The NIR region evaluated is the 6500 – 5000 cm^{-1}, as shown in **Table 13** the correlation coefficient present similar value as the 9500 – 6500 cm^{-1} spectral region.

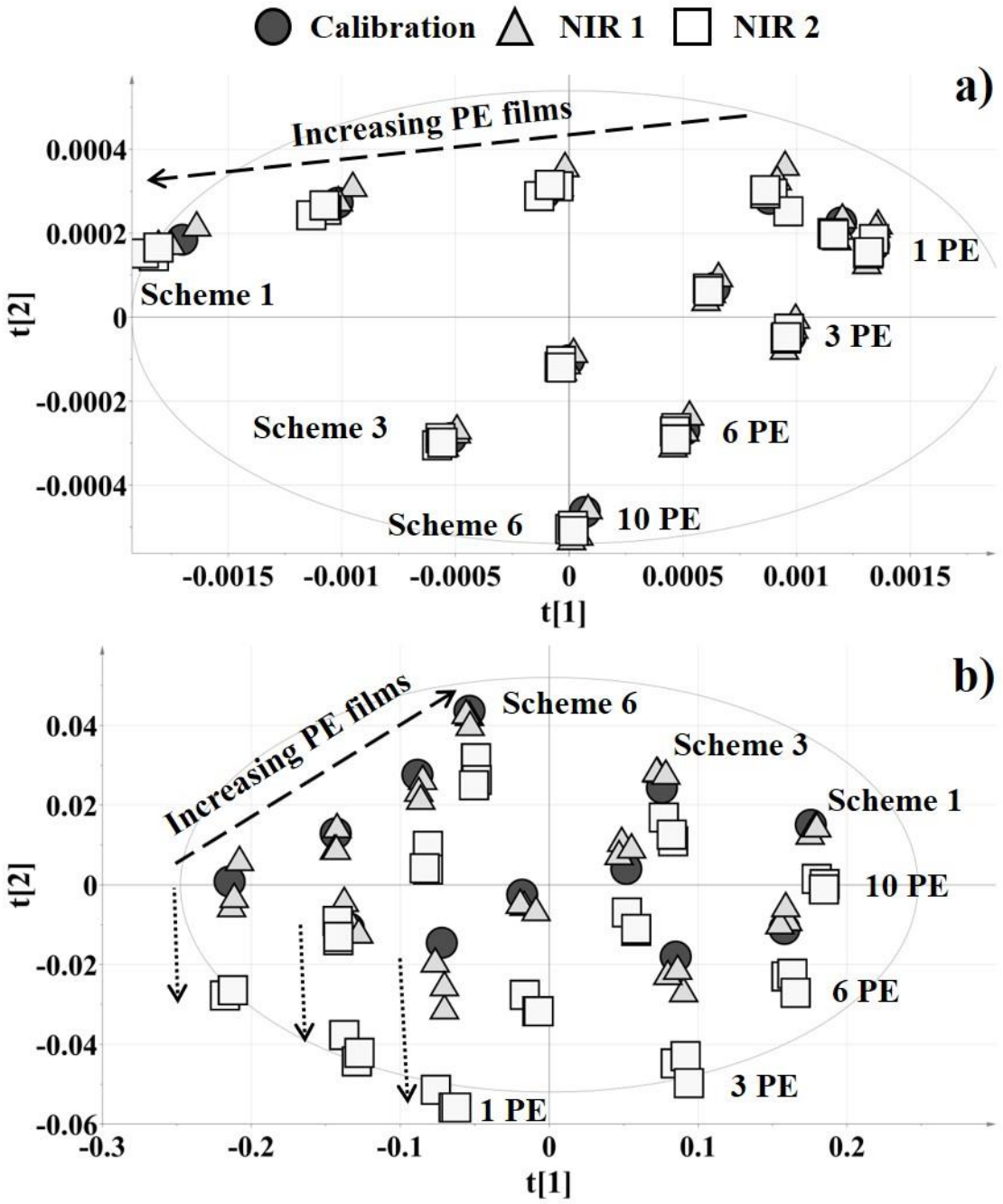

Figure 35. PLS scores of calibration and test sets with NIR1 and NIR2 in the spectral region 9500 – 6500 cm^{-1} using the spectral preprocessing. a) 2nd derivative (25-point window) and b) SNV+1st derivative (25-point window). Direction of the increasing number of polyethylene films in middle layer (dashed arrow). Dotted arrow shows the bias of the scores for test samples acquired using the NIR2.

Table **17** shows the global results (RMSEP, RSEP(%) and bias) for each validation set acquired with the first and the second FT-NIR spectrometers respectively using first derivative (25-point window), and 2nd derivative (25-point window) as spectral preprocessing in the spectral region of 6500 – 5000 cm^{-1}. As shows the table, the use of two PLS factors provides the lower error and bias regardless of the spectral preprocessing. The use of three PLS factors enhances the bias values, however the error did not improve significantly. Therefore, the evaluation was done using two PLS factors for the schemes as shown in **Table 18**. The predictions presented low error and bias values regardless of the spectral preprocessing making difficult the selection of one preprocessing as the best for the calibration model. **Figure 36** shows the PLS score plots of the calibration and test sets of the first and second FT-NIR spectrometers using the second derivative (**Figure 36a**) and SNV+1st derivative (**Figure 36b**) as preprocessing in the spectral region of 6500 – 5000 cm^{-1}. As shows the figure, the score plots of the calibration and the score plots of the test sets with the first and second FT-NIR spectrometers presented a similar pattern regardless the spectral preprocessing.

Table 17. Global results of three validations acquired with the first and second instrument until three PLS factors using the spectral region 6500 – 5000 cm-1. The RMSEP, RSEP(%), and bias values are calculated for the six schemes used in this study. Bias in cells marked with '*' indicate that zero is in the 95% confidence interval.

		Val 1 - NIR 1			Val 2 - NIR 1			Val 3 - NIR 1		
Preproc.	PLS Factors	RMSEP	RSEP (%)	Bias	RMSEP	RSEP (%)	Bias	RMSEP	RSEP (%)	Bias
2nd der	1	11.13	26.20	-0.13*	11.07	26.06	-0.21*	11.28	26.57	-0.66*
	2	2.38	5.60	0.53	1.09	2.57	-0.04*	2.41	5.69	-2.16
	3	2.43	5.71	0.56	1.05	2.46	0.14*	1.98	4.65	-1.69
SNV+1st der	1	12.15	28.61	-0.15*	12.08	28.44	-0.11*	12.08	28.44	-0.04*
	2	2.45	5.76	0.38	2.44	5.74	0.94	2.60	6.11	1.12
	3	2.92	6.87	1.46	2.95	6.94	1.69	3.36	7.90	2.38
		Val 1 - NIR 2			Val 2 - NIR 2			Val 3 - NIR 2		
2nd der	1	11.33	26.69	0.32*	11.26	26.51	0.72*	11.17	26.29	0.71*
	2	1.74	4.09	1.01	2.37	5.57	2.18	2.59	6.09	2.42
	3	1.92	4.52	1.36	2.41	5.67	2.30	2.73	6.42	2.55
SNV+1st der	1	12.04	28.35	0.01*	12.13	28.56	-0.18*	12.07	28.42	-0.14*
	2	2.35	5.53	0.03*	3.55	8.37	-2.52	3.03	7.12	-2.14
	3	2.97	6.98	1.39	2.38	5.61	0.63	2.44	5.76	1.12

2nd der: second derivative (25-point window); SNV+1st der: SNV + first derivative (25-point window).

Table 18. Statistical results by scheme of the three validations acquired with the first and second instrument using two PLS factors with the spectral region 6500 – 5000 cm^{-1}. The RMSEP, RSEP(%), and bias values are calculated for the six schemes used in this study.

NIR	*2nd derivative (25-point window)*						
	RMSEP/Bias	**Scheme 1**	**Scheme 2**	**Scheme 3**	**Scheme 4**	**Scheme 5**	**Scheme 6**
1	**Val 1**	3.81 / -3.45	2.17 / 1.71	2.53 / 2.45	0.77 / 0.18	0.76 / -0.34	2.67 / 2.63
	Val 2	0.87 / -0.42	0.96 / -0.83	1.14 / -1.07	1.47 / 1.35	0.61 / 0.36	1.29 / 0.36
	Val 3	0.95 / -0.39	3.30 / -3.25	1.88 / -1.83	2.72 / -2.67	2.18 / -2.12	2.74 / -2.69
	SNV +1st derivative (25-point window)						
	Val 1	2.74 / -1.86	1.74 / 0.76	2.52 / 2.00	1.79 / 0.69	2.87 / -0.81	2.76 / 1.50
	Val 2	2.28 / 1.07	3.79 / 3.49	2.28 / 1.18	1.48 / 0.33	2.02 / 0.73	2.15 / -1.15
	Val 3	3.73 / 2.88	2.06 / 0.04	2.84 / 2.38	1.75 / 0.25	2.68 / 2.14	1.99 / -0.97
	2nd derivative (25-point window)						
2	**Val 1**	2.94 / 2.92	2.65 / 2.62	0.86 / -0.78	0.78 / 0.67	0.50 / 0.06	0.90 / 0.55
	Val 2	3.37 / 3.32	2.14 / 2.02	1.57 / 1.52	2.06 / 2.03	1.27 / 1.16	3.06 / 3.01
	Val 3	2.13 / 1.92	1.58 / 1.46	2.71 / 2.65	2.98 / 2.94	2.38 / 2.31	3.35 / 3.23
	SNV +1st derivative (25-point window)						
	Val 1	2.77 / -0.03	2.61 / 1.79	2.03 / -0.82	2.29 / 1.53	2.45 / -1.57	1.80 / -0.73
	Val 2	2.50 / 0.58	3.47 / -2.90	2.93 / -2.46	3.59 / -2.95	4.46 / -4.05	4.01 / -3.33
	Val 3	3.58 / -2.45	3.18 / -2.52	3.24 / -2.66	2.72 / -2.10	1.93 / -0.67	3.22 / -2.47

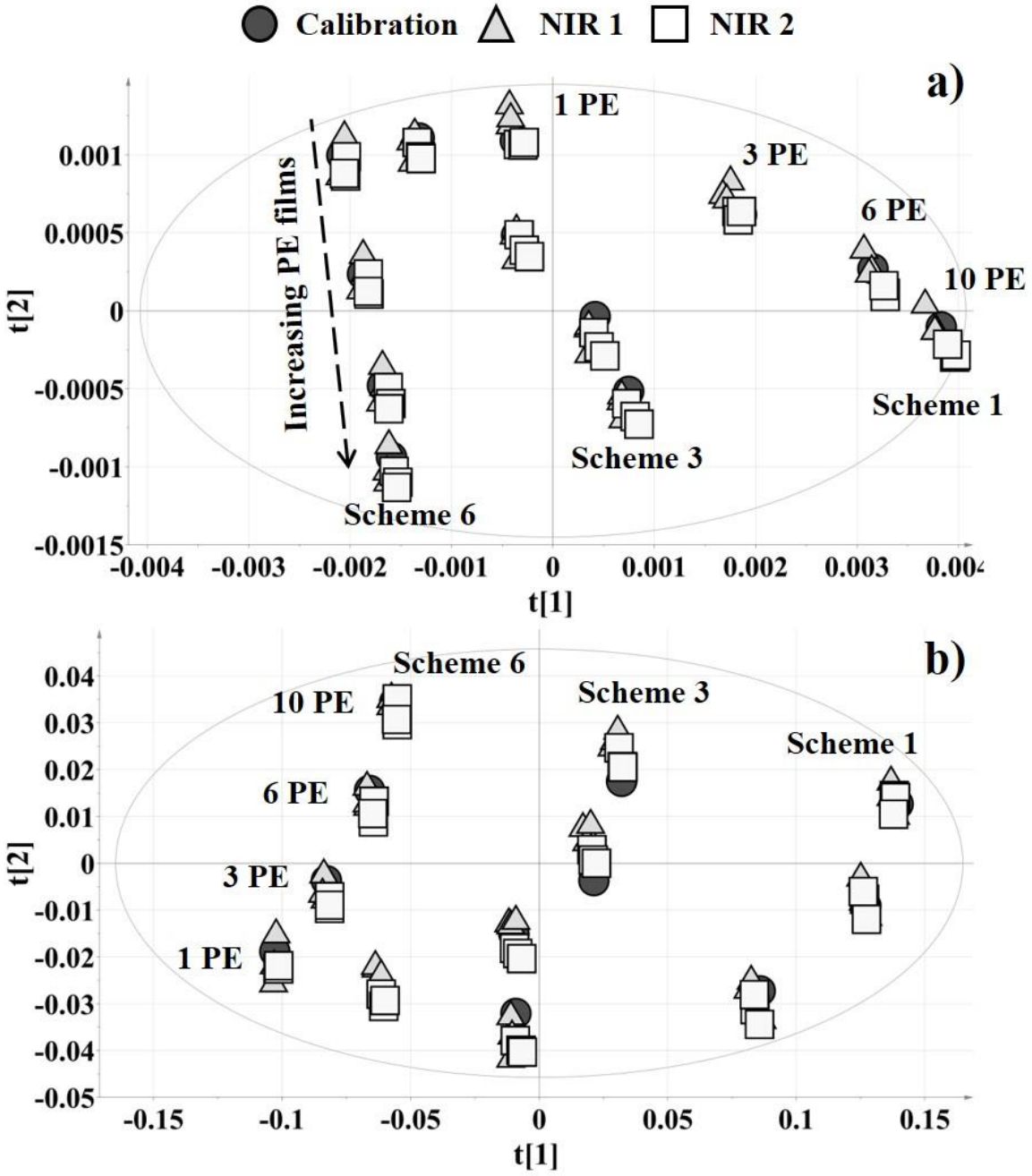

Figure 36. PCA scores of calibration and test sets with NIR1 and NIR2 in the spectral region 6500 – 5000 cm^{-1} using the spectral preprocessing. a) 2nd derivative (25-point window) and b) SNV+1st derivative (25-point window). Direction of the increasing number of polyethylene films in middle layer (dashed arrow).

An evaluation of the loading weights of the calibration models performed in the spectral region of 6500 – 5000 cm^{-1} shows similar R^2X cumulative values using two PLS factors (R^2X

[2PLS factors] = 0.998). **Figure 37** and **Figure 38** shows the PLS loading weights line plot for the models performed in the spectral region of 6500 – 5000 cm^{-1} using SNV + 1st derivative and second derivative respectively. Figures ## show, the first and second loading weight (w*c[1] and w*c[2]) represent the changes in the amount of polymer into the schemes. However, the model using second derivative shows clearly the changes in the amount of polyethylene with the first loading weight (w*c[1]) and the changes n the amount of polypropylene with the second loading weight (w*c[2]).

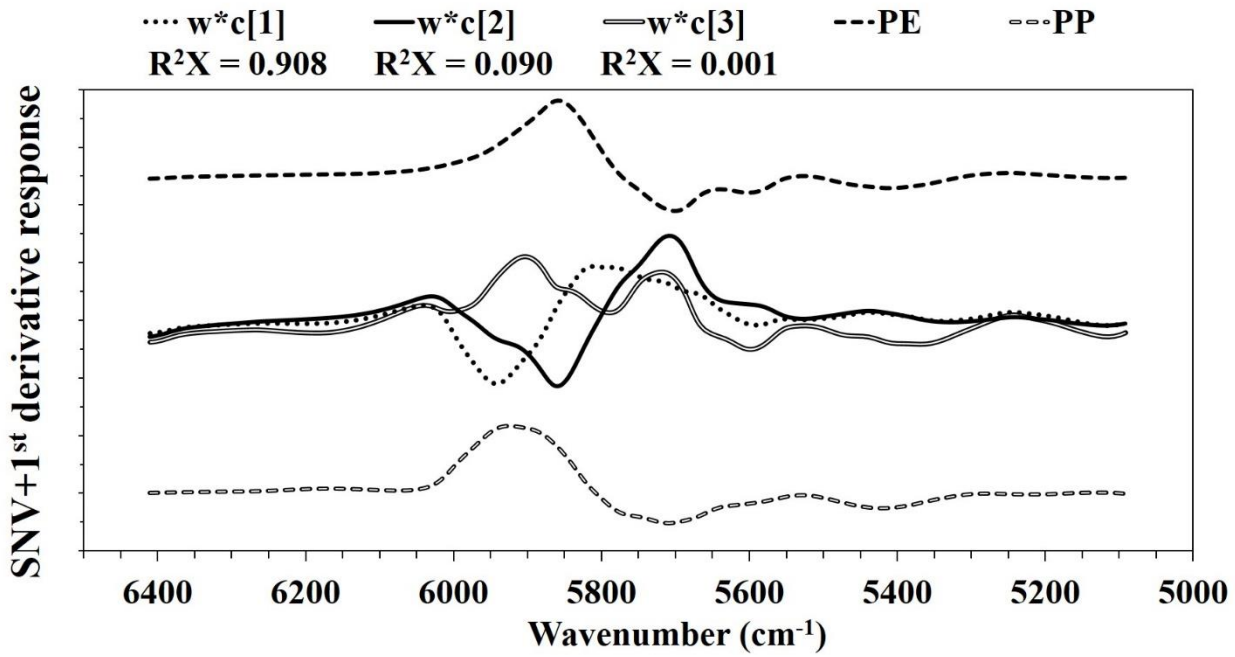

Figure 37. PLS loading-weights line plot performed on the 6500-5000 cm^{-1} spectral region using the SNV + 1st derivative (25 points) for preprocessing.

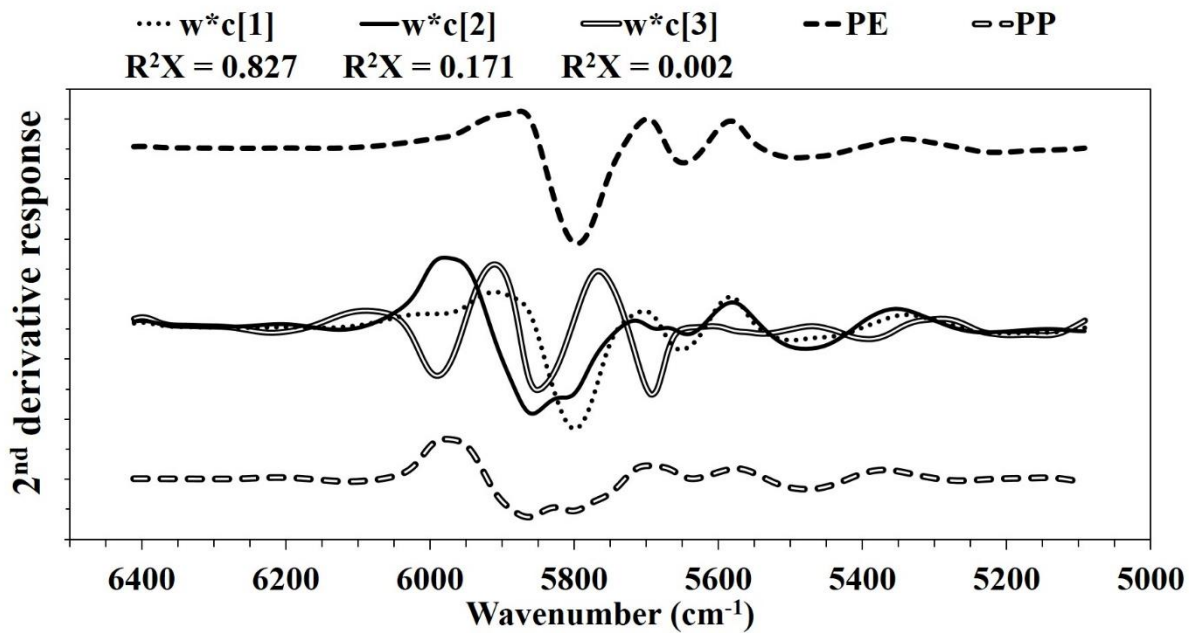

Figure 38. PLS loading-weights line plot performed on the 6500-5000 cm^{-1} spectral region using the second derivative (25 points) for preprocessing.

3.3.4. Statistical evaluation using the ANOVA method

The results were further evaluated by ANOVA according to the evaluation by PCA and PLS regression in the NIR spectral regions (9500 – 6500 cm^{-1} and 6500 – 5000 cm^{-1}). Before the analysis, the results were divided in two groups by the two spectral regions and the assumptions of the model were reviewed with the residual plots for each group (**Figure 39**). In both cases, the factors of interest with their respective levels were: the %PE composition of polyethylene (1–10 levels), the different schemes for arrangement of the polymer films (1–6), the NIR instrument used for spectral acquisition (NIR1 and NIR2), the spectral preprocessing (2^{nd}der and SNV+1^{st}der), and the validation on three different days (Val1, Val2, and Val3) was used like a block. The response variable was the residual between the reference value and the estimated values by the model with the different factor levels. The residuals presented a well adeacuacy of the model in both regions;

however, the normality and constant variance assumptions are more stable in the residuals of the 6500 – 5000 cm^{-1} spectral region.

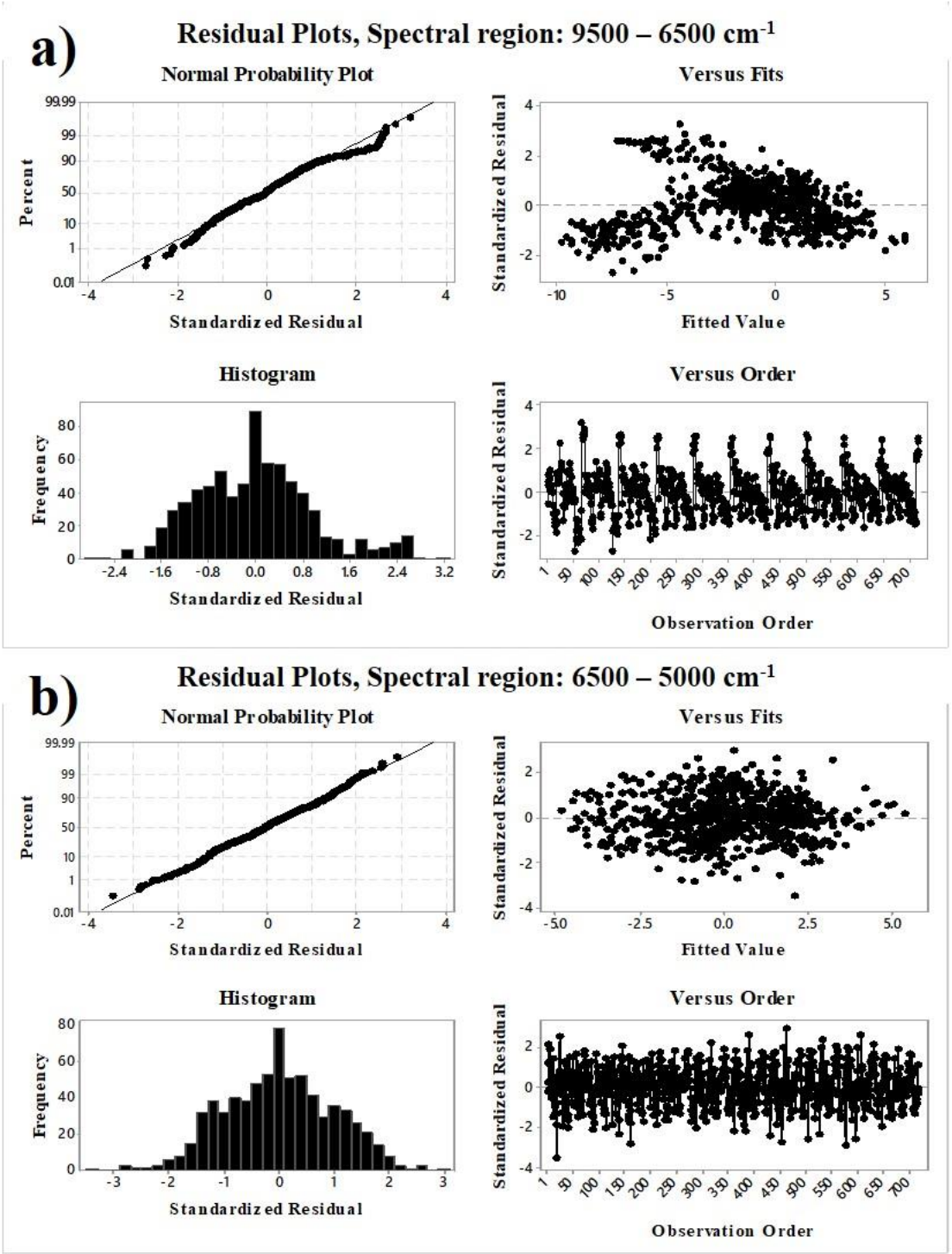

Figure 39. Residuals plot: normal probability, versus fit, histogram, and versus order performed on the spectral regions: a) 9500-6500 cm^{-1} and b) 6500-5000 cm^{-1}.

The results of the ANOVA are presented in **Table 19** for the evaluation in the spectral region 9500 – 6500 cm^{-1} and **Table 20** for the evaluation in the spectral region 6500 – 5000 cm^{-1}. The result in the spectral region of 9500 – 6500 cm^{-1} showed that all the main factors were statistically significant (p-values < 0.05). The main factors: the spectral acquisition scheme and the NIR instrument were not statistically significant in the spectral region of 6500 – 5000 cm^{-1} (p-values > 0.05). In summary, the level of the different main factors did not affect the result of the residuals significantly in the spectral region of 6500 – 5000 cm^{-1}; while residuals in the spectral region of 9500 – 6500 cm^{-1} were affected by changes in the levels of the main factors. These results showed that using the spectral region of 6500 – 5000 cm^{-1} provided NIR predictions with low residuals values that follow a normal distribution.

Table 19. ANOVA results for the spectral region of 9500 – 6500 cm^{-1}.

Source	**DF**	**Adj SS**	**Adj MS**	**F-value**	**p-value**
Val	2	917.2	458.60	62.90	0.000
%PE	9	865.3	96.15	13.19	0.000
Scheme	5	212.6	42.52	5.83	0.000
NIR	1	857.7	857.71	117.64	0.000
Preprocessing	1	3332.9	3332.86	457.12	0.000
*%PE *Scheme*	45	54.7	1.22	0.17	1.000
*%PE *NIR*	9	158.4	17.60	2.41	0.011
*%PE *Preprocessing*	9	43.5	4.84	0.66	0.742
*Scheme*NIR*	5	68.9	13.77	1.89	0.094
*Scheme*Preprocessing*	5	47.5	9.49	1.30	0.261
*NIR*Preprocessing*	1	1022.7	1022.71	140.27	0.000
Error	627	4571.4	7.29		
Total	719	12152.8			

Table 20. ANOVA results for the spectral region of 6500 – 5000 cm^{-1}.

Source	DF	Adj SS	Adj MS	F-value	p-value
Val	2	60.51	30.25	10.35	0.000
%PE	9	251.19	27.91	9.55	0.000
Scheme	5	27.82	5.56	1.90	0.092
NIR	1	0.10	0.10	0.03	0.856
Preprocessing	1	281.39	281.39	96.29	0.000
*%PE *Scheme*	45	84.60	1.88	0.64	0.967
*%PE *NIR*	9	23.55	2.62	0.90	0.529
*%PE *Preprocessing*	9	484.23	53.80	18.41	0.000
*Scheme*NIR*	5	117.56	23.51	8.05	0.000
*Scheme*Preprocessing*	5	60.71	12.14	4.16	0.001
*NIR*Preprocessing*	1	1042.38	1042.38	356.71	0.000
Error	627	1832.23	2.92		
Total	719	4266.27			

Based on the results evaluated by PCA, the error of the NIR predictions and the statistical evaluation by ANOVA, the calibration model in the spectral region of 6500 – 5000 cm^{-1} using second derivative (25 points) as spectral preprocessing was selected for the evaluation on both NIR instruments to demonstrate the performance of the method and the reliability of the analytical results. The findings in this study shows the lack of systematic error of a NIR method by PLS regression after a careful evaluation of the spectral regions, spectral preprocessing, and a statistical evaluation of the results. The use of low heterogeneous materials provides a simple system to test the reproducibility of a calibration method in two different NIR instruments with low error and bias due to material's heterogeneity and spectral differences between the instruments.

3.4. **CONCLUSIONS OF CHAPTER 3**

PLS models developed with a FT-NIR spectrometer using two polymers materials with similar thickness (polypropylene and polyethylene) presented high accuracy and precision for validation samples acquired with the first instrument and samples acquired in a second FT-NIR spectrometer in another laboratory. Calibration models in the spectral region of 9500 – 6500 cm^{-1} based on a previous study using second derivative (25-points) and SNV + 1^{st} derivative (25-points) shows high accuracy and precision in the validation samples of the first instrument; however, the predictions of the NIR spectra of the validation samples acquired with the second instrument presented a systematic error with high bias. Therefore, the statistical values of three prediction sets, the PCA, and the loading weights of the PLS models were evaluated in a second spectral region, 6500 – 5000 cm^{-1}.

The prediction errors of the PLS models in the second spectral region (6500 – 5000 cm^{-1}) showed lower values compared to the results in the spectral region of 9500 – 6500 cm^{-1} based on the spectral preprocessing used in this study, second derivative (25-points) and SNV + 1^{st} derivative (25-points). Loading weights line plot up until three PLS factors showed that first and second loading weight (w*c[1] and w*c[2]) represent the changes in the amount of polymer into the schemes. Further statistical evaluation needs to be performed to select a robust PLS model that can be used in different NIR instruments.

CHAPTER 4: DEVELOPMENT OF NEAR INFRARED SPECTROSCOPIC CALIBRATION MODELS FOR IN-LINE DETERMINATION OF LOW DRUG CONCENTRATION, BULK DENSITY, AND RELATIVE SPECIFIC VOID VOLUME WITHIN A FEED FRAME

Based on Publication in: *Journal of Pharmaceutical and Biomedical Analysis* 164 (2019) 211–222.

Carlos Ortega-Zúñiga, Carlos Pinzón-De la Rosa, Andrés D. Román-Ospino, Alberto Serrano-Vargas, Rodolfo J. Romañacha, Rafael Méndez.

This chapter is not an exact copy of the published paper. It contains original information.

4.1. INTRODUCTION

A number of Process Analytical Technology (PAT) methods have been focused on understanding blending processes and obtaining adequate blend uniformity (Gupta et al., 2005; Pestieau et al., 2014; Skibsted, Westerhuis, Smilde, & Witte, 2007). The implementation of these analytical methods in pharmaceutical manufacturing processes with low concentration of API is challenging due to powder flow properties such as segregation. The limit of quantification of the spectrometer used for monitoring the formulation could also be a limiting factor (Beach et al., 2010; D. Ely, Chamarthy, & Carvajal, 2006). However, the implementation of near infrared (NIR) spectroscopy in combination with chemometrics and sampling strategies have provided excellent results for formulations with low concentration of API. The applicability of NIR spectroscopy for real time measurement in the compression machine, more specifically on the tableting feed frame section has increased (Mateo-Ortiz, Colon, Romañach, & Méndez, 2014; Mendez, Muzzio, & Velazquez, 2010; Mendez, Muzzio, & Velazquez, 2012; Wahl et al., 2014; Ward, Blackwood, Polizzi, & Clarke, 2013). The feed frame is chosen because it is the most representative stage measurement

of API concentration possible before the final product. The operational conditions of the feed frame (paddle and die disk speed) have been demonstrated to affect the material properties of the powder blends, and in turn the final product quality (Mateo-Ortiz et al., 2014). Furthermore, changes in the physical properties of the blends due to shear stress (Hernandez et al., 2016), over-mixing (Igne, Talwar, Drennen, & Anderson, 2013), or over-lubrication (Igne et al., 2013) are some of the problems that can arise from challenging process conditions in pharmaceutical manufacturing.

Changes in physical properties of the materials due to the process within the feed frame (powder density, particle size, flowability, cohesivity), have shown a significant effect on the NIR spectra, therefore in predictions of the calibration model (Sierra-Vega et al., 2018). The determination of the API concentration by NIR spectroscopy is difficult for low concentrations in the formulation, since spectral preprocessing cannot eliminate completely the effects of the physical properties of materials on the NIR spectra (Hernandez et al., 2016; Igne et al., 2013; Singh, Román-Ospino, Romañach, Ierapetritou, & Ramachandran, 2015). The characterization of pharmaceutical materials within a feed frame using various spectroscopic techniques has been recently studied by several groups to evaluate flowability, drug concentration, content uniformity, segregation, potency in tablets, and composition of powder blends. **Table 21** provides a summary of recent studies using spectroscopic techniques in combination with chemometrics for quantitative determinations of pharmaceutical materials within a feed frame. **Table 21** also describes several conditions that affect the analysis using a spectroscopic technique. The powder dynamics within the feed frame can be significantly affected at lower paddle wheel speed which impacts the sample presentation to the sensor (Ward et al., 2013). The physical position of the probe sensor (working distance, measurement angle and location) is also an issue that has an impact on the analysis

because it significantly affects the interaction of the radiation with the particles in the powder blends (Šašić et al., 2015). Changes in paddle wheel speed significantly affects the wave behavior of the system, but the mass hold-up remains constant. Also, changes in the die disc speed affect considerably the mass hold-up, increases the speed the mass hold-up decreases, but the wave remains constant (Sierra-Vega et al., 2018).

This study describes advances in the real-time determination of drug concentration within a feed frame. A NIR calibration model was developed to determine the concentration of API at 3.00 %w/w. The calibration model was developed with a design that included a high variability of major excipients complementing a previous work that used minor variations of the excipients (Sierra-Vega et al., 2018). The calibration design facilitates the evaluation of powder density and porosity of the blends based on NIR calibration spectra. This study presents the first NIR calibration models to determine powder density and relative specific void volume for blends at low API concentrations within the feed frame. The powder density of the blends can be used to control tablet weight and therefore the content uniformity of the drug can be controlled in the die filling process in the feed frame. This work also contributes to the understanding of powder dynamics within the feed frame. Studies shows that the implementation of probe sensors for monitoring blending process facilitates the understanding powder dynamics which in practice are complex to evaluate by theoretical arguments and computational tools (**Table 21**) (Koller et al., 2011). The location of the probe sensor requires a priori knowledge of the process and the physics of the materials as shown in **Table 21**. However, working with several disciplines facilitates the analysis of the results obtained by NIR, chemometrics and computational tools to understand powder dynamics, physical properties and flow properties of the powder blends in pharmaceutical

manufacturing process. This is basically, the application of PAT in pharmaceutical industry as a process understanding, control, and risk-based approach (Dickens, 2010).

Table 21. Studies using spectroscopy and chemometrics for quantification purposes within a feed frame

Reference	Method*	Purpose	Challenge
Liu Y. and Blackwood D. (2012) (Yang & Daniel, 2012, May 1)	NIR.	Powder blend monitoring using NIR spectroscopy with chemometrics.	Dynamic of powder flow. Sample presentation. Distance of NIR probe.
Ward H.W. et al. (2013) (Ward et al., 2013)	NIR.	Monitor the powder composition circulating using NIR spectroscopy following the derivative intensity of API band vs time.	Mass throughput rate. Low paddle wheel rotational speed causes bias between weight corrected results and NIR signal.
Mateo-Ortiz D. et al (2014) (Mateo-Ortiz et al., 2014)	NIR.	Off-line and in-line calibrations of API at 5 to 15 %w/w to monitor die filling process and understand powder behavior within the feed frame	Powder accumulation on right window would represent a false signal because is analyzed the same portion of the material. Off-line calibration did not incorporate powder dynamics within the feed frame.
Wahl P.R., et al (2014) (Wahl et al., 2014)	NIR	In-line API monitoring of powder blends during manufacturing using Partial Least Squares (PLS) model of lab spectra transferred via local centering.	Stochastic segregation in hopper feeding at 12-30% LC of API. Critically at the end of process probably caused by segregation.
Šašić S. et al. (2015) (Šašić et al., 2015)	NIR.	Determination of API in powder blends at 3.5 %w/w using univariate analysis via 2nd derivative spectra assessing by PCA as further information.	Physical position of NIR probe within the feed frame causes differences in baseline spectra.
Gosselin R. et al. (2017) (Gosselin, Durão, Abatzoglou, & Guay, 2015)	LIFS, NIR, RGB color imaging.	Monitoring change in concentration of multicomponent system of three API (vitamins) using three spectroscopic tools triggered by a sensor to avoid interference between them.	Dynamics perceived by each probe varying powder composition.
Durão P. et al. (2017) (Durão, Fauteux-Lefebvre, Guay, Abatzoglou, & Gosselin, 2017)	LIFS, NIR, RGB color imaging.	Monitoring a multicomponent system of five API (vitamins) using three spectroscopic tools.	4 of the 5 vitamins could be monitored by at least one of the tools according to their physical characteristics and concentrations.
Hetrick E.M. et al. (2017) (Hetrick et al., 2017)	NIR.	Design an offline approach to mimic the full process allowing more source of variability to include in the calibration and minimizing the consumption of API and other raw materials.	Use of narrow wavelength range to increase the sensitivity of the model for the API.

Li Y. et al. (2018) (Li, Anderson, Drennen, Airiau, & Igne, 2018)	Raman.	Development and validation according to ICH-Q2 for inline and offline calibration to determine the blend content during tablet compression.	Offline modeling accurate of predicting inline data after bias correction.
De Leersnyder F. et al. (2018) (De Leersnyder et al., 2018)	NIR.	Monitoring powder blends with two different API target concentrations: 5 and 20 %w/w.	Effect of paddle wheel fingers on powder blend to avoid disturbances in NIR signal. Effect of filling degree on NIR spectra. Lower paddle speed caused more variation in predictions.
Sierra-Vega N.O. et al. (2018) (Sierra-Vega et al., 2018)	NIR.	Determination of drug concentration in 3 %w/w API in powder blends with low changes in excipient composition by NIR spectroscopy and PLS regression. Evaluation of robustness of the NIR calibration with changes of 10% and 20% of nominal paddle wheel speed. Variographic analysis to characterize sampling unit.	Changes in paddle wheel speed significantly affects the wave behavior of the system (frequency and amplitude), but the mass hold-up remains constant. Changes in the die disc speed affect considerably the mass hold-up, increases the speed the mass hold-up decreases, but the wave remains constant.

* NIR: Near Infrared, LIFS: Light-Induced Fluorescence Spectroscopy, RGB: Red Green Blue.

4.2. **MATERIALS AND METHODS**

4.2.1. Materials

Acetaminophen USP/paracetamol ph Eur semi-fine powder (APAP) from Mallinckrodt (Raleigh NC USA) was used as active pharmaceutical ingredient (API). Vivapur 102 microcrystalline cellulose PH. (MCC) from JRS Pharma LP (USA) and Tablettose 70 agglomerated lactose monohydrate PH. EUR/USP-NF/JP (Meggle Excipients & Technology, Wasserburg, Germany) were used as main excipients. Colloidal silicon dioxide (SiO_2) from Acros Organics was used to improve flow properties and magnesium stearate NF (MgSt) non-bovine from Mallinckrodt Inc. (Saint Louis, MO, USA) was used as lubricant.

4.2.2. Preparation of calibration and test set blends

The formulation components were added in layers to a 16-quart Patterson Kelley stainless steel crossflow v-blender system. Two layers of lactose monohydrate were placed in the bottom and upper part of the blender, while MCC, APAP and SiO_2 were placed in the middle. Blends are initially mixed at 15 RPMs for 60 minutes, MgSt was added afterwards and mixed for an additional 4 minutes to avoid over-lubrication effects. After blending, samples were stored in sealed plastic bags and used for the feed frame experiments within the next 24 hours. The composition of the blends is described in **Table 22**. This calibration design includes a high variability of major excipients complementing a previous work that used minor variations (Sierra-Vega et al., 2018) which facilitates the evaluation of powder density and relative specific volume of the blends based on NIR calibration spectra.

Table 22. Composition of calibration blends and test set blends

Blend	APAP (%w/w)	MCC (%w/w)	Lac (%w/w)	SiO_2 (%w/w)	MgSt (%w/w)
	Calibration Blends				
Cal 1	1.50	15.15	81.95	0.50	0.90
Cal 2	2.50	36.42	59.53	0.50	1.05
Cal 3	3.50	59.41	35.50	0.50	1.09
Cal 4	4.50	81.08	12.92	0.50	1.00
	Test Set Blends				
TS 1	3.00	47.75	47.75	0.50	1.00
TS 2	3.00	24.76	70.74	0.50	1.00
TS 3	3.00	41.04	54.46	0.50	1.00
TS 4	3.00	54.90	40.60	0.50	1.00

4.2.3. Characterization of powder blends

Bulk, tap, and true density (gas pycnometer) were characterized for all calibration and test set blends. A graduated cylinder and Rice Lake TA-120 analytical balance was used to determine bulk density. A VanKel Varian Tap density tester was used to apply 500 taps for tap density

measurements. An AccuPyc II 1340 gas displacement pycnometer (Micromeritics, Norcross, GA) was used to measure the true density from 2.0 grams of powder sample in a 10 cm^3 sample cell, and ultra-pure Helium (99.999%) from Praxair. A total of 10 purge and testing cycles at a final pressure of 19.5 psig were used for the analysis at a feed rate of 0.005 psig/min to avoid disturbing the powder sample.

4.2.4. Particle size distribution (PSD)

The particle size distribution (PSD) of raw materials and blends collected after the feed frame experiments were obtained with the Malvern Insitec Analyzer (Malvern Instruments Model IDC2000). Ten grams of each sample was analyzed three times and the PSD was reported as an average value for D10, D50 and D90.

4.2.5. Instrumentation and acquisition of NIR spectra

A Matrix-F FT-NIR spectrometer from Bruker Optics (Billerica, MA, USA) was used for near infrared spectral acquisition of the calibration and test set blends. Spectral acquisition parameters were set at 16 scans per sample, 64 scans for background, and 16 cm^{-1} of resolution. NIR spectra were obtained approximately every 5 seconds. Opus 7.2 software and its feature "Control Process" was used to control the NIR instrument and for automatic continuous data acquisition during each measurement. During the experimental runs, a significant amount of spectral data was obtained (more than 100 spectra per blend).

All NIR spectra were obtained for flowing powders within a tablet press hopper, a standard feed frame taken from a Fette 3090 tablet press as shown in **Figure 40**, and an in-house high-density polyurethane rotating die disk. The Fette 3090 feed frame is a multistage/multi-blade system, with

three blades, one at the top which reduces the consolidation of the powder material entering the feed frame, and two other blades. The polyurethane die disk consists of 36 dies of 10 mm diameter and is mounted on a rotating DC gear motor which allow to rotate the disk in counter and clockwise direction at controlled RPMs.

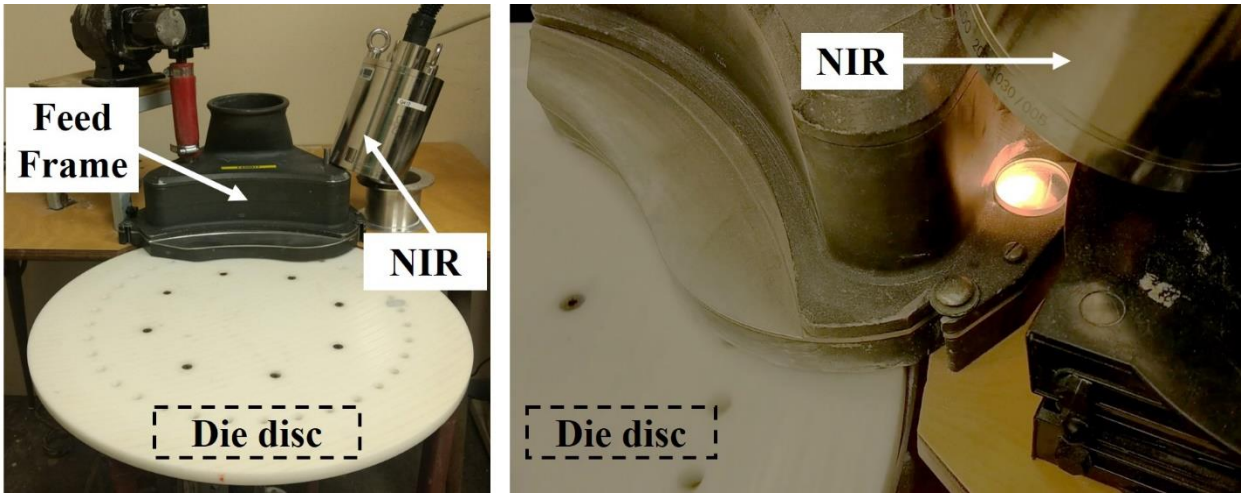

Figure 40. Fette 3090 feed frame assembly with the die disk and NIR probe.

The calibration and test set powder blends were fed into the Fette 3090 tablet press feed frame using the tablet press hopper and the attached pipe. The NIR probe was installed outside the left window on top of the feed frame. This location was selected because no stagnant material is observed on this location, and the powder flow is uniform during the experiments (Mateo-Ortiz et al., 2014). Similar observations were made in a previous study, where the effect of paddle height and the gap between paddles and the bottom part of the device was evaluated (Mateo-Ortiz et al., 2014). This study showed that the lower paddle height forces the material to pass above the paddles reducing the accumulation of the powder in the left window location. The original plastic feed frame window was replaced by a custom-made sapphire window with 30.10 mm of diameter, and

a total thickness of 10.10 mm from Guild Optical Associates, (Amherst, NH). NIR spectra were obtained through this sapphire window.

The feed frame was turned-on for the material to distribute within the feed frame and between the blades. NIR spectra of the powder material within the feed frame were acquired prior to each experimental run to ensure the optimal probe position. After setting the probe, the feed frame and rotating disk were turned-on until the system achieves steady-state. NIR spectra were acquired after the powder throughput reached steady state. Experiments were performed at 30 RPM's for feed frame and die disk rotation.

4.2.6. Development of multivariate calibration models

NIR spectral preprocessing, Principal Component Analysis (PCA) and Partial Least Squares (PLS) regression models were developed with SIMCA 15 software (Sartorious Stedim Data Analytics Solutions, Umeå, Sweden). Two different spectral regions based on APAP absorption bands were evaluated during the development of the calibration model, as well spectral preprocessing such as standard normal variate (SNV), first and second derivatives (1st der, 2nd der), and combinations of SNV with derivatives. Model performance was evaluated calculating root mean square error of prediction (RMSEP), the relative standard errors of prediction (RSEP (%)), bias, and standard deviation defined as:

$$RMSEP = \sqrt{\frac{\sum_{i=1}^{n}(\hat{y}_i - y_i)^2}{n}} \quad (1)$$

$$RSEP(\%) = 100 \times \sqrt{\frac{\sum_{i=1}^{n}(\hat{y}_i - y_i)^2}{\sum_{i=1}^{n}(y_i)^2}} \quad (2)$$

$$Bias = \sum_{i=1}^{n} \frac{(\hat{y}_i - y_i)}{n} \quad (3)$$

where n is the number of samples in the validation set, the $\hat{y}_i$ and y_i are the predicted and reference concentration values of the sample in validation.

4.3. **RESULTS AND DISCUSSION**

4.3.1. Development of calibration model

Figure 41 shows all NIR spectra obtained in a single feed-frame experiment. The first 20 spectra were obtained in the first 90 seconds of the experiments. These spectra were affected by low mass hold-up within the feed frame resulting in a high baseline (the lower the mass hold-up the farthest the powder from the NIR probe). Calibration models were developed using spectra obtained after mass steady state (# 21 – 80). After the 80 spectra the baseline increases as the mass hold-up inside the feed frame begins to decrease indicating that the system is operating outside of mass steady state.

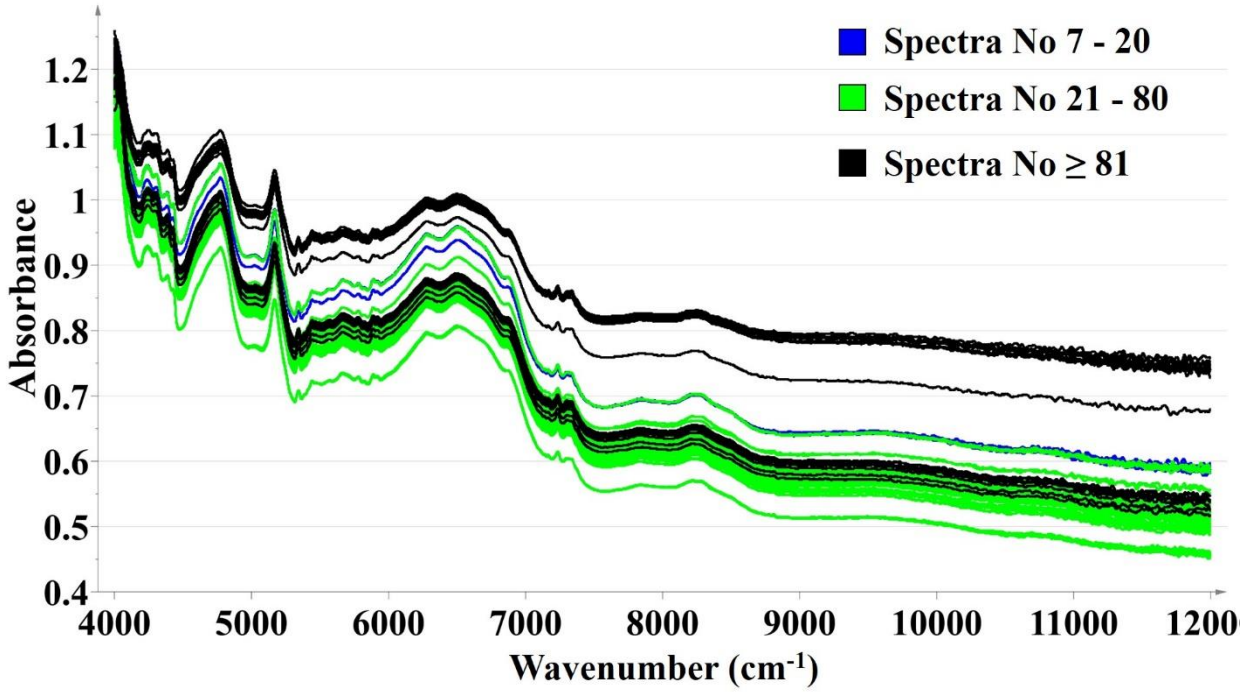

Figure 41. NIR spectra obtained during a full experimental run. Black line for the NIR spectra obtained during the first 90 seconds. Gray line for the NIR spectra during the steady state process. Light gray dashed line for the NIR spectra obtained after the steady state process.

Figure 42 shows the averaged second derivative spectra of the 1.50 and 4.50 (%w/w) blends in the 7600 – 4177 cm^{-1} spectral range where the major spectral differences were observed. Important API bands were observed from 7420 – 7125 cm^{-1} and 5580 – 5220 cm^{-1} (close up windows). The region at higher wavenumbers contains bands with moderate intensity and more energy which implies more penetration of the radiation than the bands located at the lower wavenumbers which has more intensity, but the radiation penetrates less (Iyer et al., 2002). The observation of these spectral differences is essential for the development of a PLS calibration model, where a mathematical relationship is obtained between spectral changes and API concentration.

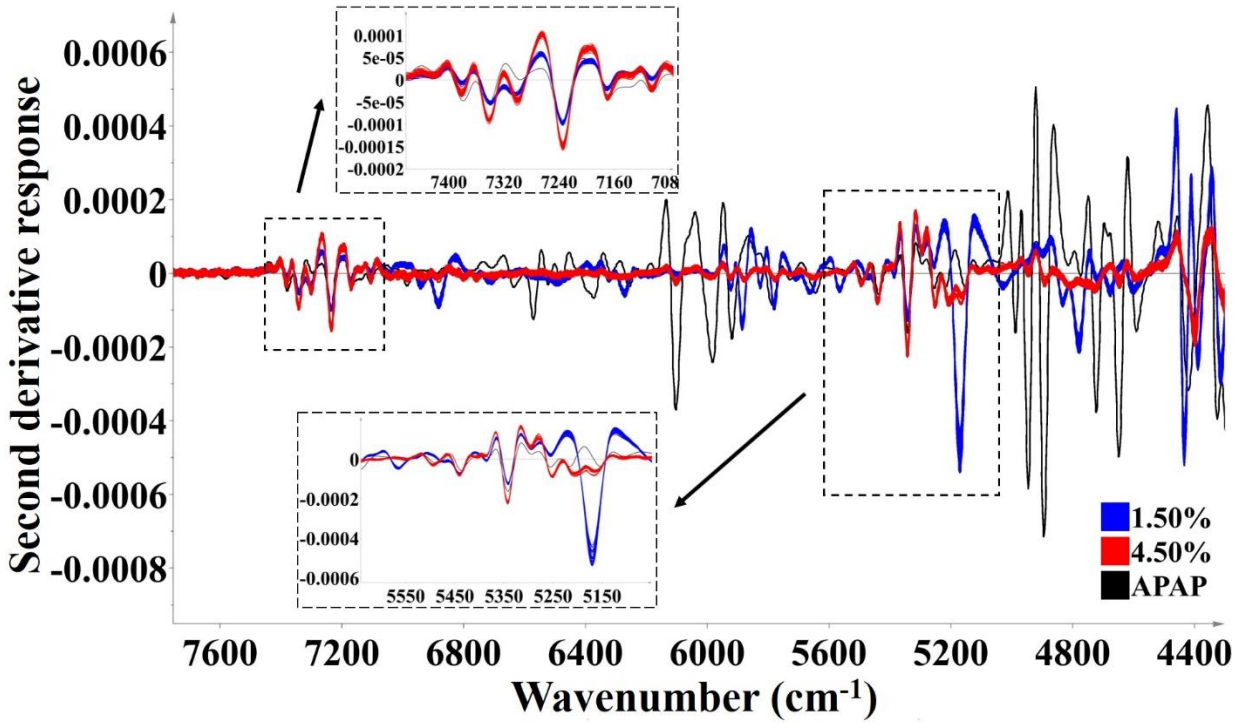

Figure 42. Second derivative (25 points) NIR spectra for calibration blends with 1.50 and 4.50 (%w/w) of API (Acetaminophen) in the spectral region 7600 – 4200 cm^{-1} (close up regions 7420 – 7125 cm^{-1} and 5580 – 5220 cm^{-1}).

Figures 28 to 33 shows the PCA score plots of the NIR spectra for the calibration blends in the spectral region of 7600 – 4177 cm^{-1} using spectral preprocessing. **Figure 43** shows the PCA of the calibration without preprocessing; the spectra of the samples are not distributed by concentration level. **Figure 44** shows the PCA of the calibration with SNV preprocessing. The explained variance is 83.3% in the first principal component and 1.36% in the second component. The samples are distributed by concentration level of the API along the first component and show variations in the second component distributed by changes in concentration of the major excipients. The PCA scores plot of the calibration blends with 1.5 and 4.5 (%w/w) of APAP, present the higher concentration of one of the major excipients (MCC or lactose) as shown in **Table 22**. The scores of these samples are aligned in the same direction of the second component as shown the PCA of the different spectral preprocessing used. **Figure 45** and **Figure 46** shows

the PCA plots using first and second derivative (25-point window) respectively. The use of the derivative preprocessing of the NIR calibration spectra provides an explained **X** variance higher than the obtained using SNV preprocessing, up to 95.5% in the first principal component with the use of second derivative. The samples are separated by concentration level along the first component and the variation in the second component is lower with the use of second derivative (1.26% of the explained variance). **Figure 46** shows all the samples are within and the plots are distributed by clusters of concentration level with the use of second derivative (25-point). **Figure 47** and **Figure 48** shows the PCA using SNV+1st and SNV+2nd derivative (25-point window), with the samples distributed along the first principal component with 91.1% and 89.5% of the explained **X** variance respectively. The explained **X** variance of the first component is slightly lower than the variance with the second derivative preprocessing. In summary, the PCA plots of the calibration spectra shows a distribution pattern separated by concentration level in the first principal component, indicating that this spectral variation could be used to develop a PLS calibration model to determine the concentration of APAP in the range of 1.50 to 4.50 (%w/w) in powder blends within the feed frame.

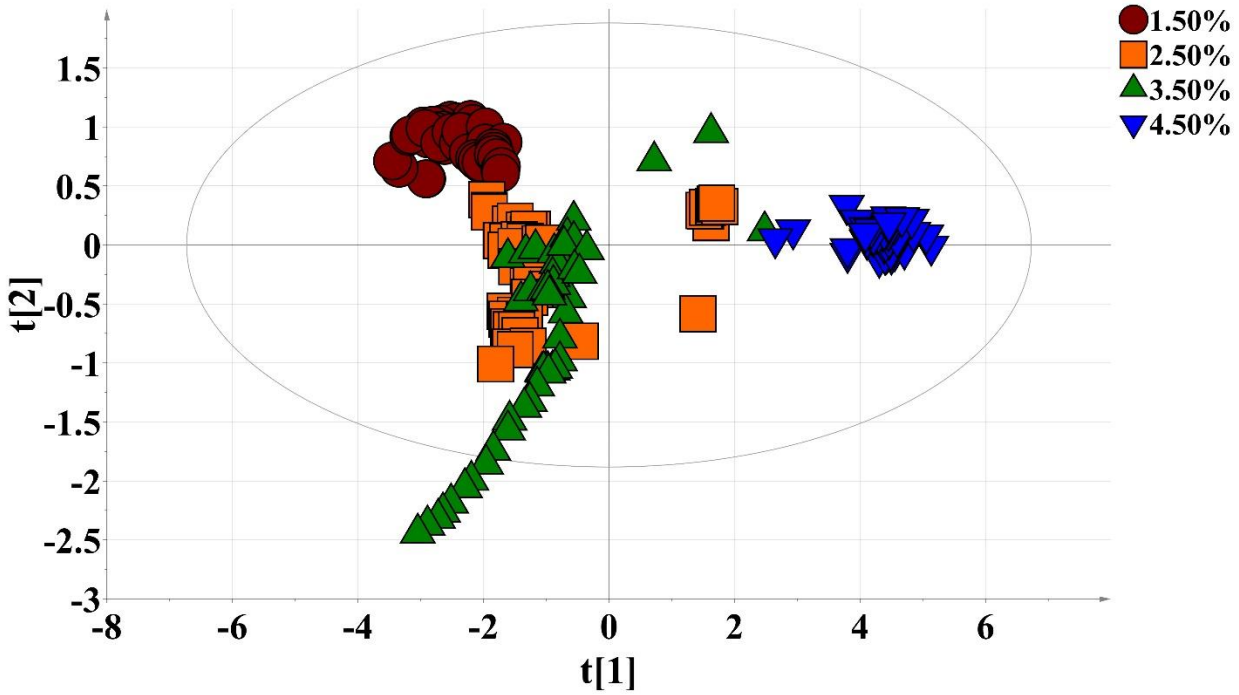

Figure 43. PCA score plots of the NIR spectra for calibration blends with 1.50, 2.50, 3.50, and 4.50 (%w/w) of API (acetaminophen) in the spectral region 7600 – 4200 cm^{-1} without spectral preprocessing.

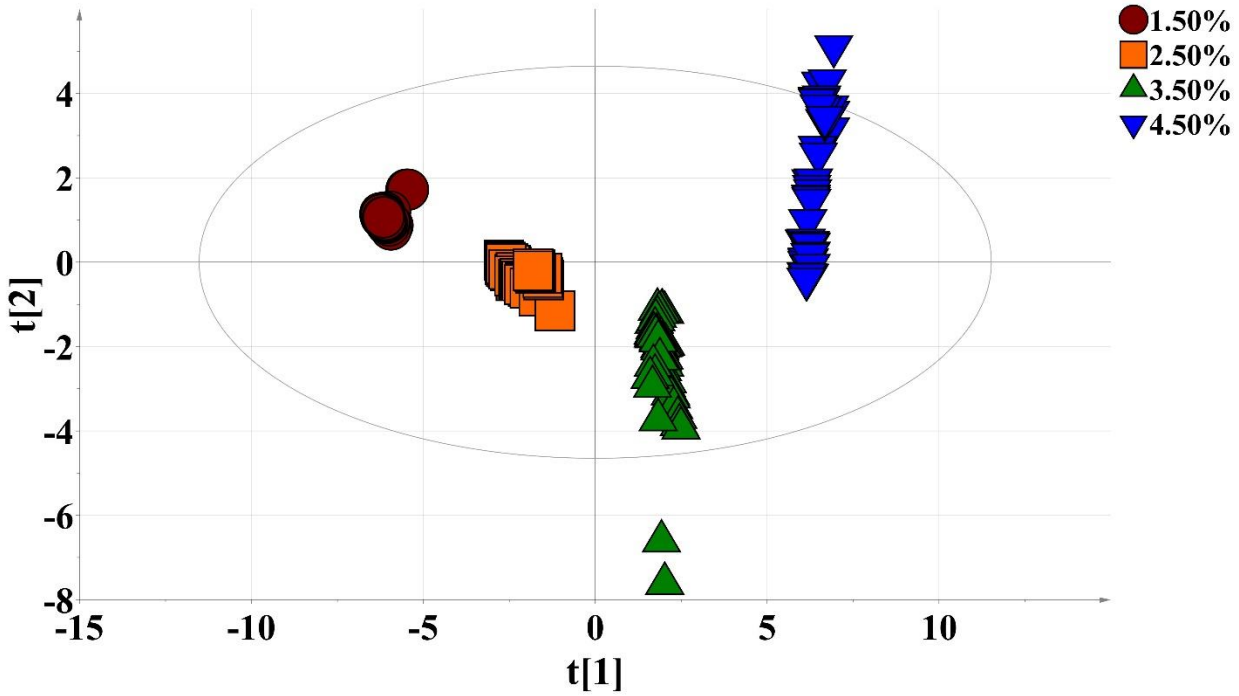

Figure 44. PCA score plots of the NIR spectra for calibration blends with 1.50, 2.50, 3.50, and 4.50 (%w/w) of API (acetaminophen) in the spectral region 7600 – 4200 cm^{-1} with spectral preprocessing SNV.

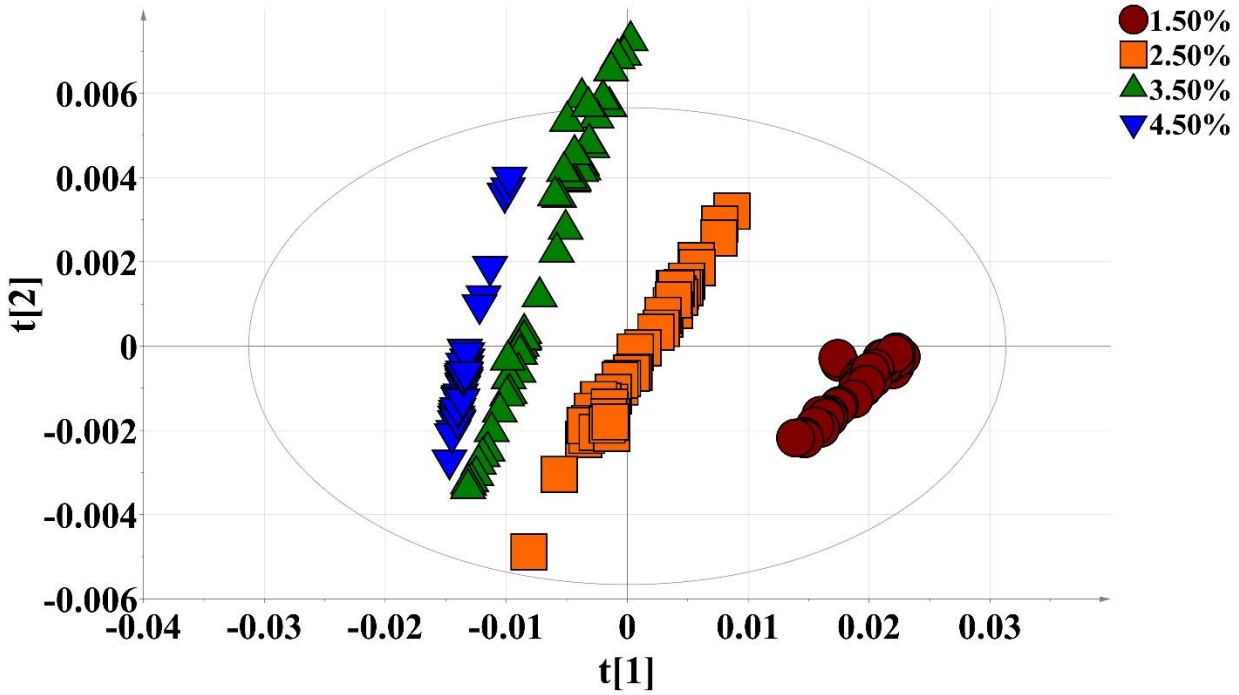

Figure 45. PCA score plots of the NIR spectra for calibration blends with 1.50, 2.50, 3.50, and 4.50 (%w/w) of API (acetaminophen) in the spectral region 7600 – 4200 cm^{-1} with spectral preprocessing 1st derivative 25-point window.

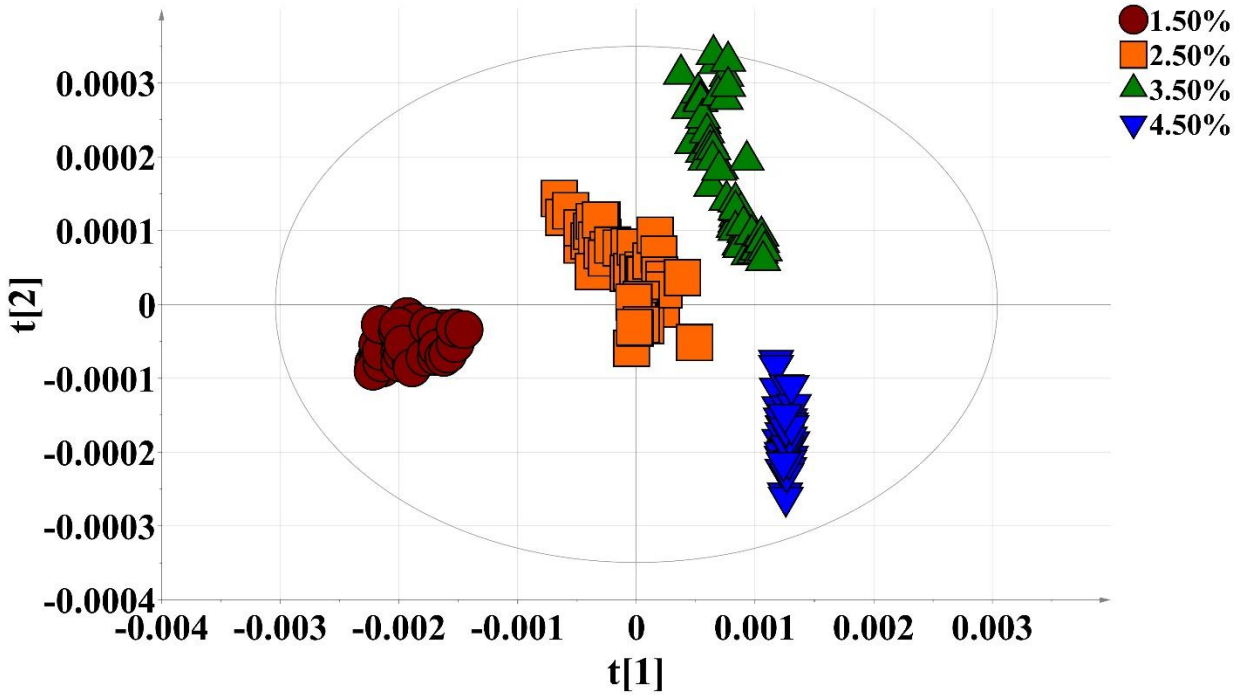

Figure 46. PCA score plots of the NIR spectra for calibration blends with 1.50, 2.50, 3.50, and 4.50 (%w/w) of API (acetaminophen) in the spectral region 7600 – 4200 cm^{-1} with spectral preprocessing 2nd derivative 25-point window.

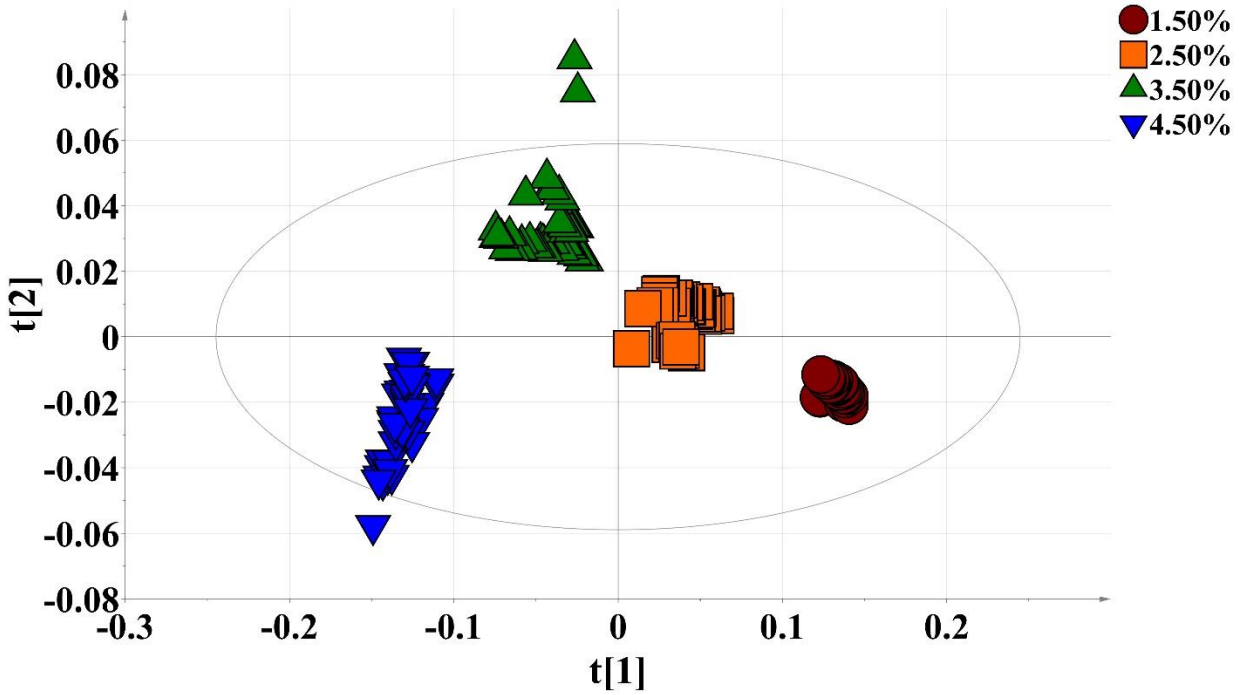

Figure 47. PCA score plots of the NIR spectra for calibration blends with 1.50, 2.50, 3.50, and 4.50 (%w/w) of API (acetaminophen) in the spectral region 7600 – 4200 cm^{-1} with spectral preprocessing SNV+1st derivative 25-point window.

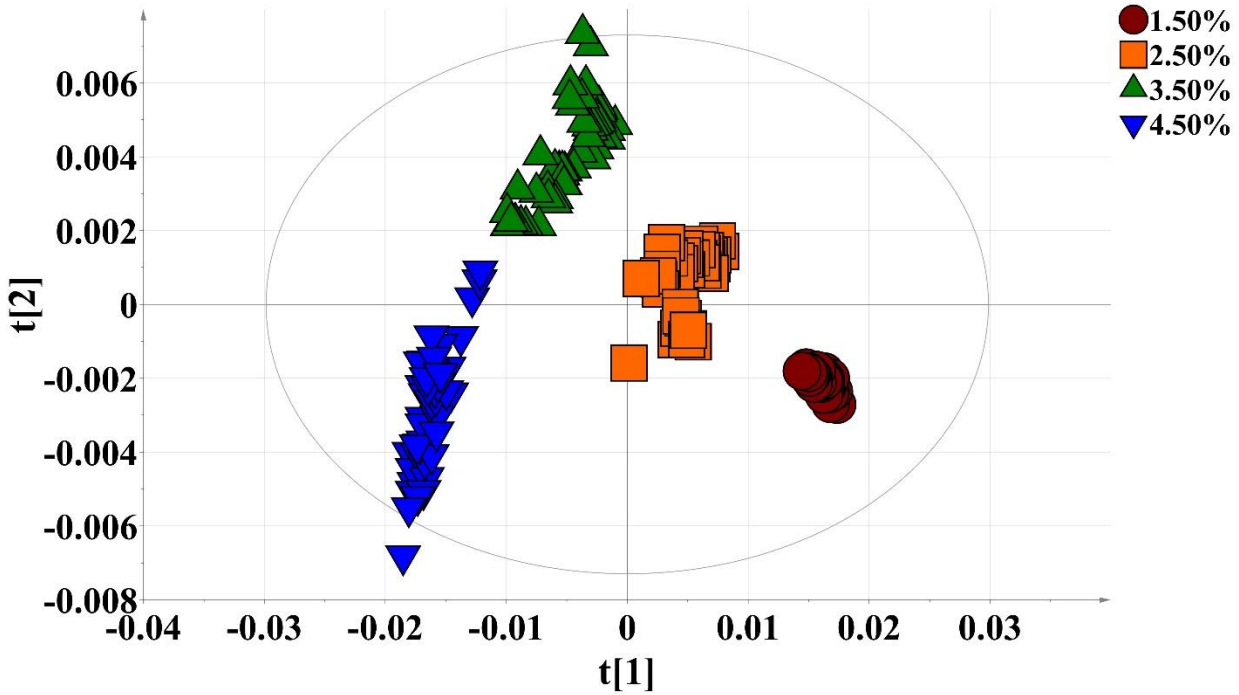

Figure 48. PCA score plots of the NIR spectra for calibration blends with 1.50, 2.50, 3.50, and 4.50 (%w/w) of API (acetaminophen) in the spectral region 7600 – 4200 cm-1 with spectral preprocessing SNV+2nd derivative 25-point window.

4.3.2. Prediction of test set blends

Table 23 shows the figures of merit of calibration models developed within the 7600 – 4177 cm^{-1} and 5446 – 4779 cm^{-1} spectral regions based on the prediction of test set blends. These spectra were obtained after steady state was achieved within the feed frame. The effectiveness of the models was evaluated by predicting independent test set blends prepared as described in **Table 22**. Test set blend 1 had equal proportions of the major excipients used in the blend (47.75 % (w/w) each). The figures of merit for test set blend 1 (**Table 23**) show low RSEP(%) and bias regardless of the preprocessing and spectral region that was used. Most of the calibration models provided excellent predictions with only 2 latent variables, and bias that varied from 0.00 to 0.22 (%w/w). The best predictions obtained for test set blend 1 were with calibration model 4 developed in the 7600 – 4177 cm^{-1} spectral region using 2 latent variables and SNV+1st derivative (25 points) as spectral preprocessing. This calibration model provided a bias of -0.01 (%w/w) and RSEP(%) of 2.21 (%w/w). Test set 1 was accurately predicted with practically all the spectral regions and spectral preprocessing described in **Table 23**.

Test set blend 2 was prepared with a greater difference in excipients (24.76 %w/w for MCC and 70.74 %w/w for lactose) as shown in **Table 22**. This variation in excipients for test set 2 is within the range of variations in the composition of calibration blends. Calibration model 4, predicted test set blend 1 with a bias of only -0.01 % (w/w), now predicts test set blend 2 with a bias of -1.15 (%w/w) with 2 latent variables and with an RSEP(%) greater than 38%. The RSEP(%) in the predictions from test set blend 2 are over 30% for several of the calibration models described in **Table 22**. The predictions of test set blend 2 present low accuracy and precision for most of the preprocessing in the spectral regions evaluated in this study, except for second derivative calibration models. The predictions after SNV transformation presented the higher bias and

standard deviation values. The calibration models developed using the 2nd derivative (25 points) provided the best accuracy and acceptable precision for the case of test set blend 2, using three latent variables, in the spectral region of 7600 – 4177 cm^{-1}. The calibration models developed using the 2nd derivative (25 points) were the only models that provided adequate accuracy in the prediction of test set blend 2.

The calibration models were further evaluated through the predictions of test set blends 3 and 4. Test set blend 3 had 41.04 (%w/w) for MCC and 54.46 (%w/w) for lactose, while test set blend 4 had 54.90 (%w/w) for MCC and 40.60 (%w/w) for lactose as shown in **Table 22**. Even though the composition of test set blends 3 and 4 are very similar with minor changes between the excipients, the accuracy and precision are different according to the spectral region and preprocessing used. The results using SNV provided high RSEP(%) values (up to 13.93%) and low accuracy even using three latent variables with bias up to 0.42 (%w/w) from the reference value (3.00 %w/w). The calibration model performed with second derivative in the 7600 – 4177 cm^{-1} spectral region using three latent variables provided a high accuracy and precision for test blend 4 but not for test blend 3. Further evaluation needs to be performed to understand the results of this calibration model.

The results described in **Table 23** shows that there is not a unique calibration model that is capable of predicting the four test set blends with high accuracy and precision. Test set blend 1 is predicted with high accuracy by practically all the calibration models developed. However, the calibration models developed have difficulty in handling the variations observed in the other test set blends. Based on the results obtained in **Table 23**, the evaluation of PLS score plot was performed on the calibration model using 2nd derivative (25-point window) as preprocessing in the 7600 – 4177 cm^{-1} spectral region.

Table 23. Summary of the predictions of an independent 3.00 (%w/w) test set (TS) blend with the developed calibration models. n≥38 spectra

TS blend	RMSEP (%)	RSEP (%)	Average (%w/w)	Bias (%w/w)	RMSEP (%)	RSEP (%)	Average (%w/w)	Bias (%w/w)
	2 Latent variables				***3 Latent variables***			
	Cal model 1: SNV 7600 – 4177 cm^{-1}							
1	0.07	2.26	3.00 ± 0.07	0.00	0.07	2.25	3.02 ± 0.06	0.02
2	1.25	41.51	1.78 ± 0.26	-1.22	1.25	41.70	1.77 ± 0.24	-1.23
3	0.34	11.47	2.66 ± 0.03	-0.34	0.30	10.03	2.70 ± 0.03	-0.30
4	0.36	12.10	3.36 ± 0.03	0.36	0.42	13.93	3.42 ± 0.03	0.42
	Cal model 2: 1^{st} der(25) 7600 – 4177 cm^{-1}							
1	0.22	7.43	3.22 ± 0.05	0.22	0.09	2.84	3.04 ± 0.08	0.04
2	0.77	25.51	2.27 ± 0.23	-0.73	0.32	10.81	2.74 ± 0.19	-0.26
3	0.09	3.14	2.91 ± 0.04	-0.09	0.48	15.90	2.52 ± 0.03	-0.48
4	0.58	19.21	3.58 ± 0.02	0.58	0.12	3.99	3.12 ± 0.03	0.12
	Cal model 3: 2^{nd} der(25) 7600 – 4177 cm^{-1}							
1	0.10	3.39	3.01 ± 0.10	0.01	0.07	2.34	3.02 ± 0.07	0.02
2	0.13	4.26	3.08 ± 0.10	0.08	0.11	3.66	3.04 ± 0.10	0.04
3	0.67	22.33	2.33 ± 0.06	-0.67	0.52	17.40	2.48 ± 0.05	-0.52
4	0.20	6.70	2.81 ± 0.06	-0.19	0.05	1.75	3.00 ± 0.05	0.00
	Cal model 4: SNV+1^{st} der(25) 7600 – 4177 cm^{-1}							
1	0.07	2.21	2.99 ± 0.07	-0.01	0.06	1.85	3.00 ± 0.06	0.00
2	1.17	39.03	1.85 ± 0.21	-1.15	1.15	38.41	1.87 ± 0.21	-1.13
3	0.29	9.52	2.72 ± 0.04	-0.28	0.24	8.13	2.76 ± 0.04	-0.24
4	0.39	12.94	3.39 ± 0.04	0.39	0.44	14.53	3.43 ± 0.03	0.43
	Cal model 5: SNV 5446 – 4779 cm^{-1}							
1	0.14	4.56	2.91 ± 0.10	-0.09	0.10	3.25	2.96 ± 0.09	-0.04
2	1.14	37.94	1.89 ± 0.25	-1.11	1.21	40.30	1.82 ± 0.25	-1.18
3	0.36	12.14	2.64 ± 0.03	-0.36	0.29	9.71	2.71 ± 0.03	-0.29
4	0.20	6.83	3.20 ± 0.03	0.20	0.32	10.75	3.32 ± 0.03	0.32
	Cal model 6: 1^{st} der(25) 5446 – 4779 cm^{-1}							
1	0.23	7.51	3.22 ± 0.06	0.22	0.12	3.90	2.94 ± 0.10	-0.06
2	0.73	24.22	2.31 ± 0.24	-0.69	0.26	8.77	2.89 ± 0.24	-0.11
3	0.11	3.62	2.90 ± 0.04	-0.10	0.65	21.74	2.35 ± 0.03	-0.65
4	0.54	18.03	3.54 ± 0.02	0.54	0.15	5.14	2.85 ± 0.04	-0.15
	Cal model 7: 2^{nd} der(25) 5446 – 4779 cm^{-1}							
1	0.13	4.44	2.98 ± 0.13	-0.02	0.06	2.01	3.03 ± 0.06	0.03
2	0.24	7.83	3.21 ± 0.11	0.21	0.21	7.00	3.19 ± 0.09	0.19
3	0.78	25.93	2.22 ± 0.06	-0.78	0.58	19.28	2.42 ± 0.05	-0.58
4	0.36	11.99	2.65 ± 0.06	-0.35	0.11	3.74	2.90 ± 0.06	-0.10
	Cal model 8: SNV+1^{st} der(25) 5446 – 4779 cm^{-1}							
1	0.13	4.45	2.89 ± 0.08	-0.11	0.12	3.91	2.91 ± 0.07	-0.09
2	1.10	36.71	1.93 ± 0.24	-1.07	1.14	38.16	1.88 ± 0.25	-1.12
3	0.43	14.35	2.57 ± 0.03	-0.43	0.40	13.26	2.60 ± 0.03	-0.40
4	0.17	5.69	3.17 ± 0.02	0.17	0.23	7.54	3.22 ± 0.03	0.22

Figure 49 shows the PLS score plot projections of the calibration and test set blends using the second derivative model (25-point window) in the 7600 – 4177 cm^{-1} spectral region. The scores of the calibration blends (white symbols) vary along the first principal component according to the

concentration of the API. However, the scores of the calibration blends differ along the second component. The PLS score plots of the calibration blends present a similar pattern distribution as the PCA score plots of the same blends shown in Figure 4d. The difference between the PLS score plots and the PCA score plots of the calibration blends is in the second principal component, in the projection of the plots in this axis, and the explained **X** variance (1.26% for the PCA and 1.08% for PLS). The scores of the calibration blends with 1.50 and 4.50 %w/w of APAP are in the positive values of the second component. Calibration blend 1 has a high lactose (81.95 %w/w) composition, while calibration blend 4 has a high MCC content (81.08 %w/w) as shown in **Table 22**. The calibration blends with 2.50 and 3.50 %w/w of APAP are observed in the opposite site of second component). Calibration blend 2 has 36.42 (%w/w) MCC and 59.53 (%w/w) lactose, while calibration blend 3 has 59.41 (%w/w) and 35.50 (%w/w) lactose. Therefore, the second principal component is related to concentration of MCC and lactose in the in the blends.

Figure 49 also shows the projection of the test set blends (gray symbols), all of which have a 3.00 (%w/w) APAP concentration. Test set blend 1 has the same content of MCC and lac (47.75 %w/w), and its scores are projected between those of the 2.50 (%w/w) and 3.50 (%w/w) calibration blends. The scores of test set blend 2 are aligned with the second component and projected away from those of the 2.50 (%w/w) and 3.50 (%w/w) calibration blends. This projection can be due to the high content of lactose in the formulation of this blend (70.74 %w/w), following a similar tendency as calibration blends with 1.50 and 4.50 %w/w APAP. However, as discussed before, the accuracy of the predictions for this blend is high, while the precision is not the best for the test set blends, but is an acceptable value as shown in **Table 23** (average 3.04 ± 0.10 %w/w using three latent variables). The test set blend 3 scores are projected with the scores of the 2.50 (%w/w) calibration

blends, explaining the negative bias observed in many of the calibration models summarized by **Table 23**.

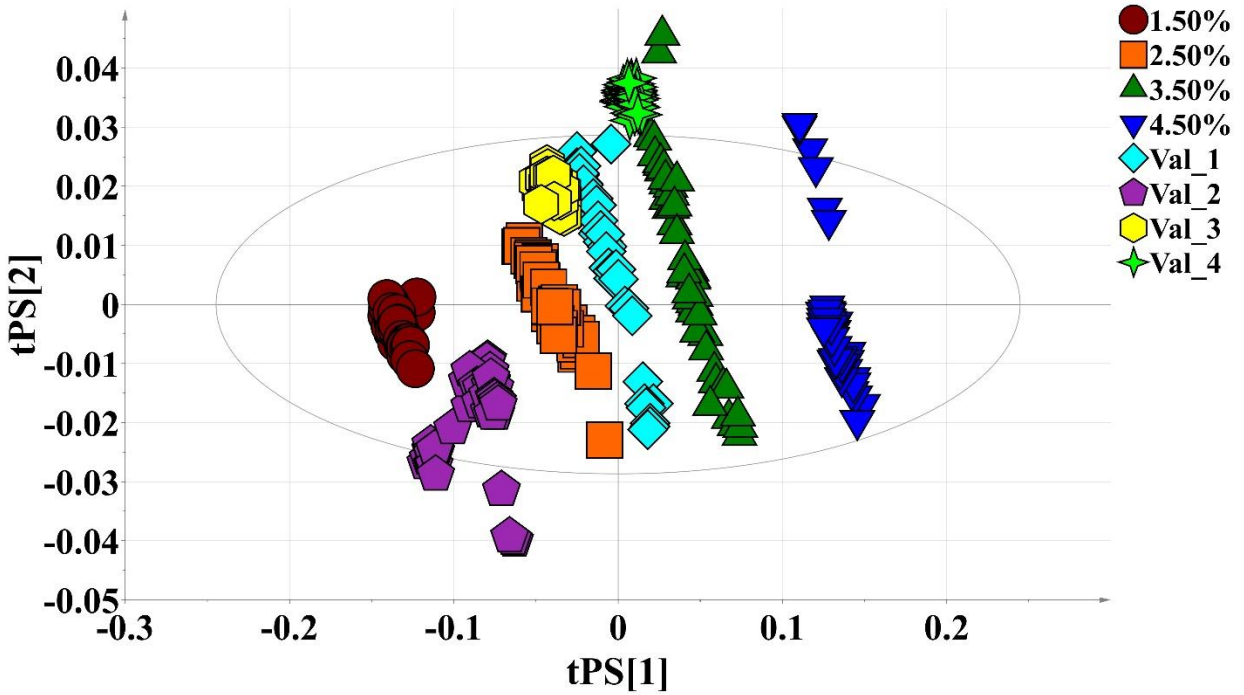

Figure 49. PLS score projections for calibration blends with 1.50, 2.50, 3.50, and 4.50 (%w/w) APAP and 3.00 (%w/w) APAP test set blends predictions. Calibration model 2nd derivative (25-point window) in the spectral region 7600 – 4177 cm^{-1}.

Test set blends 3 and 4 present intermediate values of lac and MCC (**Table 22**) and are projected in the center of the first principal component, and this is correct according to concentration of the API. As the case of the calibration blends with 2.50 and 3.50 %w/w of APAP, the projections of test set blends 3 and 4 are in the negative values of the second component. The case of the projections of the test set blend 2 need to be further evaluated. This blend presents a high concentration of one of the excipients (70.74 %w/w lactose), and it is in the range of the calibration blends.

The two excipients, Vivapur 102 microcrystalline cellulose and Tablettose 70 lactose monohydrate, differ significantly in their bulk densities as shown in **Table 24**. The APAP used

had a bulk density of 0.35 g/cm^3 while MCC had a bulk density of 0.31 g/cm^3. Lactose (tablettose 70) had a much larger bulk density of 0.52 g/cm^3. Changes in the concentration of MCC or lactose in the formulations significantly affect the physical properties of the blends which leads to changes in the spectral data, therefore these changes in spectral data leads the patterns in the PCA and PLS score projection. These figures show that a higher concentration of one the major excipients (MCC or lactose) present positive values of the scores in the second principal component using the model 2nd derivative (25-point window) in the spectral region 7600 – 4177 cm^{-1}. Equivalently, middle values in the concentration of major excipients are observed in the opposite site of second component of the projections. Therefore, the physical properties of the calibration and test set blends were characterized to obtain a better understanding of how changes in the excipient ratios affect the predictions of the calibration models.

Table 24. Determination of bulk and tap densities for calibration and test set blends.

Blend / Material	APAP (%w/w)	Average Bulk Density (g/cm^3) n=2	Average Tap Density (g/cm^3) n=2
Cal 1	1.50	0.53	0.65
Cal 2	2.50	0.48	0.63
Cal 3	3.50	0.44	0.58
Cal 4	4.50	0.41	0.56
TS 1	3.00	0.47	0.65
TS 2	3.00	0.51	0.66
TS 3	3.00	0.49	0.64
TS 4	3.00	0.45	0.61
APAP (Pure)	-	0.35	0.64
Vivapur 102 (Pure)	-	0.31	0.46
Tablettose 70 (Pure)	-	0.52	0.66

4.3.3. Characterization of the physical properties of the blends

The bulk, tap, true density (**Table 24**) of the blends, the excipients and APAP were determined, as well as their particle size distribution (**Table 25**). Particle size, like bulk density, is controlled by

the lactose concentration of the blends (low lactose concentration, low particle size distribution). The characterization of these excipients showed that the average D50 for lactose (211.5 µm) is 2 times the value on MCC (99.2 µm) creating a similar effect on bulk density.

Table 25. Particle size distribution for calibration and test set (TS) blends as determined by the Insitec Dry particle size analyzer.

Series Name	D10 (micron)			D50 (micron)			D90 (micron)		
	Value	Average	Std. Dev	Value	Average	Std. Dev	Value	Average	Std. Dev
Cal 1	97.1	57.51	11.71	272.86	196.01	21.12	615.71	420.21	100.47
Cal 2	39.74	45.28	5.35	124.75	171.21	14.82	262.46	406.95	109.58
Cal 3	39.2	37.15	2.35	144.34	141.57	7.72	482.79	377.44	41.51
Cal 4	31.65	32.91	1.37	111.38	122.42	4.98	272.53	328.12	17.13
TS 1	51.78	39.86	4.25	189.65	156.27	12.14	514.47	360.08	66.04
TS 2	46.04	48.51	6.21	153.72	181.88	14.22	320.29	387.79	64.95
TS 3	46.76	40.29	5.07	160.36	154.92	13.36	399.74	417.19	55.45
TS 4	46.28	40.46	3.36	164.62	149.94	9.27	363.32	371.64	16.61

Figure 50 shows a linear regression developed between lactose and the D50 of the blends, since lactose is affecting more significantly the particle size of the blends. This linear regression was used to calculate the amount of lactose (and hence MCC) by interpolation to the D50 of the 3.00 (%w/w) in APAP of the blends. Test set blend 3 presents a deviation of 6.5% from the average D50 in **Table 25**. This deviation of the trend of particle size can be partially the reason of the low accuracy of predictions for this test set blend as shown in Table 2 (bias of -0.52 %w/w). For the regression with the bulk density (**Figure 50** bottom) the value of the bulk density is closer to the trend and show a better correlation. This provide an opportunity to develop a calibration model base on the bulk density.

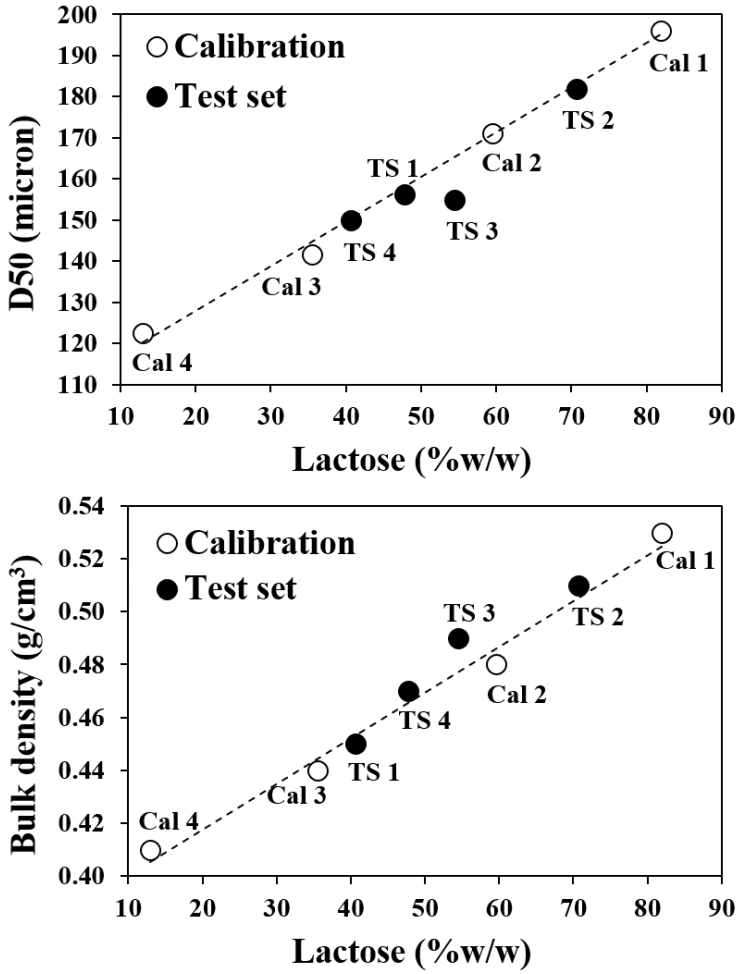

Figure 50. Linear relationship between: lactose (%w/w) and D50 particle size distribution (top), and lactose (%w/w) and bulk density (g/cm^3) (bottom) for calibration and test set (TS) blends.

4.3.4. Development of RSVV and powder bulk density models

A calibration based relative specific void volume of the powder blends was developed based on relative specific void volume (RSVV) of the powder blends since the results obtained showed that the powder density of the blends has a significant effect on the drug concentration predictions. True density would be the most representative physical property to be used as reference value, since it represents the most accurate density value measured, due to the rigorous conditions of the test (powder porosity volume is removed using an inert gas). However, the differences between the true density values of each blend are minimal. Higher numerical values were obtained

(equation 4) calculating the relative specific void volume (RSVV) with the bulk density (ρ_{bulk}) and the true density (ρ_{true}) values for all calibration and tests blends (**Table 26**). Using the measured bulk and true density (pycnometer) values for all calibration and test set blends from Table 4. The relative specific void volume is directly proportional to the porosity (relative specific void volume / relative specific bulk volume) of the blends due to the variation in excipients. These changes in the amount of lactose and MCC in each blend and the differences in mean particle size between both impacts significantly the RSVV of the void volume.

$$RSVV = \left[\frac{1}{\rho_{bulk}} - \frac{1}{\rho_{true}}\right] \quad (4)$$

Table 26. Relative specific volume and true density values for calibration and test set (TS) blends.

Blends	**Bulk Density (g/cm^3)**	**True Density (g/cm^3)**	**Relative Specific Void Volume (cm^3/g)**
Cal 1	0.53	1.571	1.263
Cal 2	0.48	1.568	1.446
Cal 3	0.44	1.566	1.611
Cal 4	0.41	1.569	1.812
TS 1	0.47	1.572	1.480
TS 2	0.51	1.571	1.330
TS 3	0.49	1.568	1.412
TS 4	0.45	1.574	1.581

* base 1 g of powder blend.

The relative specific void volume calibration models were developed with similar spectral regions and pre-treatments as in the previous sections. **Table 27** shows the results of the calibration models based on relative specific void volume of the blends. From the table several calibration models based on relative specific volume, exhibited excellent results prediction for all 4 independent test set blends. RSEP(%) below 4%, and significantly low bias values were obtained. Best results for all test set blends, were obtained using SNV+1st derivative (25 points) using one latent variable in

the spectral range 7600 – 4177 cm^{-1}. By using a physical property as reference value (bulk density, true density, RSVV), the predictions improved significantly in comparison with the predictions when concentration was used as a reference value. Most of the variation in the calibration model can be attributed in physical changes in the samples and using a physical property as reference enhances the accuracy of the model. This result indicates that the changes in porosity significantly affect the API concentration predictions and is the reason why was not be possible to find a robust model to predict the API concentration for the 4 test set blends in this study.

Table 27. Summary of the predictions for test set (TS) blends 1 - 4 based on relative specific void volume (RSVV). n≥38 spectra

TS blend	Ref. (RSVV cm3/g)	RMSEP (%)	RSEP (%)	Average (RSVV cm3/g)	Bias (RSVV cm3/g)	RMSEP (%)	RSEP (%)	Average (RSVV cm3/g)	Bias (RSVV cm3/g)
		1 Latent variable				***2 Latent variables***			
		Cal model 1: SNV 7600 – 4177 cm^{-1}							
1	1.480	0.05	3.64	1.53 ± 0.01	0.05	0.06	3.86	1.54 ± 0.01	0.06
2	1.330	0.05	3.95	1.31 ± 0.05	-0.02	0.04	3.06	1.32 ± 0.04	-0.01
3	1.412	0.06	3.93	1.47 ± 0.01	0.06	0.07	4.78	1.48 ± 0.01	0.07
4	1.581	0.01	0.87	1.59 ± 0.00	0.01	0.02	1.50	1.60 ± 0.00	0.02
		Cal model 2: 1^{st} der(25) 7600 – 4177 cm^{-1}							
1	1.480	0.11	7.44	1.56 ± 0.08	0.08	0.09	6.27	1.57 ± 0.01	0.09
2	1.330	0.10	7.85	1.42 ± 0.05	0.09	0.09	6.75	1.41 ± 0.04	0.08
3	1.412	0.03	2.32	1.44 ± 0.02	0.03	0.10	6.79	1.51 ± 0.01	0.10
4	1.581	0.07	4.57	1.51 ± 0.01	-0.07	0.04	2.78	1.62 ± 0.00	0.04
		Cal model 3: 2^{nd} der(25) 7600 – 4177 cm^{-1}							
1	1.480	0.10	6.66	1.57 ± 0.05	0.09	0.06	4.21	1.53 ± 0.03	0.05
2	1.330	0.09	6.89	1.41 ± 0.04	0.08	0.23	16.96	1.55 ± 0.02	0.22
3	1.412	0.07	4.75	1.48 ± 0.01	0.07	0.02	1.31	1.40 ± 0.01	-0.01
4	1.581	0.02	1.05	1.57 ± 0.01	-0.01	0.10	6.45	1.48 ± 0.01	-0.10
		Cal model 4: SNV+1^{st} der(25) 7600 – 4177 cm^{-1}							
1	1.480	0.05	3.39	1.52 ± 0.03	0.04	0.06	3.83	1.53 ± 0.02	0.05
2	1.330	0.04	3.26	1.36 ± 0.03	0.03	0.04	2.83	1.35 ± 0.03	0.02
3	1.412	0.04	2.87	1.45 ± 0.01	0.04	0.08	5.50	1.49 ± 0.01	0.08
4	1.581	0.03	2.14	1.55 ± 0.01	-0.03	0.02	1.45	1.60 ± 0.01	0.02
		Cal model 5: SNV 5446 – 4779 cm^{-1}							
1	1.480	0.07	4.47	1.54 ± 0.03	0.06	0.04	2.91	1.52 ± 0.02	0.04
2	1.330	0.04	2.64	1.35 ± 0.03	0.02	0.04	3.36	1.35 ± 0.04	0.02
3	1.412	0.08	5.39	1.49 ± 0.01	0.08	0.05	3.84	1.47 ± 0.01	0.05
4	1.581	0.01	0.57	1.59 ± 0.01	0.00	0.02	1.24	1.56 ± 0.00	-0.02
		Cal model 6: 1^{st} der(25) 5446 – 4779 cm^{-1}							
1	1.480	0.11	7.33	1.55 ± 0.08	0.07	0.09	6.14	1.57 ± 0.01	0.09
2	1.330	0.10	7.76	1.42 ± 0.05	0.09	0.10	7.50	1.42 ± 0.04	0.09
3	1.412	0.03	2.39	1.44 ± 0.02	0.03	0.09	6.41	1.50 ± 0.01	0.09
4	1.581	0.07	4.47	1.51 ± 0.01	-0.07	0.03	2.17	1.61 ± 0.00	0.03
		Cal model 7: 2^{nd} der(25) 5446 – 4779 cm^{-1}							
1	1.480	0.10	6.67	1.56 ± 0.05	0.08	0.06	3.87	1.53 ± 0.03	0.05
2	1.330	0.10	7.17	1.42 ± 0.04	0.09	0.25	18.85	1.58 ± 0.02	0.25
3	1.412	0.06	4.09	1.47 ± 0.01	0.06	0.03	2.07	1.39 ± 0.01	-0.03
4	1.581	0.03	1.63	1.56 ± 0.01	-0.02	0.12	7.87	1.46 ± 0.01	-0.12
		Cal model 8: SNV+1^{st} der(25) 5446 – 4779 cm^{-1}							
1	1.480	0.05	3.49	1.52 ± 0.03	0.04	0.05	3.15	1.52 ± 0.03	0.04
2	1.330	0.04	2.98	1.35 ± 0.03	0.02	0.05	3.57	1.36 ± 0.03	0.03
3	1.412	0.05	3.54	1.46 ± 0.01	0.05	0.04	2.75	1.45 ± 0.01	0.04
4	1.581	0.03	1.64	1.56 ± 0.01	-0.02	0.04	2.62	1.54 ± 0.01	-0.04

Figure 51 shows the results of the NIR predictions of APAP versus the RSVV predictions of the test set blends using the second derivative and SNV+1st derivative models. The predictions of the blends are using the first and two latent variables in the 7600 – 4177 cm^{-1} spectral region with the two spectral preprocessing mentioned before. From the figure the results of the NIR predictions present a high correlation (up to 0.976) with the results of the RSVV predictions for the four blends evaluated, except for the second derivative predictions using two latent variables. This result supports that relative specific void volume affect the NIR predictions of the API in powder blends at low concentration as mentioned. The model using second derivative with two latent variables present the lowest correlation between NIR predictions of the API and the RSVV predictions. In spite of this calibration model presents the best predictions as shown in **Table 22**, the predictions tend to be affected by relative specific void volume of the blends as shown in **Figure 51**.

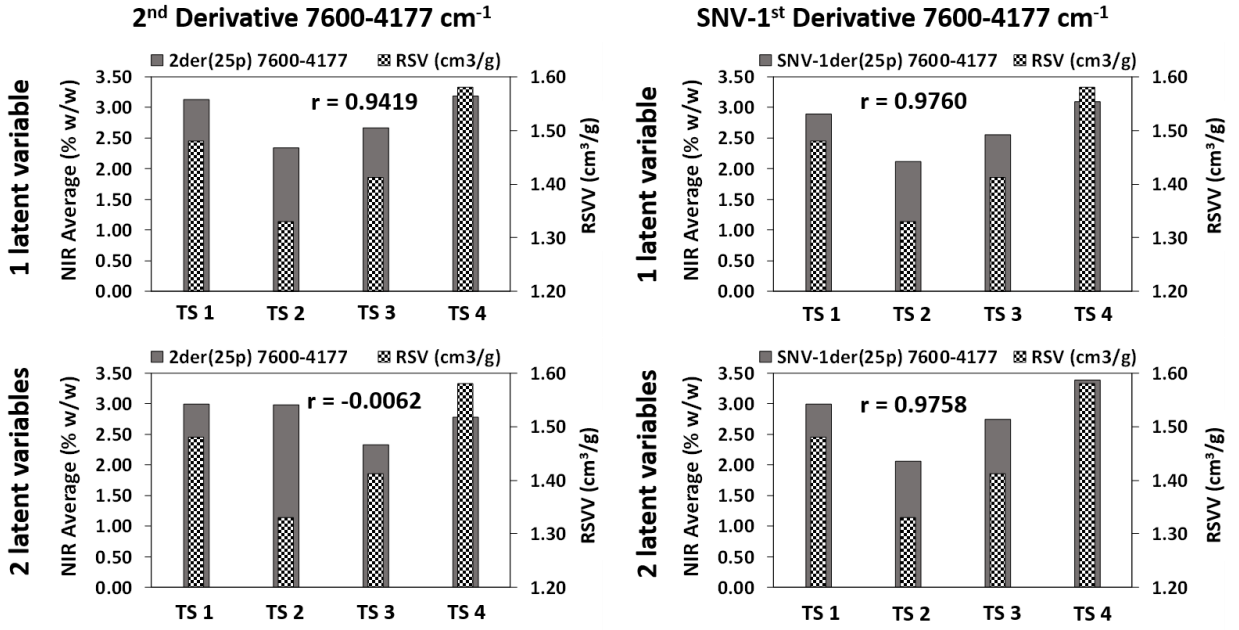

Figure 51. NIR predicted values vs reference relative specific void volume (RSVV) of the test set (TS) blends. 2nd derivative model (left graphs). SNV+1st derivative model (right graphs). 1 latent variable (upper graphs). 2 latent variables (bottom graphs). Gray columns for NIR predicted values and checker board columns for reference RSVV values.

A calibration based bulk density of the powder blends was developed based on the results described in **Figure 50**. A previous study shows that powder density of the blends has an impact on the NIR spectra at different tap density levels, different strain levels, and applying normal forces during a compressibility test with a powder rheometer (Román-Ospino et al., 2016). In this work, NIR calibration models based on bulk density of the powder blends were developed by sampling within the feed frame for blends with different excipient ratio. **Table 28** shows the results of the test set blends based on bulk density calibration models. As show the table, using one latent variable the results are excellent for the four test set blends evaluated in this study. Calibration models using SNV and SNV+1st derivative in the two spectral regions evaluated in this study present the best results with RSEP(%) values below that 2.60 % and low bias. This result, as demonstrated by a previous study (Román-Ospino et al., 2016) show that powder density of the formulations has an impact on the NIR spectra of the blends, in this case at low API concentrations. Changes on NIR spectra of the powder blends due to process within the feed frame can be used to monitor these physical changes to improve control strategies for properties such as tablet mass, hardness and dissolution.

Table 28. Summary of the predictions for test set (TS) blends 1 - 4 based on bulk density. n≥38 spectra.

TS blend	Ref. (Bulk dens. g/ cm3)	RMSEP (%)	RSEP (%)	Average (Bulk dens. g/ cm3)	Bias (Bulk dens. g/ cm3)	RMSEP (%)	RSEP (%)	Average (Bulk dens. g/ cm3)	Bias (Bulk dens. g/ cm3)
		1 Latent variable				***2 Latent variables***			
		Cal model 1: SNV 7600 – 4177 cm^{-1}							
1	0.47	0.01	1.19	0.47 ± 0.00	0.00	0.01	1.43	0.46 ± 0.00	-0.01
2	0.51	0.01	2.40	0.51 ± 0.01	0.00	0.02	3.13	0.52 ± 0.01	0.01
3	0.49	0.01	2.09	0.48 ± 0.00	-0.01	0.01	1.99	0.48 ± 0.00	-0.01
4	0.45	0.00	0.44	0.45 ± 0.00	0.00	0.00	0.29	0.45 ± 0.00	0.00
		Cal model 2: 1^{st} der(25) 7600 – 4177 cm^{-1}							
1	0.47	0.02	4.39	0.46 ± 0.02	-0.01	0.02	3.32	0.45 ± 0.00	-0.02
2	0.51	0.02	4.45	0.49 ± 001	-0.02	0.02	3.21	0.50 ± 0.01	-0.01
3	0.49	0.01	1.18	0.49 ± 0.00	0.00	0.02	4.26	0.47 ± 0.00	-0.02
4	0.45	0.02	4.47	0.47 ± 0.00	0.02	0.01	1.40	0.44 ± 0.00	-0.01
		Cal model 3: 2^{nd} der(25) 7600 – 4177 cm^{-1}							
1	0.47	0.02	3.55	0.46 ± 0.01	-0.01	0.01	2.06	0.46 ± 0.00	-0.01
2	0.51	0.02	3.85	0.49 ± 0.01	-0.02	0.04	7.16	0.47 ± 0.01	-0.04
3	0.49	0.01	2.65	0.48 ± 0.00	-0.01	0.01	1.65	0.48 ± 0.00	-0.01
4	0.45	0.01	1.63	0.46 ± 0.00	0.01	0.01	2.36	0.46 ± 0.00	0.01
		Cal model 4: SNV+1^{st} der(25) 7600 – 4177 cm^{-1}							
1	0.47	0.01	1.52	0.47 ± 0.01	0.00	0.01	1.28	0.47 ± 0.00	0.00
2	0.51	0.01	1.87	0.50 ± 0.01	-0.01	0.01	1.85	0.51 ± 0.00	0.00
3	0.49	0.01	1.50	0.48 ± 0.00	-0.01	0.01	2.10	0.48 ± 0.01	-0.01
4	0.45	0.01	2.59	0.46 ± 0.00	0.01	0.00	1.02	0.45 ± 0.00	0.00
		Cal model 5: SNV 5446 – 4779 cm^{-1}							
1	0.47	0.01	2.07	0.46 ± 0.01	-0.01	0.01	3.00	0.46 ± 0.01	-0.01
2	0.51	0.01	1.44	0.51 ± 0.01	0.00	0.01	1.63	0.52 ± 0.01	0.01
3	0.49	0.02	3.29	0.47 ± 0.00	-0.02	0.02	4.82	0.47 ± 0.00	-0.02
4	0.45	0.00	0.60	0.45 ± 0.00	0.00	0.01	2.12	0.44 ± 0.00	-0.01
		Cal model 6: 1^{st} der(25) 5446 – 4779 cm^{-1}							
1	0.47	0.02	4.32	0.46 ± 0.02	-0.01	0.02	3.47	0.45 ± 0.00	-0.02
2	0.51	0.02	4.39	0.49 ± 0.01	-0.02	0.02	3.33	0.50 ± 0.01	-0.01
3	0.49	0.01	1.22	0.49 ± 0.00	0.00	0.02	4.27	0.47 ± 0.00	-0.02
4	0.45	0.02	4.39	0.47 ± 0.00	0.02	0.01	1.34	0.44 ± 0.00	-0.01
		Cal model 7: 2^{nd} der(25) 5446 – 4779 cm^{-1}							
1	0.47	0.02	3.58	0.46 ± 0.01	-0.01	0.01	2.17	0.46 ± 0.01	-0.01
2	0.51	0.02	4.01	0.49 ± 0.01	-0.02	0.04	8.03	0.47 ± 0.01	-0.04
3	0.49	0.01	2.23	0.48 ± 0.00	-0.01	0.00	0.70	0.49 ± 0.00	0.00
4	0.45	0.01	2.13	0.46 ± 0.00	0.01	0.02	4.04	0.47 ± 0.00	0.02
		Cal model 8: SNV+1^{st} der(25) 5446 – 4779 cm^{-1}							
1	0.47	0.01	1.42	0.47 ± 0.01	0.00	0.01	1.66	0.46 ± 0.00	-0.01
2	0.51	0.01	1.70	0.51 ± 0.01	0.00	0.01	1.98	0.51 ± 0.01	0.00
3	0.49	0.01	1.97	0.48 ± 0.00	-0.01	0.02	3.30	0.47 ± 0.00	-0.02
4	0.45	0.01	2.13	0.46 ± 000	0.01	0.00	0.51	0.45 ± 0.00	0.00

These results of this study show that NIR spectroscopy could be used to monitor physical properties as bulk density and RSVV of the powder blends within the feed frame and contribute to the control of tablet weight variability. The same NIR spectra could also be used to determine low drug concentration, or for real time identification of the powder blend (Vargas et al., 2018). NIR measurements within the feed frame could become important elements within modern pharmaceutical quality control.

4.4. **CONCLUSIONS OF CHAPTER 4**

This study has described the first evaluation of powder bulk density and relative specific void volume (RSVV) or porosity of powder blends at low API concentrations within the feed frame. This determination was made possible by the large differences in powder density in the excipients used which facilitates the evaluation of powder density and RSVV of the blends based on NIR spectra.

Further evaluation using the powder density and particle size data of the blends showed a trend based on the linear regression of the D50 and bulk density vs lactose concentration (%w/w). D50 values of lactose is approximately 2 times than MCC, the bulk density of the blends. The test set blend 3 presented a deviation of this linear trend, which partially can explain the bias of the NIR predictions of this blend.

NIR calibrations based relative specific void volume and bulk density of the blends were developed since the results obtained showed that the powder density of the blends has a significant effect on the drug concentration predictions. These calibration models using the same spectral region and pretreatments as the used for API concentration presented excellent results prediction for all 4 independent test set blends using one latent variable. By using a physical property as

reference value (bulk density, true density, RSVV), the predictions were improved significantly. This result supports that most of the variation in the calibration model can be attributed to physical changes on the samples and using a physical property as reference enhances the accuracy of the model.

CHAPTER 5: NIR SPECTROSCOPY AS A NON-DESTRUCTIVE AT LINE METHOD FOR MONITORING TABLET DRUG CONCENTRATION IN A CONTINUOUS MANUFACTURING PROCESS

To be submitted, Carlos A. Ortega-Zuñiga, Jesús Torres, Rafael Méndez, Anthony Gonzalez, Yleana Colón, Eric Sánchez, Rodolfo J. Romañach

This chapter is not an exact copy of the paper to be submitted. It contains original information.

5.1. **INTRODUCTION**

This study was performed to develop an at-line near-infrared (NIR) spectroscopy method with chemometrics to determine drug concentration and confirm composition correctness of one active pharmaceutical ingredient (API) in core tablets of a combination medicine of two APIs from a Continuous Manufacturing (CM) process for real-time release testing (RTRt).

The "Guidance for Industry of the Food and Drug Administration" (FDA) (US-FDA, 2004) has increased the interest in process analytical technology (PAT) initiative in the pharmaceutical industry. One subject described in the guidance is RTRt. Real time release is a principle that provides assurance of the quality criteria specifications intended during the manufacturing process of a product with good manufacturing practice (GMP) requirements based on process data analysis (Pestieau et al., 2014; Skibsted et al., 2007). The development of an RTR system requires an in-depth and careful analysis of the quality attributes of the materials involved in all the manufacturing process. The use of NIR and chemometrics as PAT serves to monitor and evaluate the changes in the materials during the manufacturing processes and facilitates the analysis and decision making for control process (Durão et al., 2017; Ierapetritou, Muzzio, & Reklaitis, 2016; Román-Ospino et al., 2016; Singh et al., 2015).

Continuous manufacturing, as the FDA states, "often involves a higher level of process design to ensure adequate process control and product quality" (Lee et al., 2015). Since the FDA approved the use of CM for the first time on a continuous manufacturing production line, there has been growing research regarding process understanding of manufacturing and the science behind the technological advancements in CM processes (US-FDA, 2015). Puerto Rico has the second CM line approved by the FDA for tablet production of an anti-HIV product (Pharmaceutical Technology Editors, 2016, Apr 12). The use of CM to replace batch manufacturing is the result of five years of collaboration of the industry and the academia, principally Rutgers University and University of Puerto Rico at Mayaguez (Pharmaceutical Technology Editors, 2016, Apr 12). However, CM presents a challenge since the process is different to traditional batch manufacturing. An in deep understanding of the process behind the CM and a science based knowledge of the system dynamics of the materials with the use of PAT assures the improvement of the process control strategies and the manufacturing of the final drug product following the quality by design (QbD) paradigm (Singh et al., 2014; Yu et al., 2016). The success of continuous manufacturing is due to the collaborative efforts of industry and academia (Collins, 2018). The achievement of a high level of understanding regarding the science behind process changes, material characterization through continuous product manufacturing, big-data analysis for making decisions in real time, and the compliance of guidelines and regulatory requirements for GMP and QbD of a drug product, require an engagement of collaboration between the industry, academia, and government entities (O'Connor, Yu, & Lee, 2016).

This study describes the development of an at-line non-destructive method to determine drug concentration of one API in tablets of a combination medicine of two APIs from a CM process within a commercial manufacturing plant for RTRt. The development of the method follows the

PAT guidance for manufacturing and quality assurance (US-FDA, 2004), and the ICH Q2 parameters for validation of an analytical method (ICH, 2005). The model was challenged with a design of experiment of the manufacturing process variables to achieve a better understanding of the changes in the material within manufacturing and to evaluate potential parameters during the process. Also, this evaluation serves for the improvement of control strategies in the manufacturing of a drug product following the QbD paradigm.

5.2. **MATERIALS AND METHODS**

5.2.1. Materials

The formulation included the first API with a concentration lower than 20% (w/w) and the second API with a concentration greater than 60% (w/w), MCC Avicel PH102 as the filler, magnesium stearate NF/PH EUR as the lubricant, and a pre-blend material that is a formulation of MCC Ceolus and croscarmellose. All materials and excipients used in this study were acquired by the Janssen Gurabo inventory.

5.2.2. Continuous manufacturing system

The feeding system consists of five (5) gravimetric/volumetric feeders (monitored by the K-tron gravimetric feeder control). The gravimetric/volumetric feeders feed each material to maintain a constant line throughput. After, the material enters an in-line continuous paddle blender (performed using a Glatt Conti blender). Then, after the gravimetric/volumetric feeders achieved a steady state (the mass flow of all feeders in use is within its reject limits range) the compacting of powder blend was performed to make tablets (Korsch Tablet Press). **Figure 52** shows the diagram of the continuous manufacturing line. The CM includes the volumetric (V1, V2, V3, and

V4) and gravimetric feeders (G1, G2, G3, G4, and G5), the continuous blender, the interface for NIR spectra acquisition, and the tablet press for tablet compression (Image from: J.M. Vargas et al. International Journal of Pharmaceutics 538 (2018) 167–178.).

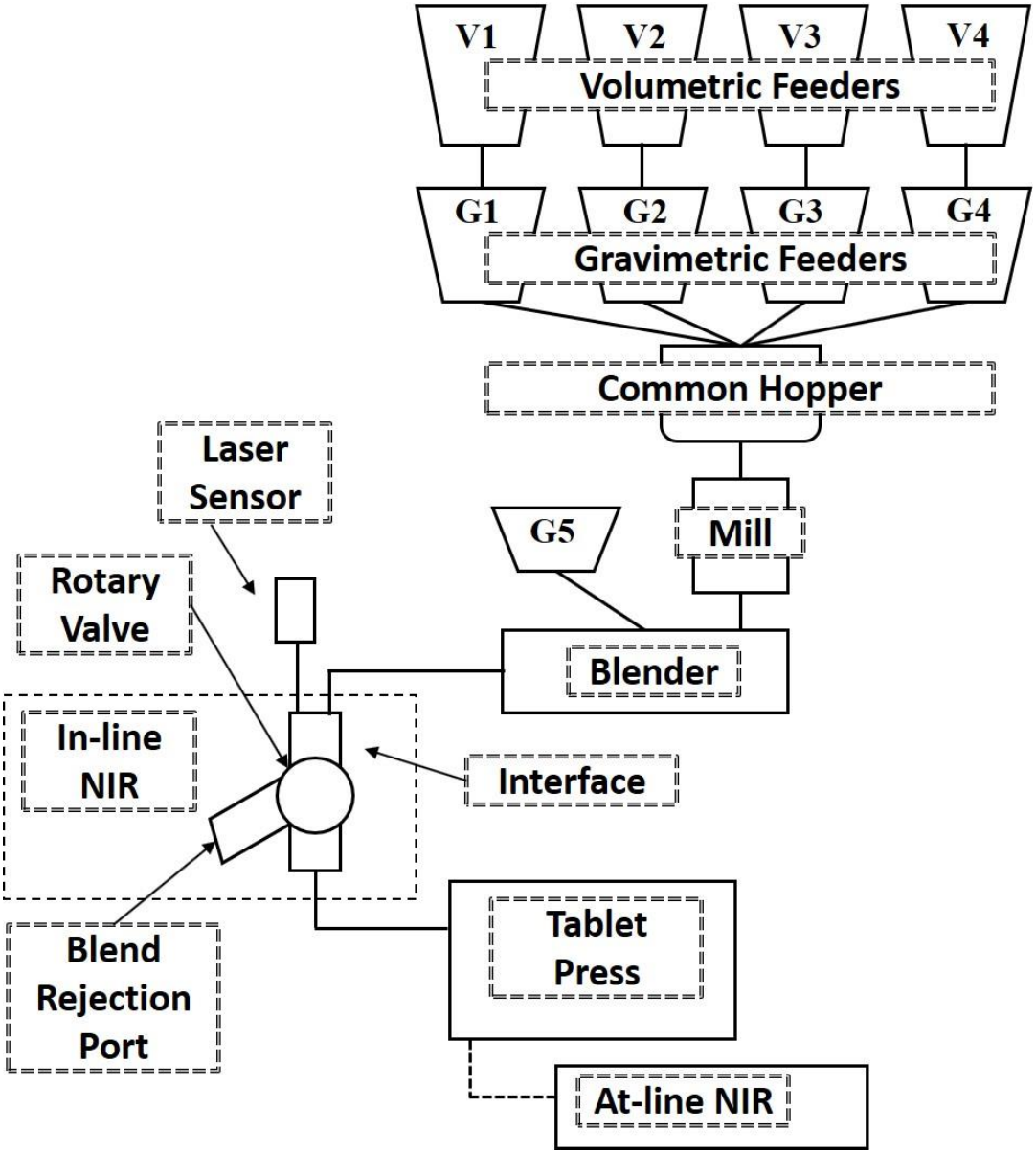

Figure 52. Diagram of the continuous manufacturing line including the volumetric (V1, V2, V3, and V4) and gravimetric feeders (G1, G2, G3, G4, and G5), the continuous blender, and the interface for NIR spectra acquisition, and the tablet press for tablet compression.

5.2.3. Preparation of the calibration and validation sets CM system

Calibration and validation tablets were produced at the CM line at concentrations in the range within 70% to 130% of label claim (LC) for API-1 at five (5) equidistant concentration levels (70%, 85%, 100%, 115%, and 130% LC). The concentration of the filler was varied to maintain the target conditions. The calibration and validation samples were prepared with the same equipment operation used for commercial processes.

5.2.4. At-line NIR spectral acquisition

Spectra from all core tablets were acquired using a Bruker FT-NIR MPA (MA, USA) coupled with a transmission probe, an integrating sphere device, and a room temperature Indium Gallium Arsenide (RT-InGaAs) external detector. The transmission mode was used for the analysis. All NIR spectra were acquired within the 14000 – 7000 cm^{-1} (714.3 – 1428.6 nm) spectral range at a resolution of 64 cm^{-1}, with 128 scans for background and 128 scans for sample.

Calibration and validation tablet spectra were acquired at the left, center, and right sides of each tablet to construct the different calibration models (5 concentration levels, 70%, 85%, 100%, 115%, and 130% LC; 10 tablets per concentration level). A second lot of the API-1 was used to produce a second set of tablets at target concentration (100% LC). A total of one-hundred and ten (110) tablets were analyzed using NIR spectroscopy in transmission mode, and UPLC was used as the reference method.

5.2.5. Development of multivariate calibration models

Principal component analysis (PCA) and partial least squares (PLS) regression calibration models were performed using SIMCA P+12 software (MKS Umetrics part of Sartorius Stedim Biotech, Umeå, Sweden). Different spectral regions and spectral preprocessing were evaluated including standard normal variate (SNV), first and second derivatives, and combination of SNV with derivatives.

The predictive performance of the calibration model was evaluated in terms of the bias, the standard deviation, the root mean square of prediction (RMSEP), and the relative standard error of prediction (RSEP (%)), defined as:

$$Bias = \sum_{i=1}^{n} \frac{\left(Y_i^{pred} - Y_i^{ref}\right)}{n} \quad (5\text{-}1)$$

$$RMSEP = \sqrt{\frac{\sum_{i=1}^{n}\left(Y_i^{pred} - Y_i^{ref}\right)^2}{n}} \quad (5\text{-}2)$$

$$RSEP\ (\%) = 100 \times \sqrt{\frac{\sum_{i=1}^{n}\left(Y_i^{pred} - Y_i^{ref}\right)^2}{\sum_{i=1}^{n}\left(Y_i^{ref}\right)^2}} \quad (5\text{-}3)$$

where n is the number of samples used in the validation set, Y^{pred} and Y^{ref} the predicted and measured reference values. The number of PLS factors was chosen by the minimum error (RMSEP and RSEP (%)), bias, and standard deviation calculated.

5.2.6. API UPLC method

The reference method used for quality control and analytical quantification of the API in tablets was a validated laboratory UPLC method. Each tablet collected was weighed and transferred to 50 mL volumetric flasks using a solution of 50% acetonitrile/50% distilled water as diluent. After sample preparation, the solution was analyzed using a UPLC equipped with a variable wavelength UV detector, stationary phase BEH C18 column, and auto-sampler.

5.3. **RESULTS**

5.3.1. NIR spectral evaluation

To identify the characteristics of the NIR spectral data for the raw materials of the core tablets, an overlay of spectra (**Figure 53**) was acquired from one tablet prepared with pure API-1, one tablet with pure API-2, and another with the pure excipient with the main components in the formulation. These spectra were examined to assess the spectral range where the absorbance bands are present.

The absorbance bands of API-1 were observed between 13530 – 13220 cm^{-1} which is related to the fourth overtone region of C-H stretching. There is a broad band at 11840 – 11220 cm^{-1} which is related to the third overtone region of C-H stretching. Also, there is an intense and narrow band at 10500 – 10000 cm^{-1} which there is no reference information, but it is in the second overtone region of O-H. This is a starting point to perform studies about the API-1 molecule because there are only a few scientific studies, and they are not related to the NIR spectra of this compound. However, the scope of this study is not a comprehensive analysis of the molecular vibrations of

the API-1, for this study it is enough to know the basics of the vibrations to understand the changes in the NIR spectra of the tablets prepared in the CM line.

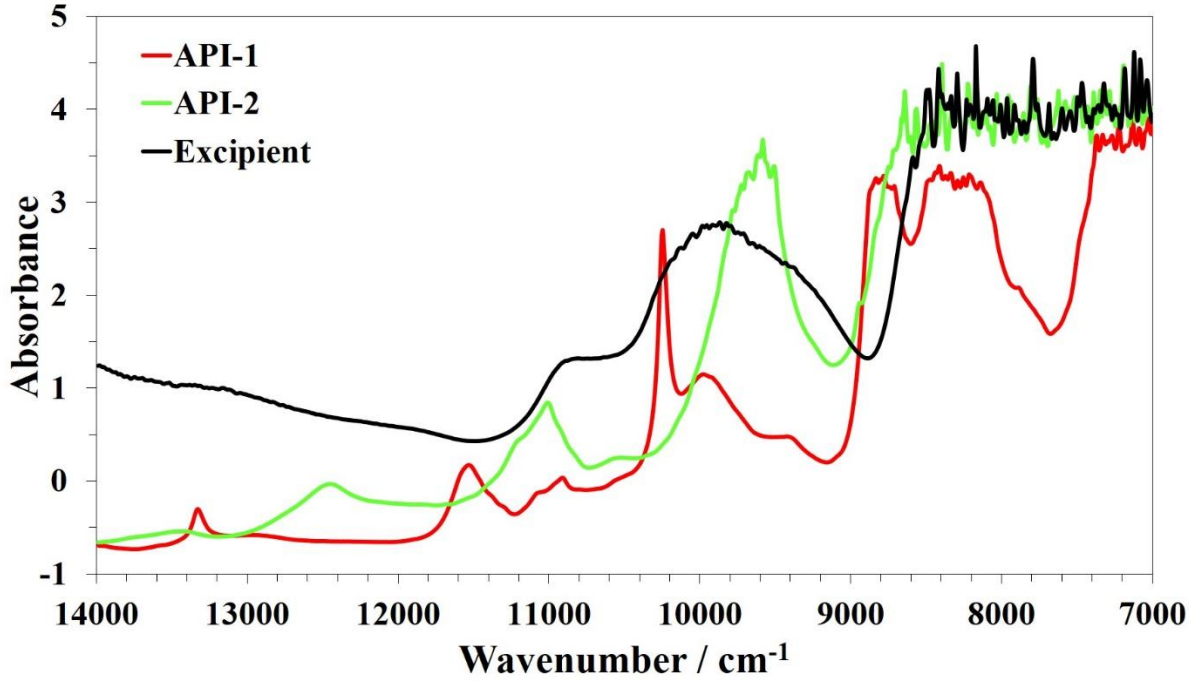

Figure 53. Raw spectra overlay of pure API-1, API-2, and one excipient tablet.

5.3.2. UPLC results

Core calibration and validation tablets sets were collected for analytical testing after their spectra was acquired using the NIR Analyzers. The UPLC results are shown in

Table *29* for the calibration set and **Table 30** for the validation set. The UPLC concentration (% LC) is considered as the reference result for each of the tablets. As shown in

Table *29* and **Table 30**, the percent relative standard deviation (% RSD) of the UPLC results per concentration ranges (n=10) were all less than 2.3% with a range of 0.9 to 2.1% for standard

deviation, showing precise preparation of the low API-1 concentration tablets for the calibration and the validation by the CM line.

Table 29. UPLC results of the calibration tablets.

Target Concentration (%LC)	Average	Std, Dev.	RSD (%)
70	70.4	1.6	2.3
85	84.1	1.4	1.7
100	100.7	1.2	1.1
115	113.5	1.1	1.0
130	129.2	2.1	1.6

Table 30. UPLC results of the validation tablets.

Target Concentration (%LC)	Average	Std, Dev.	RSD (%)
70	70.4	0.9	1.3
85	84.4	1.5	1.8
100	100.0	1.8	1.8
115	114.7	1.3	1.1
130	128.9	2.2	1.7
100 (API-1 2nd lot)	99.1	2.1	2.1

5.3.3. Development of calibration models

Based on the differences in the raw spectra (**Figure 53)** there are two major spectral regions that include the absorbance bands where the API-1, API-2 and the major excipient in tablets can be identified. **Figure 54** shows the first derivative spectra of these pure components. As shown in **Figure 54**, there are two major spectral regions that include different information. The region of 10522 – 10005 cm^{-1} shows an intense band of the API-1 and the other components does not present a notable pattern. The region of 11988 – 10754 cm^{-1} includes absorbance bands of the API-1, API-2 and the major excipient components.

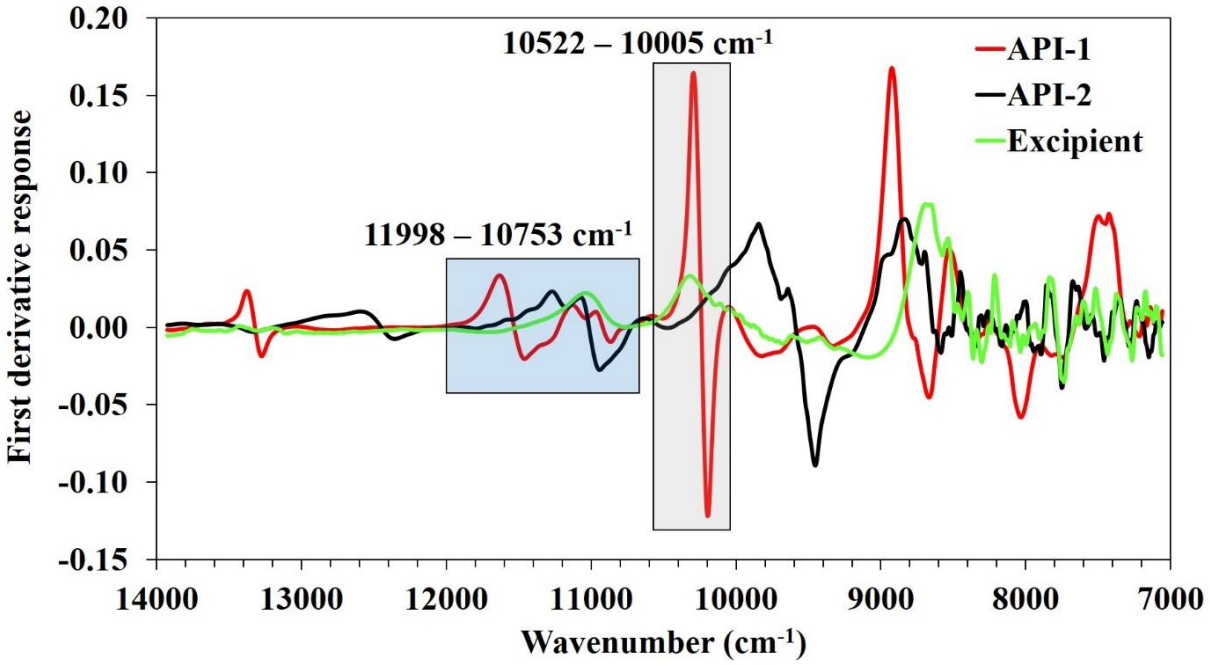

Figure 54. Overlay of the first derivative spectra of pure API-1, API-2, and one excipient tablet. Blue box: 11998 – 10753 cm^{-1} spectral region. Black box: 10522 – 10005 cm^{-1} spectral region.

5.3.4. PCA evaluation based on API-1

As shown in **Table 31**, the models present high R2X and Q2 values (above 97%) which means that there is a high variation explained by the models.

Table 31. R2X and Q2 values from the PCA in the spectral regions and spectral preprocessing selected based on the API-1 vibrational bands.

Model	Spectral region (cm^{-1})	Spectral pre-processing	1 PC		2 PCs	
			R2X(cum)	Q2(cum)	R2X(cum)	Q2(cum)
M1	12005-10152	SNV + 1st der	0.993	0.993	0.996	0.996
M2	10522-10005	SNV	0.990	0.989	0.993	0.990
M3	10522-10005	SNV + 1st der	0.997	0.996	0.998	0.997
M4	10522-10129	SNV + 1st der	0.998	0.998	0.999	0.999
M5	11988 - 10754	SNV + 1st der	0.974	0.973	0.987	0.985
M6	11998-10754 + 10522-10129	SNV + 1st der	0.994	0.994	0.997	0.997

Figure 55 through **Figure 60** show the PCA based on the spectral regions of the API-1 and the spectral preprocessing evaluated in **Table 31**. Based on the results from **Table 31**, the model with the lower values of R2X and Q2 is the M5 model; however, the PCA of this data shows well distributed plots. The model M4 has the higher values of R2X and Q2 from the table; however, the distribution of the score plots is not well defined as in M1, M6, or even M4 which has the lowest values.

From the results shown in **Table 31** and the PCA of these models, the evaluation based only in the numerical information (R2X and Q2) is not the best assessment to decide the performance of the model; furthermore, a careful inspection of the data is necessary.

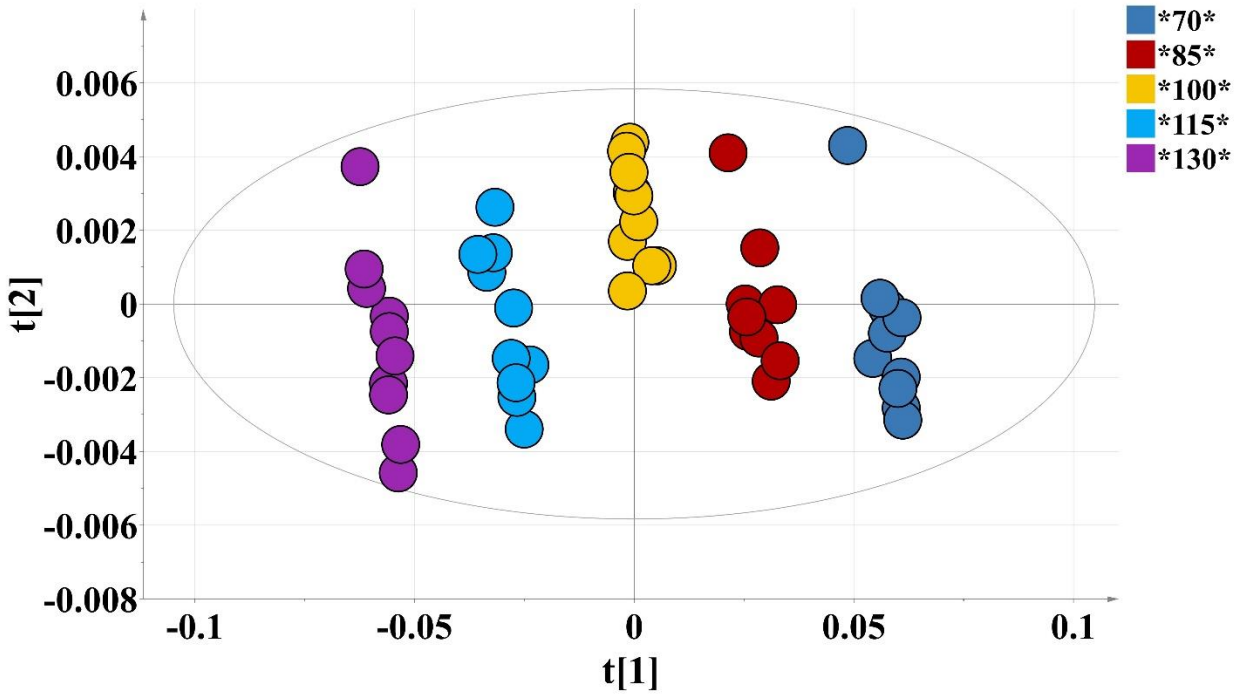

Figure 55. PCA based on the API-1, spectral region: 12005 – 10152 cm^{-1}, and spectral preprocessing: SNV + 1st derivative.

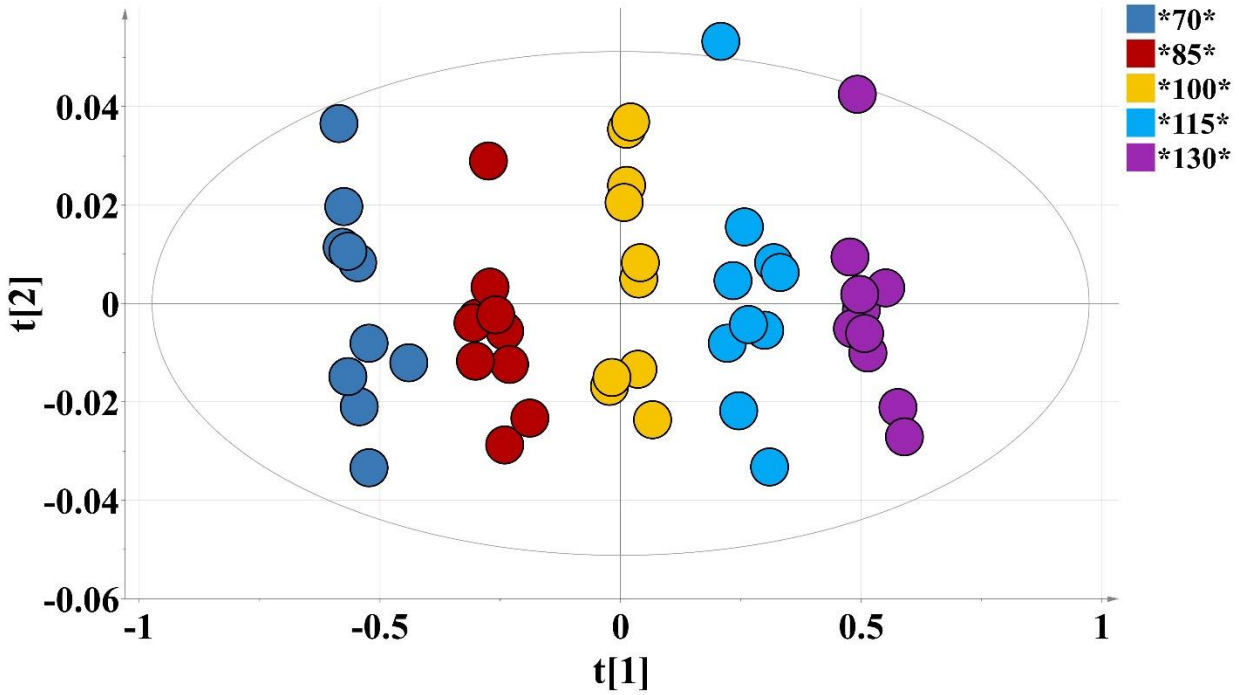

Figure 56. PCA based on the API-1, spectral region: 10522 – 10005 cm^{-1}, and spectral preprocessing: SNV.

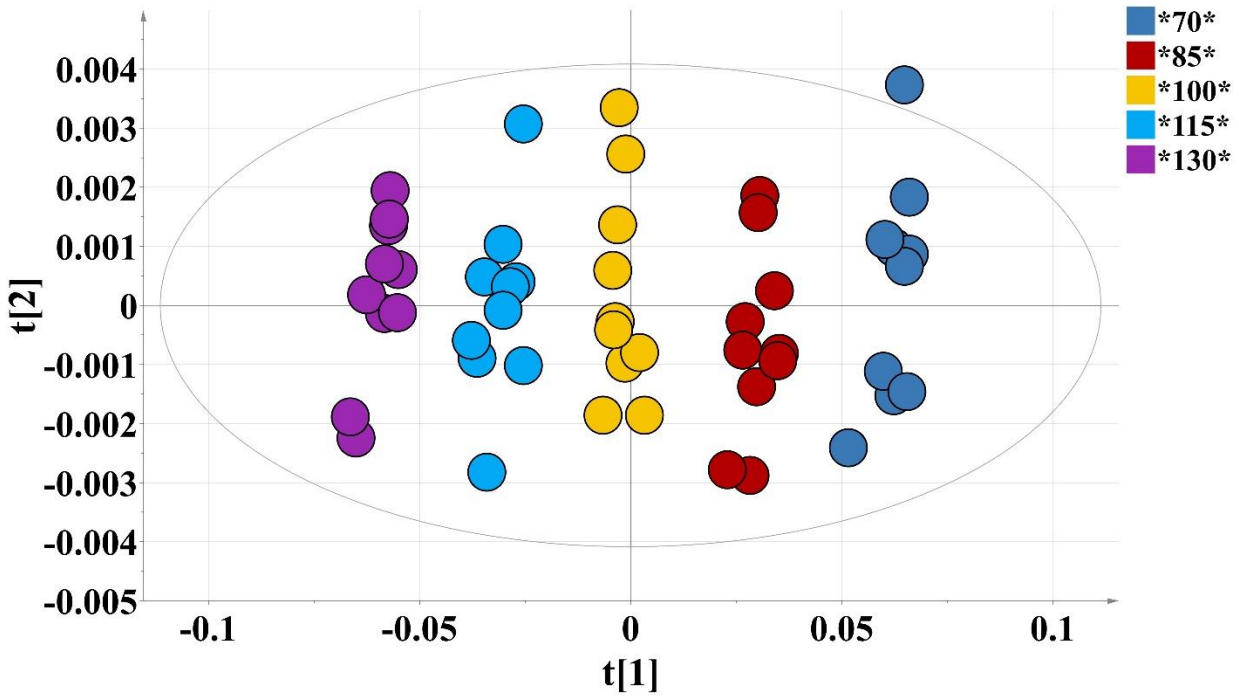

Figure 57. PCA based on the API-1, spectral region: 10522 – 10005 cm^{-1}, and spectral preprocessing: SNV + 1st derivative.

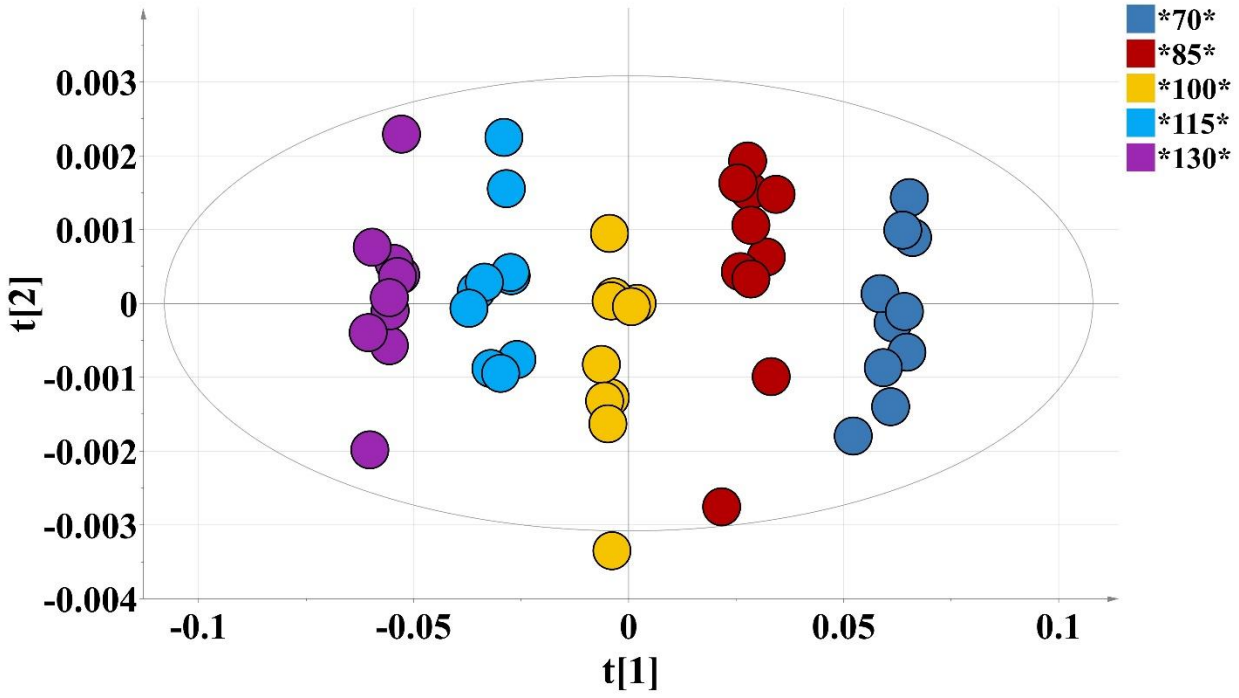

Figure 58. PCA based on the API-1, spectral region: 10522 – 10129 cm^{-1}, and spectral preprocessing: SNV + 1st derivative.

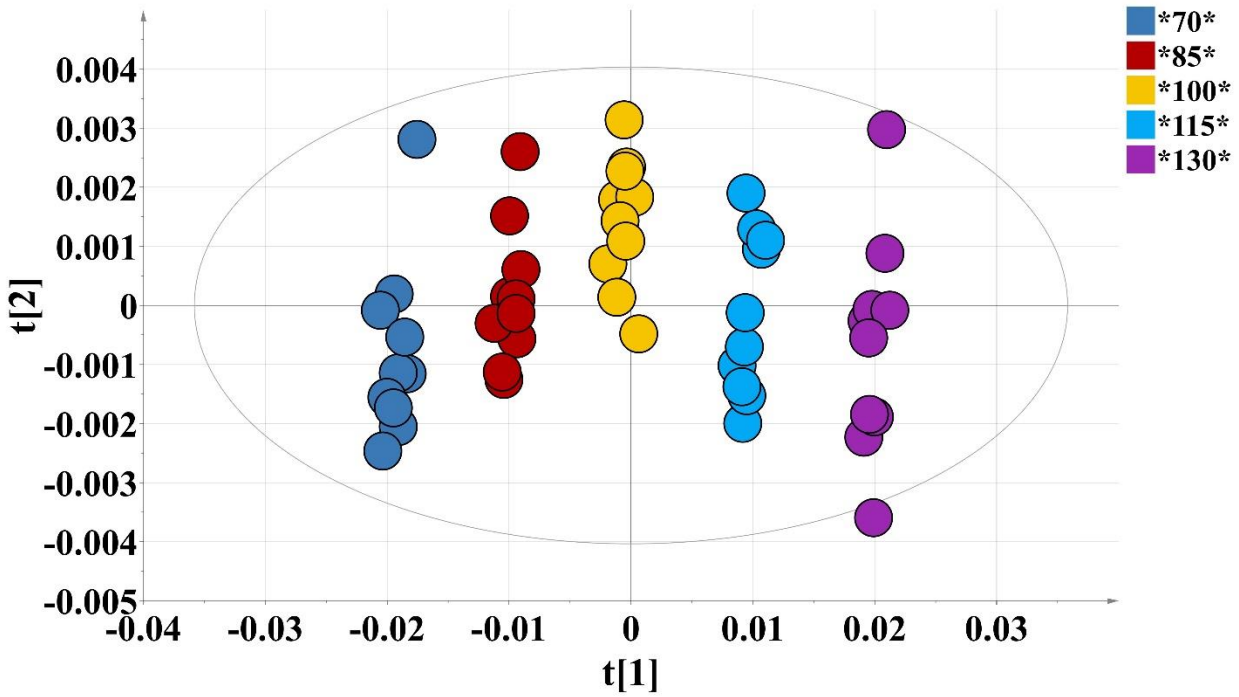

Figure 59. PCA based on the API-1, spectral region: 11988 – 10754 cm^{-1}, and spectral preprocessing: SNV + 1st derivative.

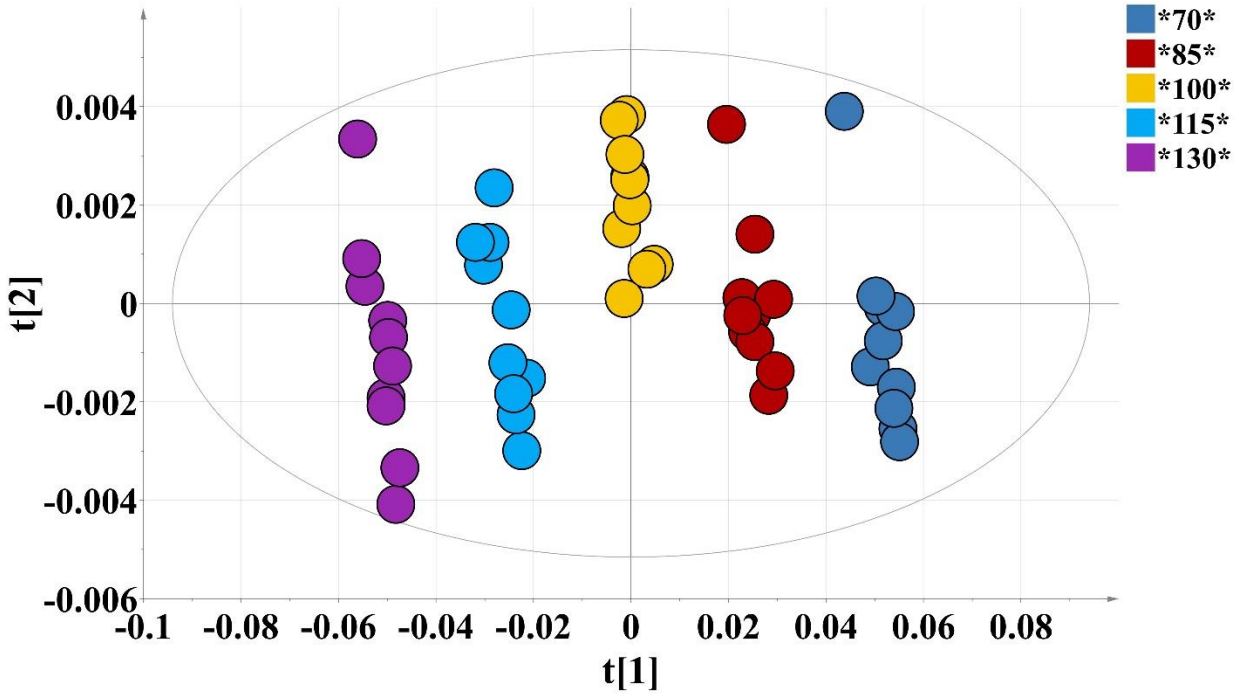

Figure 60. PCA based on the API-1, spectral region: 11998 – 10754 + 10522 – 10129 cm^{-1}, and spectral preprocessing: SNV + 1st derivative.

5.3.5. PLS models based on API-1

Table 32 displays a summary of the initial assessment performed using one (1) and two (2) PLS factors. For the NIR models evaluated, the first PLS component explains more than 97% of the variation of the samples in the calibration set. The second component contributes with no more than 1.4%. Based on the fraction of **Y**-variation modeled by the PLS components, models with 0.000 value of R2Y for the second component were not considered for evaluation since there is little information in the **Y**-variation. Therefore, models M1, M3, M4, and M6 using 2 PLS factors are not discussed further. These models have low Q2 values (in some cases negative values) explaining little information of the variation in the cross-validation.

Table 32. Description of the PLS factors for the NIR calibration models.

Model	PLS Factors	R2X	R2X(cum)	R2Y	R2Y(cum)	Q2	Q2(cum)
		SNV+1st derivative 12003-10152 cm^{-1}					
M1	1	0.998	0.998	0.996	0.996	0.995	0.995
	2	0.001	0.999	0.000	0.996	0.033	0.996
SNV 10522-10005 cm^{-1}							
M2	1	0.990	0.990	0.994	0.994	0.994	0.994
	2	0.002	0.992	0.001	0.996	0.100	0.995
SNV+1st derivative 10522-10005 cm^{-1}							
M3	1	0.981	0.981	0.995	0.995	0.995	0.995
	2	0.014	0.996	0.000	0.995	-0.015	0.995
SNV+1st derivative 10522-10129 cm^{-1}							
M4	1	0.993	0.993	0.993	0.993	0.992	0.992
	2	0.004	0.997	0.000	0.993	0.027	0.993
SNV+1st derivative 11998-10754 cm^{-1}							
M5	1	0.970	0.970	0.995	0.995	0.995	0.995
	2	0.013	0.982	0.002	0.997	0.271	0.996
SNV+1st derivative 11998-10754 + 10522-10129 cm^{-1}							
M6	1	0.980	0.980	0.996	0.996	0.995	0.995

	2	0.012	0.992	0.000	0.996	-0.025	0.995

R2X - Sum of Squares of all the x-variables explained by the extracted components.
R2Y - Sum of Squares of all the y-variables explained by the extracted components.
Q2 - The fraction of the total variation of X (PC) and Y (PLS) that can be predicted by the current component.

5.3.6. Calibration cross-validation and validation analysis

During development activities, the technique of "cross-validation" was used to obtain information regarding the suitability of the NIR calibration model performance. In Cross-Validation, the entire calibration set was split into groups of seven (10) samples, which were removed individually from the rest of the samples and tested as unknowns against the NIR calibration model that was constructed using the rest of the samples. The predictive performance of the model was evaluated using root mean square error of calibration (RMSEC), root mean square error of cross-validation (RMSECV), and root mean square error of prediction (RMSEP). Based on previous studies developed using the same CM line, the model was evaluated using a maximum of two PLS factors to optimize the ability to predict new samples (Colón, Vargas, Sánchez, Navarro, & Romañach, 2016; Vargas et al., 2018). Results for each preliminary model assessment are shown in **Table 33**. The lowest RMSEC, RMSECV, and RMSEP were obtained using the M3 and M5 models. Therefore, the NIR calibration model evaluation was developed within the range of 11998 – 10753 cm^{-1} with SNV + 1^{st} derivative as spectral preprocessing using 2 PLS factors, based on the results from **Table 32** and **Table 33**. However, the SNV + 1^{st} derivative model showed an intense API-1 band seen in the range of 10522 – 10129 cm^{-1}, shown in **Figure 54**. Both models were used to evaluate the effect of NIR spectral selection in the challenge evaluation of the models.

Table 33. Results for each preliminary model assessment for the calibration set.

PLS Factors	**RMSEC for calibration set**					
	M1	**M2**	**M3**	**M4**	**M5**	**M6**
1	1.4	1.6	1.5	1.8	1.5	1.4
2	1.3	1.4	1.5	1.7	1.2	1.3
PLS Factors	**RMSECV for calibration set**					
	M1	**M2**	**M3**	**M4**	**M5**	**M6**
1	1.4	1.6	1.5	1.8	1.5	1.4
2	1.4	1.5	1.5	1.8	1.3	1.4
PLS Factors	**RMSEP for validation set**					
	M1	**M2**	**M3**	**M4**	**M5**	**M6**
1	1.7	1.9	1.8	1.8	1.4	1.8
2	1.6	1.7	1.7	1.7	1.5	1.7

5.3.7. PLS score plot analysis of the calibration set

Score plots are useful to detect patterns, clustering, and outliers in the data. Score Plots were created for calibration set of tablets for 1 PLS and 2 PLS factors. **Figure 61** shows the score line plot of the NIR calibration model developed using 1 PLS factor (**Figure 61a**) and 2 PLS factors (**Figure 61b**) for the selected model strategy. The first PLS factor describes variation in concentration since samples are very well aligned in increasing concentration (left to right). The second PC also describes variation in the sample set, this variation is similar at the extremes of concentration ranges and very small compared to the variation described by the first PC. All samples in the score plots are within the 95% confidence interval in the 1 PC score plot; however, one sample at 130% LC concentration level in score plot using 2 PCs is outside of the 95% confidence interval. This sample outside of the limit is not treated as an outlier and will be used for the development of the NIR calibration model since there is a 5% of probability that samples will fall outside of the ellipse.

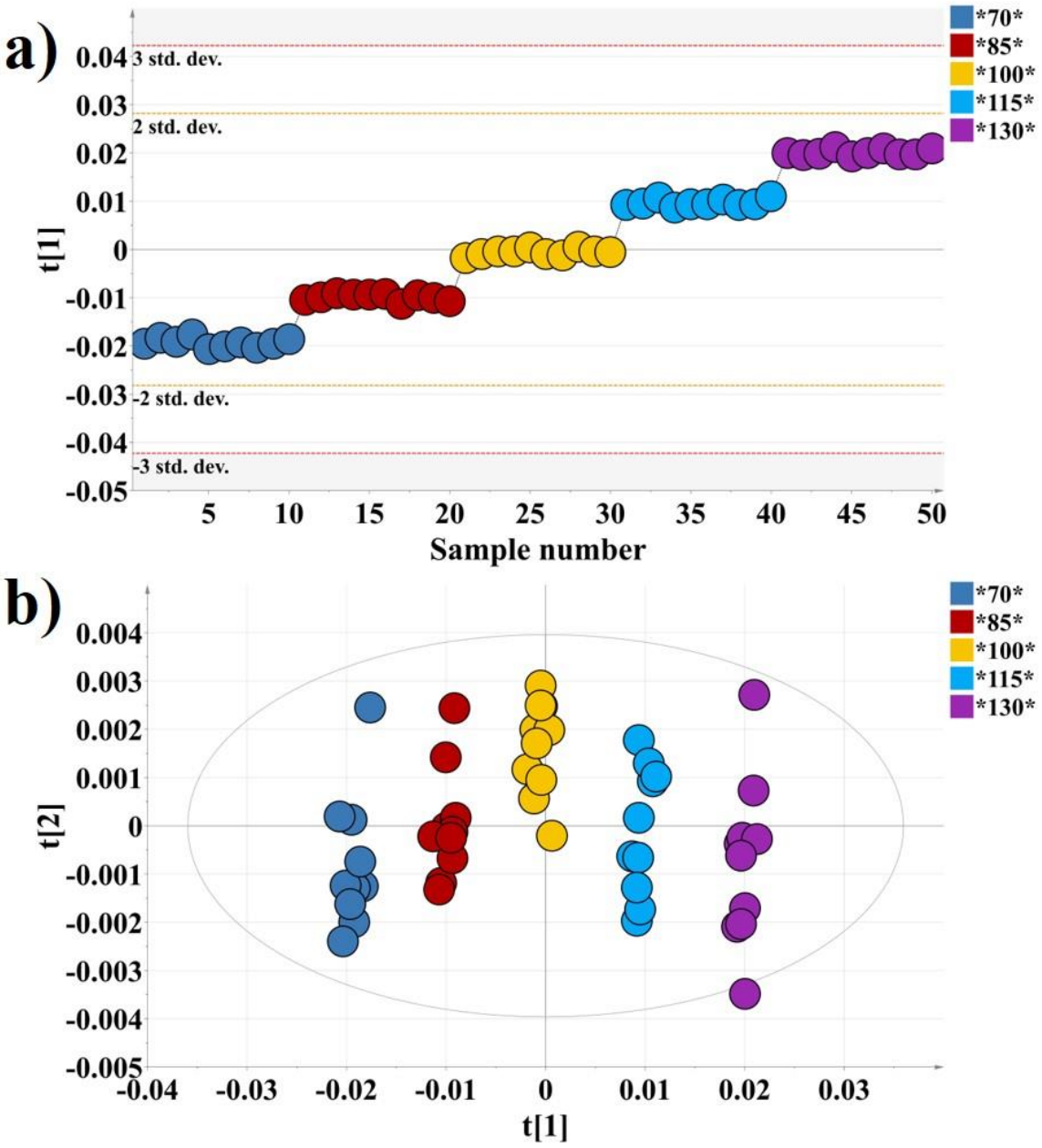

Figure 61. PLS score plots of the calibration set. a) 1 PLS Score Plot and b) 2 PLS Score Plot.

5.3.8. Predictive performance of the NIR calibration model at left, center, right, and average sides of validation set

The NIR calibration model was developed using the average of left, center, and right spectra for each tablet with the calibration set. Individual NIR spectra of left, center, and right sides, as

well as the average of the three side predictions for each tablet of the validation set were used as evaluation to test the model's performance.

NIR predictions of left, center, and right spectra for each individual tablet were compared between them to evaluate if there are differences in the results for position of measurement at each concentration level. Ten (10) tablets per concentration level of the validation set were evaluated by a single factor ANOVA.

The null hypothesis tested with the ANOVA is that there will not be differences between the means of the spectra of the experimental groups (average value of the dependent variable). The alternative or research hypothesis is that the average is not the same for all groups. In general, if the calculated F statistic in a test is larger than the table F value, we can reject the null hypothesis. The p-value is a numerical measure of the statistical significance of a hypothesis test. It says how likely it is that we could have gotten our sample data even if the null hypothesis is true. By convention, if the p-value is less than 5% ($p < 0.05$) the null hypothesis can be rejected (Wahid, Latiff, & Ahmad, 2017). **Table 34** shows a summary of the single factor ANOVA for each concentration level, evaluated by center, left, and right NIR predictions of validation set.

The F crit is 3.354 for the number of samples and groups used. Based on the results obtained, there is no statistical difference on the calculated NIR predictions of left, center, and right sides for concentration levels 85% - 130% LC with calculated F being lower than the F crit value, except for the lowest concentration level of 70% LC which resulted in a calculated F higher than F crit, and a p-value lower than 0.05. Using the Fisher LSD Method and 95% Confidence for the NIR predictions at 70% LC, **Figure 62** shows that there is a difference between the results of the left and right sides of the tablets, however, center side did not present differences with left nor right sides of the tablets. This difference on the predictions for sides of the tablets at 70% concentration

level, is expected since this is the lowest concentration level. At lower concentration levels, the particles of API are dispersed around all the tablet and there is a low probability of having the API homogeneously distributed in a relatively large tablet. A way to correct this issue is to increase the number of samples in the calibration set or increase the number of concentration levels. For this case, the concentration target is 100% and this level presents an F = 2.211, which is lower than F crit of 3.354, and the calculated p-values are higher than 0.05. These results indicate that there is no statistical difference between the NIR predictions of the left, center, and right sides of the tablets at 100% concentration level.

Table 34. Summary of ANOVA single factor analysis for each concentration level, evaluated at the center, left, and right NIR predictions of the validation set.

Summary of ANOVA: Single Factor for 70 (%LC)							
Groups	***n***	***Sum***	***Average***	***Variance***	***F***	***p-value***	***F crit***
Center	10	706.076	70.608	2.922	**6.173**	**0.006**	**3.354**
Left	10	689.599	68.960	4.382			
Right	10	722.511	72.251	5.856			
Summary of ANOVA: Single Factor for 85 (%LC)							
Center	10	850.858	85.086	2.986	**0.040**	**0.961**	**3.354**
Left	10	847.221	84.722	14.449			
Right	10	849.742	84.974	8.794			
Summary of ANOVA: Single Factor for 100 (%LC)							
Center	10	997.759	99.776	8.276	**2.211**	**0.129**	**3.354**
Left	10	976.197	97.620	2.820			
Right	10	1000.174	100.017	12.545			
Summary of ANOVA: Single Factor for 115 (%LC)							
Center	10	1154.361	115.436	8.641	**2.301**	**0.119**	**3.354**
Left	10	1127.791	112.779	13.832			
Right	10	1156.112	115.611	10.358			
Summary of ANOVA: Single Factor for 130 (%LC)							
Center	10	1302.076	130.208	3.163	**2.157**	**0.135**	**3.354**
Left	10	1275.790	127.579	8.531			
Right	10	1299.423	129.942	17.430			

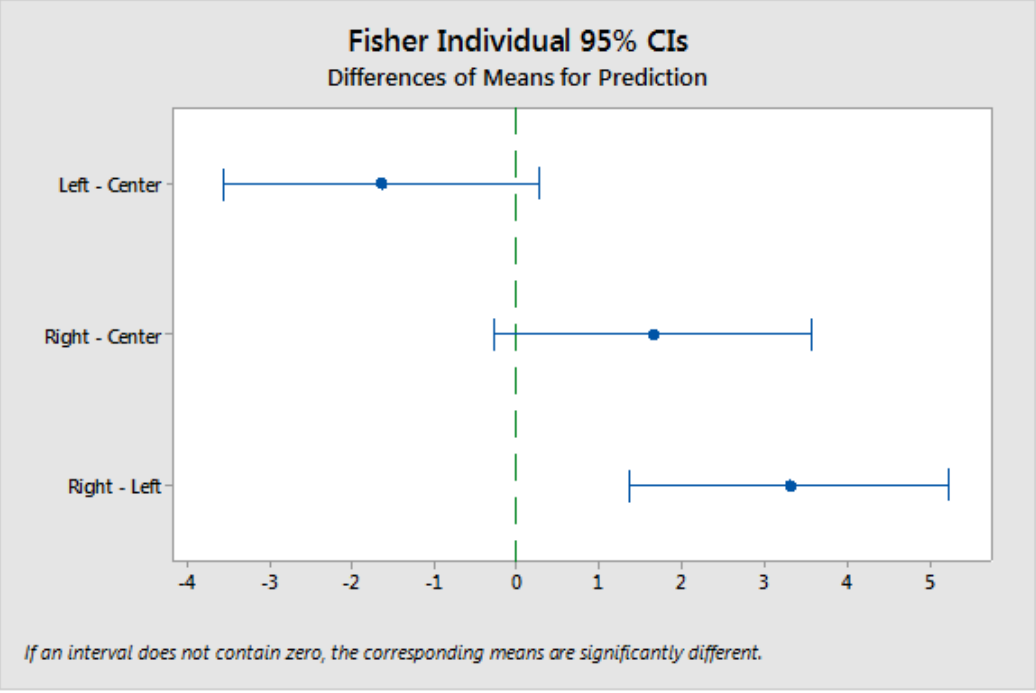

Figure 62. Fisher LSD results at 95% Confidence Interval for center, left and, right sides of the validation tablets at 70% LC.

Based on the results of **Table 34**, the NIR predictions of the center spectra of all validation tablets were compared with the NIR average predictions and UPLC results to evaluate if there are statistical differences among them. **Table 35** shows the summary of single factor ANOVAs for each concentration level. F crit is 3.354 for the number of samples and groups used. Results show that the calculated F for all the concentration levels is higher than the F crit. In addition, all p-values are higher than 0.05. These results indicate that there is no statistical difference among the NIR prediction of the spectra average, center spectra, and UPLC determinations for each tablet in the validation set. Subsequently, the NIR calibration model performance characteristics were evaluated using the center side of the NIR predictions.

Table 35. Summary of ANOVA single factor analysis of each concentration level evaluated with the average, center, and UPLC measurement of the validation set.

Summary of ANOVA: Single Factor for 70 (%LC)							
Groups	***n***	***Sum***	***Average***	***Variance***	***F***	***p-value***	***F crit***
Average	10	706.062	70.606	0.778	**0.126**	**0.882**	**3.354**
Center	10	706.076	70.608	2.922			
UPLC	10	703.691	70.369	0.788			
Summary of ANOVA: Single Factor for 85 (%LC)							
Average	10	849.274	84.927	2.684	**0.475**	**0.627**	**3.354**
Center	10	850.858	85.086	2.986			
UPLC	10	844.039	84.404	2.374			
Summary of ANOVA: Single Factor for 100 (%LC)							
Average	10	991.376	99.138	3.045	**0.390**	**0.681**	**3.354**
Center	10	997.759	99.776	8.276			
UPLC	10	999.693	99.969	3.231			
Summary of ANOVA: Single Factor for 115 (%LC)							
Average	10	1146.088	114.609	6.612	**0.366**	**0.697**	**3.354**
Center	10	1154.361	115.436	8.641			
UPLC	10	1146.982	114.698	1.647			
Summary of ANOVA: Single Factor for 130 (%LC)							
Average	10	1292.430	129.243	3.781	**1.173**	**0.325**	**3.354**
Center	10	1302.076	130.208	3.163			
UPLC	10	1288.992	128.899	4.822			

5.3.9. Score plot analysis of the validation set

Figure 63 shows the score projection of the validation set. All samples present a linear tendency with increasing concentration from 70% to 130% LC along the first PLS factor axis. The projections of the validation set present a small degree of variation along the second PLS factor that needs another diagnostic to detect outliers. For the validation data, a Normal Probability Plot of Residuals serves to detect outliers in the dataset. If the residuals are random and normally distributed, the normal probability plot of the residuals has all the points lying on a straight line between the standardized deviations. Experimental runs lying outside the line of standardized deviations are considered outliers.

Figure 64 shows a Normal Probability Plot of Residuals for the validation set. From this data, there are only one observation that is far from the rest of the data, however its value lying between a straight line of standardized deviations. Therefore, all the observations of the validation set can be used to test the validity of the model.

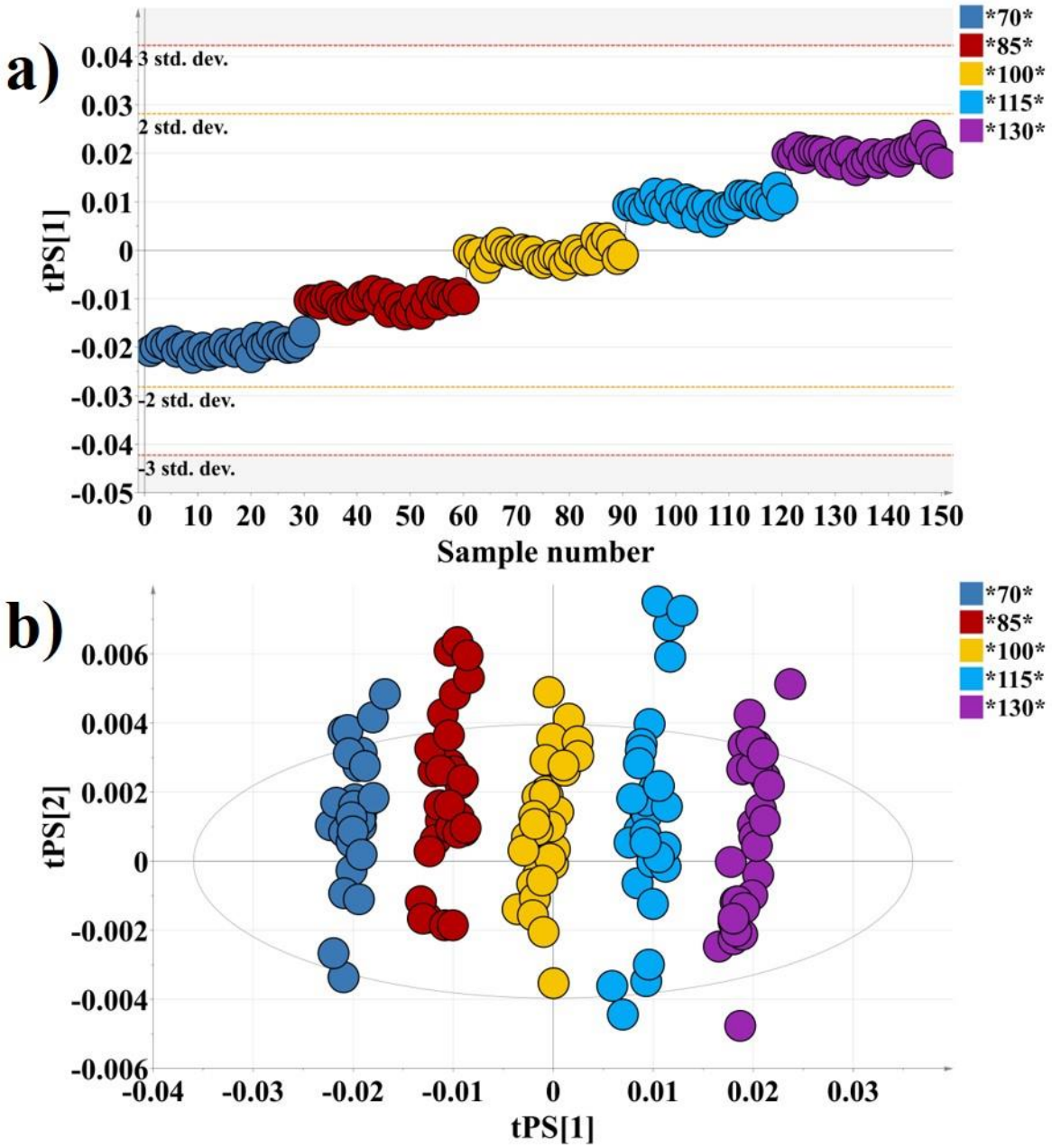

Figure 63. PLS score plots of the validation set. a) 1 PLS Score Plot and b) 2 PLS Score Plot.

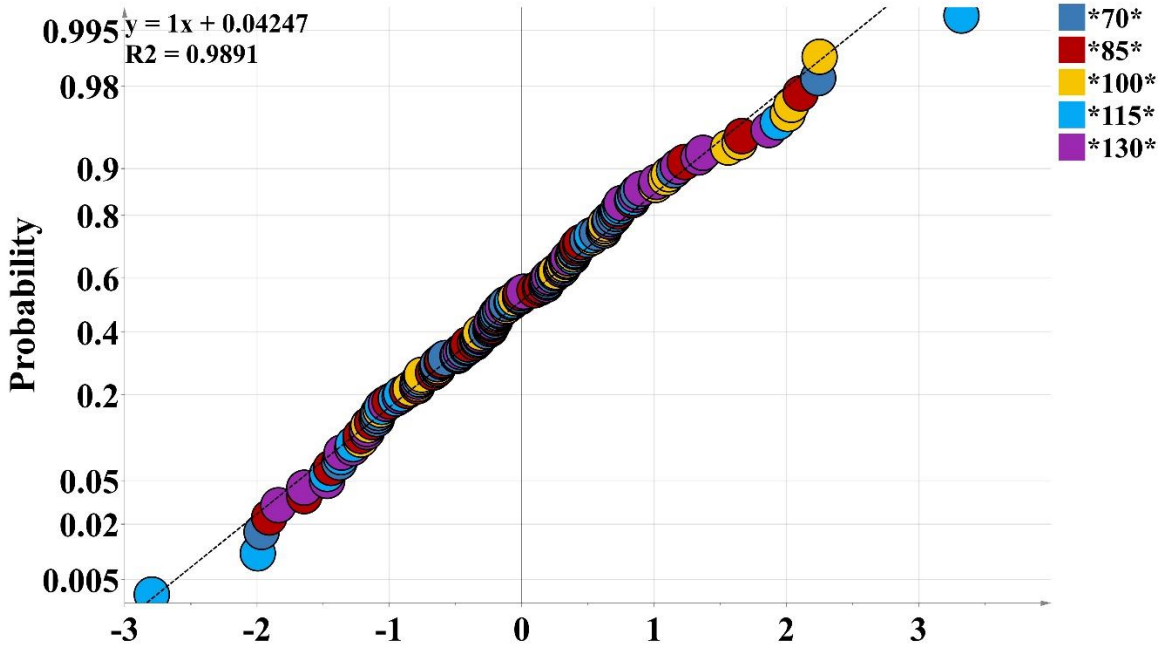

Figure 64. Normal probability plot of residuals for the validation set.

5.3.10. Method performance characteristics (ICH Q2 parameters)

The NIR calibration model performance characteristics evaluated are: accuracy, precision, linearity, range, robustness, and specificity (ICH, 2005; Olivieri, 2015). This evaluation was performed by the analysis of the validation set (target concentrations of 70%, 85%, 100%, 115%, and 130% LC).

5.3.10.1. Accuracy

Accuracy was determined with using thirty (30) spectra per concentration level, three (3) spectra from each tablet, and ten (10) tablets per concentration level. **Table 36** shows the center measurement NIR results of the validation set, the corresponding UPLC results, and the RMSEP. From the table, all the NIR prediction standard deviations and RMSEP values for 70%-130% LC

validation samples are below to 1.5 and 2.0, respectively demonstrating a high level of accuracy achieved by the developed NIR model.

A difference in results was observed for the 100% API-1 second lot samples. These API-1 2nd lot samples were prepared using a different granulation API-1 lot from the one used for 70%-130% LC validation samples. In average, this API-1 2nd lot granulation was found to be low in assay, also a higher standard deviation (Std. Dev.) between the granulation.

Table 36. Accuracy results of the validation set.

Target Concentration (%LC)	Center NIR Average	NIR Std. Dev	RMSEP
70	70.6	0.7	0.8
85	85.1	0.9	1.2
100	99.8	1.5	2.0
115	115.4	1.4	1.7
130	130.2	1.3	1.2
100 (API-1 2nd lot)	100.6	2.6	1.3

5.3.10.2. Precision

Two sources of variation were evaluated as part of the NIR calibration model precision assessment. The NIR concentration predictions were assessed in terms of system repeatability and reproducibility.

- **System repeatability**

The system repeatability was evaluated by analyzing 1 validation tablet of high, target, and low concentration levels (70%, 100%, and 130% LC). A total of ten (10) consecutive spectra per tablet (same side of the tablet, center measurement only) were acquired. **Table 37** shows the NIR concentration predictions for the system repeatability study. The evaluation was performed by the evaluation of the standard deviation and % RSD. All NIR results standard deviations and % RSD

values were between 0.3 and 0.8 for all concentration levels which means that variations between measurements are low and have similar values.

Table 37. Repeatability results of the validation set.

Target Concentration (%	Average	Std.	RSD
70	70.0	0.5	0.8
100	110.6	0.6	0.6
130	132.9	0.4	0.3

- **Intermediate precision**

The intermediate precision analysis was performed using three (3) concentration levels, two (2) analysts and one FT-NIR Analyzer. A total of six (6) spectra (same side of the tablet, center measurement only, at high, target and low concentration) per concentration level were acquired. **Table 38** and **Table 39** show the NIR results for the reproducibility study. The evaluation was performed by the standard deviation, RSD (%) and pooled Std. Dev.

The intermediate precision shows a standard deviation from 0.3 to 0.7, RSD (%) from 0.3 to 0.8, the pooled standard deviation between analysts for the three (3) concentration levels were 0.4, 0.6 and 0.4 for concentration levels 70%, 100%, 130% LC, respectively. These results have low variations and they are similar to values of the repeatability discussed before, which means that variations from analyst to analyst are minimum and reproducible.

Table 38. Intermediate precision results of the validation set for the analyst 1.

Target Concentration (% LC)	Average	Std. Dev.	RSD
70	68.2	0.4	0.6
100	97.6	0.5	0.5
130	132.0	0.4	0.3

Table 39. Intermediate precision results of the validation set for the analyst 2.

Target Concentration (% LC)	Average	Std. Dev.	RSD
70	68.4	0.4	0.6
100	97.6	0.7	0.7
130	131.9	0.3	0.2

5.3.10.3. Linearity

Linearity was determined by analyzing all ten (10) tablets at all five (5) concentration levels of the validation set (target concentrations of 70%, 85%, 100%, 115%, and 130% LC API). The linearity was evaluated between the API-1 concentration determined by the NIR calibration model predictions of the center measurement only and the corresponding UPLC results of the fifty (50) tablets of the validation set. The plot of the NIR predicted values versus the UPLC results and the linear equation regression coefficients are shown in **Figure 65.** Comparison between the predictions and UPLC results produced a correlation coefficient of 0.990 showing strong correlation between both methods.

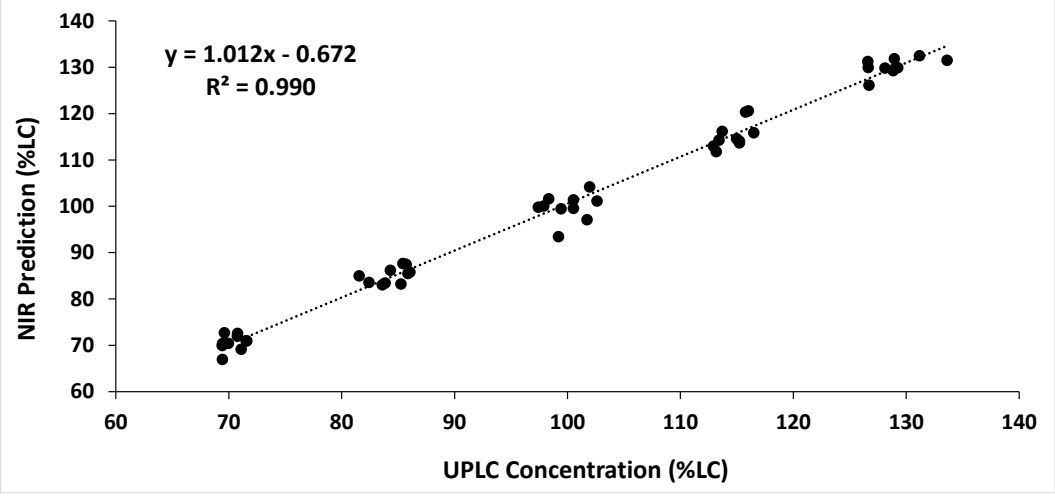

Figure 65. Plot of the center NIR predictions vs UPLC results of the validation set.

5.3.10.4. Robustness

Robustness was evaluated by measuring the capacity of the NIR calibration model predictions to remain unaffected by the deliberate variations of the tablet side positioning (top debossed side vs bottom debossed side) in the FT-NIR Analyzer. The sample holder was not evaluated as a measurement characteristic since all holders to be used are from the same manufacturer and set.

The average prediction, pooled standard deviation, p-values of the paired t-test of the predictions performed on one tablet of the 70, 100, and 130% LC concentration levels (tablets from the validation set) at the different tablet positioning were calculated and presented in **Table 40**.

The t-test showed no statistical significant differences between the measurements taken from the different sides of the tablets, for the 100% and 130% LC concentration levels with p-values higher than 0.05. However, at the lowest concentration level (70% LC) there is a statistical difference on the NIR prediction of the spectra acquired from the same tablet of the sides. This result is expected due to low concentration level of API-1 in a relatively large tablet and the small amounts of samples used for this analysis. In addition, the p-value of the analysis increases as the concentration level of API increases in the tablet. Moreover, at target concentration (100% LC) the NIR predictions are not statistically different.

Table 40. t-test statistic on the top vs bottom debossed side comparison of the validation tablets.

Target Concentration (% LC)	NIR Prediction % LC (bottom Side)	NIR Prediction % LC (top Side)	Pooled Std. Dev.	p value
70	72.177	70.340	1.9	0.025
	70.281	68.414		
	72.328	71.245		
Average	**71.6**	**70.0**		
100	100.803	100.335	2.2	0.089
	98.911	97.653		
	101.394	100.811		
Average	**100.4**	**99.6**		
130	136.218	137.482	9.5	0.601
	124.993	125.379		
	127.677	127.041		
Average	**129.6**	**130.0**		

5.3.10.5. Specificity

The purpose of the specificity exercise is to evaluate the capacity of the NIR calibration model to respond to the analyte of interest (API-1) at the range of concentrations of the development. An overlay of the tablet spectra containing API-1 target concentrations at 70%, 100%, 130% LC, pure API-1, API-2 and one excipient were analyzed. **Figure 66** illustrates these spectra.

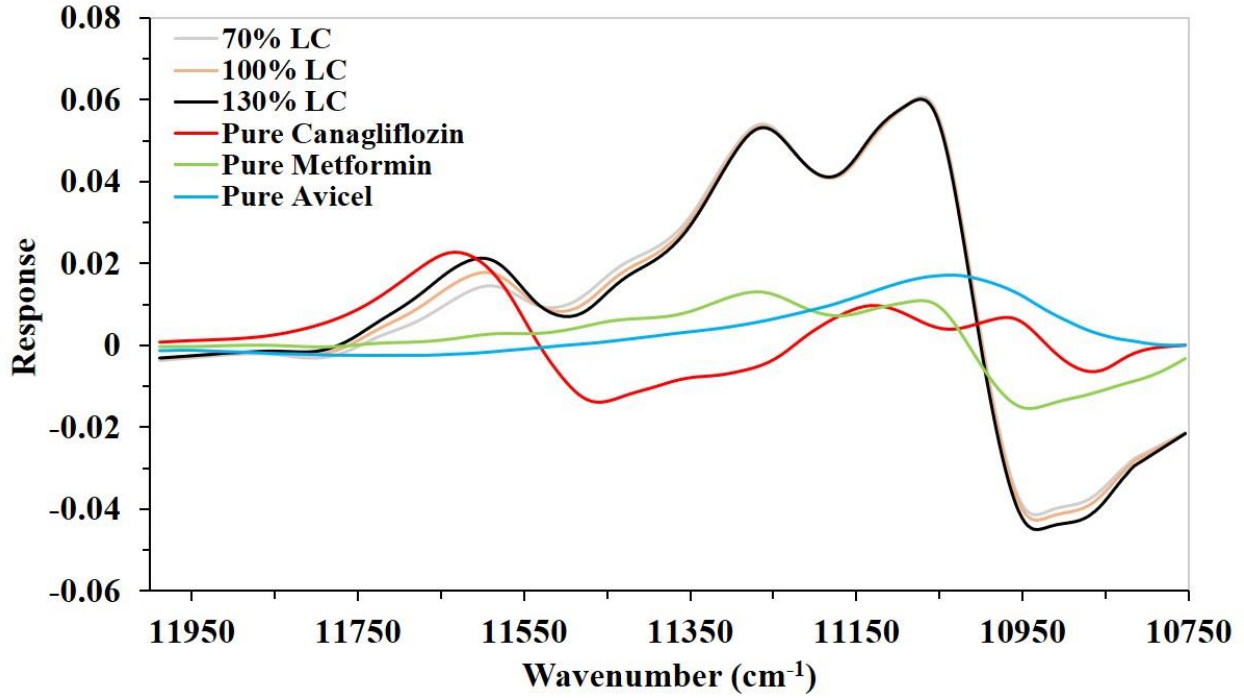

Figure 66. Overlay spectra of API-1 at target concentrations at 70%, 100%, 130% LC tablets, pure API-1, pure API-2, and one pure excipient tablets.

Tablet spectra containing 70%, 100%, and 130% LC API-1 in the formulation show the same pattern of variation. As the concentration of API-1 increases in the formulation, bands associated with this (red line) increase in response showing the same characteristic bands as the tablet containing pure API-1. The opposite is observed for the excipient. No variation (response) or bands are observed in the excipient spectra associated to the API-1 (orange line) in this spectra region.

In addition, an overlay of the NIR model regression vector and a pure API-1 spectrum is shown in **Figure 67**. The NIR model regression vector (black line) is aligned with the maximum variance of the pure API-1 spectra (red line) indicating that the model is specific to changes in API-1.

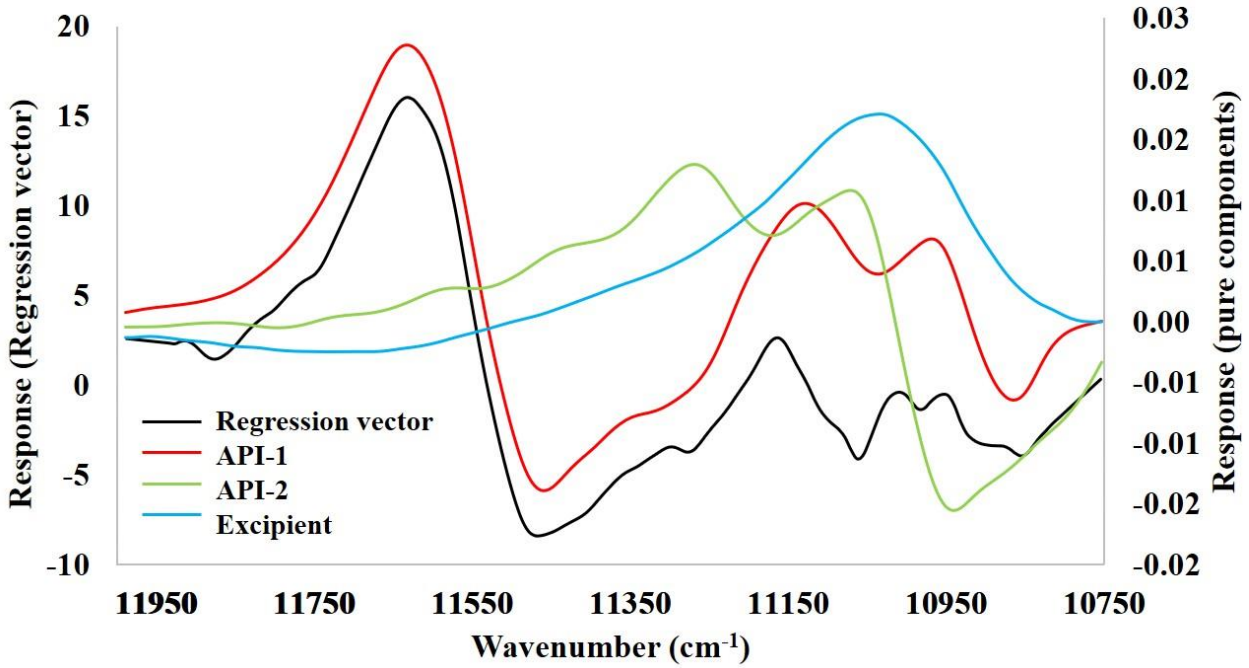

Figure 67. Overlay spectra of the regression vector, pure API-1, pure API-2 and one pure excipient tablets.

The NIR calibration model selected resulted on a 2 PLS factors in the 11988-10753 cm^{-1} spectral region using SNV followed by first derivative, 17-point window spectra preprocessing. The model was developed using an average of 128 scans per spectrum and a resolution of 64 cm^{-1}, at the center side of each tablet.

Challenge to the developed model was performed within the designed space of process in the continuous manufacturing line. In addition, an evaluation was performed of the model selected in the 11988-10753 cm^{-1} and the 10522-10005 cm^{-1} spectral region.

5.3.11. Evaluation of potential critical process parameters in the CM line

The model developed is based on target conditions of process variables in the CM line that are part of a normal run for commercial purposes. Based on this condition, the model was

challenged with a design of experiment (DoE) of the manufacturing process variables to evaluate potential Critical Process Parameters (pCPPs) to assess their criticality during the manufacturing shown in **Table 41**. The changes in the variables in the table are three (3) levels of evaluation, high, target and low level. These levels were selected according to the target process, and the high and low levels are within the limits of the product manufacturing. The first process variable is the blender speed, which defines the mixing of the materials and the heterogeneity of the powder blend (Vanarase et al., 2010). The second variable is the lubricant feed rate, which improve the flowability of the materials and adherence to metallic parts of the CM line (Boukouvala, Niotis, Ramachandran, Muzzio, & Ierapetritou, 2012). The third and fourth variables are the API-1 and API-2 feed rates, which define the amount of materials used and therefore, the predicted concentration. The fifth and sixth variables are the tablet weight and main compression force that are part of the final process and have been studied (Ervasti et al., 2015; Järvinen et al., 2013; Singh et al., 2014; Ward et al., 2013). With these variables, 20 compression profiles were performed, the first and last profiles are runs at targets conditions of manufacturing.

Table 41. Design of experiment of the manufacturing process variables. Relative to target values (%).

Comp. Profile	Blender Speed (% rpm)	Lubricant Feed Rate (% kg/h)	API-1 Feed Rate (% kg/h)	API-2 Feed Rate (% kg/h)	Tablet Weight (% mg)	Main Compression Force (% kN)
1	100	100	100	100	100	100
2	117	78	107	96	103	80
3	117	78	107	104	97	80
4	83	100	107	104	103	80
5	83	122	92	96	103	120
6	100	78	92	96	103	120
7	100	100	100	100	97	80
8	83	78	100	96	100	100
9	117	122	100	104	97	80
10	83	122	107	96	97	120
11	83	78	92	104	103	120
12	117	122	107	96	100	80
13	117	122	92	100	100	100
14	100	100	100	100	103	100
15	83	78	107	100	97	120
16	117	78	92	104	103	80
17	117	100	92	96	97	120
18	100	122	107	104	97	100
19	83	122	92	104	100	120
20	100	100	100	100	100	100

The NIR calibration model in the 10522 – 10005 cm^{-1} region (first model) and the 11988 – 10753 cm^{-1} region (second model) were used to predict the content of six (6) tablets for each individual run, also the UPLC analytical concentration were measured to obtain the reference value. The reason to use the content instead of concentration of tablets is that the NIR calibration models were developed at target conditions of process manufacturing (Blanco & Alcalá, 2006). This implies that NIR predictions of concentration are to tablet weight at the target weight. The DoE from **Table 41** includes variations of tablet weight at high and low levels, if the NIR concentration is used at these levels, the predictions result in values away from the real value. The use of NIR content serves to correct the differences in tablet weight and to obtain the amount of API of interest in the tablet.

Figure 68 shows the NIR prediction content of the tablets at the different profile runs of the DoE using the NIR concentration (**Figure 68a**) and the NIR content (**Figure 68b**). The first two runs correspond to target profiles of all variables evaluated. As show the figure, the first model (red color) present high values in almost all the profiles compared to UPLC values, except the profile 8 that has low levels in the variables blender speed, lubricant feed rate, and API-2 feed rate, the rest of the variables are in target conditions. The second model (green color) present similar values to UPLC at the two target conditions (profiles 1 and 20). From this figure there are a notable pattern to highlight, the second model at the profiles 2, 10, and 12, predict low values compared to UPLC, and this model at the profiles 11, 16, and 19, predict high values compared to UPLC. From **Table 41**, the profiles where the second model predict low values have the variables API-1 feed rate at high level and the API-2 feed rate at low level; the profiles where the second model predict at high values have the variables in the inverse scenario. The principal reason for the differences in the predictions of the second model is that this model was develop using a spectral region with absorbance bands of the API-1, API-2 and the major excipient in the formulations. With this information of the second model (the 11988 – 10753 cm^{-1} region) can be evaluated the source of variations in the predictions and decide the changes that need to be done in the control process.

In deep analysis need to be done to have a better understanding for the relationship of the rest of the process variables and their influence in the NIR predictions. In this study chemometrics analysis were performed to facilitate the evaluation of the process variables and their relationship with NIR predictions. From the **Figure 68** was evaluated how is the change in NIR predictions with variations at high and low levels of the API-1 and API-2 feed rates, however is not easily to understand the relationship of the rest of process variables. An evaluation was performed using

PCA between the process variables of manufacturing (**Table 41**) and the NIR predictions of the second model (in content values), also was included the time of the NIR spectral acquisition to estimate if this variable has a relationship in the predictions of the model.

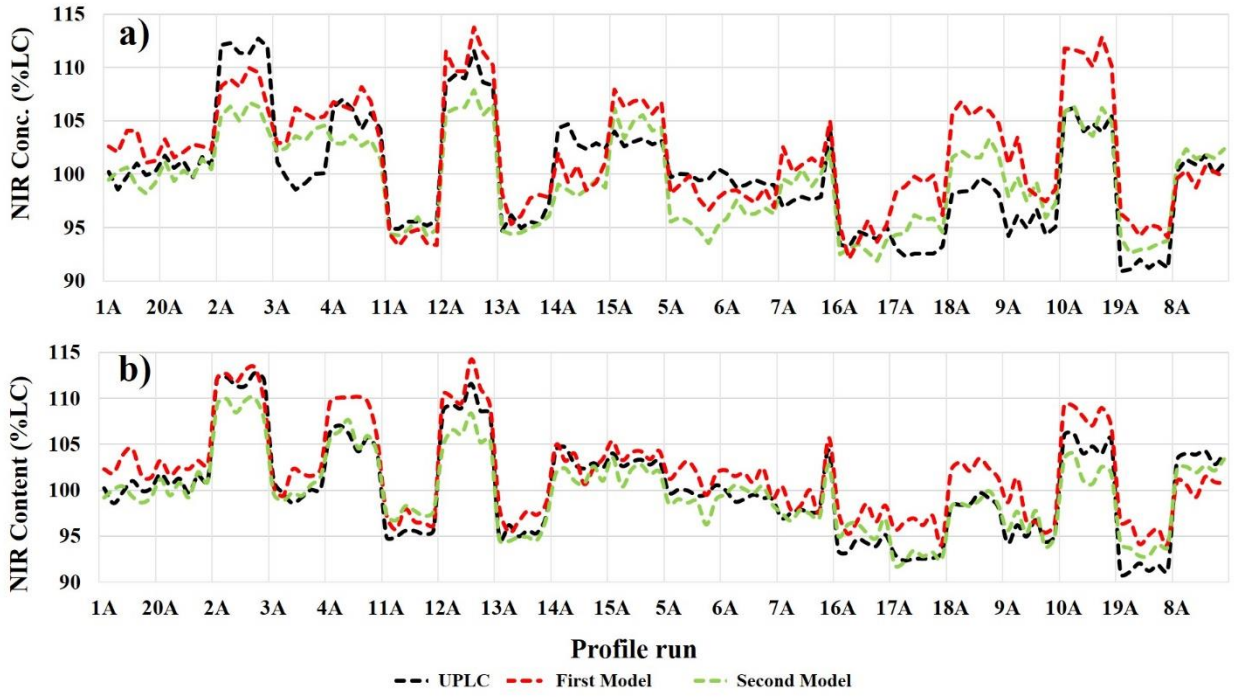

Figure 68. NIR predictions of the tablets from the DoE of manufacturing process runs. a) NIR concentration (%LC) and b) NIR content (%LC).

Figure 69 shows the result of the PCA loadings between the process variables, the NIR predictions (content values) and the time of the NIR spectral acquisitions. The green columns represent the first loading, the blue columns the second loading and the yellow columns the third loading. As shows the figure the NIR predictions has a positive relationship with the API-1 feed rate in the first loading, and this can be explained because the NIR calibration model is based in the API-1. The time has a negative relationship with the NIR predictions, and this is an important issue that can be resolved with a plan of execution for NIR spectral acquisition of the tablets.

Blender speed and lubricant feed rate have moderate relationship with the NIR predictions, however the second loading show that these process variables have major and inverse relationship with the predictions. In the final process of manufacturing the tablet weight has minor relationship with the predictions in the first loading, and this is because the NIR predictions have been corrected by tablet weight and the values are the content. Main compression has a negative an strong relationship with the predictions in the three loadings of the PCA, this can be explained because this produce the compaction of the tablets and therefore, the scattering of the NIR radiation into the tablets is not the same at the different levels of compression (Blanco & Alcalá, 2006).

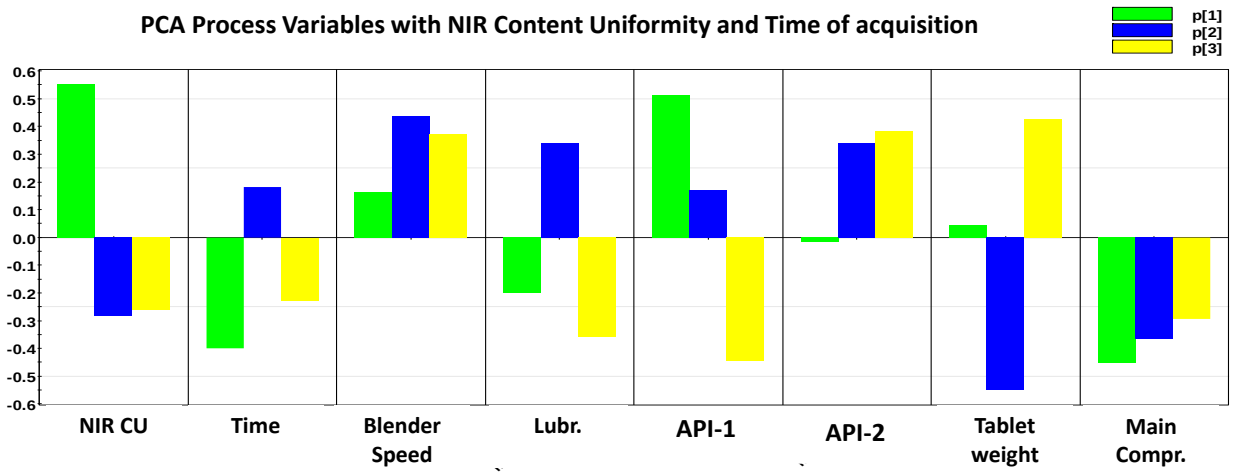

Figure 69. Relationship between process variables by PCA from the DoE of manufacturing process runs.

The PCA score plot between the process variables, the NIR predictions (content values) and the time of the NIR spectral acquisitions are shown in **Figure 70**. In the figure are shown the directions of the variations according to NIR predictions in content values (**Figure 70a**), the main compression force (**Figure 70b**), and the tablet weight (**Figure 70c**). The blue plots indicate low level, the green color middle level, and the red color high level of the variables. For each PCA

score plot is attached the loading of the process variable to link the weight of the variable and the direction in the score plot. As shown in **Figure 70**, the main compression and the tablet weight have a direct relationship with the second PC as NIR predictions has the same direction. This indicate that the process at the tablet press is one of the major sources of impact in the NIR predictions in this study.

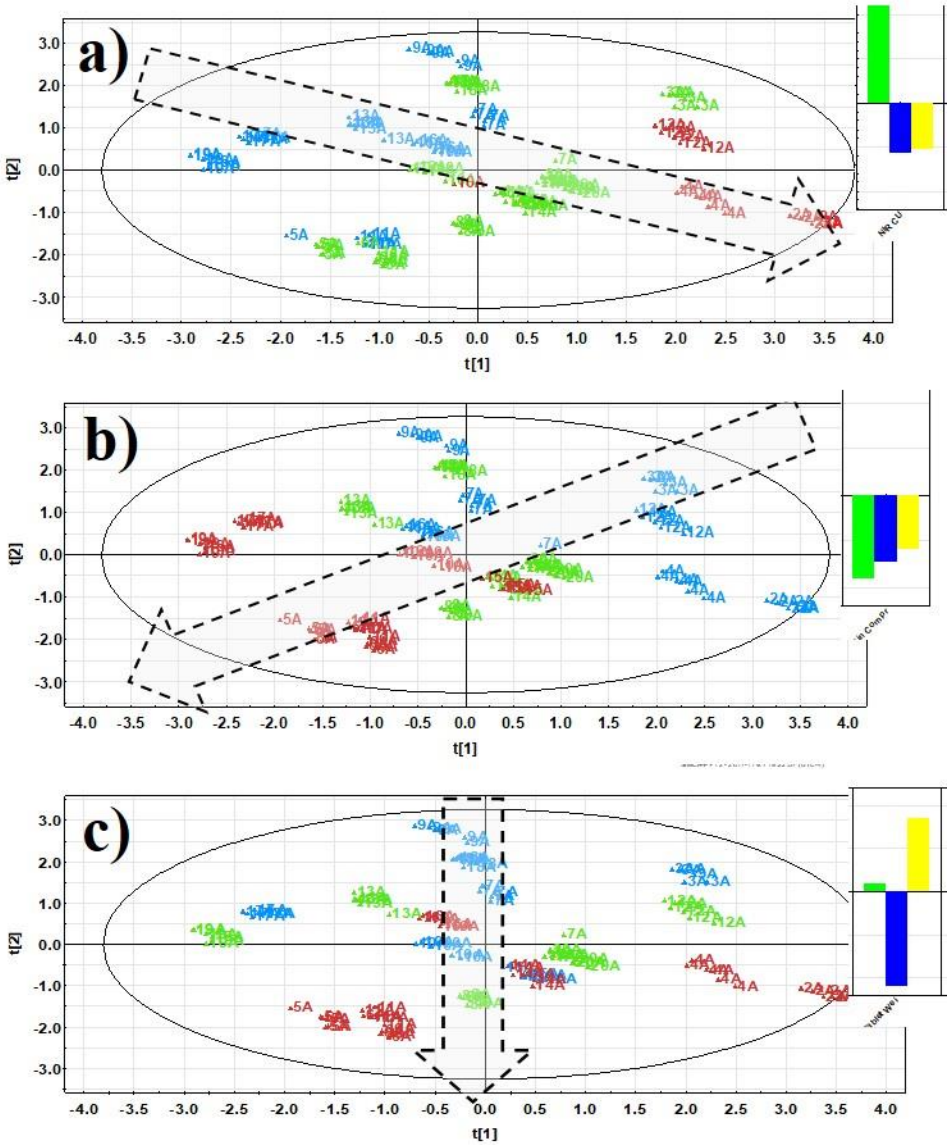

Figure 70. PCA score plots of the DoE of manufacturing process runs. a) Color according to NIR predictions (content values). b) Color according to main compression force. c) Color according to tablet weight. Blue: low level, green: middle level, and red: high level.

5.4. **CONCLUSIONS OF CHAPTER 5**

The NIR calibration model for tablets of a drug product containing two APIs was successfully developed. This development resulted on a 2 PLS factors model in the 11998 – 10753 cm^{-1} spectral range using SNV followed by first derivative, 17-point window as spectral preprocessing. The analytical configuration was develop using an average of 32 scans per spectrum and a resolution of 64 cm^{-1}, at three sides (left, center and right side) of each tablet.

The model was challenged with extreme limits of process variables of manufacturing and the relationship of these variables was evaluated with the NIR predictions. It was found that model at target conditions of process manufacturing remains similar to the UPLC analytical reference method, however at the extreme and inverse limits between the API-1 and API-2 feed rates, the model result in positive or negative bias, according to the relationship between the feed rate values.

PCA shows that variables at the tablet press have a relationship with the NIR predictions and this information suggest that more attention need to be done in this final process. Finally, based on the results obtained in this work, critical process parameters can be estimate in the product development in the continuous manufacturing line and the relationship with the predictions obtained with a NIR calibration model.

CHAPTER 6: CONCLUSIONS AND FUTURE WORK

This dissertation describes four studies to evaluate the prediction errors observed in partial least squares (PLS) calibration models by diffuse reflectance and transmission near infrared (NIR) spectroscopy.

The NIR method was found to be unbiased as long as the optical sampling of the FT-NIR instrument is representative of the samples to be analyzed and samples with very low heterogeneity are measured. The reproducibility and linearity of two FT-NIR instruments can be evaluated using low heterogeneous polymer films to avoid errors due to the heterogeneity of the samples.

The powder density and porosity of pharmaceutical powder blends at low concentration of active pharmaceutical ingredient (API) has an effect on the prediction errors of PLS calibration models that can be evaluated in a real time process by NIR spectroscopy.

The impact of production process parameters in the prediction of one API content of tablets (with two APIs) from a continuous manufacturing (CM) line can be evaluated efficiently using NIR spectroscopy. The results shown that using the spectral region with moderate intensity of both APIs and excipients, presented low prediction error and bias that using the high intensity band of the API of interest.

The first study in chapter 2, based on the test of representative layer theory, contributed an uncomplicated, efficient, and economic method to have a better understanding of the physics of diffuse reflectance in solid materials using low heterogeneous polymer films (polypropylene). The results shown that NIR method is unbiased as long as the number of samples are within the depth of penetration of the NIR radiation. The error due to sampling procedures can stem from the

heterogeneity of the materials and for the case of NIR reflectance measurements it can occur due to optical sampling by the depth of penetration of the NIR radiation. The sampling error was reduced by using a system with low heterogeneity in this study since as theory of sampling indicates, heterogeneity is the major source of all sampling errors. The optical sampling of the NIR radiation into the polymer films was determined and it was estimated the maximum sampling depth that can penetrates this specific samples of polypropylene non-glare films

The second study in chapter 3, contributed with an analytic method to evaluate the absorption and scattering of NIR radiation in PLS calibration models using two materials with a NIR spectra that presented spectral regions with correlations that affects the prediction errors. The study provided an uncomplicated, economic, and efficient method to test the reproducibility and linearity of two FT-NIR instruments using two low heterogeneous polymer films (polyethylene and polypropylene) with similar thickness (for the polyethylene film was 0.083 ± 0.002 mm, and the polypropylene film was 0.086 ± 0.002 mm). The results shown in this experimental design that both FT-NIR instruments presented statistical differences in the second overtones spectral region (9500 – 6500 cm^{-1}) depending the preprocessing applied. However, the first overtone region (6500 – 5000 cm^{-1}) did not show statistical differences no matter the spectral preprocessing applied. In conclusion. The reproducibility and linearity of both FT-NIR instruments was tested using validation samples from three random days for spectral acquisition, and the results in the 6500 – 5000 cm^{-1} spectral region using the second derivative passed satisfactorily the statistical tests applied.

The third study in chapter 4, described the first evaluation of powder bulk density and porosity of powder blends at low API concentration (3.00% w/w) within a feed frame. The evaluation of powder density and porosity of powder blends based on NIR spectra within a feed

frame was possible using large differences in powder density due to their excipients concentrations which facilitates the evaluation. The results show that PLS calibration models are affected by the porosity of the powder blends and it presents a high correlation with the predictions of API concentration in the first latent variable (PLS factor) which indicates that at low concentration of API (for this case 3.00% w/w), the physical properties of the samples presented a high impact on the errors observed by the PLS model.

The fourth study in chapter 5, described the efforts in the development of a PLS calibration model using NIR transmission in tablets with two APIs from a continuous manufacturing process. In conclusion, the real time determination of one API can be achieved satisfactorily saving effort, and time of analysis using an spectral region with moderate intensity of both APIs and excipients, instead of use a high intensity band of the API of interest but with few spectral bands of the other ingredients of the tablets. The impact of process parameters in the manufacturing of tablets can be determined by NIR spectroscopy, and the results shown that low prediction errors and bias can be observed in the spectral region with information of APIs and excipients. Based on the evaluation of process parameters, the main compression force and tablet weight presented and effects on the predictions by the PLS calibration model.

Future works could be performed for the evaluation of errors for NIR predictions of a more complex system of polymer films. Combinations of different polymer materials could be used with a design of experiment using a number of films below the infinite depth of penetration of the NIR radiation.

A future study based on the work in chapters 2 and 3 is to evaluate the performance of two (or more) NIR instruments using polymer films standards. The polymer films standards will provide homogeneous materials with few variations with time. Variability from the instruments

can be evaluated and it will be easier to perform an analysis of calibration models that works statistically equal on both NIR instruments.

Another study could be the evaluation of polymer pellets to simulate pharmaceutical powder materials and to reduce the waste of particulate compounds. This experiment could be a future work that helps to compare PLS regression as well as classical least squares regression and to evaluate the performance of both methods. This study also can be evaluated on two (or more) NIR instruments.

References

Abrahamsson, C., Johansson, J., Andersson-Engels, S., Svanberg, S., & Folestad, S. (2005). Time-Resolved NIR Spectroscopy for Quantitative Analysis of Intact Pharmaceutical Tablets. *Analytical Chemistry, 77*(4), 1055-1059. doi:10.1021/ac0487754

Alcalà, M., Blanco, M., Moyano, D., Broad, N. W., O'Brien, N., Friedrich, D., . . . Siesler, H. W. (2013). Qualitative and Quantitative Pharmaceutical Analysis with a Novel Hand-Held Miniature near Infrared Spectrometer. *Journal of Near Infrared Spectroscopy, 21*(6), 445-457. doi:10.1255/jnirs.1084

Alves, J. C. L., & Poppi, R. J. (2013). Biodiesel content determination in diesel fuel blends using near infrared (NIR) spectroscopy and support vector machines (SVM). *Talanta, 104*, 155-161. doi:10.1016/j.talanta.2012.11.033

Andersson, M., Josefson, M., Langkilde, F. W., & Wahlund, K. G. (1999). Monitoring of a film coating process for tablets using near infrared reflectance spectrometry. *Journal of Pharmaceutical and Biomedical Analysis, 20*(1), 27-37. doi:https://doi.org/10.1016/S0731-7085(98)00237-4

Barnes, R., Dhanoa, M., & Lister, S. J. (1989). Standard normal variate transformation and de-trending of near-infrared diffuse reflectance spectra. *Applied Spectroscopy, 43*(5), 772-777.

Batten, G. D. (1998). An Appreciation of the Contribution of NIR to Agriculture. *Journal of Near Infrared Spectroscopy, 6*(1), 105-114. doi:10.1255/jnirs.127

Beach, L., Ropero, J., Mujumdar, A., Alcalà, M., Romañach, R. J., & Davé, R. N. (2010). Near-Infrared Spectroscopy for the In-Line Characterization of Powder Voiding Part II: Quantification of Enhanced Flow Properties of Surface Modified Active Pharmaceutical Ingredients. *Journal of Pharmaceutical Innovation, 5*(1-2), 1-13. doi:10.1007/s12247-010-9075-1

Beebe, K. R., Pell, R. J., & Seasholtz, M. B. (1998). *Chemometrics: A practical guide*. New York: Wiley-Interscience.

Bellamy, L. J., Nordon, A., & Littlejohn, D. (2008). Real-time monitoring of powder mixing in a convective blender using non-invasive reflectance NIR spectrometry. *Analyst, 133*(1), 58-64. doi:10.1039/B713919E

Berntsson, O., Burger, T., Folestad, S., Danielsson, L. G., Kuhn, J., & Fricke, J. (1999). Effective Sample Size in Diffuse Reflectance Near-IR Spectrometry. *Analytical Chemistry, 71*(3), 617-623. doi:10.1021/ac980652u

Berntsson, O., Danielsson, L. G., & Folestad, S. (1998). Estimation of effective sample size when analysing powders with diffuse reflectance near-infrared spectrometry1. *Analytica Chimica Acta, 364*(1–3), 243-251. doi:10.1016/S0003-2670(98)00196-2

Blanco, M., & Alcalá, M. (2006). Content uniformity and tablet hardness testing of intact pharmaceutical tablets by near infrared spectroscopy: A contribution to process analytical technologies. *Analytica Chimica Acta, 557*(1–2), 353-359. doi:10.1016/j.aca.2005.09.070

Blanco, M., Alcalá, M., Planells, J., & Mulero, R. (2007). Quality control of cosmetic mixtures by NIR spectroscopy. *Anal Bioanal Chem, 389*(5), 1577-1583. doi:10.1007/s00216-007-1541-3

Blanco, M., Bautista, M., & Alcalá, M. (2008). Preparing calibration sets for use in pharmaceutical analysis by NIR spectroscopy. *Journal of Pharmaceutical Sciences, 97*(3), 1236-1245. doi:10.1002/jps.21105

Blanco, M., Coello, J., Iturriaga, H., Maspoch, S., & Pou, N. (2001). Influence of the procedure used to prepare the calibration sample set on the performance of near infrared spectroscopy in quantitative pharmaceutical analyses. *Analyst, 126*(7), 1129-1134. doi:10.1039/B102090K

Bondi, R. W., Igne, B., Drennen, J. K., & Anderson, C. A. (2012). Effect of Experimental Design on the Prediction Performance of Calibration Models Based on Near-Infrared Spectroscopy for Pharmaceutical Applications. *Applied Spectroscopy, 66*(12), 1442-1453. doi:10.1366/12-06689

Boukouvala, F., Niotis, V., Ramachandran, R., Muzzio, F. J., & Ierapetritou, M. G. (2012). An integrated approach for dynamic flowsheet modeling and sensitivity analysis of a continuous tablet manufacturing process. *Computers & Chemical Engineering, 42*, 30-47. doi:10.1016/j.compchemeng.2012.02.015

Cairós, C., Coello, J., & Maspoch, S. (2008). Application of representative layer theory to near-infrared reflectance spectra of powdered samples. *Applied Spectroscopy, 62*(12), 1363-1369.

Cao, N. (2013). Calibration optimization and efficiency in near infrared spectroscopy.

Càrdenas, V., Blanco, M., & Alcalà, M. (2014). Strategies for Selecting the Calibration Set in Pharmaceutical Near Infrared Spectroscopy Analysis. A Comparative Study. *Journal of Pharmaceutical Innovation, 9*(4), 272-281. doi:10.1007/s12247-014-9192-3

Cárdenas, V., Cordobés, M., Blanco, M., & Alcalà, M. (2015). Strategy for design NIR calibration sets based on process spectrum and model space: An innovative approach for process analytical technology. *Journal of Pharmaceutical and Biomedical Analysis, 114*, 28-33. doi:10.1016/j.jpba.2015.05.002

Clarke, F. C., Hammond, S. V., Jee, R. D., & Moffat, A. C. (2002). Determination of the Information Depth and Sample Size for the Analysis of Pharmaceutical Materials Using Reflectance Near-Infrared Microscopy. *Applied Spectroscopy, 56*(11), 1475-1483. doi:10.1366/00037020260377797

Collins, P. C. (2018). Chemical engineering and the culmination of quality by design in pharmaceuticals. *AIChE Journal, 64*(5), 1502-1510. doi:10.1002/aic.16154

Colón, Y. M., Florian, M. A., Acevedo, D., Méndez, R., & Romañach, R. J. (2014). Near Infrared Method Development for a Continuous Manufacturing Blending Process. *Journal of Pharmaceutical Innovation, 9*(4), 291-301. doi:10.1007/s12247-014-9194-1

Colón, Y. M., Vargas, J., Sánchez, E., Navarro, G., & Romañach, R. J. (2016). Assessment of Robustness for a Near-Infrared Concentration Model for Real-Time Release Testing in a Continuous Manufacturing Process. *Journal of Pharmaceutical Innovation, 12*(1), 14-25. doi:10.1007/s12247-016-9265-6

Da-Col, J. A., & Poppi, R. (2018). Optimization of Experimental Parameters in Analysis of Pharmaceutical Pellets by Near Infrared-Chemical Imaging (NIR-CI) and Multivariate Curve Resolution with Alternating Least Squares (MCR-ALS). *Journal of the Brazilian Chemical Society*. doi:10.21577/0103-5053.20180059

Dahm, D. (2005). Effect of particle size on absorbance (for real). *NIR news, 16*(4), 5-6.

Dahm, D., & Dahm, K. (2014). Review: Formulae for absorption spectroscopy related to idealised cases. *Journal of Near Infrared Spectroscopy, 22*(4), 249-259. doi:10.1255/jnirs.1123

Dahm, D., Dahm, K., & Norris, K. (2000). Test of the representative layer theory of diffuse reflectance using plane parallel samples. *Journal of Near Infrared Spectroscopy, 8*(3), 171-181. doi:10.1255/jnirs.276

Dahm, D., Dahm, K., & Norris, K. (2002). Obtaining material absorption properties from remission spectra of directly illuminated, layered samples. *Journal of Near Infrared Spectroscopy, 10*(1), 1-13. doi:10.1255/jnirs.316

Dahm, D. J. (2013). Explaining some light scattering properties of milk using representative layer theory. *Journal of Near Infrared Spectroscopy, 21*(5), 323-339.

Dahm, D. J., & Dahm, K. D. (2001). The Physics of Near Infrared Scattering. In P. Williams & K. Norris (Eds.), *Near Infrared Technology in the Agricultural and Food Industry* (2 edition ed., pp. 1-17). St. Paul: American Association of Cereal Chemists.

De Leersnyder, F., Peeters, E., Djalabi, H., Vanhoorne, V., Van Snick, B., Hong, K., . . . De Beer, T. (2018). Development and validation of an in-line NIR spectroscopic method for continuous blend potency

determination in the feed frame of a tablet press. *Journal of Pharmaceutical and Biomedical Analysis, 151*, 274-283. doi:10.1016/j.jpba.2018.01.032

Dickens, J. E. (2010). Overview of Process Analysis and PAT. In K. A. Bakeev (Ed.), *Process Analytical Technology* (pp. 1-15). New Jersey: A John Wiley & Sons, Ltd.

Dou, Y., Sun, Y., Ren, Y., Ju, P., & Ren, Y. (2005). Simultaneous non-destructive determination of two components of combined paracetamol and amantadine hydrochloride in tablets and powder by NIR spectroscopy and artificial neural networks. *Journal of Pharmaceutical and Biomedical Analysis, 37*(3), 543-549. doi:10.1016/j.jpba.2004.11.017

Durão, P., Fauteux-Lefebvre, C., Guay, J.-M., Abatzoglou, N., & Gosselin, R. (2017). Using multiple Process Analytical Technology probes to monitor multivitamin blends in a tableting feed frame. *Talanta, 164*, 7-15. doi:10.1016/j.talanta.2016.11.013

Ely, D., Chamarthy, S., & Carvajal, M. T. (2006). An investigation into low dose blend uniformity and segregation determination using NIR spectroscopy. *Colloids and Surfaces A: Physicochemical and Engineering Aspects, 288*(1), 71-76. doi:https://doi.org/10.1016/j.colsurfa.2006.04.032

Ely, D. R., Thommes, M., & Carvajal, M. T. (2008). Analysis of the effects of particle size and densification on NIR spectra. *Colloids and Surfaces A: Physicochemical and Engineering Aspects, 331*(1–2), 63-67. doi:10.1016/j.colsurfa.2008.07.017

Ervasti, T., Simonaho, S.-P., Ketolainen, J., Forsberg, P., Fransson, M., Wikström, H., . . . Abrahmsén-Alami, S. (2015). Continuous manufacturing of extended release tablets via powder mixing and direct compression. *Int J Pharm, 495*(1), 290-301. doi:10.1016/j.ijpharm.2015.08.077

Esbensen, K., & Julius, L. P. (2009). Representative sampling, data quality, validation-a necessary trinity in chemometrics *Comprehensice Chemometrics* (pp. 1-20): Wiley.

Esbensen, K. H., & Geladi, P. (2010). Principles of Proper Validation: use and abuse of re-sampling for validation. *Journal of Chemometrics, 24*(3-4), 168-187. doi:10.1002/cem.1310

Esbensen, K. H., Guyot, D., Westad, F., & Houmoller, L. P. (2002). *Multivariate data analysis: in practice: an introduction to multivariate data analysis and experimental design*: Multivariate Data Analysis.

Esbensen, K. H., & Paasch-Mortensen, P. (2010). Process Sampling: Theory of Sampling – the Missing Link in Process Analytical Technologies (PAT). In K. A. Bakeev (Ed.), *Process Analytical Technology* (pp. 37-80). New York: John Wiley & Sons, Ltd.

Esbensen, K. H., Paoletti, C., & Minkkinen, P. (2012). Representative sampling of large kernel lots I. Theory of Sampling and variographic analysis. *TrAC Trends in Analytical Chemistry, 32*, 154-164. doi:10.1016/j.trac.2011.09.008

Esbensen, K. H., Roman-Ospino, A. D., Sanchez, A., & Romanach, R. J. (2016). Adequacy and verifiability of pharmaceutical mixtures and dose units by variographic analysis (Theory of Sampling) - A call for a regulatory paradigm shift. *Int J Pharm, 499*(1-2), 156-174. doi:10.1016/j.ijpharm.2015.12.038

Esbensen, K. H., & Wagner, C. (2014). Theory of sampling (TOS) versus measurement uncertainty (MU)–A call for integration. *TrAC Trends in Analytical Chemistry, 57*, 93-106.

Ferrage, E., Martin, F., Micoud, P., Petit, S., Beziat, D., & Ferret, J. (2003). Cation site distribution in clinochlores: a NIR approach. *Clay Minerals, 38*(3), 329-338.

Frake, P., N. Luscombe, C., R. Rudd, D., Gill, I., Waterhouse, J., Frake, P., & A. Jayasooriya, U. (1998). Near-infrared mass median particle size determination of lactose monohydrate, evaluating several chemometric approaches. *Analyst, 123*(10), 2043-2046. doi:10.1039/A802532K

Furukawa, T., Watari, M., Siesler, H. W., & Ozaki, Y. (2003). Discrimination of various poly(propylene) copolymers and prediction of their ethylene content by near-infrared and Raman spectroscopy in combination with chemometric methods. *Journal of Applied Polymer Science, 87*(4), 616-625. doi:10.1002/app.11351

Gobrecht, A., Bendoula, R., Roger, J.-M., & Bellon-Maurel, V. (2015). Combining linear polarization spectroscopy and the Representative Layer Theory to measure the Beer–Lambert law absorbance of highly scattering materials. *Analytica Chimica Acta, 853*, 486-494.

Gosselin, R., Durão, P., Abatzoglou, N., & Guay, J.-M. (2015). Monitoring the concentration of flowing pharmaceutical powders in a tableting feed frame. *Pharmaceutical Development and Technology, 22*(6), 699-705. doi:10.3109/10837450.2015.1102278

Gowen, A., Downey, G., Esquerre, C., & O'Donnell, C. (2011). Preventing over-fitting in PLS calibration models of near-infrared (NIR) spectroscopy data using regression coefficients. *Journal of Chemometrics, 25*(7), 375-381.

Gupta, A., Peck, G. E., Miller, R. W., & Morris, K. R. (2005). Real-time near-infrared monitoring of content uniformity, moisture content, compact density, tensile strength, and young's modulus of roller compacted powder blends. *Journal of Pharmaceutical Sciences, 94*(7), 1589-1597. doi:10.1002/jps.20375

Hernandez, E., Pawar, P., Keyvan, G., Wang, Y., Velez, N., Callegari, G., . . . Romañach, R. J. (2016). Prediction of dissolution profiles by non-destructive near infrared spectroscopy in tablets subjected to different levels of strain. *Journal of Pharmaceutical and Biomedical Analysis, 117*, 568-576. doi:https://doi.org/10.1016/j.jpba.2015.10.012

Hetrick, E. M., Shi, Z., Barnes, L. E., Garrett, A. W., Rupard, R. G., Kramer, T. T., . . . Castle, B. C. (2017). Development of Near Infrared Spectroscopy-based Process Monitoring Methodology for Pharmaceutical Continuous Manufacturing Using an Offline Calibration Approach. *Analytical Chemistry, 89*(17), 9175-9183. doi:10.1021/acs.analchem.7b01907

Heymann, K., Mirschel, G., & Scherzer, T. (2010). Monitoring of the Thickness of Ultraviolet-Cured Pigmented Coatings and Printed Layers by Near-Infrared Spectroscopy. *Applied Spectroscopy, 64*(4), 419-424. doi:10.1366/000370210791114310

Heymann, K., Mirschel, G., Scherzer, T., & Buchmeiser, M. R. (2009). In-line determination of the thickness of UV-cured coatings on polymer films by NIR spectroscopy. *Vibrational Spectroscopy, 51*(2), 152-155. doi:10.1016/j.vibspec.2009.04.001

Himmelsbach, D. S., Barton, F. E., & Akin, D. E. (1986). Comparison of Responses of 13C NMR and NIR Diffuse Reflectance Spectroscopies to Changes in Particle Size and Order in Cellulose. *Applied Spectroscopy, 40*(7), 1054-1058. doi:10.1366/0003702864508133

ICH. (2005). International Conference on Harmonisation (ICH) of technical Requirements for Registration of Pharmaceuticals for Human Use *Validation of Analytical Procedures: Text and Methodology Q2(R1)*. Geneva.

Ierapetritou, M., Muzzio, F., & Reklaitis, G. (2016). Perspectives on the continuous manufacturing of powder-based pharmaceutical processes. *AIChE Journal, 62*(6), 1846-1862. doi:10.1002/aic.15210

Igne, B., Talwar, S., Drennen, J. K., & Anderson, C. A. (2013). Online Monitoring of Pharmaceutical Materials Using Multiple NIR Sensors—Part II: Blend End-point Determination. *Journal of Pharmaceutical Innovation, 8*(1), 45-55. doi:10.1007/s12247-012-9146-6

Ito, M., Suzuki, T., Yada, S., Nakagami, H., Teramoto, H., Yonemochi, E., & Terada, K. (2010). Development of a method for nondestructive NIR transmittance spectroscopic analysis of acetaminophen and caffeine anhydrate in intact bilayer tablets. *Journal of Pharmaceutical and Biomedical Analysis, 53*(3), 396-402. doi:10.1016/j.jpba.2010.04.029

Iyer, M., Morris, H., & Drennen III, J. (2002). Solid dosage form analysis by near infrared spectroscopy: comparison of reflectance and transmittance measurements including the determination of effective sample mass. *Journal of Near Infrared Spectroscopy, 10*(4), 233-245. doi:10.1255/jnirs.340

Järvinen, K., Hoehe, W., Järvinen, M., Poutiainen, S., Juuti, M., & Borchert, S. (2013). In-line monitoring of the drug content of powder mixtures and tablets by near-infrared spectroscopy during the continuous direct compression tableting process. *European Journal of Pharmaceutical Sciences, 48*(4-5), 680-688. doi:10.1016/j.ejps.2012.12.032

Johansson, J., Folestad, S., Josefson, M., Sparén, A., Abrahamsson, C., Andersson-Engels, S., & Svanberg, S. (2002). Time-resolved NIR/Vis spectroscopy for analysis of solids: pharmaceutical tablets. *Applied Spectroscopy, 56*(6), 725-731.

Johansson, J., Sparén, A., Svensson, O., Folestad, S., & Claybourn, M. (2007). Quantitative Transmission Raman Spectroscopy of Pharmaceutical Tablets and Capsules. *Applied Spectroscopy, 61*(11), 1211-1218. doi:10.1366/000370207782597085

Kalivas, J. H., & Palmer, J. (2014). Characterizing multivariate calibration tradeoffs (bias, variance, selectivity, and sensitivity) to select model tuning parameters. *Journal of Chemometrics, 28*(5), 347-357.

Koçak, A., Lucania, J. P., & Berets, S. L. (2009). Some Advances in Fourier Transform Infrared Transflection Analysis and Potential Applications in Forensic Chemistry. *Applied Spectroscopy, 63*(5), 507-511. doi:10.1366/000370209788346887

Kohler, A., Zimonja, M., Segtnan, V., & Martens, H. (2009). Standard normal variate, multiplicative signal correction and extended multiplicative signal correction preprocessing in biospectroscopy.

Koller, D. M., Posch, A., Hörl, G., Voura, C., Radl, S., Urbanetz, N., . . . Khinast, J. G. (2011). Continuous quantitative monitoring of powder mixing dynamics by near-infrared spectroscopy. *Powder Technology, 205*(1-3), 87-96. doi:10.1016/j.powtec.2010.08.070

Lee, S. L., O'Connor, T. F., Yang, X., Cruz, C. N., Chatterjee, S., Madurawe, R. D., . . . Woodcock, J. (2015). Modernizing pharmaceutical manufacturing: from batch to continuous production. *Journal of Pharmaceutical Innovation, 10*(3), 191-199.

Li, Y., Anderson, C. A., Drennen, J. K., Airiau, C., & Igne, B. (2018). Method Development and Validation of an Inline Process Analytical Technology Method for Blend Monitoring in the Tablet Feed Frame Using Raman Spectroscopy. *Analytical Chemistry, 90*(14), 8436-8444. doi:10.1021/acs.analchem.8b01009

Mark, H. (1991). *Principles and practice of spectroscopic calibration* (Vol. 118): John Wiley & Sons.

Mark, H., & Workman Jr, J. (2010). *Chemometrics in spectroscopy*: Elsevier.

Mateo-Ortiz, D., Colon, Y., Romañach, R. J., & Méndez, R. (2014). Analysis of powder phenomena inside a Fette 3090 feed frame using in-line NIR spectroscopy. *Journal of Pharmaceutical and Biomedical Analysis, 100*, 40-49. doi:https://doi.org/10.1016/j.jpba.2014.07.014

Mauritz, J. M. A., Morrisby, R. S., Hutton, R. S., Legge, C. H., & Kaminski, C. F. (2010). Imaging pharmaceutical tablets with optical coherence tomography. *Journal of Pharmaceutical Sciences, 99*(1), 385-391. doi:10.1002/jps.21844

Mendez, R., Muzzio, F., & Velazquez, C. (2010). Study of the effects of feed frames on powder blend properties during the filling of tablet press dies. *Powder Technology, 200*(3), 105-116. doi:https://doi.org/10.1016/j.powtec.2010.02.010

Mendez, R., Muzzio, F. J., & Velazquez, C. (2012). Powder hydrophobicity and flow properties: Effect of feed frame design and operating parameters. *AIChE Journal, 58*(3), 697-706. doi:10.1002/aic.12639

Miller, C. E. (2001). Chemical principles of near-infrared technology. *Near-infrared technology in the agricultural and food industries, 2*.

Næs, T., Isaksson, T., Fearn, T., & Davies, T. (2002). *A user friendly guide to multivariate calibration and classification*: NIR publications.

Nagata, T., Ohshima, M., & Tanigaki, M. (2000). In-line monitoring of polyethylene density using near infrared (NIR) spectroscopy. *Polymer Engineering & Science, 40*(5), 1107-1113. doi:doi:10.1002/pen.11238

Norris, K. H. (1989). Near infrared reflectance spectroscopy (NIRS): Analysis of forage quality. In G. C. Marten, J. Shenk, & F. Barton (Eds.), *Agriculture handbook No 643*. USA.

O'Connor, T. F., Yu, L. X., & Lee, S. L. (2016). Emerging technology: A key enabler for modernizing pharmaceutical manufacturing and advancing product quality. *Int J Pharm, 509*(1-2), 492-498. doi:10.1016/j.ijpharm.2016.05.058

Oelkrug, D., Brun, M., Rebner, K., Boldrini, B., & Kessler, R. (2012). Penetration of Light into Multiple Scattering Media: Model Calculations and Reflectance Experiments. Part I: The Axial Transfer. *Applied Spectroscopy, 66*(8), 934-943. doi:10.1366/11-06518

Olivieri, A. C. (2015). Practical guidelines for reporting results in single- and multi-component analytical calibration: A tutorial. *Analytica Chimica Acta, 868*, 10-22. doi:10.1016/j.aca.2015.01.017

Ortega-Zúñiga, C., Pinzón-De la Rosa, C., Román-Ospino, A. D., Serrano-Vargas, A., Romañach, R. J., & Méndez, R. (2019). Development of near infrared spectroscopic calibration models for in-line determination of low drug concentration, bulk density, and relative specific void volume within a feed frame. *Journal of Pharmaceutical and Biomedical Analysis, 164*, 211-222.

Ortega-Zuñiga, C., Reyes-Maldonado, K., Méndez, R., & Romañach, R. J. (2017). Study of near infrared chemometric models with low heterogeneity films: The role of optical sampling and spectral preprocessing on partial least squares errors. *Journal of Near Infrared Spectroscopy, 25*(2), 103-115. doi:10.1177/0967033516686653

Pell, R. J., Seasholtz, M. B., Beebe, K. R., & Koch, M. V. (2014). Process analytical chemistry and chemometrics, Bruce Kowalski's legacy at The Dow Chemical Company. *Journal of Chemometrics, 28*(5), 321-331. doi:10.1002/cem.2535

Pestieau, A., Krier, F., Thoorens, G., Dupont, A., Chavez, P.-F., Ziemons, E., . . . Evrard, B. (2014). Towards a real time release approach for manufacturing tablets using NIR spectroscopy. *Journal of Pharmaceutical and Biomedical Analysis, 98*, 60-67. doi:10.1016/j.jpba.2014.05.002

Petersen, L., Minkkinen, P., & Esbensen, K. H. (2005). Representative sampling for reliable data analysis: Theory of Sampling. *Chemometrics and Intelligent Laboratory Systems, 77*(1-2), 261-277. doi:10.1016/j.chemolab.2004.09.013

Petit, S., Decarreau, A., Martin, F., & Buchet, R. (2004). Refined relationship between the position of the fundamental OH stretching and the first overtones for clays. *Physics and Chemistry of Minerals, 31*(9), 585-592. doi:10.1007/s00269-004-0423-x

Petit, S., Martin, F., Wiewiora, A., De Parseval, P., & Decarreau, A. (2004). Crystal-chemistry of talc: A near infrared (NIR) spectroscopy study. *American Mineralogist, 89*(2-3), 319. doi:10.2138/am-2004-2-310

Pharmaceutical Technology Editors. (2016, Apr 12). FDA Approves Tablet Production on Janssen Continuous Manufacturing Line. Retrieved from http://www.pharmtech.com/fda-approves-tablet-production-janssen-continuous-manufacturing-line

Roggo, Y., Chalus, P., Maurer, L., Lema-Martinez, C., Edmond, A., & Jent, N. (2007). A review of near infrared spectroscopy and chemometrics in pharmaceutical technologies. *Journal of Pharmaceutical and Biomedical Analysis, 44*(3), 683-700. doi:10.1016/j.jpba.2007.03.023

Rohe, T., Becker, W., Kölle, S., Eisenreich, N., & Eyerer, P. (1999). Near infrared (NIR) spectroscopy for in-line monitoring of polymer extrusion processes. *Talanta, 50*(2), 283-290. doi:10.1016/S0039-9140(99)00035-1

Román-Ospino, A. D., Singh, R., Ierapetritou, M., Ramachandran, R., Méndez, R., Ortega-Zuñiga, C., . . . Romañach, R. J. (2016). Near infrared spectroscopic calibration models for real time monitoring of powder density. *Int J Pharm, 512*(1), 61-74. doi:10.1016/j.ijpharm.2016.08.029

Romañach, R. J. (2017). *Theory of Sampling - From Missing Link to Key Enabler for Process Analytical Technology (PAT)*. Paper presented at the Keynote Lecture 8th World Conference on Sampling and Blending, Perth, Australia.

Romañach, R. J., Hernández-Torres, E., Roman-Ospino, A., Pastrana-Otero, I., & Semidei-Ortiz, F. M. (2014). NIR and Raman Spectroscopic Experiments to Train the Next Generation of PAT Scientists. *American Pharmaceutical Review, 17*(16), 82-87.

Romañach, R. J., Román-Ospino, A. D., & Alcalà, M. (2016). A Procedure for Developing Quantitative Near Infrared (NIR) Methods for Pharmaceutical Products. In M. G. Ierapetritou & R. Ramachandran (Eds.), *Process Simulation and Data Modeling in Solid Oral Drug Development and Manufacture* (pp. 133-158). New York, NY: Springer New York.

Römer, M., Heinämäki, J., Strachan, C., Sandler, N., & Yliruusi, J. (2008). Prediction of Tablet Film-coating Thickness Using a Rotating Plate Coating System and NIR Spectroscopy. *AAPS PharmSciTech, 9*(4), 1047-1053. doi:10.1208/s12249-008-9142-9

Rosas, J., Blanco, M., Santamaría, F., & Alcalà, M. (2013). Assessment of chemometric methods for the non-invasive monitoring of solid blending processes using wireless near infrared spectroscopy. *Journal of Near Infrared Spectroscopy, 21*(2), 97-106. doi:10.1255/jnirs.1041

Sánchez-Paternina, A., Román-Ospino, A., Ortega-Zuñiga, C., Alvarado, B., Esbensen, K. H., & Romañach, R. (2015). *When "homogeneity" is expected—Theory of Sampling in pharmaceutical manufacturing.* Paper presented at the TOS forum.

Sánchez-Paternina, A., Román-Ospino, A. D., Martínez, M., Mercado, J., Alonso, C., & Romañach, R. J. (2016). Near infrared spectroscopic transmittance measurements for pharmaceutical powder mixtures. *Journal of Pharmaceutical and Biomedical Analysis, 123*, 120-127. doi:10.1016/j.jpba.2016.02.006

Sarraguca, M. C., Cruz, A. V., Amaral, H. R., Costa, P. C., & Lopes, J. A. (2011). Comparison of different chemometric and analytical methods for the prediction of particle size distribution in pharmaceutical powders. *Anal Bioanal Chem, 399*(6), 2137-2147. doi:10.1007/s00216-010-4230-6

Šašić, S., Blackwood, D., Liu, A., Ward, H. W., & Clarke, H. (2015). Detailed analysis of the online near-infrared spectra of pharmaceutical blend in a rotary tablet press feed frame. *Journal of Pharmaceutical and Biomedical Analysis, 103*, 73-79. doi:10.1016/j.jpba.2014.11.008

Savitzky, A., & Golay, M. J. (1964). Smoothing and differentiation of data by simplified least squares procedures. *Analytical Chemistry, 36*(8), 1627-1639.

Shi, Z., & Anderson, C. A. (2010). Application of Monte Carlo Simulation-Based Photon Migration for Enhanced Understanding of Near-Infrared (NIR) Diffuse Reflectance. Part I: Depth of Penetration in Pharmaceutical Materials. *Journal of Pharmaceutical Sciences, 99*(5), 2399-2412. doi:https://doi.org/10.1002/jps.22013

Shimoyama, M., Ninomiya, T., Sano, K., Ozaki, Y., Higashiyama, H., Watari, M., & Tomo, M. (1998). Near infrared spectroscopy and chemometrics analysis of linear low-density polyethylene. *Journal of Near Infrared Spectroscopy, 6*(1), 317-324.

Sierra-Vega, N. O., Sánchez-Paternina, A., Maldonado, N., Cárdenas, V., Romañach, R. J., & Méndez, R. (2018). In line monitoring of the powder flow behavior and drug content in a Fette 3090 feed frame at different operating conditions using Near Infrared spectroscopy. *Journal of Pharmaceutical and Biomedical Analysis, 154*, 384-396. doi:10.1016/j.jpba.2018.03.017

Siesler, H. W. (2007). Basic principles of near-infrared spectroscopy *Handbook of Near-Infrared Analysis, Third Edition* (pp. 25-38): CRC press.

Singh, R., Román-Ospino, A. D., Romañach, R. J., Ierapetritou, M., & Ramachandran, R. (2015). Real time monitoring of powder blend bulk density for coupled feed-forward/feed-back control of a

continuous direct compaction tablet manufacturing process. *Int J Pharm, 495*(1), 612-625. doi:10.1016/j.ijpharm.2015.09.029

Singh, R., Sahay, A., Karry, K. M., Muzzio, F., Ierapetritou, M., & Ramachandran, R. (2014). Implementation of an advanced hybrid MPC–PID control system using PAT tools into a direct compaction continuous pharmaceutical tablet manufacturing pilot plant. *Int J Pharm, 473*(1-2), 38-54. doi:10.1016/j.ijpharm.2014.06.045

Skibsted, E. T. S., Westerhuis, J. A., Smilde, A. K., & Witte, D. T. (2007). Examples of NIR based real time release in tablet manufacturing. *Journal of Pharmaceutical and Biomedical Analysis, 43*(4), 1297-1305. doi:10.1016/j.jpba.2006.10.037

Sulub, Y., & DeRudder, J. (2013). Determination of polymer blends composed of polycarbonate and rubber entities using near-infrared (NIR) spectroscopy and multivariate calibration. *Polymer Testing, 32*(4), 802-809. doi:10.1016/j.polymertesting.2013.03.008

Tankeu, S. Y., Vermaak, I., Kamatou, G. P. P., & Viljoen, A. M. (2014). Vibrational spectroscopy and chemometric modeling: An economical and robust quality control method for lavender oil. *Industrial Crops and Products, 59*, 234-240. doi:10.1016/j.indcrop.2014.05.005

Torricelli, A., Contini, D., Pifferi, A., Caffini, M., Re, R., Zucchelli, L., & Spinelli, L. (2014). Time domain functional NIRS imaging for human brain mapping. *NeuroImage, 85*, 28-50. doi:10.1016/j.neuroimage.2013.05.106

US-FDA. (2004). Guidance for Industry – PAT A Framework for Innovative Pharmaceutical Development, Manufacturing, and Quality Assurance. Rockville, MD, USA.

US-FDA. (2015). Summary review of regulatory action NDA Number 206038.

Vanarase, A. U., Alcalà, M., Jerez Rozo, J. I., Muzzio, F. J., & Romañach, R. J. (2010). Real-time monitoring of drug concentration in a continuous powder mixing process using NIR spectroscopy. *Chemical Engineering Science, 65*(21), 5728-5733. doi:10.1016/j.ces.2010.01.036

Vargas, J. M., Nielsen, S., Cárdenas, V., Gonzalez, A., Aymat, E. Y., Almodovar, E., . . . Romañach, R. J. (2018). Process analytical technology in continuous manufacturing of a commercial pharmaceutical product. *Int J Pharm, 538*(1-2), 167-178. doi:10.1016/j.ijpharm.2018.01.003

Wahid, Z., Latiff, A. I., & Ahmad, K. (2017). Application of one-way ANOVA in completely randomized experiments. *Journal of Physics: Conference Series, 949*, 012017. doi:10.1088/1742-6596/949/1/012017

Wahl, P. R., Fruhmann, G., Sacher, S., Straka, G., Sowinski, S., & Khinast, J. G. (2014). PAT for tableting: Inline monitoring of API and excipients via NIR spectroscopy. *European Journal of Pharmaceutics and Biopharmaceutics, 87*(2), 271-278. doi:https://doi.org/10.1016/j.ejpb.2014.03.021

Ward, H. W., Blackwood, D. O., Polizzi, M., & Clarke, H. (2013). Monitoring blend potency in a tablet press feed frame using near infrared spectroscopy. *Journal of Pharmaceutical and Biomedical Analysis, 80*, 18-23. doi:https://doi.org/10.1016/j.jpba.2013.02.008

Watari, M., & Ozaki, Y. (2004). Prediction of Ethylene Content in Melt-State Random and Block Polypropylene by Near-Infrared Spectroscopy and Chemometrics: Comparison of a New Calibration Transfer Method with a Slope/Bias Correction Method. *Applied Spectroscopy, 58*(10), 1210-1218. doi:10.1366/0003702042336082

Williams, P., & Norris, K. (1987). *Near-infrared technology in the agricultural and food industries*: American Association of Cereal Chemists, Inc.

Workman, J., & Weyer, L. (2012). *Practical Guide and Spectral Atlas for Interpretive Near-Infrared Spectroscopy*: CRC Press.

Workman Jr., J. J. (2001). *Handbook of organic compounds NIR, IR, Raman, and UV spectra featuring polymers and surfaces* (1 ed.). San Diego: Academic Press.

Yang, L., & Daniel, B. (2012, May 1). Sample Presentation in Rotary Tablet Press Feed Frame Monitoring by Near Infrared Spectroscopy. Retrieved from

https://www.americanpharmaceuticalreview.com/Featured-Articles/116357-Sample-Presentation-in-Rotary-Tablet-Press-Feed-Frame-Monitoring-by-Near-Infrared-Spectroscopy/

Yu, L. X., Akseli, I., Allen, B., Amidon, G., Bizjak, T. G., Boam, A., . . . Zezza, D. (2016). Advancing Product Quality: a Summary of the Second FDA/PQRI Conference. *The AAPS Journal, 18*(2), 528-543. doi:10.1208/s12248-016-9874-5

Zhang, M., Hui, Q., Lou, X.-J., Redfern, S. A. T., Salje, E. K. H., & Tarantino, S. C. (2006). Dehydroxylation, proton migration, and structural changes in heated talc: An infrared spectroscopic study. *American Mineralogist, 91*(5-6), 816-825. doi:10.2138/am.2006.1945